

AN ABSTRACT OF THE THESIS OF

Therese Michelle Pflaum for the degree of Master of Science in Civil Engineering presented on August 12, 2013.

Title: Non-Destructive Determination of Yield Stress for In-Situ Gusset Plates

Abstract approved: _____

Christopher C. Higgins

Failure of a gusset plate that caused the I-35W Bridge collapse in Minneapolis, MN resulted in mandated rating of connections by the Federal Highway Administration (FHWA). Rating connections requires material properties as an input. The material properties are generally reported on the available detailed drawings for bridges. However, some bridges do not have documented materials or it is uncertain if the as-built properties are those reported in the design documents. To ensure ratings that adequately reflect the in-situ connections, the material properties must be obtained. Unfortunately, at present there are no recognized, non-destructive testing methods available to establish the yield stress of in-service steel gusset plates. To address this need, a prototype testing device was developed to determine the yield stress of in-service connection plates. The device applies an out of plane load to the free edge of a gusset plate and

simultaneously, the load applied by the device and plate deflection under the load point are measured. These measurements are then correlated to the yield stress which is determined based on calibrated finite element models for various materials and thicknesses. The non-destructive testing device can serve three major functions for connection evaluations. It will 1) allow bridge owners to establish the material properties for bridges that do not have documentation of the materials used in construction, 2) allow rating engineers to determine if the yield stress is above the minimum required for the plate to achieve a specific rating, or 3) enable rating engineers to use the actual yield stress of the plate to extract the most capacity from the connection. The research outcome allows bridge owners to effectively and non-destructively collect as-built yield stress of gusset plate connections thereby enabling connection capacity to be established with greater certainty.

©Copyright by Therese Michelle Pflaum

August 12, 2013

All Rights Reserved

Non-Destructive Determination of Yield Stress for In-Situ Gusset Plates

by

Therese Michelle Pflaum

A THESIS

submitted to

Oregon State University

in partial fulfillment of

the requirements for the

degree of

Master of Science

Presented August 12, 2013

Commencement June 2014

Master of Science thesis of Therese Michelle Pflaum presented on August 12, 2013

APPROVED:

Major Professor, representing Civil Engineering

Head of the School of Civil and Construction Engineering

Dean of the Graduate School

I understand that my thesis will become part of the permanent collection of Oregon State University libraries. My signature below authorizes release of my thesis to any reader upon request.

Therese Michelle Pflaum, Author

ACKNOWLEDGEMENTS

First and foremost I would like to thank Dr. Chris Higgins for taking me on as his research assistant and for his continued guidance throughout my project; I am not sure what I would have done without him. Also, I would like to thank Dr. Andre Barbosa, Dr. Burkan Isgor, and Dr. John Sessions for being on my committee.

Thank you to NCHRP for their funding of this project.

I would like to thank Dr. Tugrul Turan for his assistance on my ABAQUS models and Manfred Dietrich and Michael Dyson for helping me with the construction of my prototype and experimental testing setup. I also want to recognize my undergrad assistant Brandon Zaikoski for his help with strain gauging and experimental testing.

School would not have been the same without all of my friends who put up with my constant need for activity. You all helped make school more fun than it was work. The faculty and staff here at OSU have been unbelievable and have helped me so much, both in and out of the classroom.

Lastly, I would like to thank my amazing family for all of their love and support, without whom I would not be the person that I am today.

TABLE OF CONTENTS

	<u>Page</u>
1 INTRODUCTION AND BACKGROUND.....	1
2 LITERATURE REVIEW	3
2.1 Relationship Between Hardness and Yield Stress	3
2.2 Non-Destructive Testing Method of Metallic Materials.....	5
2.3 Determining Both Dynamic and Static Yield Stress	7
2.4 Bridge Steels.....	12
3 METHODOLOGY	16
3.1 Prototype Design	16
3.2 Finite Element Modeling	20
3.2.1 Boundary Conditions.....	20
3.2.2 Free Plates	24
3.2.3 Axially Loaded Plates.....	34
3.2.4 Plate Cut Layout.....	38
3.3 Material Testing.....	41
3.3.1 Sample Preparation.....	41
3.3.2 Sample Testing	42
3.3.3 Data Reduction	43
3.3.4 Material Results.....	49

TABLE OF CONTENTS (Continued)

	<u>Page</u>
4 EXPERIMENTAL TESTING	60
4.1 Free Plates.....	60
4.1.1 Setup and Instrumentation.....	60
4.1.2 Testing Methodology.....	65
4.2 Axially Loaded Plates.....	68
4.2.1 Setup and Instrumentation.....	68
4.2.2 Effects of Bending Within the Plate.....	69
5 RESULTS	71
5.1 Pressure Gauge vs. Load Cell.....	71
5.2 Prototype Load vs. Strain Gauge Data	72
5.3 Prototype Load vs. Mill Scale Flaking	74
5.4 Prototype Load vs. Time	77
5.5 Prototype Load vs. Plate Deflection	80
5.6 Prototype Load Correlation with Finite Element Model	81
5.7 Analysis Results	83
5.7.1 Development of Offset Method Concept.....	83
5.7.2 Demonstration of Offset Method.....	88
5.7.3 Prototype Device Testing on Spare Gusset Plate	98

TABLE OF CONTENTS (Continued)

	<u>Page</u>
6 CONCLUSIONS.....	100
7 BIBLIOGRAPHY	102
APPENDECIES	104

LIST OF FIGURES

<u>Figure</u>	<u>Page</u>
Figure 2-1: Typical indentation load versus depth of penetration curve Murty <i>et al.</i> [1998].....	6
Figure 2-2: Schematic representation of the indentation profile in an ABI test, Murty <i>et al.</i> [1998]	6
Figure 2-3: Visual of yield stress terms from Rao, Lohrman, and Tall [1966] Fig. 1	8
Figure 2-4: Typical stress vs. strain diagram from Rao, Lohrmann and Tall [1966] Fig 8	10
Figure 2-5: Estimated curves relating dynamic yield stress level, static yield stress level, and strain rate from Rao, Lohrmann, and Tall [1966]	11
Figure 3-1: Side view of prototype design.....	17
Figure 3-2: Elevation view of prototype design.....	18
Figure 3-3: Load cell with 10 kip capacity (http://www.futek.com/product.aspx?t=load&m=lca305)	19
Figure 3-4: Final prototype design.....	19
Figure 3-5: AutoCAD drawings for idealized beam model	21
Figure 3-6: Load and deflection curves for various support conditions	23
Figure 3-8: Free plate generic model	24
Figure 3-9: Varying length and width effect on prototype device load for 3/8 in. thick A36 material set to 0.05 in. displacement.....	25
Figure 3-11: Load vs. deflection for plate widths 6 in. to 24 in. and length 16 in. for 3/8 in. thick A36 material.....	27
Figure 3-13: Mesh refinement plot for a 20 in. wide and 16 in. long 3/8 in. thick A36 plate	30
Figure 3-14: Mesh seed size vs. run time.....	31
Figure 3-15: Final mesh layout for free plate model	32
Figure 3-16: Adjusted FE load vs. deflection curve based on various stiffness values for 3/8 in. A36 plate.....	33
Figure 3-18: Partition layout for the axially stressed induced plate model.....	36

LIST OF FIGURES (Continued)

<u>Figure</u>	<u>Page</u>
Figure 3-19: Final mesh layout for the axially stressed induced plate model.....	36
Figure 3-20: Axially loaded plate stress distribution from FE Model for 3/8 in. thick A36 plate loaded to 38 kips, stresses in ksi	37
Figure 3-21: Final dimensions for axially loaded plates tested in UTM.....	37
Figure 3-22: Labeling scheme for plates and coupons.....	38
Figure 3-23: Plate and coupon sample cut layout for free plates	39
Figure 3-24: Axially loaded plate and coupon labeling scheme	40
Figure 3-25: Axially loaded plate and coupon sample cut layout.....	40
Figure 3-26: Coupon labeling scheme	41
Figure 3-28: Typical engineering stress vs. engineering strain data before post-processing.....	43
Figure 3-29: Engineering stress vs. time filtering process using low pass option	44
Figure 3-30: Engineering stress vs. engineering strain filtered data	45
Figure 3-31: Filtered stress vs. time dynamic and static yield plateaus.....	46
Figure 3-32: Dynamic yield for 0.2% offset	47
Figure 3-33: Example of 0.2% offset used for materials with no yielding plateau.....	48
Figure 3-34: Static yield stress drop over time	48
Figure 3-36: Example of elastic and early plastic region of engineering stress vs. engineering strain curve.....	51
Figure 3-37: True stress vs. true plastic strain for all rolling directions of 3/8 in. thick A36 steel	54
Figure 3-38: Plot of all coupon tests averaged by plate type and rolling direction.....	56
Figure 3-39: Varying dynamic yield true stress vs. true plastic strain plots based on average tensile coupon results	58
Figure 3-40: Load vs. deflection for various plate thicknesses using A36 and Gr. 50 properties	59

LIST OF FIGURES (Continued)

<u>Figure</u>	<u>Page</u>
Figure 4-1: Image of micrometer used to measure plate deflection.....	61
Figure 4-2: Displacement sensors attached to support beam of prototype	62
Figure 4-3: Displacement sensors attached to prototype and free edge of plate.....	63
Figure 4-4: White wash on plate	64
Figure 4-5: Mill scale flaking of white wash after plate yielding	64
Figure 4-6: Typical strain gauge	64
Figure 4-7: Free plate testing setup.....	65
Figure 4-9: Axially loaded plate strain gauge setup	69
Figure 4-10: Plate test setup in UTM.....	69
Figure 5-1: Comparison of pressure gauge and load cell outputs.....	72
Figure 5-2: Strain gauge data from ½ in. thick A36 plate TN1	73
Figure 5-4: Spread of Plasticity (B).....	75
Figure 5-5: Spread of Plasticity (C).....	75
Figure 5-6: Spread of Plasticity (D).....	75
Figure 5-7: Progression of mill scale flaking in relation to load vs. deflection curve	76
Figure 5-9: Load reductions occurring at hold plateaus increases as yielding increases across plate.....	79
Figure 5-10: Absolute change in load at each 60 sec. hold interval.	80
Figure 5-11: Typical experimental results load vs. deflection plot.....	81
Figure 5-12: Load drop between dynamic and static yield properties giving first yielding	82
Figure 5-13: FE model - first yielding	83
Figure 5-14: FE model - 2 in. spread of plasticity at the load point	83

LIST OF FIGURES (Continued)

<u>Figure</u>	<u>Page</u>
Figure 5-15: A36 various material inputs	84
Figure 5-16: A514 various material inputs	84
Figure 5-17: Load-deformation response for analyses of different material models.	85
Figure 5-18: Load vs. deflection response and device load at 0.005 in. offset for 3/8 in. thick plate.....	86
Figure 5-19: Load vs. deflection response and device load at 0.005 in. offset for 1 in. thick plate	86
Figure 5-20: 3/8 in. thick A36 (2.51 kip) spread of plasticity.....	87
Figure 5-21: 3/8 in. thick A514 (5.87 kip) spread of plasticity.....	87
Figure 5-22: 1 in. thick A36 (19.21 kip) spread of plasticity.....	87
Figure 5-23: 1 in. thick A514 (47.86 kip) spread of plasticity.....	87
Figure 5-24: Prototype device yielding load using offset method for 3/8 in. thick A36 plate BW1	88
Figure 5-25: FE predicted effect of axial stresses on P_Y for 1/2 in. thick A36 plate.....	89
Figure 5-26: Strain gauge locations on specimen	90
Figure 5-27: Measured strain gauge readings (microstrain) in 1/2 in. thick A36 plate with 10 ksi nominal axial stresses	90
Figure 5-29: Load-deformation response for 3/8 in. thick plate with different yield stress materials.....	92
Figure 5-30: Prototype device load at 0.005 in. offset correlated to yield stress for 3/8 in. thick steel plate	93
Figure 5-31: Relationship between dynamic yield stress and prototype device load for various plate thicknesses with no yield stress prediction safety factor.....	98
Figure 5-32: Gusset plate test with spare plate in OSU laboratory.....	99

LIST OF TABLES

<u>Table</u>	<u>Page</u>
Table 2-2: Various structural steel designations	13
Table 3-2: Percent difference between FEA model support conditions and beam experimental results	23
Table 3-4: Percent difference between results of various mesh sizes	31
Table 3-6: Summary of results for all material samples – US Customary Units	52
Table 3-7: Summary of results for all material samples – Metric Units	53
Table 3-9: Average FE material inputs used in each model – Metric Units	55
Table 3-11: Material properties for specific rolling direction – Metric Units	57
Table 5-3: Predicted yield stress results from plate specimens.....	94
Table 5-4: Predicted yield stress	96
Table 5-5: Yield stress prediction safety factor for various test readings	97

LIST OF APPENDICIES

<u>Appendix</u>	<u>Page</u>
A. MATERIALS TESTING RESULTS.....	105
B. MATERIAL FABRICATION DOCUMENTS	163
C. EXPERIMENTAL RESULTS 0.005 IN. OFFSET	169

APPENDIX LIST OF FIGURES

<u>Figure</u>	<u>Page</u>
Figure A-1: Engineering stress vs. engineering strain for the parallel rolling direction 3/8 in. thick A36 sample PN1	105
Figure A-2: True stress vs. true plastic strain for the parallel rolling direction 3/8 in. thick A36 sample PN1	105
Figure A-3: Engineering stress vs. engineering strain for the parallel rolling direction 3/8 in. thick A36 sample PN2	106
Figure A-4: True stress vs. true plastic strain for the parallel rolling direction 3/8 in. thick A36 sample PN2	106
Figure A-5: Engineering stress vs. engineering strain for the parallel rolling direction 3/8 in. thick A36 sample PN3	107
Figure A-6: True stress vs. true plastic strain for the parallel rolling direction 3/8 in. thick A36 sample PN3	107
Figure A-7: Engineering stress vs. engineering strain for the parallel rolling direction 3/8 in. thick A36 sample PW1	108
Figure A-8: True stress vs. true plastic strain for the parallel rolling direction 3/8 in. thick A36 sample PW1	108
Figure A-9: Engineering stress vs. engineering strain for the parallel rolling direction 3/8 in. thick A36 sample PW2	109
Figure A-10: True stress vs. true plastic strain for the parallel rolling direction 3/8 in. thick A36 sample PW2	109
Figure A-11: Engineering stress vs. engineering strain for the parallel rolling direction 3/8 in. thick A36 sample PW3	110
Figure A-12: True stress vs. true plastic strain for the parallel rolling direction 3/8 in. thick A36 sample PW3	110
Figure A-13: Engineering stress vs. engineering strain for the transverse rolling direction 3/8 in. thick A36 sample TN1	111
Figure A-14: True stress vs. true plastic strain for the transverse rolling direction 3/8 in. thick A36 sample TN1	111
Figure A-15: Engineering stress vs. engineering strain for the transverse rolling direction 3/8 in. thick A36 sample TN2	112

APPENDIX LIST OF FIGURES (Continued)

<u>Figure</u>	<u>Page</u>
Figure A-16: True stress vs. true plastic strain for the transverse rolling direction 3/8 in. thick A36 sample TN2	112
Figure A-17: Engineering stress vs. engineering strain for the transverse rolling direction 3/8 in. thick A36 sample TN3	113
Figure A-18: True stress vs. true plastic strain for the transverse rolling direction 3/8 in. thick A36 sample TN3	113
Figure A-19: Engineering stress vs. engineering strain for the transverse rolling direction 3/8 in. thick A36 sample TW1	114
Figure A-20: True stress vs. true plastic strain for the transverse rolling direction 3/8 in. thick A36 sample TW1	114
Figure A-21: Engineering stress vs. engineering strain for the transverse rolling direction 3/8 in. thick A36 sample TW2	115
Figure A-22: True stress vs. true plastic strain for the transverse rolling direction 3/8 in. thick A36 sample TW2	115
Figure A-23: Engineering stress vs. engineering strain for the transverse rolling direction 3/8 in. thick A36 sample TW3	116
Figure A-24: True stress vs. true plastic strain for the transverse rolling direction 3/8 in. thick A36 sample TW3	116
Figure A-25: Engineering stress vs. engineering strain for the 45° bias rolling direction 3/8 in. thick A36 sample BN1	117
Figure A-26: True stress vs. true plastic strain for the 45° bias rolling direction 3/8 in. thick A36 sample BN1	117
Figure A-27: Engineering stress vs. engineering strain for the 45° bias rolling direction 3/8 in. thick A36 sample BN2	118
Figure A-28: True stress vs. true plastic strain for the 45° bias rolling direction 3/8 in. thick A36 sample BN2	118
Figure A-29: Engineering stress vs. engineering strain for the 45° bias rolling direction 3/8 in. thick A36 sample BN3	119

APPENDIX LIST OF FIGURES (Continued)

<u>Figure</u>	<u>Page</u>
Figure A-30: True stress vs. true plastic strain for the 45° bias rolling direction 3/8 in. thick A36 sample BN3.....	119
Figure A-31: Engineering stress vs. engineering strain for the 45° bias rolling direction 3/8 in. thick A36 sample BW1	120
Figure A-32: True stress vs. true plastic strain for the 45° bias rolling direction 3/8 in. thick A36 sample BW1	120
Figure A-33: Engineering stress vs. engineering strain for the 45° bias rolling direction 3/8 in. thick A36 sample BW2	121
Figure A-34: True stress vs. true plastic strain for the 45° bias rolling direction 3/8 in. thick A36 sample BW2.....	121
Figure A-35: Engineering stress vs. engineering strain for the 45° bias rolling direction 3/8 in. thick A36 sample BW3	122
Figure A-36: True stress vs. true plastic strain for the 45° bias rolling direction 3/8 in. thick A36 sample BW3.....	122
Figure A-37: Engineering stress vs. engineering strain for the parallel rolling direction 1/2 in. thick A36 sample P1	147
Figure A-38: True stress vs. true plastic strain for the parallel rolling direction 1/2 in. thick A36 sample P1	147
Figure A-39: Engineering stress vs. engineering strain for the parallel rolling direction 1/2 in. thick A36 sample P2	148
Figure A-40: True stress vs. true plastic strain for the parallel rolling direction 1/2 in. thick A36 sample P2	148
Figure A-41: Engineering stress vs. engineering strain for the parallel rolling direction 1/2 in. thick A36 sample P3	149
Figure A-42: True stress vs. true plastic strain for the parallel rolling direction 1/2 in. thick A36 sample P3	149
Figure A-43: Engineering stress vs. engineering strain for the transverse rolling direction 1/2 in. thick A36 sample T1	150

APPENDIX LIST OF FIGURES (Continued)

<u>Figure</u>	<u>Page</u>
Figure A-44: True stress vs. true plastic strain for the transverse rolling direction 1/2 in. thick A36 sample T1	150
Figure A-45: Engineering stress vs. engineering strain for the transverse rolling direction 1/2 in. thick A36 sample T2	151
Figure A-46: True stress vs. true plastic strain for the transverse rolling direction 1/2 in. thick A36 sample T2	151
Figure A-47: Engineering stress vs. engineering strain for the transverse rolling direction 1/2 in. thick A36 sample T3	152
Figure A-48: True stress vs. true plastic strain for the transverse rolling direction 1/2 in. thick A36 sample T3	152
Figure A-49: Engineering stress vs. engineering strain for the parallel rolling direction 3/8 in. thick Gr. 50 sample P1	155
Figure A-50: Engineering stress vs. engineering strain for the parallel rolling direction 3/8 in. thick Gr. 50 sample P1	155
Figure A-51: Engineering stress vs. engineering strain for the parallel rolling direction 3/8 in. thick Gr. 50 sample P2	156
Figure A-52: Engineering stress vs. engineering strain for the parallel rolling direction 3/8 in. thick Gr. 50 sample P2	156
Figure A-53: Engineering stress vs. engineering strain for the parallel rolling direction 3/8 in. thick Gr. 50 sample P3	157
Figure A-54: Engineering stress vs. engineering strain for the parallel rolling direction 3/8 in. thick Gr. 50 sample P3	157
Figure A-55: Engineering stress vs. engineering strain for the transverse rolling direction 3/8 in. thick Gr. 50 sample T1	158
Figure A-56: True stress vs. true plastic strain for the transverse rolling direction 3/8 in. thick Gr. 50 sample T1	158
Figure A-57: Engineering stress vs. engineering strain for the transverse rolling direction 3/8 in. thick Gr. 50 sample T2	159

APPENDIX LIST OF FIGURES (Continued)

<u>Figure</u>	<u>Page</u>
Figure A-58: True stress vs. true plastic strain for the transverse rolling direction 3/8 in. thick Gr. 50 sample T2.....	159
Figure A-59: Engineering stress vs. engineering strain for the transverse rolling direction 3/8 in. thick Gr. 50 sample T3.....	160
Figure A-60: True stress vs. true plastic strain for the transverse rolling direction 3/8 in. thick Gr. 50 sample T3.....	160
Figure B-1: Mill certification for titanium plate 1	163
Figure B-2: Mill certification for titanium plate 2	164
Figure B-3: Mill certification for titanium plate 3	165
Figure B-4: Mill certification for steel ½ in. thick A36 plate	166
Figure B-5: Mill certification for steel 3/8 in. thick A36 plate	167
Figure B-6: Mill certification for steel 3/8 in. thick Gr. 50 plate.....	168
Figure C-1: 3/8 in. thick A36 plate PW1	169
Figure C-2: 3/8 in. thick A36 plate PW1s.....	170
Figure C-3: 3/8 in. thick A36 plate PW2	170
Figure C-4: 3/8 in. thick A36 plate PW2s.....	171
Figure C-5: 3/8 in. thick A36 plate PW3	171
Figure C-6: 3/8 in. thick A36 plate PW3s.....	172
Figure C-7: 3/8 in. thick A36 plate TW1s1	172
Figure C-8: 3/8 in. thick A36 plate TW2.....	173
Figure C-9: 3/8 in. thick A36 plate TW2s	173
Figure C-10: 3/8 in. thick A36 plate TW3s	174

APPENDIX LIST OF FIGURES (Continued)

<u>Figure</u>	<u>Page</u>
Figure C-11: 3/8 in. thick A36 plate BW1s	174
Figure C-12: 3/8 in. thick A36 plate BW2.....	175
Figure C-13: 3/8 in. thick A36 plate BW2s	175
Figure C-14: 1/2 in. thick A36 plate PN1	176
Figure C-15: 1/2 in. thick A36 plate PN3	176
Figure C-16: 1/2 in. thick A36 plate TN3.....	177
Figure C-17: 3/8 in. thick Gr 50 plate PN3.....	177
Figure C-18: 3/8 in. thick Gr 50 plate TN1.....	178
Figure C-19: 3/8 in. thick Gr 50 plate TN3.....	178

APPENDIX LIST OF TABLES

<u>Table</u>	<u>Page</u>
Table A-1: Static yield stress for the parallel rolling direction 3/8 in. thick A36 plate	123
Table A-2: Static yield stress for the transverse rolling direction 3/8 in. thick A36 plate	125
Table A-3: Static yield stress for the 45° bias rolling direction 3/8 in. thick A36 plate	127
Table A-4: Dynamic yield stress for the parallel rolling direction 3/8 in. thick A36 plate	129
Table A-5: Dynamic yield stress for transverse rolling direction for 3/8 in. thick A36 plate	131
Table A-6: Dynamic yield stress for 45° bias rolling direction for 3/8 in. thick A36 plate	133
Table A-7: Final strain and tensile strength for the parallel rolling direction 3/8 in. thick A36 plate –US Customary Units	135
Table A-8: Final strain and tensile strength for the parallel rolling direction 3/8 in. thick A36 plate –Metric Units	136
Table A-9: Final strain and tensile strength for the transverse rolling direction 3/8 in. thick A36 plate- English Units	137
Table A-10: Final strain and tensile strength for the transverse rolling direction 3/8 in. thick A36 plate- Metric Units	138
Table A-11: Final strain and tensile strength for the 45° bias rolling direction for 3/8 in. thick A36 plate- English Units	139
Table A-12: Final strain and tensile strength for the 45° bias rolling direction for 3/8 in. thick A36 plate- Metric Units	140
Table A-13: Results summary for the parallel rolling direction 3/8 in. thick plate	141
Table A-14: Results summary for the transverse rolling direction 3/8 in. thick plate	143
Table A-15: Results summary for the 45° bias rolling direction 3/8 in. thick plate	145
Table A-16: Results summary for the parallel rolling direction 1/2 in. thick A36 plate	153
Table A-17: Results summary for the transverse rolling direction 1/2 in. thick A36 plate	154
Table A-18: Results for parallel rolling direction 3/8 in. thick Gr. 50 plate	161
Table A-19: Results for transverse rolling direction 3/8 in. thick Gr. 50 plate	162

1 INTRODUCTION AND BACKGROUND

On August 1, 2007 the I-35W bridge that crosses the Mississippi River in Minneapolis, MN suddenly collapsed. An investigation of the collapse by the National Transportation Safety Bureau (NTSB) [NTSB, 2008] concluded that the bridge collapse was due to an under designed gusset plate. Between its lifespan of 1967 and 2007, the bridge members had been evaluated several times, however the gusset plates were not evaluated and the fact that they were under-designed was not identified prior to collapse. In response, the FHWA mandated rating of gusset plate connections. These new mandated ratings were presented in *Load Rating Guidance and Examples for Bolted and Riveted Gusset Plates in Truss Bridges* [FHWA Guide, FHWA 2009]. As a result, all transportation agencies now must evaluate their inventory of gusset plate connections which is costly and time consuming.

Currently, most transportation agencies are conducting analyses using the specified material properties and design drawings as the analysis inputs. Yet, to produce the intended outcome of ensuring bridge safety without excessive and costly conservatism, it is best to have connection ratings performed with inputs that reflect the as-built conditions. These include both geometrical and material properties. While geometrical dimensions can easily be obtained in the field, there is no recognized non-destructive testing method currently available to field verify the yield stress of plate materials [AASHTO Manual for Bridge Evaluation, 2008]. Typically, the minimum yield stress of steel is obtained using tensile coupons tested in accordance with the ASTM E8 standard, but to collect the samples is destructive and most bridge owners are reluctant to remove samples from in-service gusset plates.

To overcome this limitation, a practical device that can induce inelastic bending of connection plates in the field was investigated. The device applies an out of plane load to the edge of a plate

and creates a deflection that can be measured using displacement sensors. The approach relies on small deflection thin plate theory, in which shear deformations are neglected when the plate span width or length is at least 10 times the plate thickness and the deflections are smaller than one tenth of the thickness [Szilard, 1974]. These conditions are reasonable for gusset plate connection materials.

Development of a non-destructive method for establishing yield stress will serve three major roles for connection evaluations. It will 1) allow bridge owners to establish the material properties for bridges that do not have documentation of the materials used in construction, 2) allow rating engineers to determine if the yield stress is above the minimum required for the plate to achieve a specific rating, or 3) enable rating engineers to use the actual yield stress of the plate to extract the most capacity from the connection. The research outcome allows bridge owners to effectively and non-destructively collect as-built yield stress of gusset plate connections thereby enabling connection capacity to be established with greater certainty.

2 LITERATURE REVIEW

With new regulations for evaluation of gusset plates in truss bridges, the need to determine the in-situ material properties, specifically the yield stress, has arisen. For engineers to perform accurate and economic analyses of these gusset plates, obtaining the actual yield stress as opposed to the nominal yield stress that is found in design drawings is highly beneficial. A few methods of determining these properties non-destructively do exist, however the universally accepted method is performing tensile tests in conformance with the American Society for Testing and Materials (ASTM) *Standard Test Methods for Tension Testing of Metallic Materials* [E8/E8M-11].

Topics covered in the following literature review include previous research in regard to hardness testing and its relationship with material properties, studies relating static and dynamic yield stress, and material testing on older bridge steels.

2.1 Relationship Between Hardness and Yield Stress

While several researches have attempted to correlate the tensile strength of metals with hardness, there are few correlations between hardness and yield stress.

Hardness is a measure of the material resistance to localized plastic deformation. Researchers who have explored these connections include Tabor [1951], Speich and Warlimont [1968], Cahoon *et al.* [1971], Cahoon [1972], Datsko *et al.* [2001], Kowalkowski and Varma [2007], and Pavlina and Van Tyne [2008].

Tabor [1951] stated that for work-hardened metals, yield stress can be taken as:

$$F_y = \frac{H_D}{3} \quad [2.1]$$

where H_D is the Vickers hardness of the material and F_y is in kg/mm^2 . This derivation applies to the yield stress of severely cold worked materials and assumes the strain hardening coefficient equals zero. Cahoon *et al.* [1971] and Cahoon [1972] proposed formulations for 0.2% offset yield stress for steels in either the cold rolled or tempered condition which includes the strain hardening coefficient:

$$F_y (0.2\% \text{ offset}) = \frac{H_D}{3} (0.1)^n \quad [2.2]$$

where H_D is as defined above and n is the strain hardening coefficient. The strain hardening coefficient can be approximately calculated using $m-2$ where m is the Meyer's hardness coefficient. F_y is expressed in kg/mm^2 . For these experiments, H_D was determined using a Vickers Hardness Tester and at least ten indentations were made in each specimen. Samples were machined from 65S aluminum alloy strips and 1040 steel strips. The aluminum specimens were machined as-is while the 1040 steel strips were either cold rolled or austenized, water quenched, and then tempered to obtain a wide spread of hardness values. Tensile tests were performed at an initial strain rate of $3.3 \times 10^{-4} \text{ sec}^{-1}$.

Pavlina and Van Tyne [2008] tested over 150 nonaustenitic steels with yield stress ranging from 44 ksi (300MPa) to 247 ksi (1700 MPa). The results showed the correlation of hardness to yield stress as:

$$F_y = -90.7 + 2.876H_D \quad [2.3]$$

where F_y is defined in MPa and H_D in kg/mm^2 .

When analyzing this yield stress equation, large standard deviations were found. It was therefore assumed that strain hardening factors into the correlation. It is recognized that the maximum amount of hardening a steel can achieve during plastic deformation can be measured using the strain-hardening potential of the material. One way to measure this strain-hardening potential is through the tensile strength to yield stress ratio of F_u/F_y . Samples were sorted by the ratio F_u/F_y which showed the predicted strength to be greater for steels with low ratios compared to those with a high ratio. Due to the effects of strain-hardening, it was determined that yield stress has a linear correlation with hardness for higher yield stress steels ranging from 47 ksi (325 MPa) to 247 ksi (1700 MPa).

2.2 Non-Destructive Testing Method of Metallic Materials

Drawing from past research relating hardness to other material properties, Advanced Technology Corporation developed a device that works based on an Automated Ball Indentation (ABI) principle. A unique aspect of the device is that the ABI method automatically measures all impression parameters. The testing method behind this device is described by Murty *et al.* [1998]. The necessary equipment to perform these tests include the stress-strain microprobe (SSM) system, high resolution penetration transducer and load cell, a personal computer, a 16-bit data acquisition system, and copyrighted ABI software. Unlike standard tensile tests where uniaxial deformation is confined to within the specimens gauge length, with constant loading of the ball indenter into the plate, material is simultaneously experiencing both elastic and plastic deformation throughout the test. Therefore the load vs. depth shown in Figure 2-1 does not resemble the typical linear elastic curve followed by non-linear work hardening of the material.

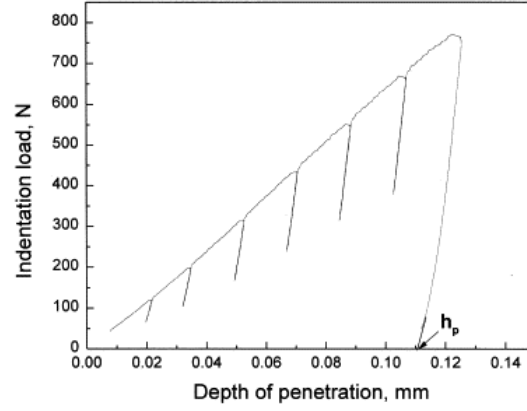


Figure 2-1: Typical indentation load versus depth of penetration curve Murty *et al.* [1998]

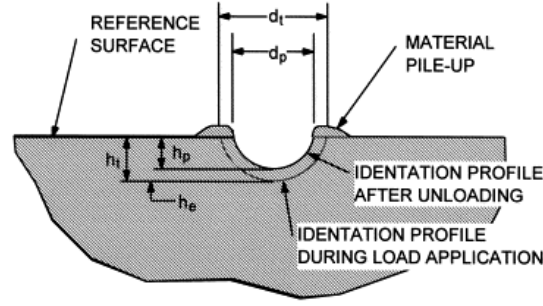


Figure 2-2: Schematic representation of the indentation profile in an ABI test, Murty *et al.* [1998]

For each ABI loading cycle, the total penetration depth (h_t) is measured while the load is applied, and the depth is converted to a total indentation diameter (d_t) using the equation:

$$d_t = 2\sqrt{Dh_t - h_t^2} \quad [2.4]$$

where D is the diameter of the indenter. Various loading cycles are applied up to a maximum value of $\frac{d_t}{D} = 1.0$. These results are then fit by a linear regression analysis to the relationship:

$$\frac{P}{d_t^2} = A\left(\frac{d_t}{D}\right)^{m-2} \quad [2.5]$$

where P is the applied indentation load, m is the Meyer's coefficient and A is a material parameter obtained from the regression. Once the material parameter A is known, the yield stress (σ_y) is calculated by:

$$\sigma_y = \beta_m A \quad [2.6]$$

β_m is a constant for a given class of materials that was determined through standard tensile tests. For all carbon steels, whether hot or cold rolled, β_m is taken to be 0.2285. A drawback of this test is that it cannot be performed in the field.

2.3 Determining Both Dynamic and Static Yield Stress

As shown in Figure 2-3 the yield stress of steel can be expressed in many different ways. These definitions are found in the Structural Stability Research Council *Standard Methods and Definitions for Tests for Static Yield Stress* and definitions for static yield stress and are based off of the ASTM *Standard Terminology Relating to Methods of Mechanical Testing* [E6].

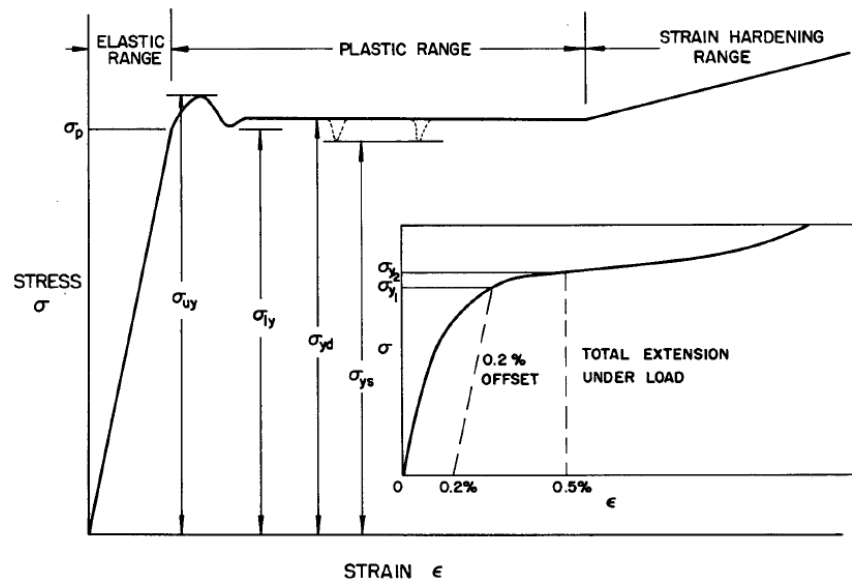


Figure 2-3: Visual of yield stress terms from Rao, Lohrman, and Tall [1966] Fig. 1

- 1) Upper Yield Stress (σ_{uy}): the first stress in a material, less than the maximum attainable stress, at which an increase in strain occurs without an increase in stress.
- 2) Lower Yield Stress (σ_{ly}): the lowest level of yield stress immediately following the upper yield point while maintaining a constant strain rate.
- 3) Dynamic Yield Stress (σ_{yd}): the average stress during actual yielding in the plastic range. It remains fairly constant, provided that the strain rate remains constant.
- 4) Static Yield Stress (σ_{ys}): the average stress during actual yielding in the plastic range at a zero strain rate.

While there are various definitions of yield stress, the most commonly used is the dynamic yield stress. The method for calculating this value is found in ASTM E8 and consists of either finding the intersection between the stress/strain curve at a 0.2% offset of the elastic portion of the

stress/strain curve or retrieving the stress value at 0.5% strain. Typically, the 0.2% offset method is used.

As stated in Nadai [1950], yield stress of steel is directly affected by the rate of straining and often, the higher the rate, the higher the yield stress. ASTM Methods and Definitions for Mechanical Testing of Steel Products [370-12a] limits the maximum testing speed to 1/16 in/min/in of reduced section. However, using lower speeds than others can result in inconsistencies of up to 20 percent [Beedle and Tall, 1960]. Therefore, unless the yield stress is specified along with a strain rate or crosshead speed, the term has a rather limited significance.

Due to these high discrepancies, a less common, but reliable measure of yield stress is the static stress value. Because it corresponds to a strain rate of zero, it is independent of testing procedures and machine behavior [Structural Stability Research Council, 1987].

Rao, Lohrmann, and Tall [1966], describe the method for determining the static yield stress of steel specimens. First, various steel plate type specimens were tested using three material types: 1) A36 cut from hot rolled square hollow tube shapes 2) A441 from webs and flanges of W shapes and 3) quenched and tempered (Q-T) from plates and bar stock. Coupon thicknesses ranged from $\frac{1}{4}$ in. to $\frac{3}{4}$ in. and were tested at a rate of 1/16 in/min/in of gauge length until it was shown that the specimen had reached the plastic range. At this point, the test was paused and it was seen that the load indicator reached a stable position in about three (3) minutes. A unique aspect of lower strength steels, such as A36, is that they have a defined yield plateau as seen in Figure 2-4.

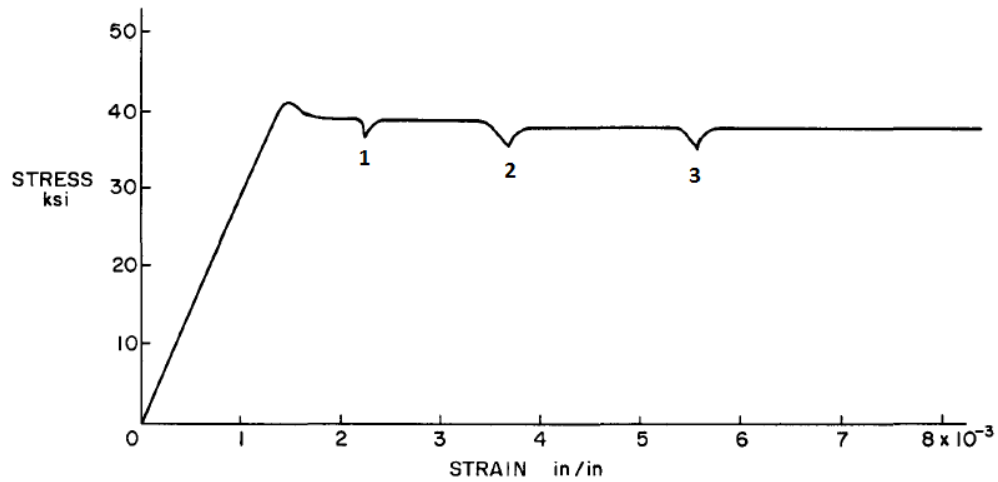


Figure 2-4: Typical stress vs. strain diagram from Rao, Lohrmann and Tall [1966] Fig 8

The static yield stress was found by drawing a line to connect points 1, 2 and 3. If the line is horizontal, that value is considered the yield stress, but if it is at an incline the static yield stress is taken as the stress at 0.5% strain.

After testing was completed, a dynamic yield stress ratio $\frac{\sigma_{yd}}{\sigma_{ys}}$ and strain rate were related by the equation:

$$\frac{\sigma_{yd}}{\sigma_{ys}} = 1 + k\varepsilon^n \quad [2.4]$$

where σ_{yd} and σ_{ys} are as defined above, ε is the strain rate, and k and n are constants. Figure 2-5 shows that the dynamic yield stress ratio is less affected by strain rate for higher strength steels.

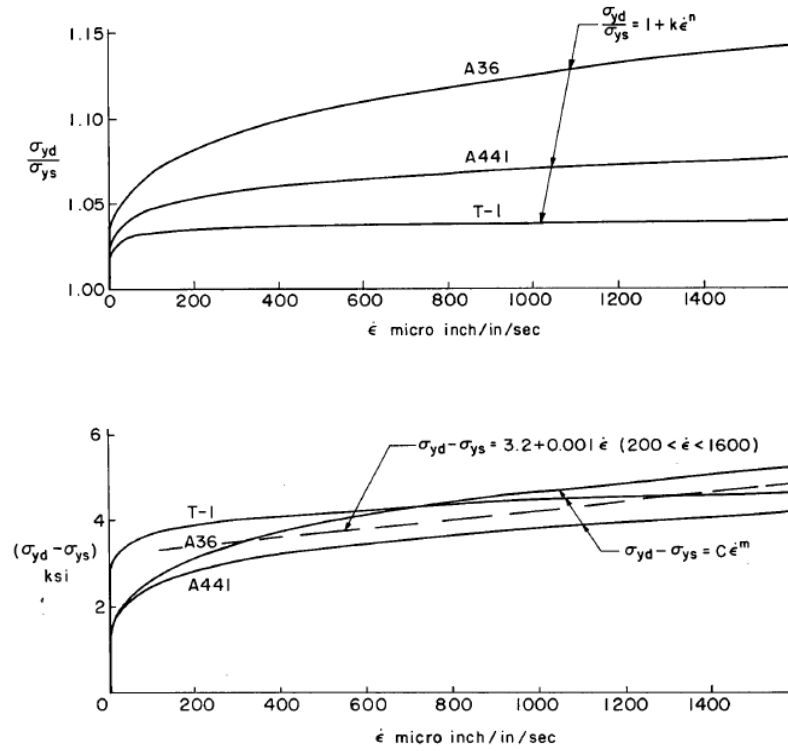


Figure 2-5: Estimated curves relating dynamic yield stress level, static yield stress level, and strain rate from Rao, Lohrmann, and Tall [1966]

Differences between the dynamic yield stress, static yield stress, and strain rate are related by:

$$\sigma_{yd} - \sigma_{ys} = c\epsilon^m \quad [2.5]$$

with c and m as constants. Due to the small variance in dynamic and static yield stress, an average curve that related $(\sigma_{yd} - \sigma_{ys})$ and ϵ was found to be:

$$\sigma_{yd} - \sigma_{ys} = 3.2 + 0.001\epsilon \quad [2.6]$$

where $\sigma_{yd} - \sigma_{ys}$ is in ksi and ϵ is in $\mu\text{in/in/sec}$.

2.4 Bridge Steels

In an unpublished report received from the FHWA (Moore *et al.*, 2001), experiments were performed on eight in-service bridges to determine various material properties of bridges constructed before 1930. The first specification from ASTM was issued in 1901, and while it gave requirements for steel properties such as yield stress, tensile strength, phosphorus content and sulfur content, all other characteristics were left up to the steel manufacturer. This resulted in a wide range of steel compositions until more specifications were added to the ASTM standard in 1930 which specified chemical composition. The following table shows various elements found in steels as well as the influence they have on the steel properties [Moore, 2001].

Table 2-1: Alloying elements and their influence on steel properties

Alloying Element	Influence on Steel	Typical Content, %
Carbon (C)	Hardness, strength, wear	0 - 3
Chromium (Cr)	Corrosion resistance, hardenability	0 - 0.8
Lead (Pb)	Machinability	Variable
Manganese (Mg)	Strength, hardenability, increased response to heat treatment	0 - 1.4
Aluminum (Al)	Deoxidation	Variable
Nickel (Ni)	Toughness, strength	0 - 0.5
Silicon (Si)	Deoxidation, hardenability	0 - 0.9
Molybdenum (Mo)	High temperature strength, hardenability	0 - 0.3
Sulfur (S)	Machinability	0 - 0.07
Copper (Cu)	Corrosion strength, strength	0 - 0.4
Phosphorus (P)	Hardness, wear	0 - 0.4

While higher amounts of each element will have a greater effect on the steel properties, it is rare for any alloying element to exceed 2%. Low carbon structural steels (0.05% - 0.35% carbon) are not as hard or strong as other steels but are easier to machine during manufacturing. Quenched and tempered steels have better impact resistance at lower temperatures, and better corrosion

resistance. They are more expensive and are usually used where greater strength and corrosion resistance is required.

Throughout the years, various structural steel designations for bridges were allowed by the American Association of State Highway Transportation Officials (AASHTO). A significant reason behind the discontinued use of some steels was due to a lack of weldability. From the early 1900's to 1967, ASTM A7 steel was the most widely used structural steel. ASTM A373 steel was introduced in 1954 but discontinued in 1965 after the introduction of ASTM A36 which had superior weldability and strength characteristics. High-strength, low-alloy steels are used where weight reduction is required and increased durability and corrosion resistance are desired. A few designations of structural steels for bridges can be seen below in Table 2-2.

Table 2-2: Various structural steel designations

ASTM (AASHTO) Designation	Grade or Thickness ^a	F _y ksi (MPa)	F _u ksi (MPa)	Steel Type
A 36 (M94)	-	36 (248)	58-80 (400-551)-	Structural Steel
A 242 (M161)	less than 3/4 in.	50 (345)	70 (483)	High-Strength, Low- Alloy Structural Steel
	3/4 to 1.5 in.	46 (317)	67 (462)	
A 514 (M244)	3/4 in to 2.5 in	100 (689)	110-130 (759-896)	High-Yield-Strength, Quenched and Tempered Alloy Steel Plate
A 572 (M223)	Grade 42	42 (290)	60 (414)	Structural-Quality, High-Strength, Low- Alloy Columbium- Vanadium Steel
	Grade 50	50 345()	65 (448)	
	Grade 55	55 (379)	70 (483)	
	Grade 60	60 (414)	75 (517)	
	Grade 65	65 (448)	80 (552)	
A 588 (M222)	4 in. and under	50 (345)	70 (483)	High –Strength Low- Alloy Structural Steel
A 852	4 in. and under	70 (483)	90-110 (621-758)	Quenched and Tempered Low-Alloy Structural Steel Plate

Three of the main mechanical properties of bridge steels are tensile strength, brittleness (inverse of ductility), and hardness. Generally, as one property increases the others also increase, and vice versa. Through the experimental program of the FHWA, tests were performed to determine the chemical composition, tensile properties, and hardness of older steels which were removed from eight in-service bridges. The following tables show the bridge names and locations as well as their year of construction and applicable ASTM specification for that time.

Bridge	Member Geometry	State
Harvard	Eye-shaped	Massachusetts
Brandywine Creek	I-shaped	Delaware
7 th Street	Eye-shaped	Pennsylvania
Old Dog River	I-shaped	Alabama
6 th Street	Plate	West Virginia
Walnut	Plate	Pennsylvania
#005-2714-0.02	Circular shaped	West Virginia
Severn River	Plate	Maryland

Bridge	Year of Construction	Applicable ASTM Specification
Harvard	1891	N/A
Brandywine Creek	1924	A7 (1914)
7 th Street	1928 -1929	A7 (1914)
Old Dog River	1929	A7 (1914)
6 th Street	1935	A7 (1934)
Walnut	1935	A7 (1934)
#005-2714-0.02	1915	A7 (1915)
Severn River	1922-24	A7 (1922-25)

N/A - ASTM specification did not exist at the time of the bridge construction

Figure 2-6: Description of bridges and materials tested by FHWA

Material samples were removed and subsequently tested at the FHWA's Turner-Fairbank Highway Research Center. A few key conclusions that resulted from the research were:

1. Moderate carbon content steel members exhibit, on average, a higher tensile strength, ductility, elongation, and higher reduction of area at failure than higher carbon content.
2. Higher nickel and copper content steel members exhibit a higher fracture toughness and yield stress for moderate carbon content steels.
3. Steel members from older bridges display greater chemical compositional variability.
4. Older bridges will likely have material with greater compositional variability, but this may not necessary reflect the quality of the steel.

While some of the hardness conversions may be able to indicate yield stress, one concern with the data is that most results are for metallic materials with relatively high strength or processing methods that are different than those of bridge steels considered in this research. Bridge steels, specifically those used on older bridges and the main focus of this study, are on the lower end of yield stress and are typically hot rolled. There are therefore, no currently available, non-destructive methods of determining yield stress for in-situ bridge gusset plates.

3 METHODOLOGY

A prototype non-destructive testing device was developed that applies an out of plane load to the free edge of a steel plate. During application of the load, the load magnitude, time, and plate deflection data are collected. A proof of concept test program was developed to correlate device measurements with the material properties of steel plates determined using traditional tensile coupons. Two different plate types were considered; the first set was free standing and free of externally applied stresses and the second set contained externally applied axial stress. Analytical modeling of the steel plates was performed using the finite element (FE) analysis program ABAQUS/Standard Version 6.12-2. (Hibbitt, Karlsson & Sorensen, 2002, Abaqus User Manual).

3.1 Prototype Design

A non-destructive testing device to assess the yield stress of gusset plates must apply a relatively large magnitude load to induce plate bending at the free edge of a steel plate. It must be self-reacting and must also be field portable and therefore lightweight. To achieve these criteria, a prototype device was developed as illustrated in Figures 3-1 and 3-2. The center to center span length between the supports was chosen to be 10 in. (254 mm). While the minimum size thickness for a gusset plate is 3/8 in. (9.5 mm) [AASHTO 1944] this span allows for plate thickness of up to 1 in. (25.4 mm) to be tested and still be operating within the definition of thin plate theory. All other dimensions were designed around a mini bottle jack that is 2.5 in. (63.5 mm) tall and has a loading capacity of 10 kips (59 MN). While other, larger sized jacks were available, the smaller jack was the only one available that had a pressure gauge attachment. In order for the prototype to be as lightweight as possible, it was constructed out of titanium due to its high strength to weight ratio. Grade 5 titanium (ASTM B265) with a yield stress of 130 ksi

(896 MPa) was used. Structural analysis of the device components verified it would remain elastic at the maximum loading applied by the jack.

The prototype was fabricated at Oregon State University and multiple load and support conditions were analyzed and tested before the final design was complete. In the following design figures, all dimensions are in inches.

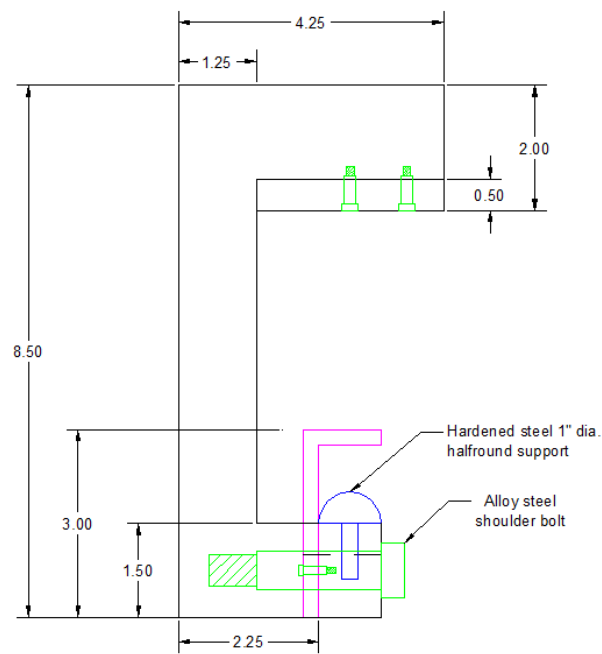


Figure 3-1: Side view of prototype design



Figure 3-3: Load cell with 10 kip capacity (<http://www.futek.com/product.aspx?t=load&m=lca305>)

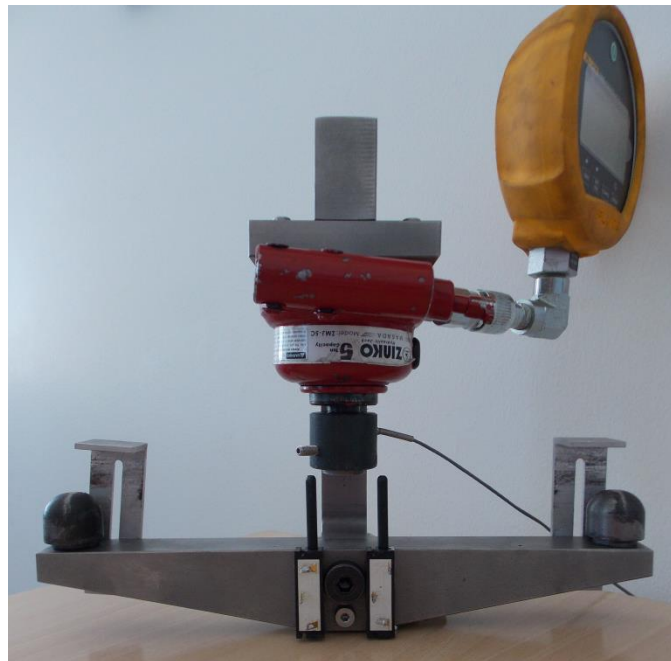


Figure 3-4: Final prototype design

The final weight of the prototype was just under 10 lbs (44.5 N) and the total cost was approximately \$4,000 as detailed in Table 3-1.

Table 3-1: Cost break down for prototype device

Titanium	\$ 502.50
Alloy Steel Bolt	\$ 2.50
Hydraulic Jack	\$ 436.50
Pressure Gauge	\$ 925.00
Gauge Calibration	\$ 208.00
Load Cell	\$ 575.00
Data Acquisition System	#
Labor Costs	\$ 1,344.00
TOTAL	\$3,993.50

#Depends on user preference.

3.2 Finite Element Modeling

Plate sizes for the experimental program were initially determined based on FE analyses that used idealized material properties prior to collection of the actual tensile material properties from the specimens. Once results were obtained, as explained in Section 3.3, the specific material properties were used as the inputs into all FE models to verify that the original assumptions were valid. In the following sections, the actual material properties are shown in the results. Free standing rectangular plates were modeled first, followed by similar plates that were tested with axial loading applied to the plate to simulate service level stress conditions.

3.2.1 Boundary Conditions

The model was made using shell elements because they account for thin plate theory. To appropriately determine what load and support conditions should be used in the FE model, two methods were considered to establish the contact surface areas at the loading and reaction points. The first used pressure paper which was placed between the plate and contact points. Image

processing of the color spread induced by the pressure applied was used to calculate the contact areas of 0.18 in. (4.6 mm) at the load point and 0.12 in. (3.0 mm) at the supports. These results were taken at the estimated yield load of 2.5 kip (11.1 kN) for the test plates. The second approach used one (1) inch wide plate specimens tested in the device to idealize the behavior of a simply supported beam. Hand calculations were used to verify the FE model for the load and deflection results as well as the yielding load of the prototype.

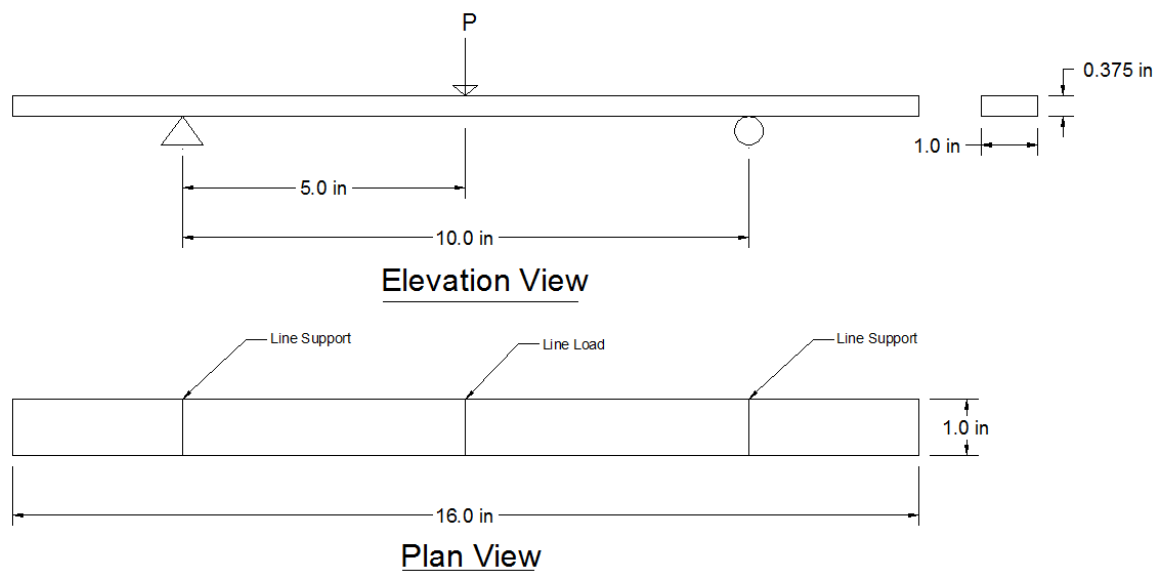


Figure 3-5: AutoCAD drawings for idealized beam model

The yielding load and plastic load capacity were calculated using the expressions:

$$\sigma_y = \frac{M_y}{S} \quad [3-1]$$

$$\sigma_y = \frac{M_p}{Z} \quad [3-2]$$

where σ_y is the yield stress of the material, S is the elastic section modulus $\frac{1}{6}bh^2$, and Z is the plastic section modulus $\frac{1}{4}bh^2$. Based on the geometry shown in Figure 3-5, $M = \frac{5P}{2}$ which results in a load at first yield $P_Y = 0.4$ kip (1.8 kN) and load at plastic moment $P_p = 0.6$ kip (2.7 kip). As shown in Figure 3-6 these hand calculations match the experimental results closely, however, the calculations are still slightly lower because the prototype does not induce the ideal line load conditions assumed in the calculations and is therefore stiffer than the idealized model. Subsequently, various contact areas were modeled until the two curves were within approximately 3% of each other. To achieve this correlation, the model was loaded with a true point load in the center and two, 0.02 in. (0.51 mm) diameter round patches as the supports.

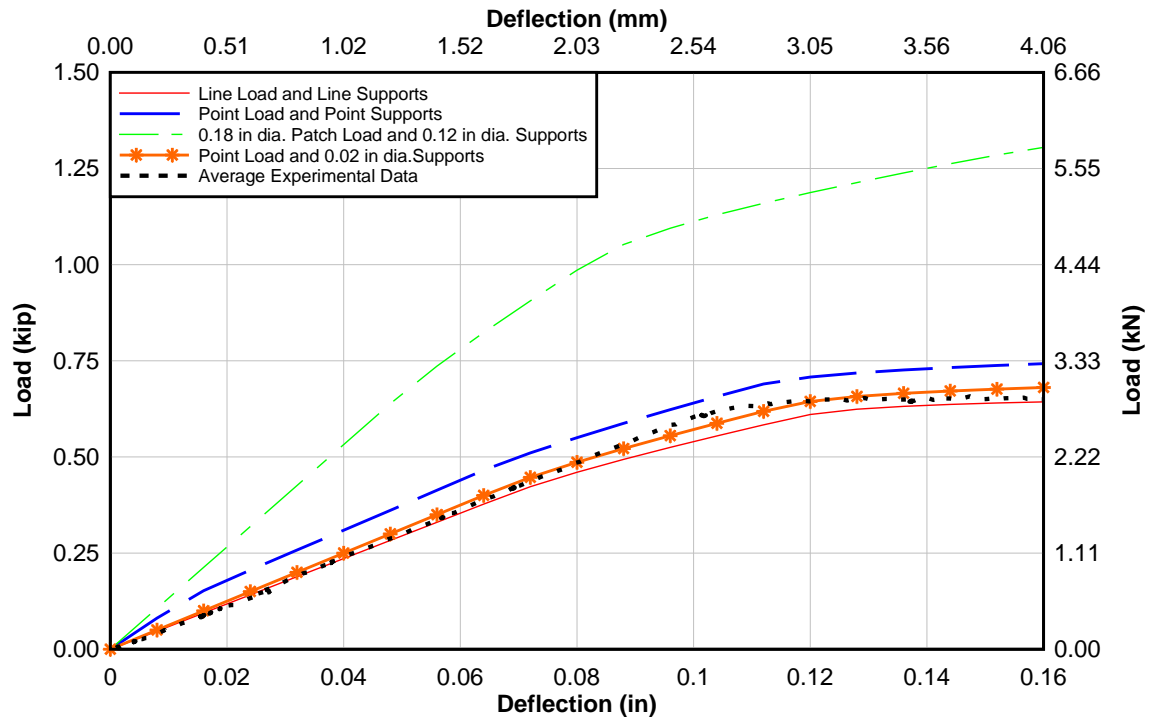


Figure 3-6: Load and deflection curves for various support conditions

Table 3-2: Percent difference between FEA model support conditions and beam experimental results

Deflection (in)	Experimental Load (kip)	FEA Load (kip)	% Difference
0.00	0.000	0.000	0.00
0.02	0.112	0.125	10.26
0.04	0.238	0.250	4.64
0.06	0.362	0.375	3.56
0.08	0.486	0.486	0.11
0.10	0.604	0.571	5.68
0.12	0.633	0.611	3.55
0.14	0.652	0.668	2.48
0.16	0.649	0.681	4.59
		Average	3.87

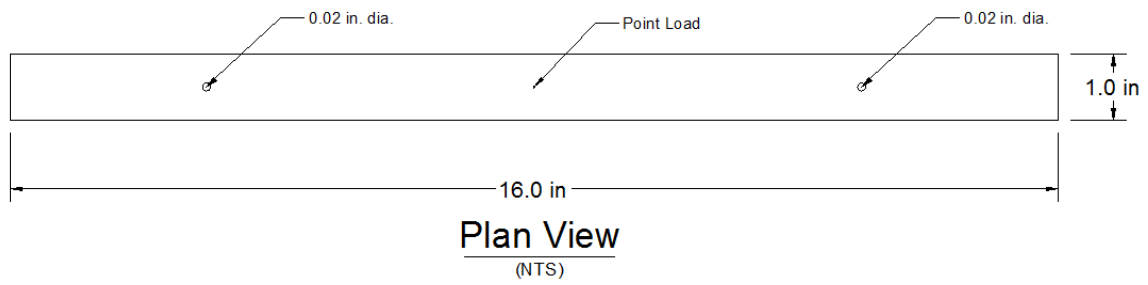


Figure 3-7: Final design of FE support conditions

3.2.2 Free Plates

Using these support conditions, a generic rectangular shaped plate was designed. In order to analyze various plate sizes, the scripting program Python was modified to generate widths between 2 in. (51 mm) and 24 in. (914 mm) and lengths of 14 in. (356 mm) and 24 in. (914 mm). The plate was modeled as a 3D, homogenous shell element with a thickness of 3/8 in. (9.5 mm).

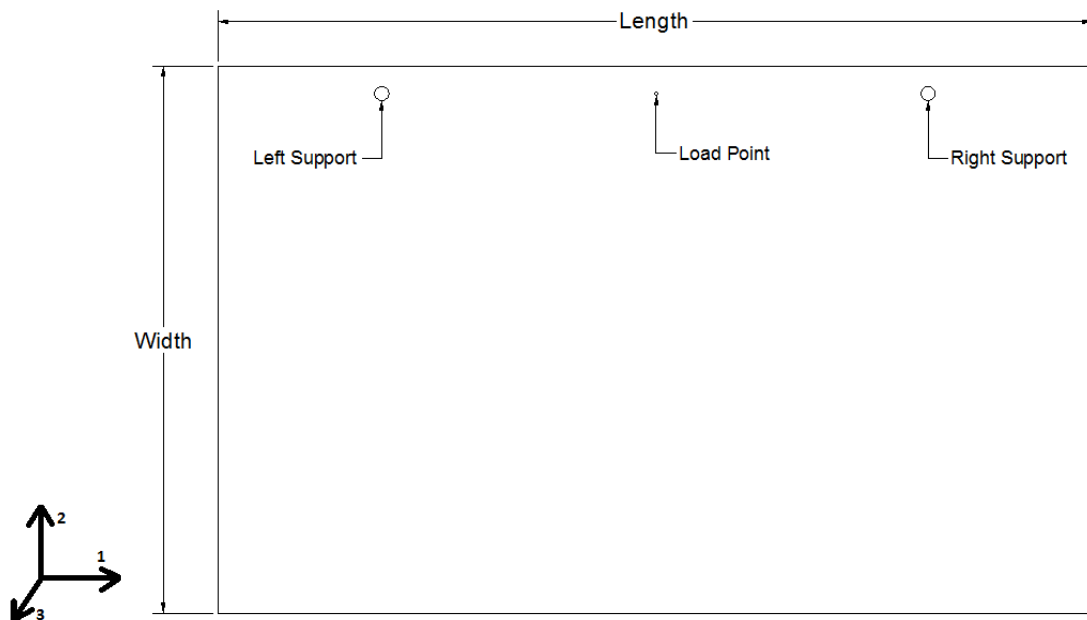


Figure 3-8: Free plate generic model

A displacement controlled analysis was run to simulate the loading applied to the plate by the prototype. The load point was set to a displacement of 0.05 in. (1.27 mm) in the out-of-plane direction ($U_3 = -0.05$ in.) with all other parameters unrestrained ($U_1 = U_2 = U_{R1} = U_{R2} = U_{R3} = \text{Free}$). In order to allow for bending within the plate, the left support rotations were unrestrained about the plane axes ($U_1 = U_2 = \text{Free}$) while all other movements were fixed ($U_1 = U_2 = U_3 = U_{R3} = 0$). To insure no induced stresses were applied to the plate from restrained boundary conditions, movement on the right support was permitted in all directions except for the opposing load direction ($U_3 = 0$). A static step increment of the displacement condition was set to 0.05 which means the specified displacement value was applied at five percent increments. This assists with stability of the analysis and allows for easier data collection of the results. Select results for various plate sizes are shown below in Figure 3-9 .

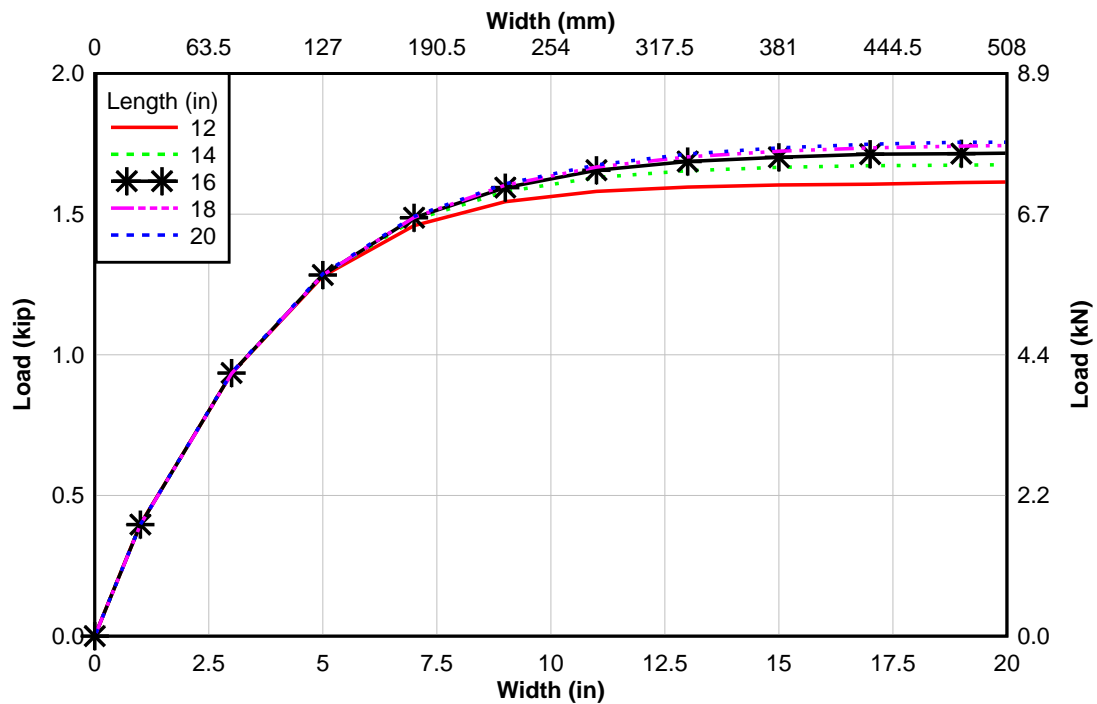


Figure 3-9: Varying length and width effect on prototype device load for 3/8 in. thick A36 material set to 0.05 in. displacement

Plate sizes used in the experimental analysis were chosen based on the smallest width and length that no longer had more than a 3% effect on the terminal load vs. deflection. As the curves move closer together, they resemble an infinitely large plate. Figure 3-9 indicates that starting at a width of 10 in. (254 mm), the results begin to level out. It also shows that the length of the plate does not have as significant an effect on the results.

An additional model was analyzed to clearly demonstrate the differences between plate and beam behaviors by setting the load point to an arbitrary value of -4.25 kip (-18.9 kN). The beam was modeled as a 2 in. (51 mm) wide strip. Figure 3-10, shows that as the width exceeds 2 in. (51 mm) the response changes dramatically because the model more closely resembles plate behavior as opposed to beam behavior. With the increased plate area, the prototype device load is resisted by more material and therefore requires additional load to be applied to obtain the same deflections. In Figure 3-11, the 2 in. (51 mm) and 4 in. (102 mm) wide plates were removed to enable distinction between the differences in the larger sized plates. A plate width of 10 in. (254 mm) and 20 in. (508 mm) were chosen for testing. The variation between the results for the two plate sizes is approximately 3%. The variance between each varying length curve is less than 1%, therefore, a length value of 16 in. (406 mm) was chosen.

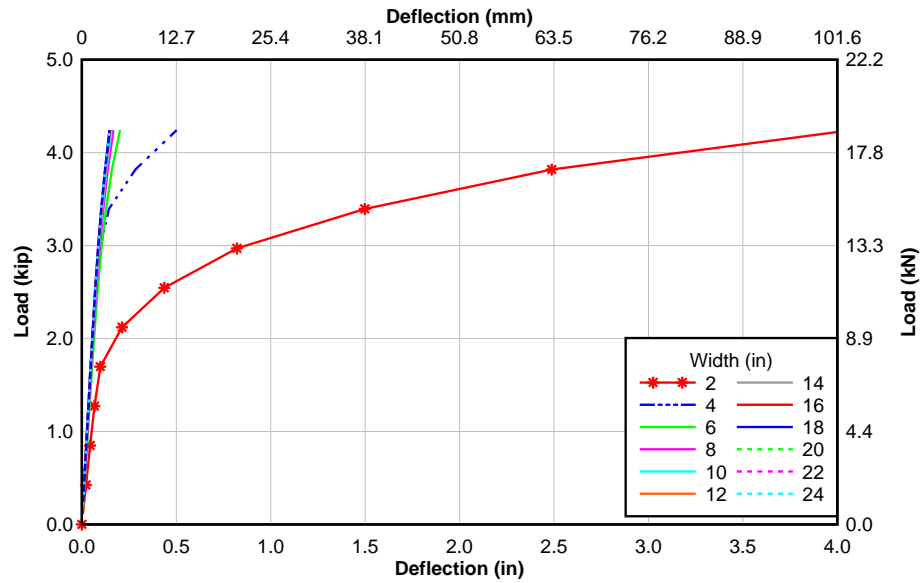


Figure 3-10: Load vs. deflection for plate widths 2 in. to 24 in. for 3/8 in. thick A36 material

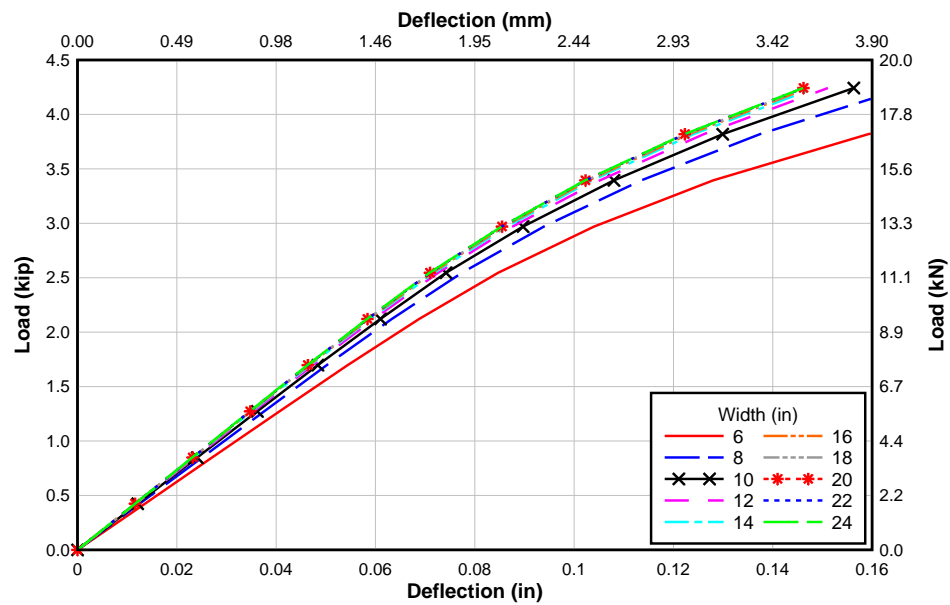


Figure 3-11: Load vs. deflection for plate widths 6 in. to 24 in. and length 16 in. for 3/8 in. thick A36 material

3.2.2.1 Mesh Refinement

A mesh refinement analysis was performed on the 20 in. (508 mm) plate to determine what elements sizes should be used for the FE models. To mesh the model, the structured quad element S4R was used. This is a 4-node, reduced integration, doubly curved shell with hourglass control and finite membrane strains (Hibbitt, Karlsson & Sorensen, 2002). Partitions were made in the part module to help simplify the mesh layout, predominately around the small circles for the supports and load point as shown in Figure 3-12.

As stated in the Abaqus Theory Manual, all elements use numerical integration. Specific details on numerical integration are:

For full integration the number of integration points is sufficient to integrate the virtual work expression exactly, at least for linear material behavior. All triangular and tetrahedral elements in Abaqus use full integration. Reduced integration can be used for quadrilateral and hexahedral elements; in this procedure the number of integration points is sufficient to integrate exactly the contributions of the strain field that are one order less than the order of interpolation. The (incomplete) higher-order contributions to the strain field present in these elements will not be integrated.

One should reference the Abaqus Theory Manual (6.11) section 3.1.1 found online for a more detailed description of the element types.

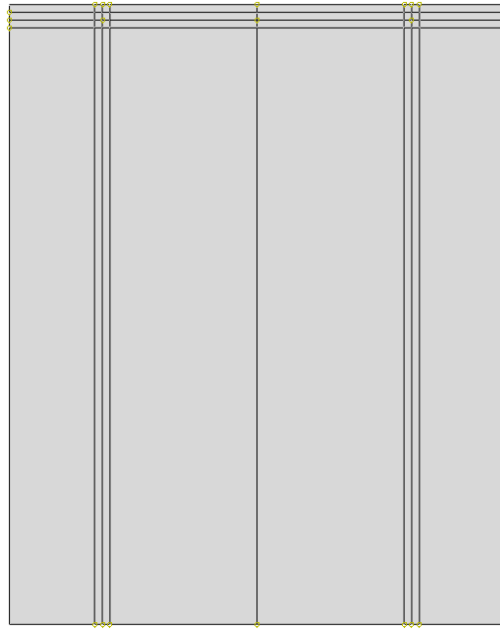


Figure 3-12: Partition layout for free plate model

Figure 3-13 plots the load vs. deflection results of this analysis and Table 3-3 and Table 3-4 calculate the percent differences between various mesh sizes. The seed size is roughly the dimension, in inches, of a square mesh. For example: a seed size of 0.5 equates to a 0.5 in. x 0.5 in. square. Determining the most accurate and efficient mesh size was found by comparing the results of percent differences between the calculated load for given deflections and model runtime. As seed size decreases the results become more refined, but there is a point where decreasing the size is no longer essential because it has only a slight effect on the results. Consequently, the runtime increases significantly for smaller seed sizes because of the effort required to analyze the additional nodes. A 0.2 seed size varies by less than 1% with seed sizes 0.1 and 0.05 without causing a high increase in model run time. Therefore, 0.2 was used for all subsequent FE models.

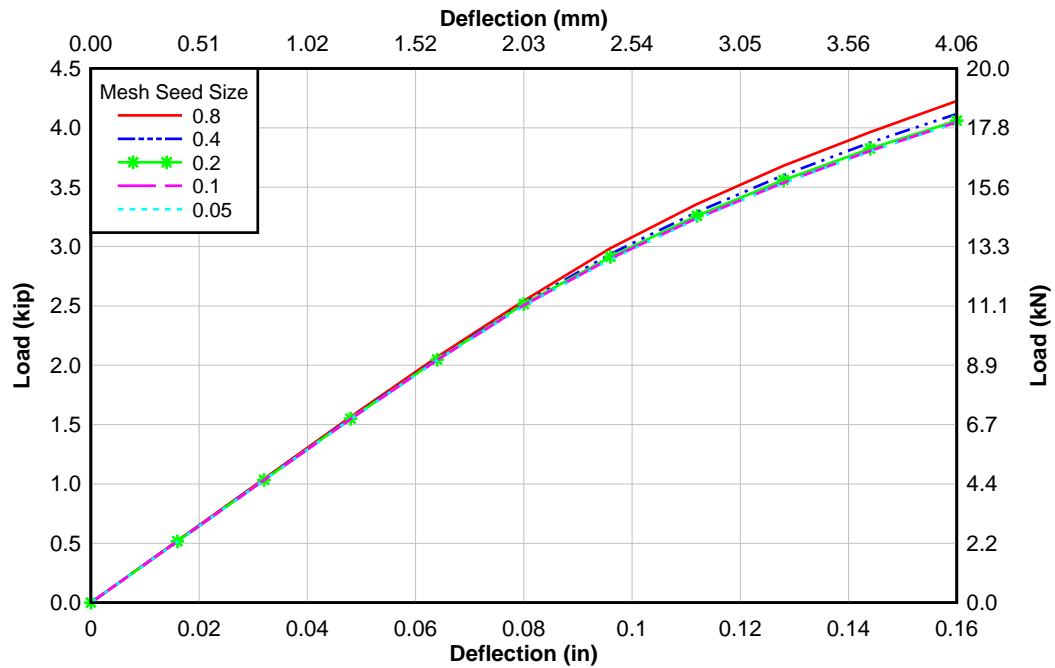


Figure 3-13: Mesh refinement plot for a 20 in. wide and 16 in. long 3/8 in. thick A36 plate

Table 3-3: Applied load for a given deflection with various mesh sizes

Step	Deflection (in)	Applied Prototype Load (kip)				
		Mesh Seed Size 0.8	Mesh Seed Size 0.4	Mesh Seed Size 0.2	Mesh Seed Size 0.1	Mesh Seed Size 0.05
0.00	0.00	0.00	0.00	0.00	0.00	0.00
0.10	0.02	0.52	0.52	0.52	0.52	0.52
0.20	0.03	1.04	1.04	1.03	1.03	1.03
0.30	0.05	1.57	1.55	1.55	1.55	1.54
0.40	0.06	2.07	2.05	2.05	2.04	2.04
0.50	0.08	2.54	2.52	2.52	2.51	2.50
0.60	0.10	2.99	2.94	2.91	2.90	2.89
0.70	0.11	3.36	3.29	3.26	3.24	3.23
0.80	0.13	3.68	3.60	3.56	3.54	3.53
0.90	0.14	3.96	3.88	3.82	3.81	3.80
1.00	0.16	4.23	4.12	4.06	4.05	4.04
Run Time (min)		3.00	4.00	4.00	8.00	34.00

Table 3-4: Percent difference between results of various mesh sizes

Step	% Difference of Seed 0.8 and Seed 0.2	% Difference of Seed 0.2 and Seed 0.1	% Difference of Seed 0.2 and Seed 0.05
0.00	0.00	0.00	0.00
0.10	0.94	0.16	0.30
0.20	0.94	0.16	0.30
0.30	0.98	0.19	0.33
0.40	1.11	0.17	0.30
0.50	1.09	0.40	0.66
0.60	2.44	0.49	0.78
0.70	2.95	0.60	0.82
0.80	3.29	0.60	0.72
0.90	3.52	0.49	0.62
1.00	3.93	0.32	0.47

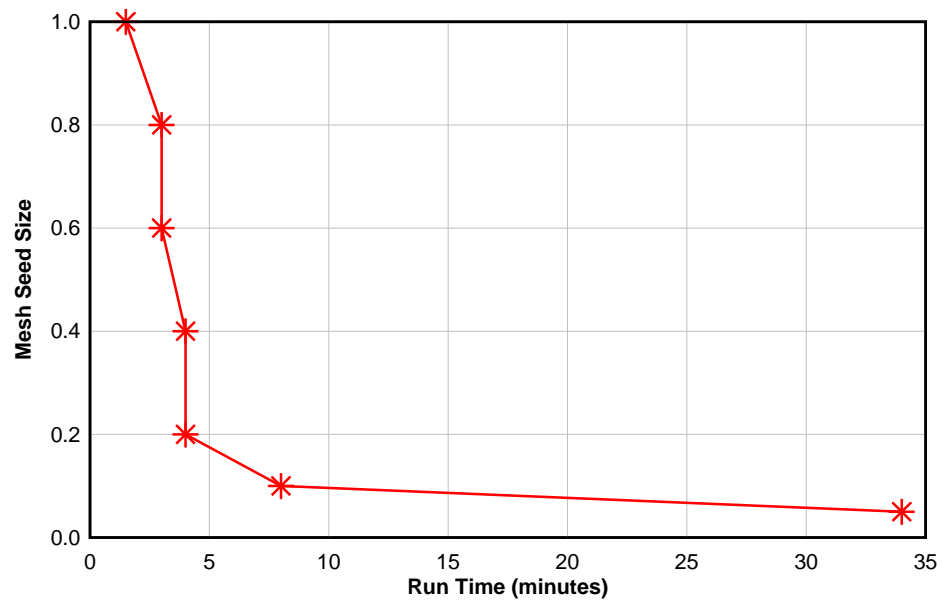


Figure 3-14: Mesh seed size vs. run time

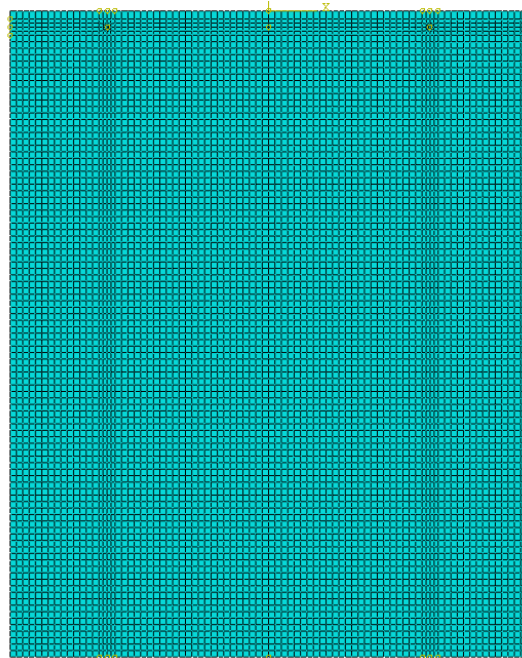


Figure 3-15: Final mesh layout for free plate model

3.2.2.2 *Stiffness Adjustment*

While the FE analyses were developed to reasonably model the prototype loading conditions on the plate surface, they do not incorporate the deformations taking place in the prototype device. In practice, the plate deformations are measured not in absolute terms, but relative to the prototype device, which also experiences elastic deformations. Therefore, modifications had to be made to the load and deflection curve for the FE results to emulate the experimentally measured responses that use displacement sensors mounted to the device. Even though any point can be referenced as zero, there are deformations attributed to multiple sources including the support beam bending, shear deformations of the bolted connections, and elongation and bending of the handle. While these could be estimated analytically, the stiffness of the prototype was determined empirically.

The average of all free plate, 3/8 in. (9.5 mm) A36 test data was compared with the analytically predicted FE results, and the elastic stiffness was computed as.

$$k = \frac{F}{\Delta} \quad [5-1]$$

where Δ is the deflection (units of in.) of the prototype device , F is the applied prototype device load (kip). To correct the measured plate deflections for the elastic deformations of the device, additional deflections were added to the FE deflections to provide an adjusted curve until the values matched within an average of 1% as shown below in Figure 3-16. Using this method, a stiffness value of $k = 200$ kip/in was determined.

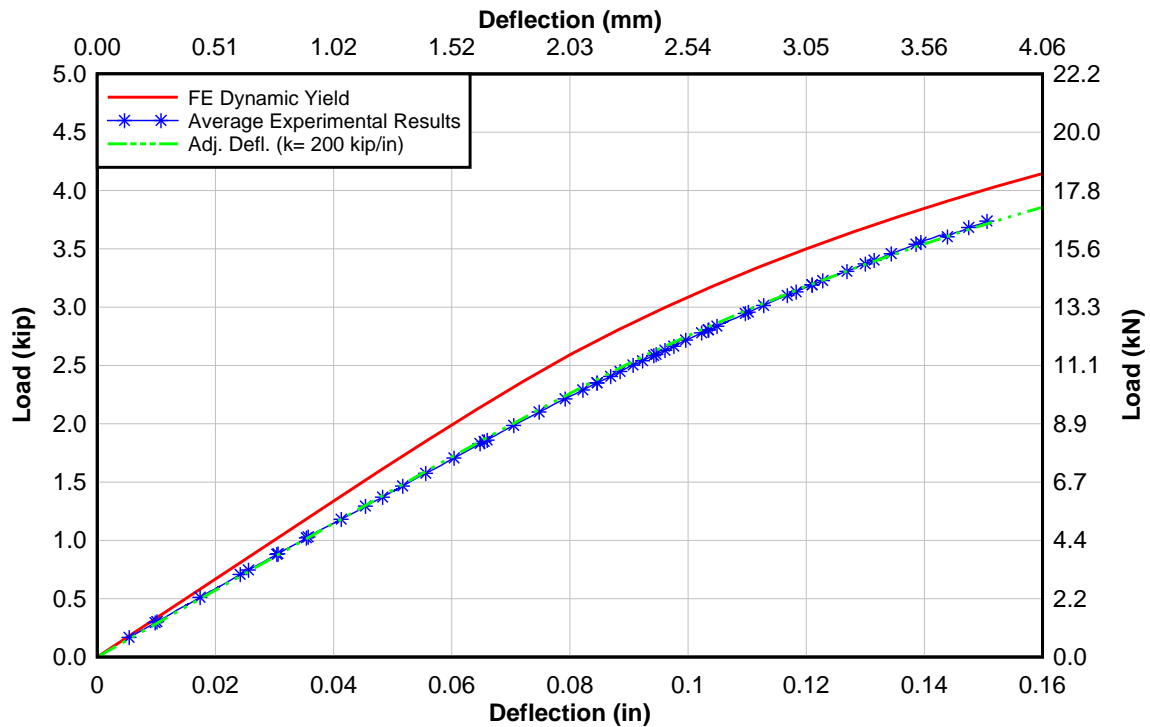


Figure 3-16: Adjusted FE load vs. deflection curve based on various stiffness values for 3/8 in. A36 plate

Table 3-5: Percent difference between initial FE results and results adjusted with $k=200$ kip/in.

Deflection (in)	Load Experimental (kip)	Load Adjusted Curve (kip)	% Difference
0.00	0.00	0.00	0.00
0.02	0.59	0.57	3.39
0.04	1.15	1.15	0.00
0.06	1.7	1.71	0.59
0.08	2.23	2.26	1.35
0.1	2.72	2.75	1.10
0.12	3.17	3.18	0.32
0.14	3.57	3.54	0.84
AVERAGE			1.08

The differences between the experimental and shifted finite element results was within 1% for the 3/8 in. thick A36 plate, however the results for the other two plate models came within 4%. This variance was accepted because there was significantly less test data for these plates.

3.2.3 *Axially Loaded Plates*

A second set of plates were designed to analyze what effects induced stresses in a gusset plate may have on the prototype results. Even with no live loads on a bridge, gusset plates are still subject to service loads coming in to the connections. These plates were designed to fit in the universal testing machine (UTM) in order to apply tension to the ends of the plate and simulate stresses.

The model was run for plate thicknesses of 3/8 in. (9.5 mm) and 1/2 in. (12.7 mm) and steel strengths A36 and A572, Gr. 50. Plate dimensions were chosen based on which width to length ratio provided uniform stresses within the portion of the plate the prototype would be applied.

Shown in Figure 3-17 is a generic sketch of the modeled plate. Measurements taken of the UTM resulted in a maximum possible length of 40 in. (1016 mm), a width of 22 in. (559 mm), and a grip width of 3 in. (76.2 mm). Dimension w_1 varied based on the chosen length and width dimensions allowing for a 45° tapered angle to the grips.

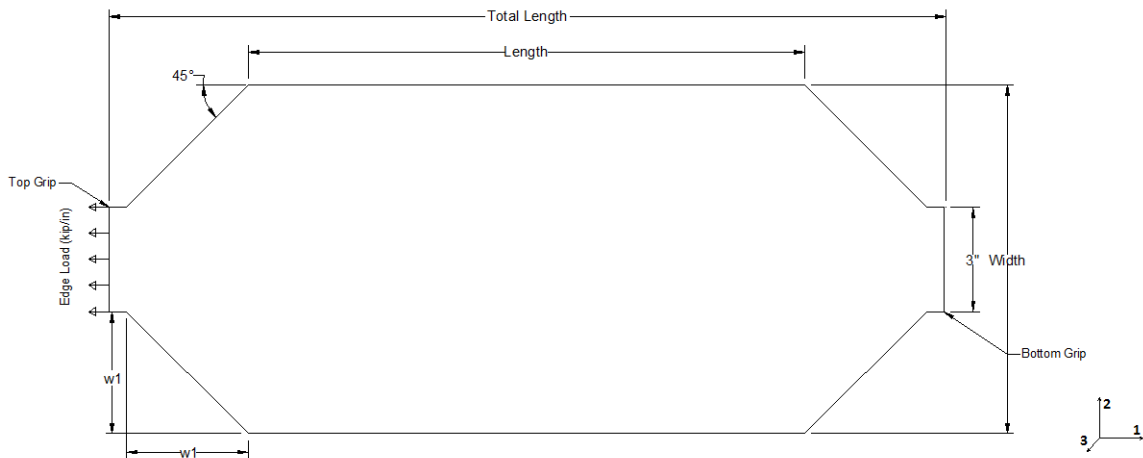


Figure 3-17: Generic design of plate modeled in ABAQUS for uniform stress calculations

The bottom grip was modeled with a boundary condition fixing translational movement in the U_1 and U_2 direction ($U_1 = U_2 = 0$) at one corner while the opposite corner was only restrained in the U_1 direction ($U_1 = 0$). Loading at the top grip was applied in a static, general step with an edge load in units of kip/in. Due to the 110 kip (490 kN) capacity of the UTM, the maximum edge load that could be applied was 36 kip/in. (6304 kN/m).

Due to the varied geometry and sharper corners, a free S3R mesh was used as opposed to the structured S4R for the free rectangular plates. S3R mesh consists of 3-node triangular shell with finite membrane strains (Hibbitt, Karlsson & Sorensen, 2002). Using a similar mesh and analysis

check as detailed before, a seed size of 0.1 was used for this model. The partition model and final mesh layout can be seen in Figure 3-18 and Figure 3-19 below.

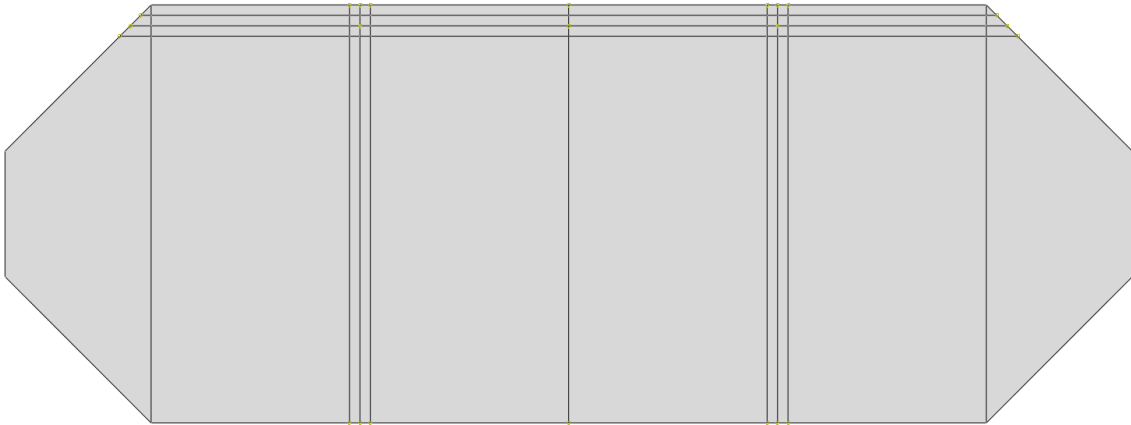


Figure 3-18: Partition layout for the axially stressed induced plate model

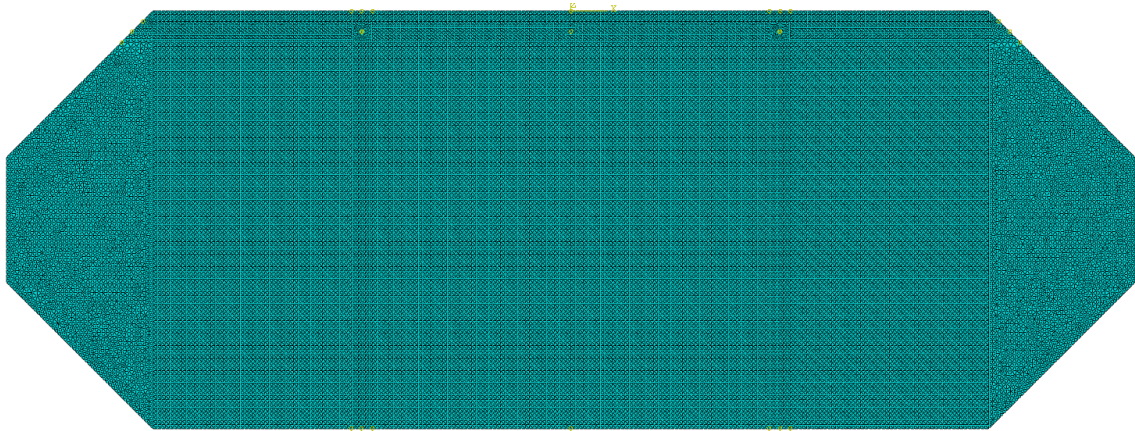


Figure 3-19: Final mesh layout for the axially stressed induced plate model

Based on the stress distribution results, a plate with a length of 20 in. (508 mm) and width of 10 in. (254 mm) was chosen. Figure 3-20 shows the pattern of uniform stress within the center of the plate and the final dimensions can be seen in Figure 3-21.

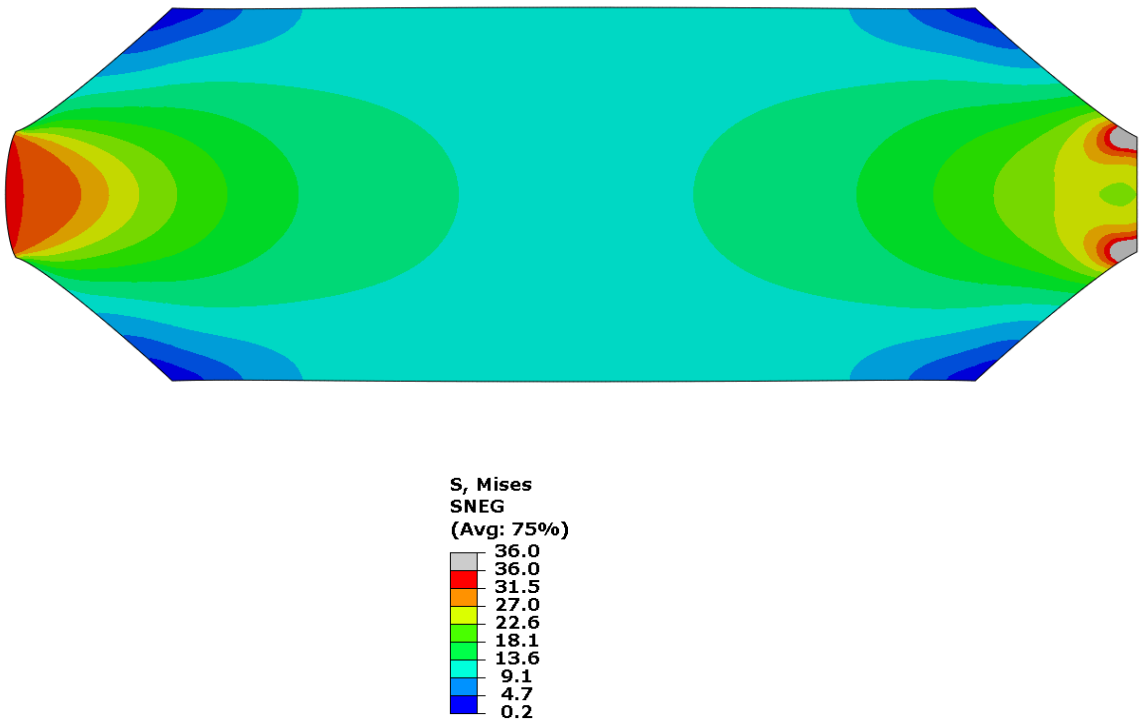


Figure 3-20: Axially loaded plate stress distribution from FE Model for 3/8 in. thick A36 plate loaded to 38 kips, stresses in ksi

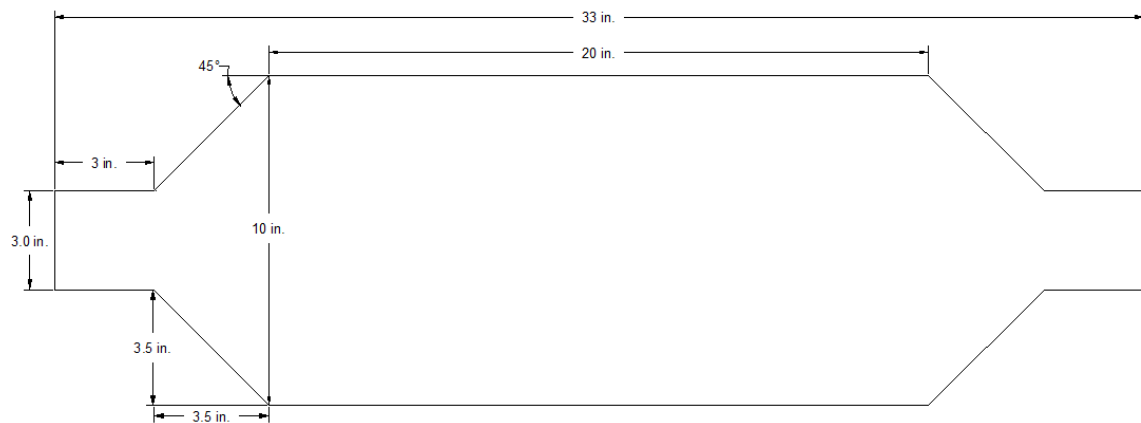


Figure 3-21: Final dimensions for axially loaded plates tested in UTM

3.2.4 *Plate Cut Layout*

Once the plate dimensions were finalized, multiple samples were ordered for both sets of plate models. The free plates were cut from three directions which were parallel, transverse, and at a 45° bias to the rolling direction. For each direction, three (3) 10 in. x 16 in. (254 mm x 406 mm) and 20 in. x 16 in. (508 mm x 406 mm), totaling eighteen (18) plates, were cut from 3/8 in. (9.5 mm) thick A36 material. The different cutting directions were chosen to determine whether or not they varied the material properties or the prototype measurements. Additionally, eighteen (18) 11 in. x 4.5 in. (279 mm x 114.3 mm) samples were cut in conjunction with each plate and used to machine coupon samples for tensile testing.

Each plate was labeled with the format shown in Figure 3-22 by the steel fabricator to easily differentiate which direction and sample was being tested. Only the first three symbols are necessary for plate labels while the fourth is used to differentiate the coupon samples. Coupon sample details and testing are described in 3.3.

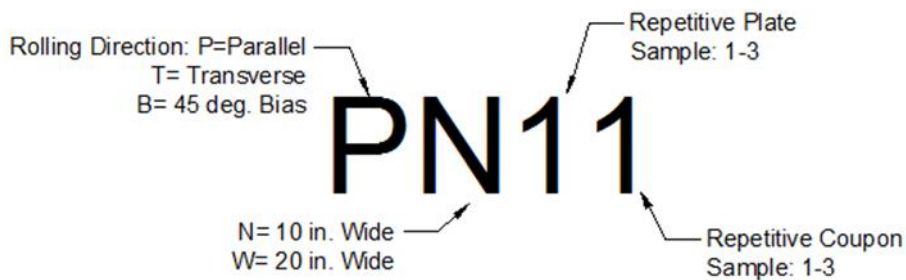


Figure 3-22: Labeling scheme for plates and coupons

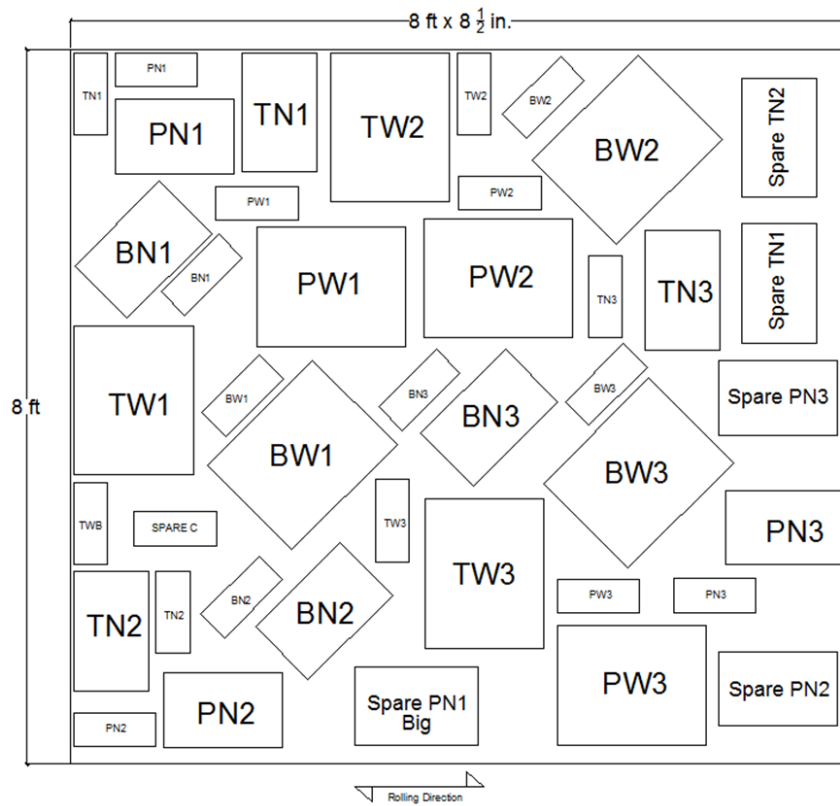


Figure 3-23: Plate and coupon sample cut layout for free plates

For the axially loaded plates 3/8 in. (9.5 mm) thick Gr. 50 and 1/2 in. (12.7 mm) thick A36 material were chosen based on the results shown in Figure 3-40. Unlike the free plate samples, these plates and coupon specimens were cut from only the parallel and transverse directions. The labeling is similar to that of the free plates which can be seen in Figure 3-24 and the cut layout is shown in Figure 3-25.

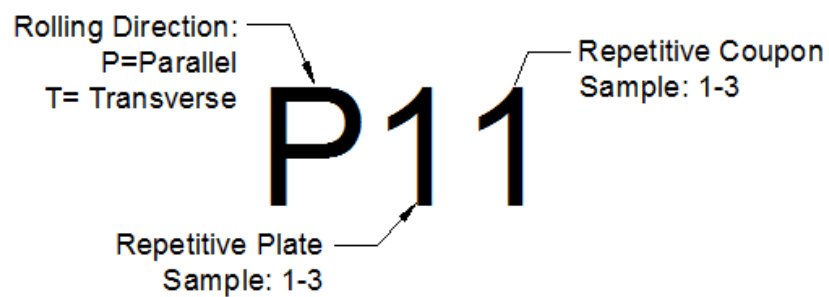


Figure 3-24: Axially loaded plate and coupon labeling scheme

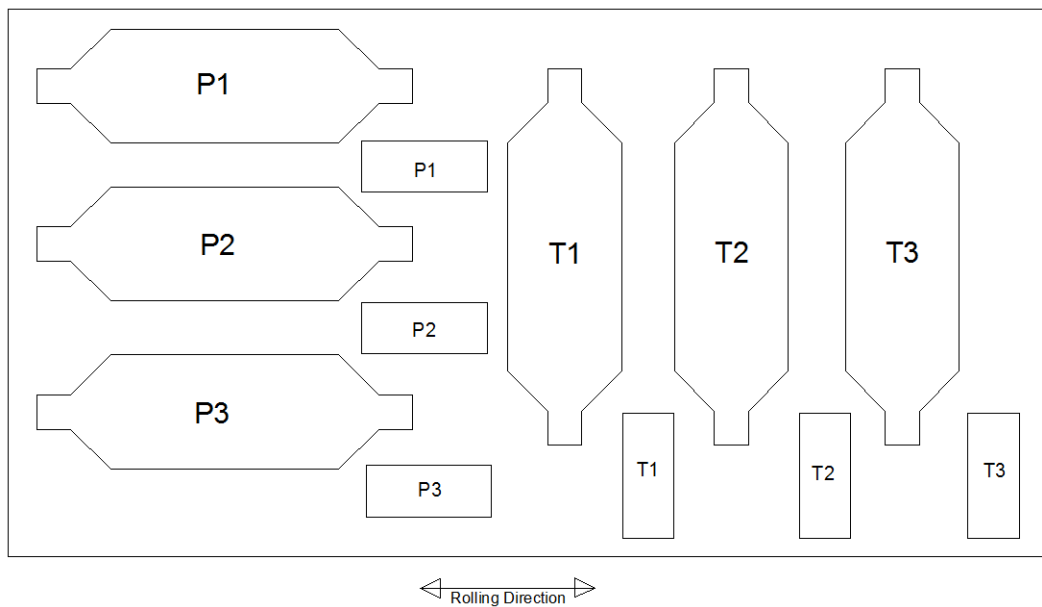


Figure 3-25: Axially loaded plate and coupon sample cut layout

3.3 Material Testing

Once the plate sizes were determined, tensile tests were performed on the coupon samples in accordance with ASTM E8-11 specification. The resulting stress and strain data were used in the FE models to verify the previous model results based off of idealized material properties. Testing also determined whether or not the rolling direction orientation influenced the material properties.

3.3.1 Sample Preparation

As shown in the layout of Figure 3-23:, eighteen plates were cut to provide material for the coupon samples. From each of the eighteen plates, three samples were machined (See Figure 3-26), resulting in fifty-four (54) samples along with three (3) sample specimens which were not used in the data reduction.

ASTM E8 verifies the sheet type specimen is valid for material thickness up to 0.75 in. (19 mm). All pretest measurements and markings were also performed in accordance with this specification.

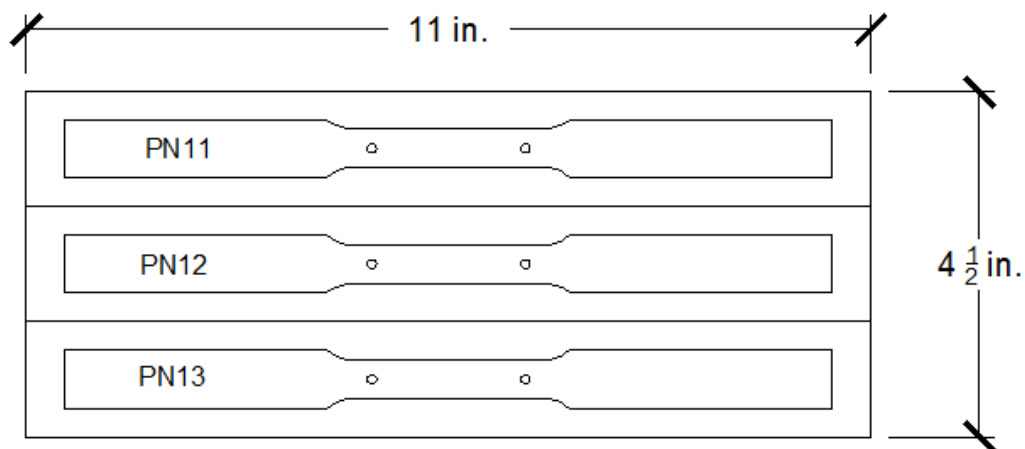


Figure 3-26: Coupon labeling scheme

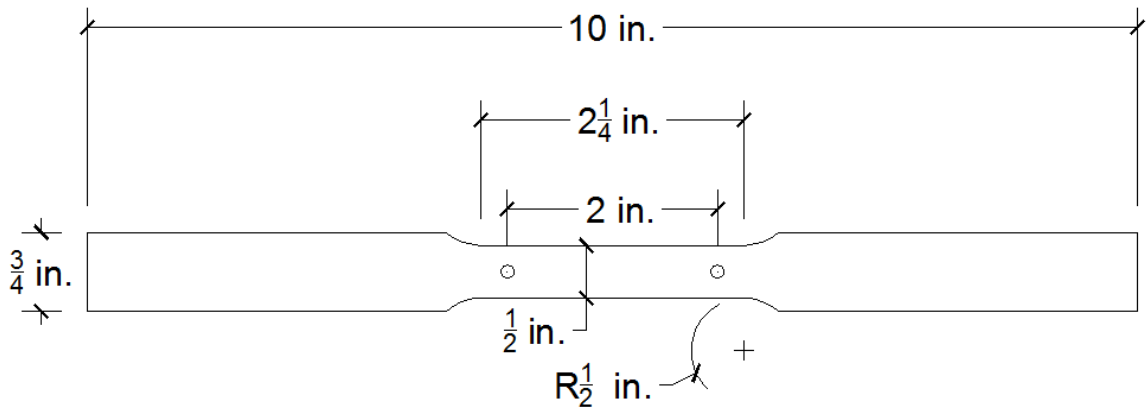


Figure 3-27: Sheet type sample dimensions

The area for each coupon sample was calculated using the average of three measurements for both the width and thickness and 2 inch gauge marks were punched onto the narrowed portion of the sample to retrieve final elongation. These areas and elongation results can be found in Appendix A. For specimens PN1, PN2, and PW1, punch marks were not made in the samples and therefore, the final elongation was estimated using the ratio of the elongation between the 2.0 in. gauge length and narrowed length from the three sample coupons.

3.3.2 *Sample Testing*

Tension tests were performed on a two-post 110 kip capacity universal testing machine with top-loading hydraulic wedge grips. The machine controls allowed for the displacement rate command to be changed in the middle of the test. Strain measurements were found using a clip-on extensometer that had a fixed 2.0 in. (51 mm) gauge length and a 0.5 in. (12 mm) stroke range. The data collection software permitted viewing of the stress vs. strain diagram through the duration of the test, allowing for first yield to be visually observed.

Specimens were initially loaded at a rate of 0.0003 in/sec. Once the specimen reached the upper yield point, the static yield was attained by pausing the displacement rate for a period of 60 seconds, in three locations along the yield plateau. When strain hardening began, the loading rate was gradually increased to 0.005 in/sec until the specimen fractured. It took approximately 20 minutes to test a specimen.

3.3.3 *Data Reduction*

Sample PW13 provides a representation of the typical results collected from all the samples and is therefore used in the following explanation of the data reduction process and its results are plotted below.

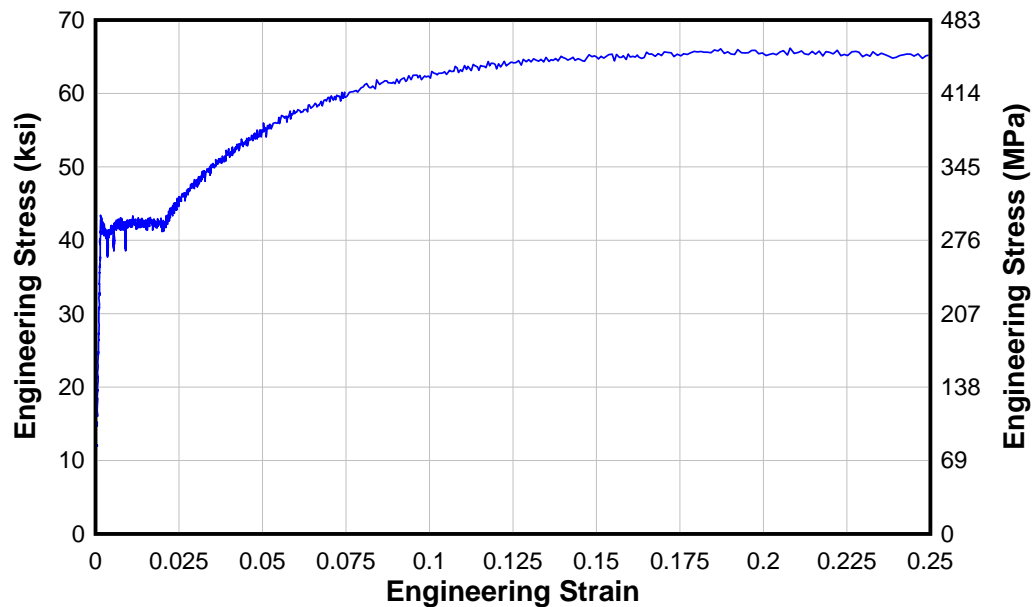


Figure 3-28: Typical engineering stress vs. engineering strain data before post-processing

To remove the random noise in the collected data, the stress values were filtered using a low-pass option with a commercially available plotting program. Figure 3-29 shows the filtered and unfiltered data taken from a stress vs. time graph, resulting in the new stress vs. strain plot seen in Figure 3-30.

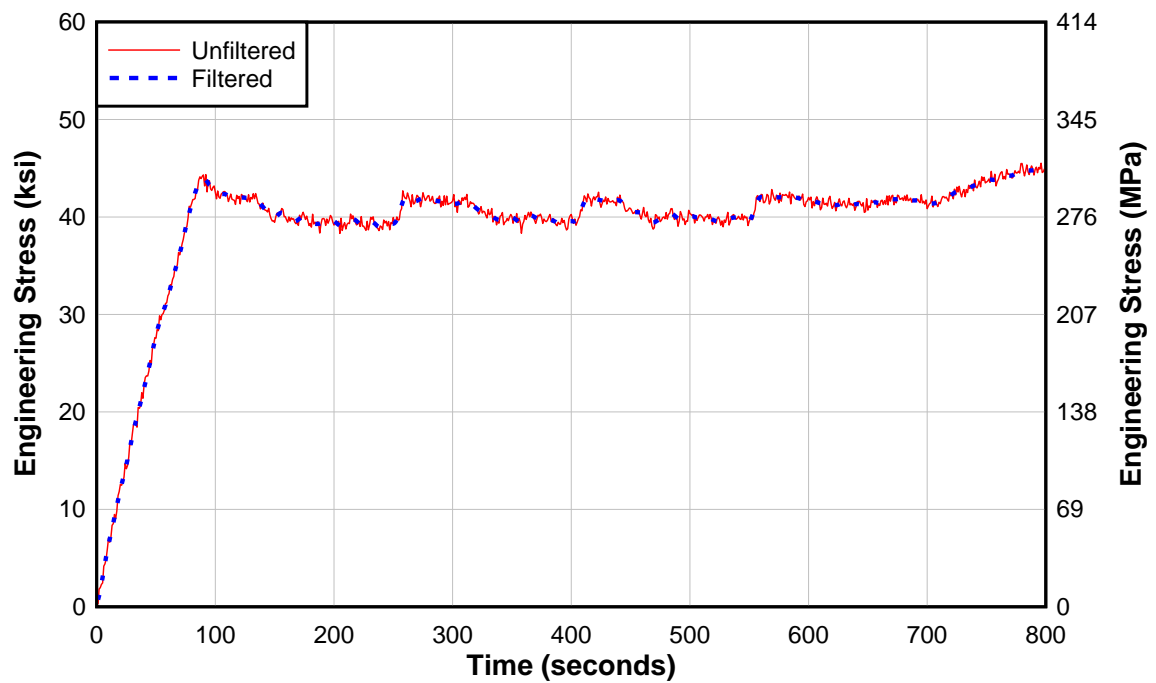


Figure 3-29: Engineering stress vs. time filtering process using low pass option

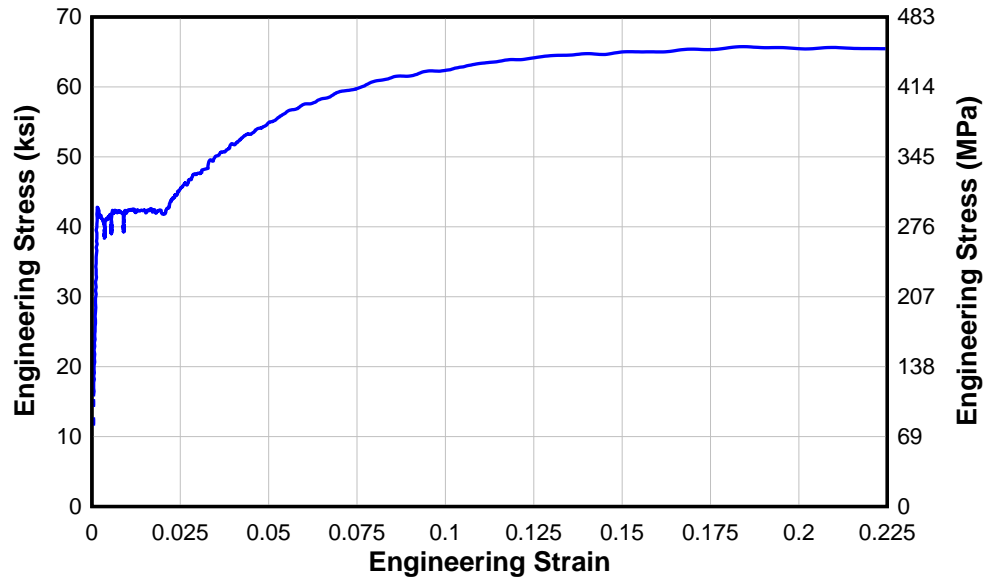


Figure 3-30: Engineering stress vs. engineering strain filtered data

Both the static yield stress and dynamic yield stress were calculated by finding the minimum and maximum values, respectively, as well as the mean value and standard deviation of each plateau on the filtered data plot. The static yield was the plateau from the maximum stress right before the test was held to the minimum value before the testing rate was then increased. The dynamic yield was the period of constant displacement rate in between the held test intervals seen in Figure 3-31. Calculated results can be seen in Appendix A. Averaging the values for each plateau gave the mean yield stress for each coupon sample. For the three different cut directions, all samples were averaged to determine the yield stress in each direction.

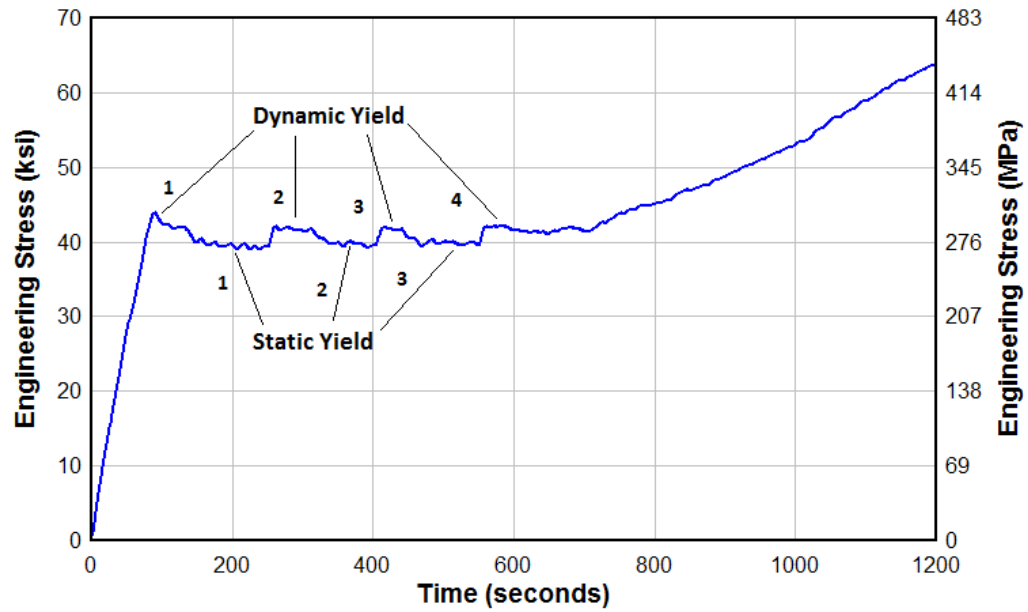


Figure 3-31: Filtered stress vs. time dynamic and static yield plateaus

The dynamic yield stress was also found using the 0.2% offset method specified in ASTM E8 and is displayed in Figure 3-32. Because the ASTM standard focuses on the dynamic yield stress and not the static yield stress, if the intersection of the offset and the curve fell within one of the static yield locations, the nearest dynamic yield value was chosen. For the final material results, only the 0.2% offset dynamic yield values were used.

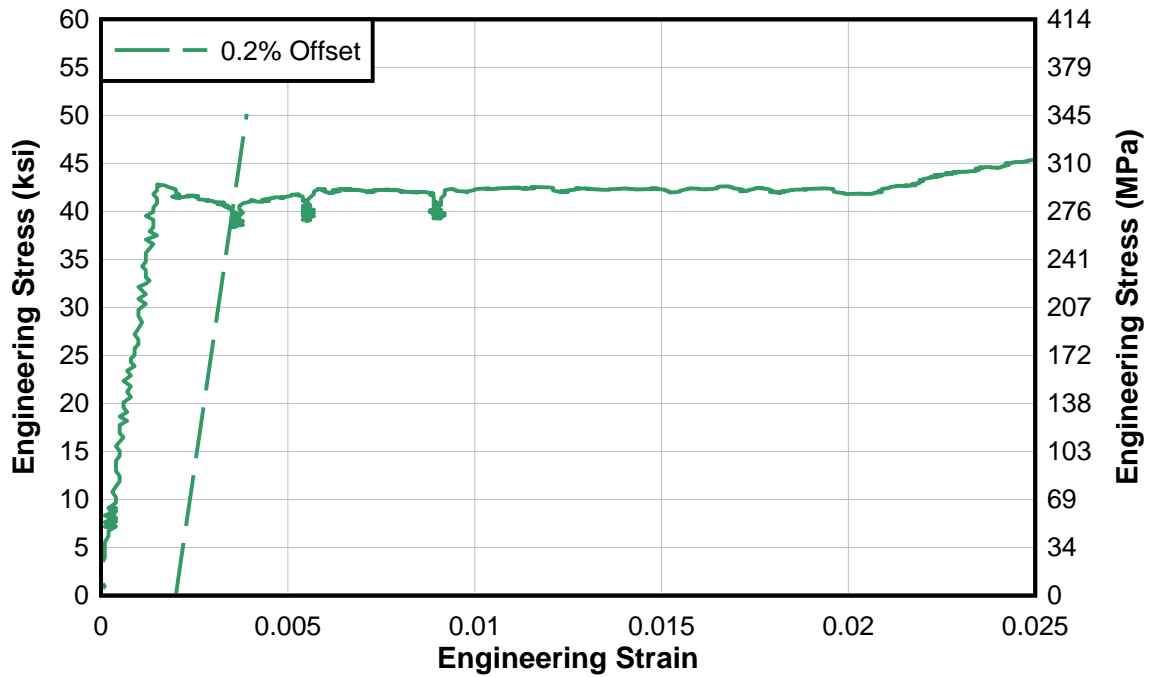


Figure 3-32: Dynamic yield for 0.2% offset

Data reduction for the second set of plates was very similar to that of the 3/8 in. thick A36 plate material but with a few slight changes. The higher strength material and thicker plate did not produce the large yield plateau that was seen in the previous data; therefore, the calculation for the dynamic and static yield stresses was adjusted. For the dynamic yield stress only the 0.2% offset was calculated. The static yield was determined by subtracting the minimum yield stress from the maximum value for each of the three periods in which the crosshead testing speed was held at zero. Each total yield stress drop was averaged together and subtracted from the 0.2% offset average to obtain the static yield.

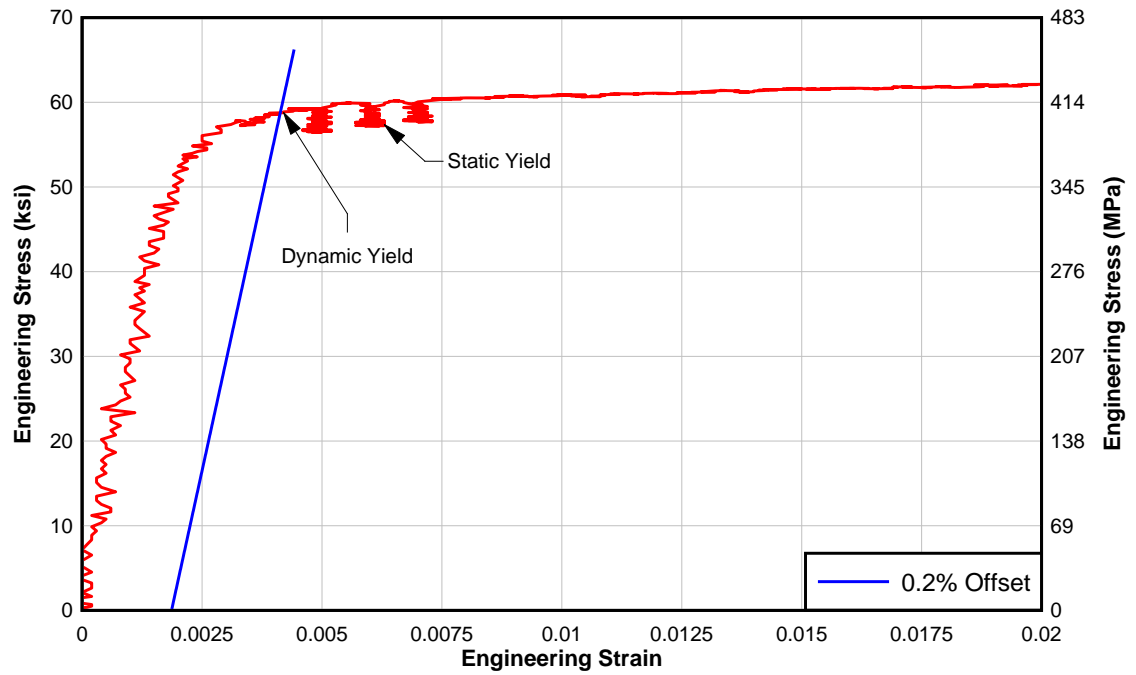


Figure 3-33: Example of 0.2% offset used for materials with no yielding plateau

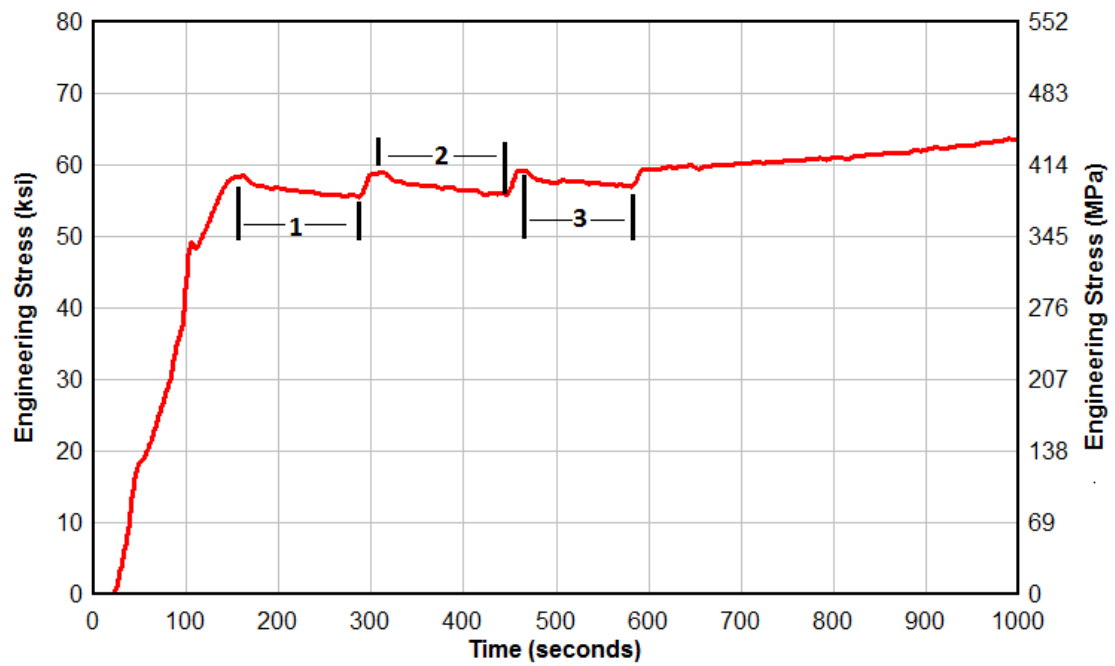


Figure 3-34: Static yield stress drop over time

3.3.4 *Material Results*

A summary of all key plate specimen properties is presented in Table 3-6. Data reported includes the average dynamic yield 0.2 % offset (F_{YD}), average static yield (F_{YS}), yield stress drop, average tensile stress (F_U), as well as the total averages and standard deviation for each rolling direction. Other specific material properties such as modulus of elasticity, % elongation, and % area reduction can be found in Appendix A. When a testing mistake, such as an incorrect loading rate, produced erroneous data, it was noted with a dash (-) in the summary table and the results were not included in the plots or statistical analysis. In Appendix A, two graphs are presented for each set of coupon samples. The first shows engineering stress vs. engineering strain while the second shows true stress vs. true plastic strain. The FE program requires true stress and strain because, unlike with engineering stress values, true stress accounts for the instantaneous area reduction of a sample throughout the test. The differences in these plots can be seen in Figure 3-35.

Conversions from engineering stress (σ) and strain (ϵ) to true stress (σ_T) and true plastic strain (ϵ_T) (Callister 2000) are made by

$$\epsilon_T = \ln(1 + \epsilon) \quad [3-1]$$

$$\sigma_T = \sigma(1 + \epsilon) \quad [3-2]$$

$$\epsilon_{plastic} = \epsilon_T - (\sigma_T / E) \quad [3-3]$$

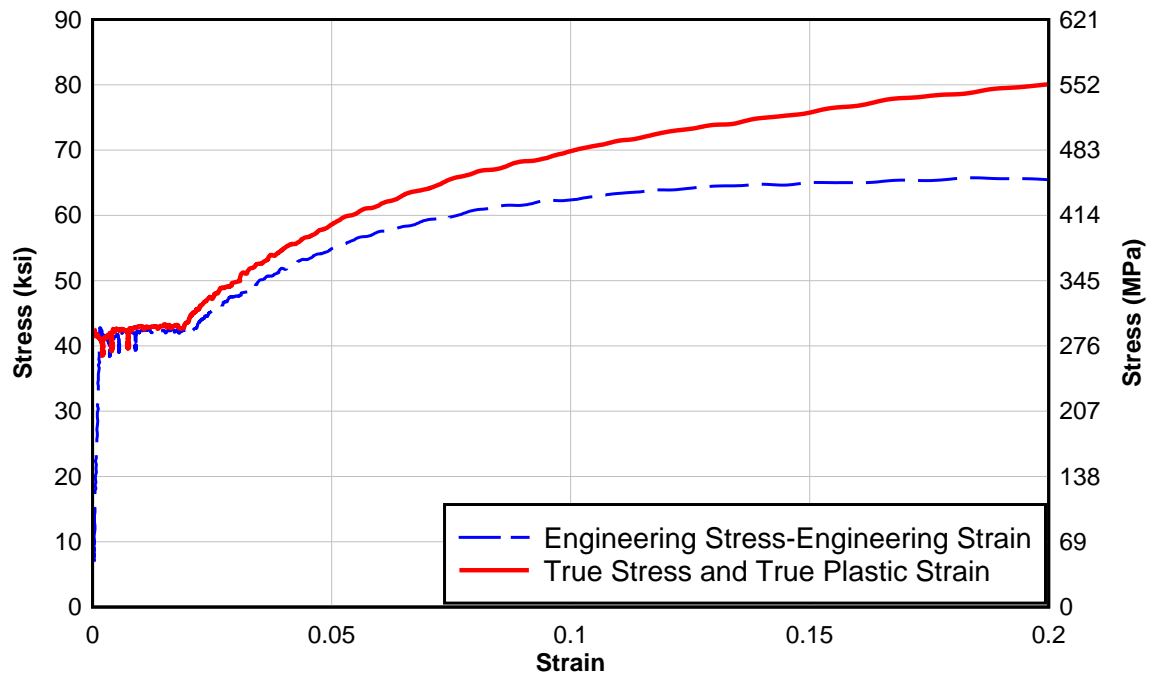


Figure 3-35: Engineering stress and engineering strain vs. true stress and true plastic strain example curves

All stress-strain graphs in Appendix A show only the elastic and early plastic regions of the curves. This is the main focus of the data and allows for each plot to be more easily differentiated.

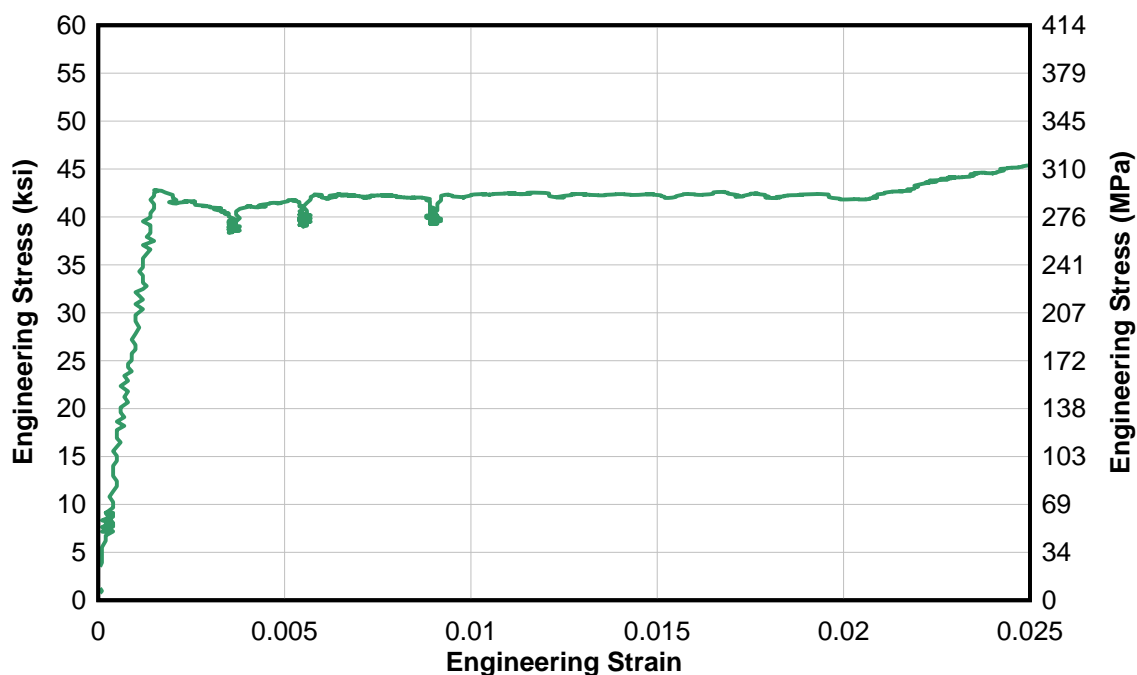


Figure 3-36: Example of elastic and early plastic region of engineering stress vs. engineering strain curve

A side by side comparison of each of the three material samples shows that the rolling direction has only a slight effect on the measured material properties. For the lower strength, thinner material, there was no noticeable difference in the rolling direction results. The higher strength and thicker samples do show some differences between the rolling directions, however this variance is less than 3 ksi (21 MPa) as shown in Figure 3-38.

Table 3-6: Summary of results for all material samples – US Customary Units

3/8 A36				
Rolling Direction	Average F_{YD} 0.2% Offset (ksi)	Average F_{YS} (ksi)	Yield Stress Drop (ksi)	Average F_u (ksi)
Parallel	41.73	39.60	2.13	65.90
Transverse	41.61	39.34	2.27	66.17
45° Bias	42.01	39.57	2.44	66.30
<i>AVERAGE</i>	<i>41.79</i>	<i>39.50</i>	<i>2.29</i>	<i>66.12</i>
<i>Std. Dev.</i>	<i>1.02</i>	<i>1.26</i>	<i>0.64</i>	<i>0.55</i>
1/2 A36				
Rolling Direction	Average F_{YD} 0.2% Offset (ksi)	Average F_{YS} (ksi)	Yield Stress Drop (ksi)	Average F_u (ksi)
Parallel	42.13	39.39	2.74	66.05
Transverse	44.89	42.92	1.97	65.92
<i>AVERAGE</i>	<i>43.51</i>	<i>41.16</i>	<i>2.36</i>	<i>65.99</i>
<i>Std. Dev.</i>	<i>2.03</i>	<i>1.70</i>	<i>0.59</i>	<i>1.09</i>
3/8 Gr. 50				
Rolling Direction	Average F_{YD} 0.2% Offset (ksi)	Average F_{YS} (ksi)	Yield Stress Drop (ksi)	Average F_u (ksi)
Parallel	56.84	53.52	3.32	66.63
Transverse	58.72	55.79	2.93	68.2
<i>AVERAGE</i>	<i>57.72</i>	<i>54.66</i>	<i>3.13</i>	<i>67.42</i>
<i>Std. Dev.</i>	<i>2.54</i>	<i>2.1</i>	<i>0.97</i>	<i>1.19</i>

Table 3-7: Summary of results for all material samples – Metric Units

3/8 A36				
Rolling Direction	Average F_{YD} 0.2% Offset (MPa)	Average F_{YS} (MPa)	Yield Stress Drop (MPa)	Average F_u (MPa)
Parallel	288	273	15	454
Transverse	287	271	16	456
45° Bias	290	273	17	457
<i>AVERAGE</i>	<i>288</i>	<i>272</i>	<i>16</i>	<i>456</i>
<i>Std. Dev.</i>	<i>7.03</i>	<i>8.69</i>	<i>4.41</i>	<i>3.77</i>
1/2 A36				
Rolling Direction	Average F_{YD} 0.2% Offset (MPa)	Average F_{YS} (MPa)	Yield Stress Drop (MPa)	Average F_u (MPa)
Parallel	290	272	19	66
Transverse	310	296	14	66
<i>AVERAGE</i>	<i>300</i>	<i>284</i>	<i>16</i>	<i>66</i>
<i>Std. Dev.</i>	<i>14.00</i>	<i>11.72</i>	<i>4.07</i>	<i>7.52</i>
3/8 Gr. 50				
Rolling Direction	Average F_{YD} 0.2% Offset (MPa)	Average F_{YS} (MPa)	Yield Stress Drop (MPa)	Average F_u (MPa)
Parallel	392	369	23	459
Transverse	405	385	20	470
<i>AVERAGE</i>	<i>57.72</i>	<i>376.84</i>	<i>21.55</i>	<i>464.81</i>
<i>Std. Dev.</i>	<i>17.51</i>	<i>14.48</i>	<i>6.69</i>	<i>8.20</i>

Dynamic material properties for the finite element model were calculated using the average of all three rolling directions shown in Figure 3-37. The static yield input values came from the average curve offset by the calculated yield stress drop shown in Table 3-6.

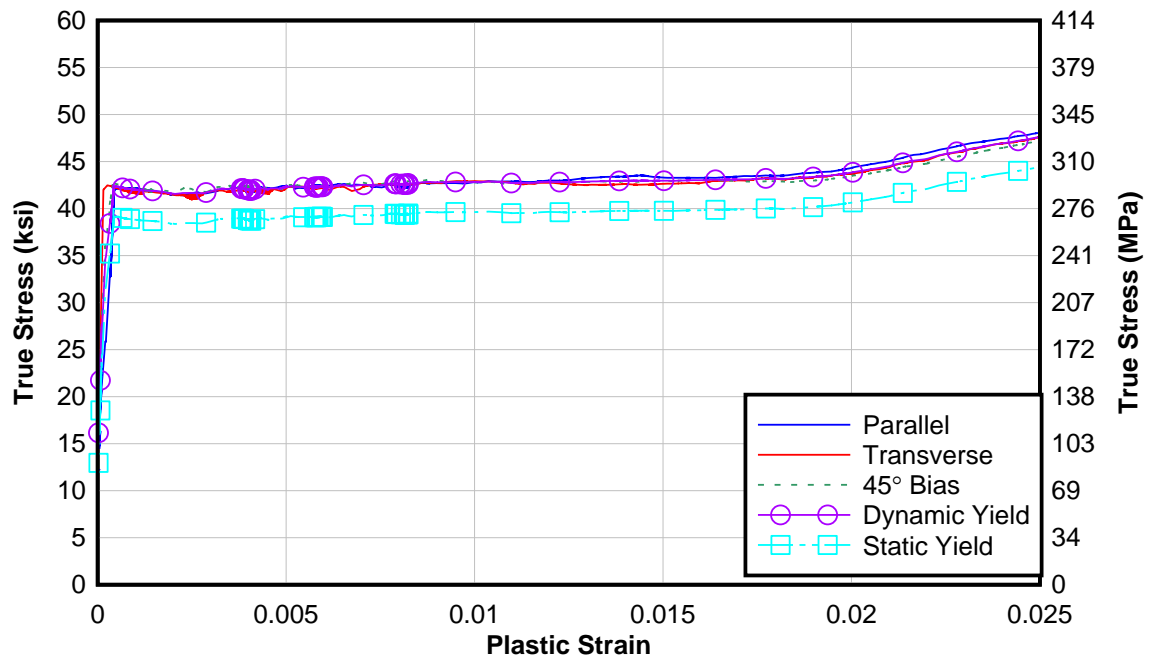


Figure 3-37: True stress vs. true plastic strain for all rolling directions of 3/8 in. thick A36 steel

The average values for each set of material results can be found in Table 3-8 and Table 3-9.

Figure 3-38 shows the stresses separated by rolling direction. Because the 3/8 in. thick A36 plate properties do not show any significant difference, the results were kept as the average of the rolling directions.

Table 3-8: Average FE material inputs used in each model – US Customary Units

	3/8 in A36		1/2 in A36		3/8 in Gr. 50	
True Plastic Strain	True Static Stress (ksi)	True Dynamic Stress (ksi)	True Static Stress (ksi)	True Dynamic Stress (ksi)	True Static Stress (ksi)	True Dynamic Stress (ksi)
0.00	39.50	41.79	41.16	43.51	54.66	57.72
0.01	40.04	42.84	46.38	48.33	57.64	60.70
0.02	41.03	43.83	51.19	53.14	59.88	62.94
0.03	47.62	50.42	55.22	57.17	61.73	64.79
0.04	52.15	54.95	58.58	60.53	63.39	66.45
0.06	58.90	61.70	63.45	65.40	66.36	69.42
0.08	63.63	66.43	66.99	68.94	68.69	71.75
0.10	67.24	70.04	69.78	71.73	70.82	73.88
0.12	69.97	72.77	71.92	73.87	72.65	75.71
0.14	72.33	75.13	73.67	75.62	74.12	77.18
0.18	76.04	78.84	76.35	78.30	76.07	79.13

Table 3-9: Average FE material inputs used in each model – Metric Units

	3/8 in A36		1/2 in A36		3/8 in Gr. 50	
True Plastic Strain	True Static Stress (MPa)	True Dynamic Stress (MPa)	True Static Stress (MPa)	True Dynamic Stress (MPa)	True Static Stress (MPa)	True Dynamic Stress (MPa)
0.00	272	288	284	300	377	398
0.01	276	295	320	333	397	419
0.02	283	302	353	366	413	434
0.03	328	348	381	394	426	447
0.04	360	379	404	417	437	458
0.06	406	425	437	451	458	479
0.08	439	458	462	475	474	495
0.10	464	483	481	495	488	509
0.12	482	502	496	509	501	522
0.14	499	518	508	521	511	532
0.18	524	544	526	540	524	546

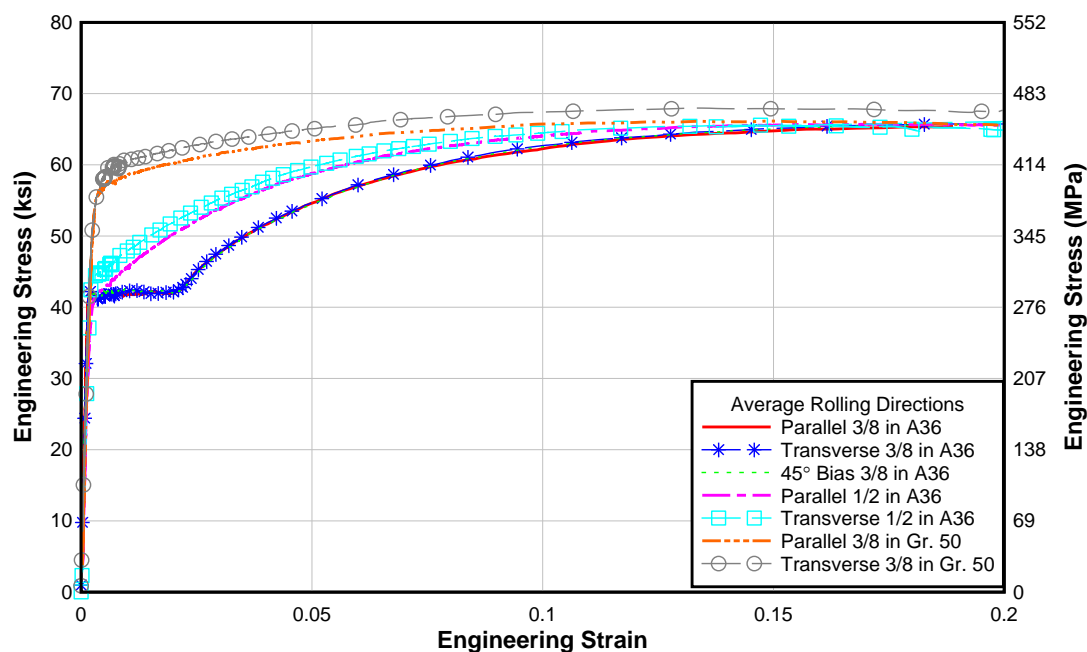


Figure 3-38: Plot of all coupon tests averaged by plate type and rolling direction

Table 3-10: Material properties for specific rolling directions – US Customary Units

	A36 3/8	A36 1/2 Parallel	A36 1/2 Transverse	Gr 50 3/8 Parallel	Gr 50 3/8 Transverse
True Strain	True Stress (ksi)	True Stress (ksi)	True Stress (ksi)	True Stress (ksi)	True Stress (ksi)
0.00	41.79	42.13	44.89	56.84	58.72
0.01	42.84	47.27	49.58	59.74	61.79
0.02	43.83	52.35	54.18	62.02	64.00
0.03	50.42	56.62	57.97	63.94	65.79
0.04	54.95	60.01	61.28	65.63	67.39
0.06	61.70	65.06	66.09	68.53	70.43
0.08	66.43	68.65	69.54	70.81	72.83
0.10	70.04	71.57	72.24	72.98	74.91
0.12	72.77	73.90	74.27	74.70	76.86
0.14	75.13	75.76	75.91	76.21	78.29
0.18	78.84	78.71	79.22	78.62	81.17

Table 3-11: Material properties for specific rolling direction – Metric Units

	A36 3/8	A36 1/2 Parallel	A36 1/2 Transverse	Gr 50 3/8 Parallel	Gr 50 3/8 Transverse
True Strain	True Stress (MPa)	True Stress (MPa)	True Stress (MPa)	True Stress (MPa)	True Stress (MPa)
0.00	288	290	310	392	405
0.01	295	326	342	412	426
0.02	302	361	374	428	441
0.03	348	390	400	441	454
0.04	379	414	423	453	465
0.06	425	449	456	473	486
0.08	458	473	479	488	502
0.10	483	493	498	503	516
0.12	502	510	512	515	530
0.14	518	522	523	525	540
0.18	544	543	546	542	560

In order to extrapolate the finite element results and apply them to a wide range of plate materials, ratios from the inputted properties were used to model the constitutive relationship between the A36 and Gr. 50 results. From these ratios, steel strengths ranging from $F_y = 30$ ksi to 56 ksi (207 MPa and 386 MPa) were formed. For clarity, select stress vs. strain curves are shown below in Figure 3-39:. Similar plots were made in both the parallel and transverse directions for the experimental analysis while general material properties would be used in practice.

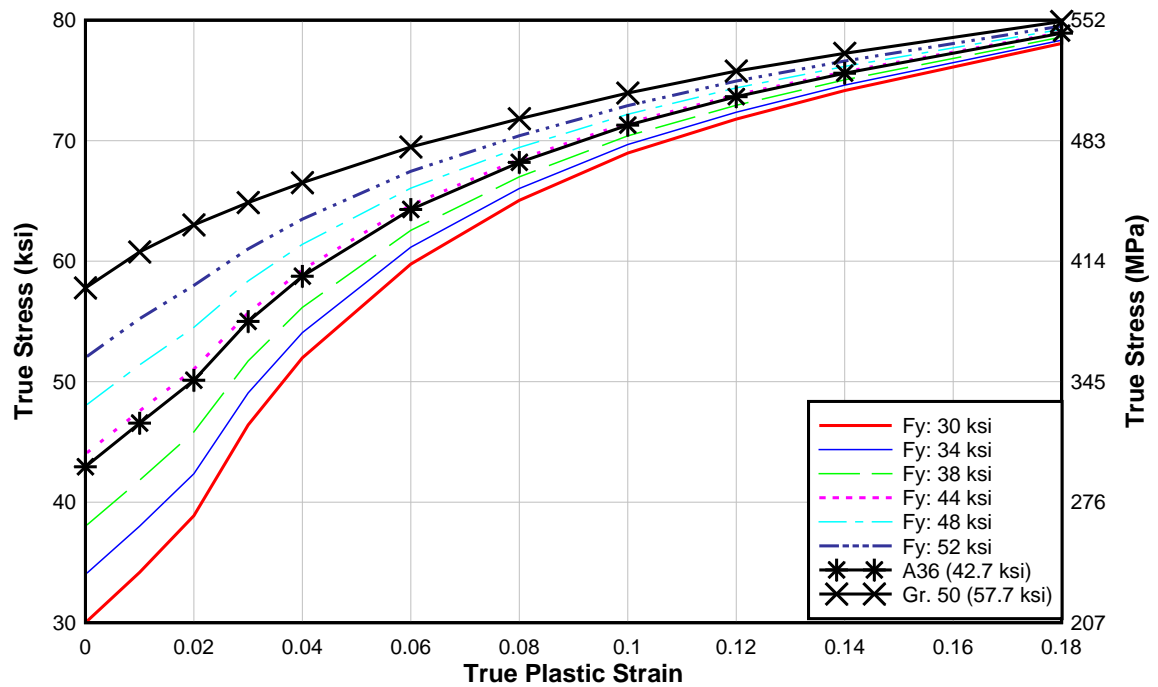


Figure 3-39: Varying dynamic yield true stress vs. true plastic strain plots based on average tensile coupon results

Once the FE model was finalized and all material samples were tested, various plate thicknesses were analyzed to provide the range of plate sizes that could be tested with the available prototype loading capacity.

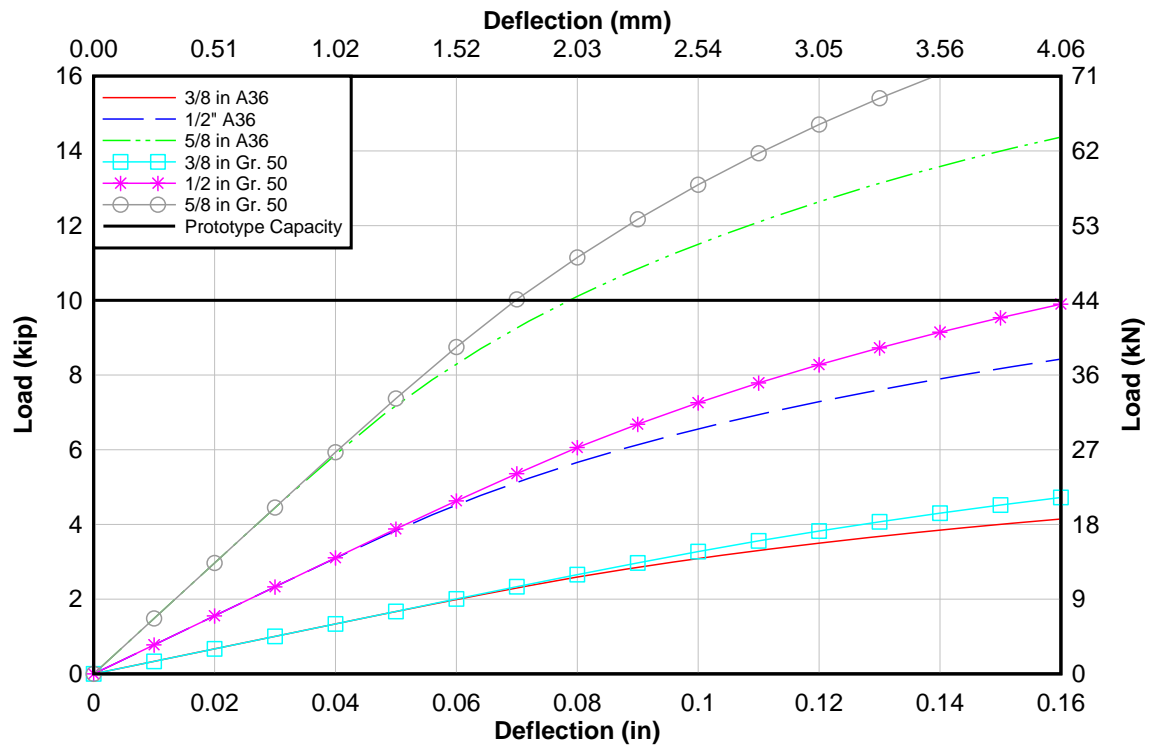


Figure 3-40: Load vs. deflection for various plate thicknesses using A36 and Gr. 50 properties

All material property results confirmed that the original plate dimensions and steel materials could be tested with the prototype device.

4 EXPERIMENTAL TESTING

To obtain experimental load and deflection data from the prototype device to compare with the FE models, fifty two (52) tests were performed. Forty four (44) tests were conducted on the free plates and eight (8) tests were conducted on the axially stressed plates. The free plates were supported in a stand that was constructed to hold them vertically, while the axially loaded plates were tested using the UTM. An out-of-plane load was applied to the plate samples by the prototype device. During application of the load, the load, time, and plate deflection data were collected.

4.1 Free Plates

4.1.1 *Setup and Instrumentation*

The stand for the free plates was made to support both sample sizes and account for slight variability in fabrication dimensions by providing a 1/8 in. (3.2 mm) clearance. Three screws were placed at the top and bottom, which were hand tightened, to keep the plate from moving during testing. An image of the stand can be seen in Figure 4-7.

Various instrumentation was attached to the plate and prototype device to obtain load and deflection readings. To measure the applied load, three different methods were used: 1) a pressure gauge connected to the bottle jack, 2) strain gauges attached to the inner and outer sides of the prototype device, and 3) a load cell placed at the loading point. The strain gauges and load cell were used to verify the accuracy of the pressure gauge. In order to acquire more precise pressure measurements, the analog dial gauge that came with the bottle jack was replaced with a high-resolution digital pressure gauge which also allowed for data to be logged and uploaded to a computer.

To measure plate deflections relative to the prototype device, a micrometer was clamped to the edge of the prototype handle which gave readings relative to the center of the support beam. The legs of the micrometer were bent to conform to the handle and a small indentation was made in the prototype directly below the load cell to ensure that all measurements were taken from the same location. This location was 0.5 in. (12.7 mm) from the edge of the plate and directly below the applied load.



Figure 4-1: Image of micrometer used to measure plate deflection

Electronic displacement sensors were also attached between the prototype device and plate sample to obtain redundant measurements. For the narrow plates, two sensors were glued to the outer side of the support beam on either side of the shoulder bolt (Figure 4-2). The sensors were averaged together to obtain an approximate value that measured 1.1 in. (27.9 mm) in from the edge of the plate, in line with the load cell.

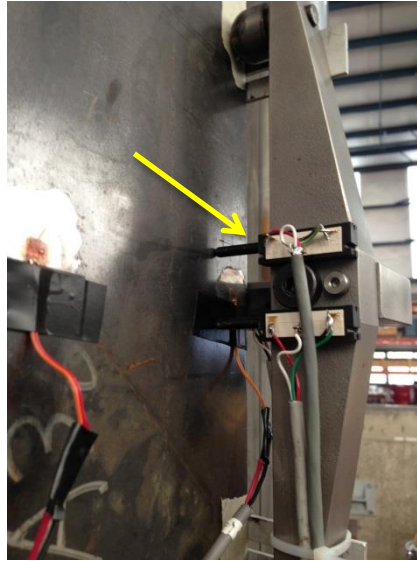


Figure 4-2: Displacement sensors attached to support beam of prototype

It was later determined that an additional sensor was needed at the free edge of the plate to obtain more accurate deflection results under the load point, which could not be measured directly with the available displacement sensors. The steel plate material in the original location of the displacement sensors remains in the elastic range for a longer period of time and therefore affects the ability to characterize the load-displacement response under the load point. To account for this, in the testing of the wide plates, an additional sensor was attached to the free edge of the plate (Figure 4-3), also in line with the load cell. This sensor was averaged with the two prototype displacement sensors to obtain the displacement at approximately the same location as the micrometer.

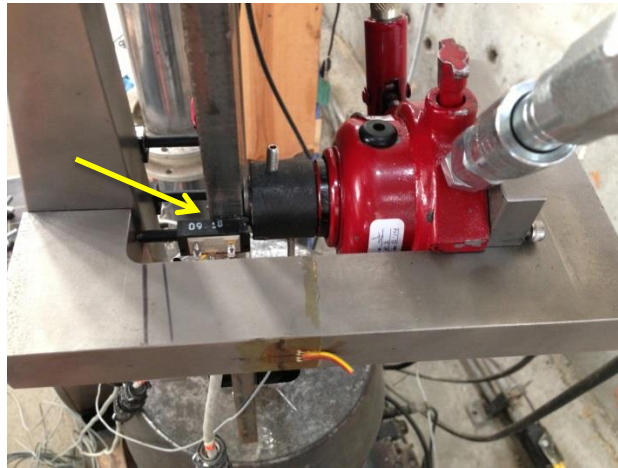


Figure 4-3: Displacement sensors attached to prototype and free edge of plate

Prior to each test, one side of the plate was painted with slaked lime whitewash to visually observe flaking of the mill scale as the plate yielded (Figure 4-4). For the wide plates, a grid with spacing at 0.5 in. (12.7 mm) was applied over the whitewash, providing a visual scale for the progression of mill scale flaking (Figure 4-5). A strain gauge was attached to the opposite side of the plate, directly below the load point, to serve as another measurement of local plate yielding (Figure 4-6). The strain gauge length was 0.062 in. (1.57 mm).



Figure 4-4: White wash on plate

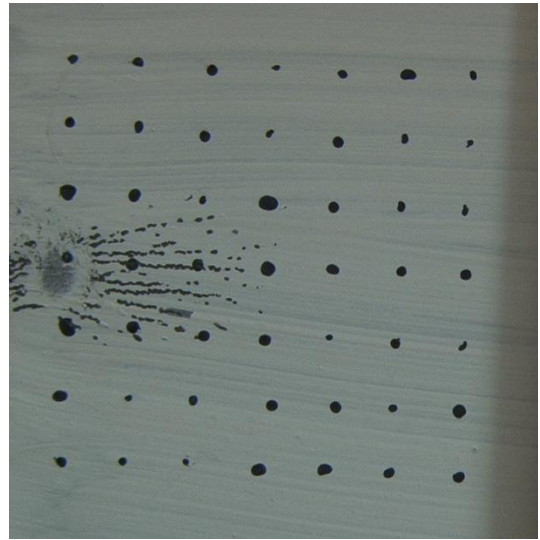


Figure 4-5: Mill scale flaking of white wash after plate yielding

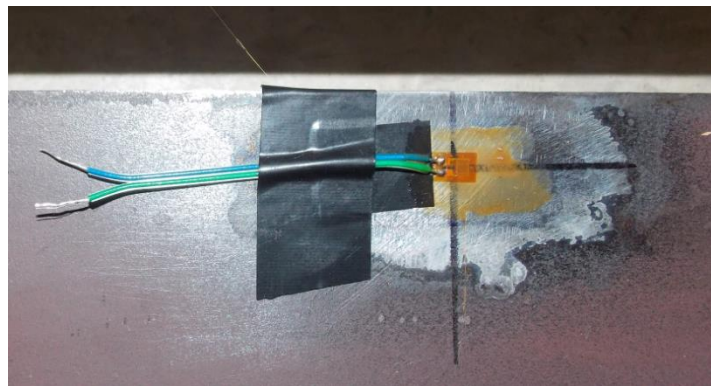


Figure 4-6: Typical strain gauge

4.1.2 *Testing Methodology*

Once the plate was secured in the stand, the prototype was held in place by applying a small initial load of approximately 0.3 kips (1.3 kN). This allowed the device to be self-supported during the rest of the experimental setup.



Figure 4-7: Free plate testing setup

All narrow plates were tested first, followed by the wide plates. In addition to the third displacement sensor that was added for the wide plates, the prototype was loaded and unloaded three times to approximately 1.0 kip (4.5 kN). This allowed for seating of the supports which helped remove slight variations in displacement measurements due to local imperfections of the plate surface at the load and reaction points.

Throughout the testing, load readings from the pressure gauge were taken at consistent micrometer measurements for each test as shown in Table 4-1. Originally, the readings were taken until slightly past yield, but for the wide plates, additional readings were taken well into the plastic region to obtain a much more nonlinear load vs. displacement curve. At each reading shown in bold in Table 4-1, a digital picture was taken of the whitewashed surface of the plate around the loading point.

Table 4-1: Specified points for manual load and deflection readings

Narrow Plate Micrometer Reading (in)	Wide Plates Micrometer Reading (in)	Narrow Plate Micrometer Reading (in)	Wide Plates Micrometer Reading (in)
0.000	0.000	0.088	0.088
0.005	0.005	0.090	0.090
0.010	0.010	0.092	0.092
0.015	0.015	0.094	0.094
0.020	0.020	0.096	0.096
0.025	0.025	0.098	0.098
0.030	0.030	0.100	0.100
0.035	0.035	0.102	0.103
0.040	0.040	0.105	0.107
0.045	0.045	0.110	0.110
0.050	0.050	0.113	0.115
0.055	0.055	0.115	0.118
0.060	0.060	0.120	0.120
0.065	0.065	-	0.125
0.070	0.070	-	0.130
0.075	0.074	-	0.135
0.077	0.077	-	0.140
0.080	0.080	-	0.145
0.082	0.082	-	0.150
0.084	0.084	-	0.160
0.086	0.086		

After completion of the test, the prototype was removed from the plate and a straight edge ruler was placed along the face of the plate to measure any residual deformations at the loaded region of the sample. No macro-measurable residual deformations were observed for any of the specimens after testing. Even for the wide plates that were tested well into the plastic range, the largest residual deformation was no larger than a 0.03 in. (0.76 mm).



Figure 4-8: No macro-measurable residual deformation of plate after yielding

The 1986 LRFD Manual of steel construction states that a deviation from flatness of up to 0.25 in. (6.36 mm) is tolerable. Therefore, because the measured deformation is much less than 0.25 in. the test method is verified as non-destructive.

4.2 Axially Loaded Plates

Through the process of testing the free plates, insights were found from the measured responses. Based on the earlier findings, refinements were made to the testing methods to include not only load vs. displacement but also, load vs. time. Due to this later evolution, only a few plates were tested with externally applied axial stress to the plates. Eight of the twelve plates were tested in the UTM but with no externally applied axial stress, which allowed for more control data similar to the free plates. The additional two plates for each of the different steel materials were tested by applying axial load to the samples creating average axial stress levels in the plate specimens at 10 ksi (69 MPa) for one set of tests and 20 ksi (138 MPa) for the second set of tests. The higher stress level would be considered close to the allowable working stress (live and dead load effects) in the lower strength plate materials.

4.2.1 *Setup and Instrumentation*

For the plates with no externally applied axial stress, strain gauges were placed on the specimens directly below the prototype device load point and in the center of the plate. Four strain gauges were added to the plates that were subjected to externally applied axial stress because it was observed that in addition to the intended axial stress, there was unintended bending (both strong and weak direction) within the plate due to non-uniform gripping of the plate in the UTM. The four strain gauges allowed for resolution of the biaxial bending to be determined. Prior to testing, the prototype device was initially loaded and unloaded three times up to a load of approximately 1.0 kip (4.4 kN). Subsequently, the prototype device load was incrementally applied and held for 30 seconds at each increment until well past yielding.



Figure 4-9: Axially loaded plate strain gauge setup



Figure 4-10: Plate test setup in UTM

4.2.2 *Effects of Bending Within the Plate*

The rationale for the externally applied axial stress levels of 10 ksi (68.9 MPa) and 20ksi (139.9 MPa) was to approximate the upper level of expected service stresses in a plate. It is assumed that the prototype device would be deployed while no live loads or transient live loads are present. Further, because it is applied at the free edge of the plate, the stresses are expected to be lower than in other regions of high stress flow. However, the lower stress level of 10 ksi approximates larger amplitude stresses that could be anticipated due to dead loads acting in the region being tested with the prototype device.

Due to the unanticipated bending, the yield stress comes from both axial and bending stresses in the plate calculated as:

$$\sigma_Y = \sigma_{Axial} + \sigma_{Bending} \quad [4.1]$$

$$\sigma_Y = \frac{P}{A} + \frac{Mc}{I} \quad [4.2]$$

where $M = \frac{5P}{2}$ as described in Figure 3-5 it is expected that the applied prototype device load that will produce yielding of the plate will be lower for plates with internal stresses from dead loads. This difference is slight for 10 ksi but is more significant for 20 ksi as shown in Figure 5-25. Obviously as the external stress becomes smaller, the influence on the prototype load will also become smaller.

Note: These plate models forced the high stresses to be at the free edge of the plate, but in reality, the 10 ksi or 20 ksi stresses would be at the connections and the free edge of the plate would have little to no stress applied.

5 RESULTS

The experimental results were analyzed in multiple ways to determine the yielding load of the prototype device, defined here as P_Y . The various analysis methods compared the prototype load to the strain gauge readings, onset and spread of mill scale flaking, load decay over time during hold periods, and load-deflection response. The experimental results were further compared with the finite element results. These analyses resulted in an offset method, similar to that used in tensile testing, to determine P_Y . For the early tests of the narrow plates, only strain gauge data was used for the analysis because these were the only continuous data available in the first phase. Later refinements allowed more and redundant data comparisons.

5.1 Pressure Gauge vs. Load Cell

Specifications provided by the hydraulic bottle jack manufacturer stated that the ram area was 1 in² (645 mm²) which should result in a direct equivalent output from the high-resolution pressure gauge of (psi) to load (lbs). However, tests with the pressure gage, as shown in Figure 5-1, demonstrated that the pressure gauge readings did not correlate to those of the load cell. Further, the internal circuit of the pressure gage is believed to have a built in filter which does not allow dynamic measurements to be made. The calibration of the pressure gage was found to be nonlinear when compared with the load cell. The factory calibrated load cell was recalibrated twice during this test program and gave the same output. Because of the nonlinearity and uncertainty of the pressure gauge, only the load cell readings were used in the following analyses.

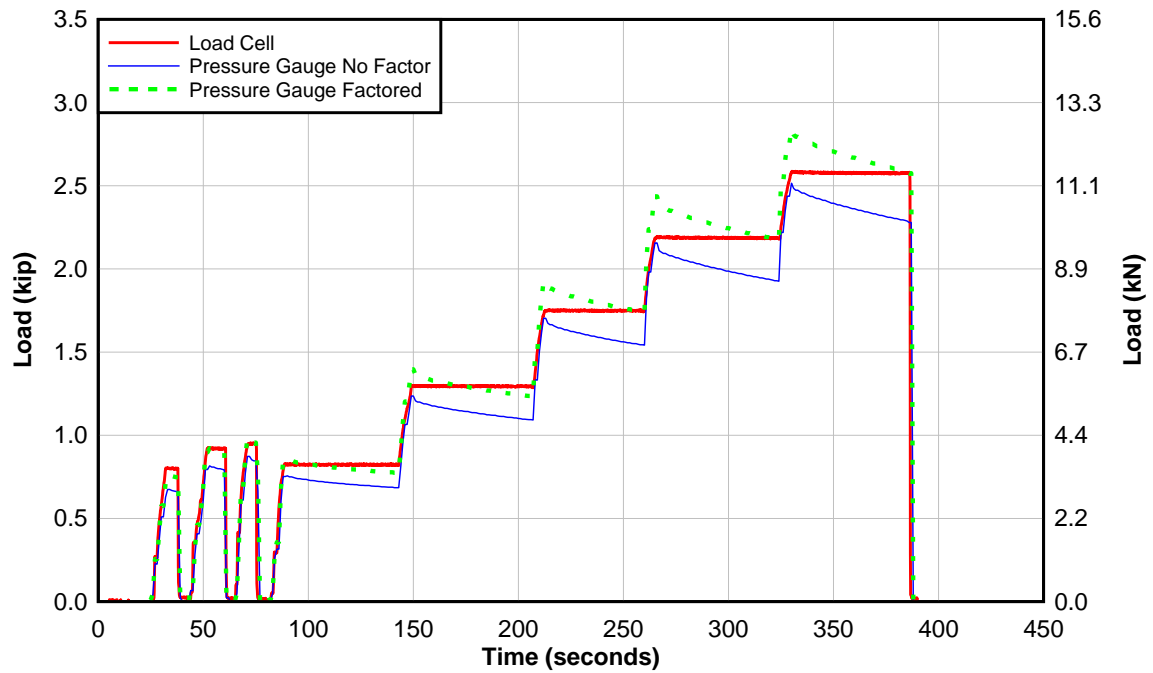


Figure 5-1: Comparison of pressure gauge and load cell outputs

5.2 Prototype Load vs. Strain Gauge Data

The first method used to predict P_Y was to take the strain measurement from the strain gauge placed below the loading point, convert strain to stress, and plot the stress vs. load cell data.

Using the coupon nominal yield stress, P_Y was determined for each test.

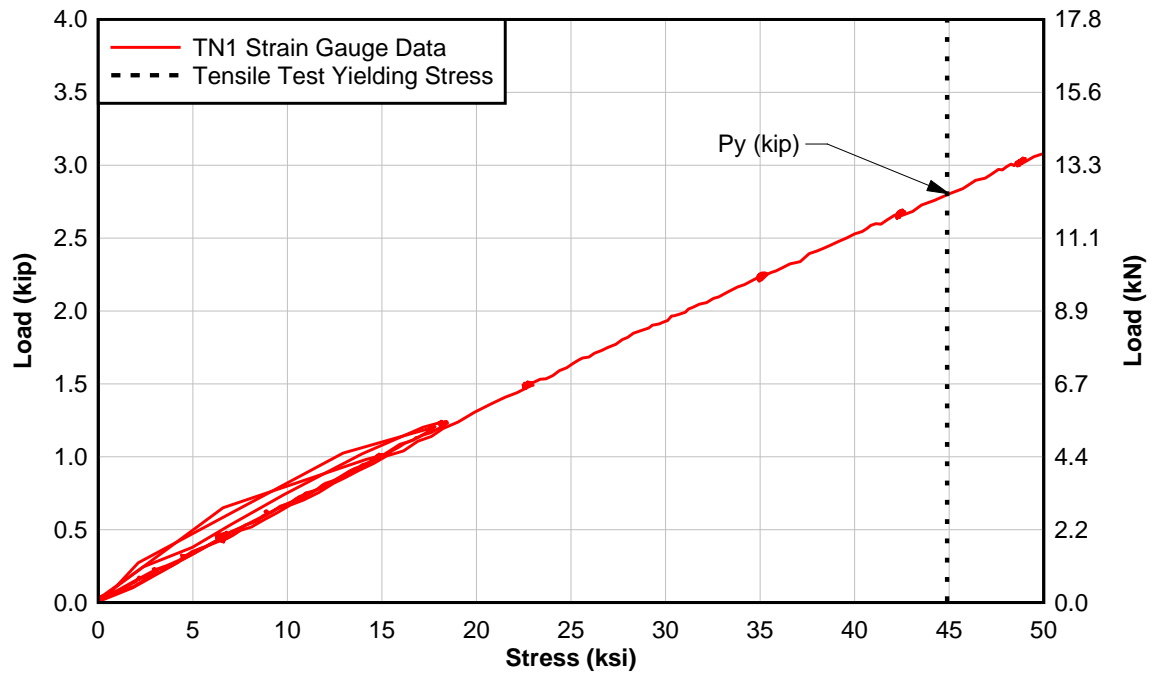


Figure 5-2: Strain gauge data from 1/2 in. thick A36 plate TN1

Because the strain gauge length is very small and thus represents a point or micro measure of yielding, P_Y was found to occur earlier than in other methods and represents a value of micro yielding rather than macro yielding. These differences are explained in more detail in section 5.6. In addition, to use this method, the yield stress from tensile coupons needs to be known previously because the strain gages do not become highly nonlinear at the expected yield stress. Therefore, this is not a reasonable method for determining the yield stress.

Table 5-1: Prototype yielding load based off strain gauge data

Sample	Strain Gauge Stress (ksi)	Associated P_y (kip)	Sample	Strain Gauge Stress (ksi)	Associated P_y (kip)
<i>A36 3/8 in</i>			<i>A36 1/2 in</i>		
			PN1	42.13	2.46
PN1	41.79	1.62	PN2a	42.13	-
PN3	41.79	1.26	PN2b	42.13	-
PW1s1	41.79	1.59	PN3	42.13	2.62
PW1s2	41.79	1.60	TN1	44.89	2.96
PW2	41.79	1.46	TN2a	44.89	2.47
PW3	41.79	1.50	TN2b	44.89	2.65
TN1	41.79	1.45	TN3	44.89	2.90
TN2	41.79	1.42	<i>Standard Deviation, σ</i>		
TN3	41.79	1.30	<i>Average, μ (ksi)</i>		
TW1s1	41.79	1.46	COV		
TW1s2	41.79	1.50	<i>Gr. 50 3/8 in</i>		
TW2	41.79	1.40	PN1a	56.84	1.84
TW3	41.79	1.42	PN2	56.84	-
BN1	41.79	1.66	PN3	56.84	1.82
BN2	41.79	1.47	TN1	58.72	2.14
BN3	41.79	1.42	TN2a	58.72	1.71
BW1s	41.79	1.47	TN2b	58.72	1.52
BW2s	41.79	1.47	TN3	58.72	-
<i>Standard Deviation, σ</i>		0.10	<i>Standard Deviation, σ</i>		0.23
<i>Average, μ (ksi)</i>		1.47	<i>Average, μ (ksi)</i>		1.81
COV		0.07	COV		0.12

5.3 Prototype Load vs. Mill Scale Flaking

As the prototype load is applied above the yield stress of the plate, the mill scale, which acts as a brittle coating, will flake off the plate. Application of whitewash allows the mill scale flaking to be more easily observed. The progression of mill scale flaking during the test of plate TW3s is shown in Figure 5-3 through Figure 5-6 and is located in reference to the load vs. deflection curve

in Figure 5-7. As previously stated, the grid points are spaced at 0.5 in. (12.7 mm). As seen in these figures, mill scale flaking occurs after the load-deflection response deviates from the linear elastic region. Thus, mill scale flaking is more of an indication of macro yielding of the plate in the region of the prototype device load point.

While mill scale flaking is a visual indication of plate yielding, it can be difficult to see. It occurs on the compression face of the plate and the very first initial flaking is likely hidden below the load cell. To use this as a measure of yielding in the field would require removing the paint on the plate, but not removing the mill scale, and adding a whitewash coating, allowing it to dry, and then testing. This is not practical.



Figure 5-3: Spread of Plasticity (A)



Figure 5-4: Spread of Plasticity (B)



Figure 5-5: Spread of Plasticity (C)

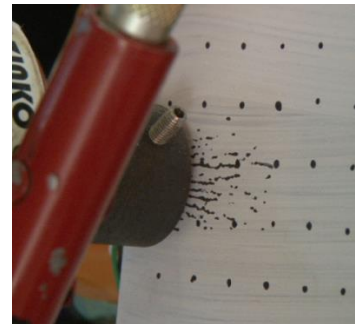


Figure 5-6: Spread of Plasticity (D)

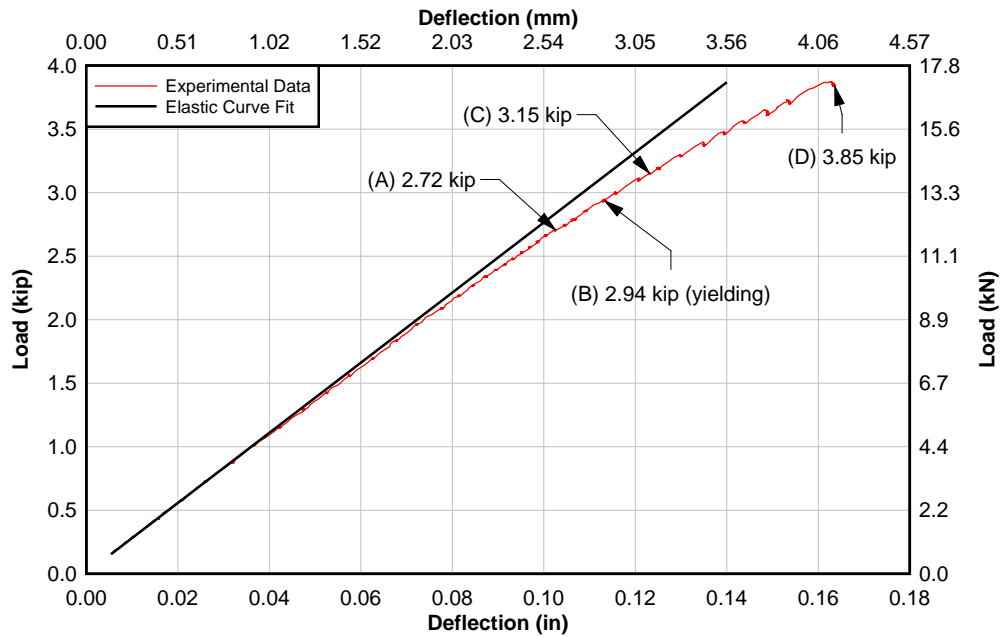


Figure 5-7: Progression of mill scale flaking in relation to load vs. deflection curve

Based on a similar set of images taken for each of the wide plate tests, P_Y was chosen at the first sign of flaking and associated to a predicted yield stress, σ_Y , value as shown in Table 5-2. The calculations of σ_Y and the test over-prediction safety factor, α , are explained in section 5.7.2.

Table 5-2: Predicted yield stress at first sign of mill scale flaking.

Sample	Deflection (in)	P_y (kip)	Predicted σ_y (ksi)	Predicted σ_y /Actual σ_y (Bias)
PW1	0.12	3.13	46.77	1.12
PW1s	0.10	2.83	41.45	0.99
PW2	0.11	2.91	42.88	1.03
PW2s	0.11	2.91	42.88	1.03
PW3	0.13	3.34	50.63	1.21
PW3s	0.11	2.87	42.14	1.01
TW1s1	0.10	2.73	39.73	0.95
TW1s2	-	-	-	-
TW2	0.11	2.79	40.77	0.98
TW2s	0.11	2.72	39.56	0.95
TW3s	-	-	-	-
TW3s	0.11	2.95	43.62	1.04
BW1	0.11	2.90	42.60	1.02
BW1s	0.10	2.88	42.27	1.01
BW2	0.12	3.07	45.75	1.09
BW2s	0.12	3.09	46.10	1.10
BW3	-	-	-	-
BW3s	-	-	-	-
<i>Standard Deviation, σ</i>		0.17	3.03	0.07
<i>Average, μ (ksi)</i>		2.94	43.37	1.04
COV		0.06	0.07	0.07
			$\alpha=$	0.77

5.4 Prototype Load vs. Time

The painted plates were only tested for load vs. time data and the results are shown in Figure 5-8.

When the plate is still in the elastic range there is no change in the load magnitude over the hold time interval, however, as the plate yields, the load drops during the hold period. Similar to the

tensile test specimens, the rate of change of the load in time is initially rapid and then slows. The load magnitude drop occurring over the hold interval increases as yielding spreads across the plate around the load point, as seen in Figure 5-9.

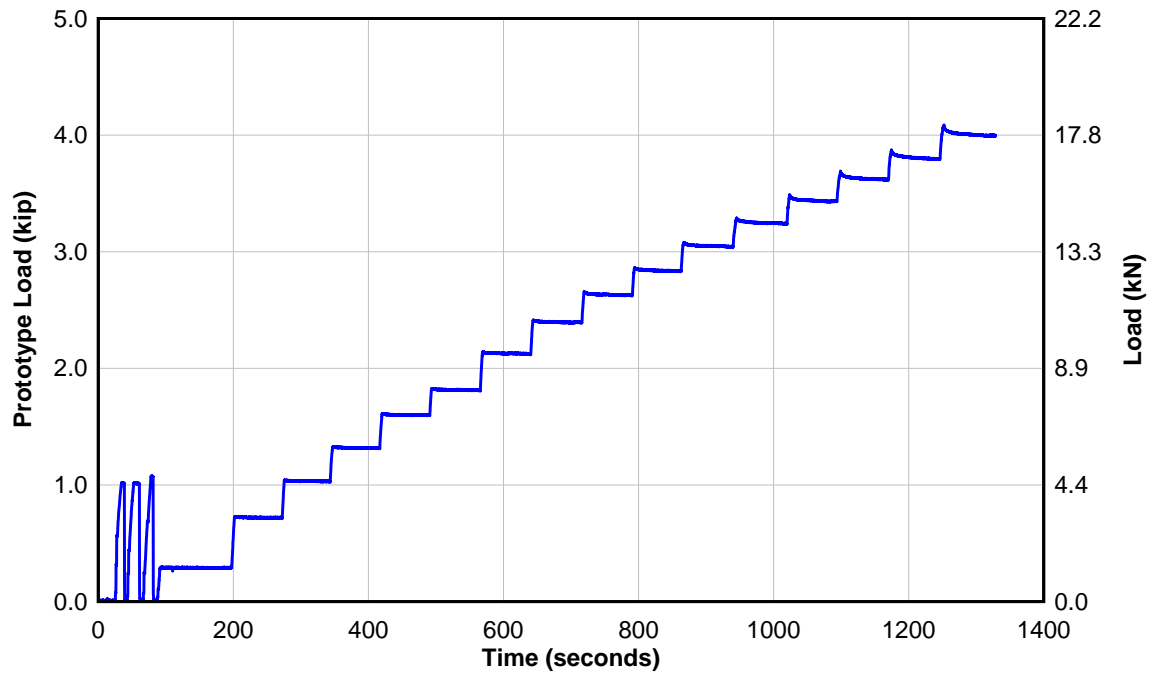


Figure 5-8: Load vs. time for 3/8 in A36 painted plate PN2

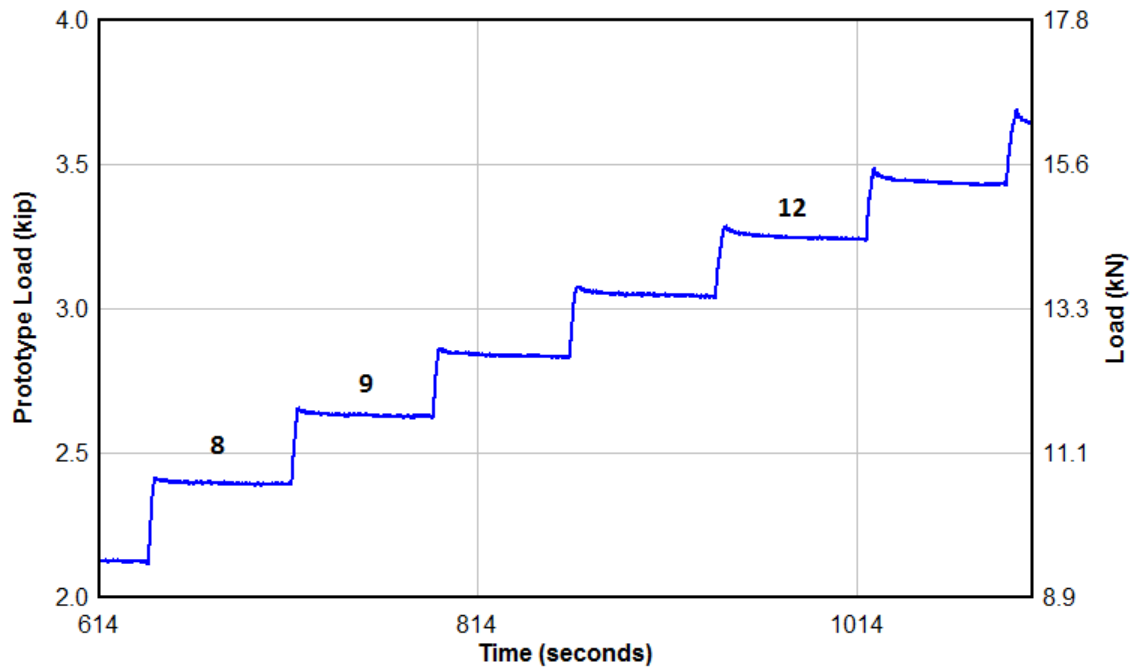


Figure 5-9: Load reductions occurring at hold plateaus increases as yielding increases across plate

The change in load magnitude occurring over a plate test is shown in Figure 5-10. For each plateau in Figure 5-8, correlating to a one minute pause in the prototype loading, the absolute drop in load was calculated by subtracting each value from the maximum peak at the start of holding. It can be seen that the first large drop in the load occurs at plateau 9 for PN2. This corresponds to a device load of 2.9 kip (12.9 kN). Any drop in load between ± 0.005 kip could be attributed to the effects of the 10 pounds of noise associated with the data acquisition system. First yielding and macro yielding were determined through a comparison of all test methods and is explained in section 5.6.

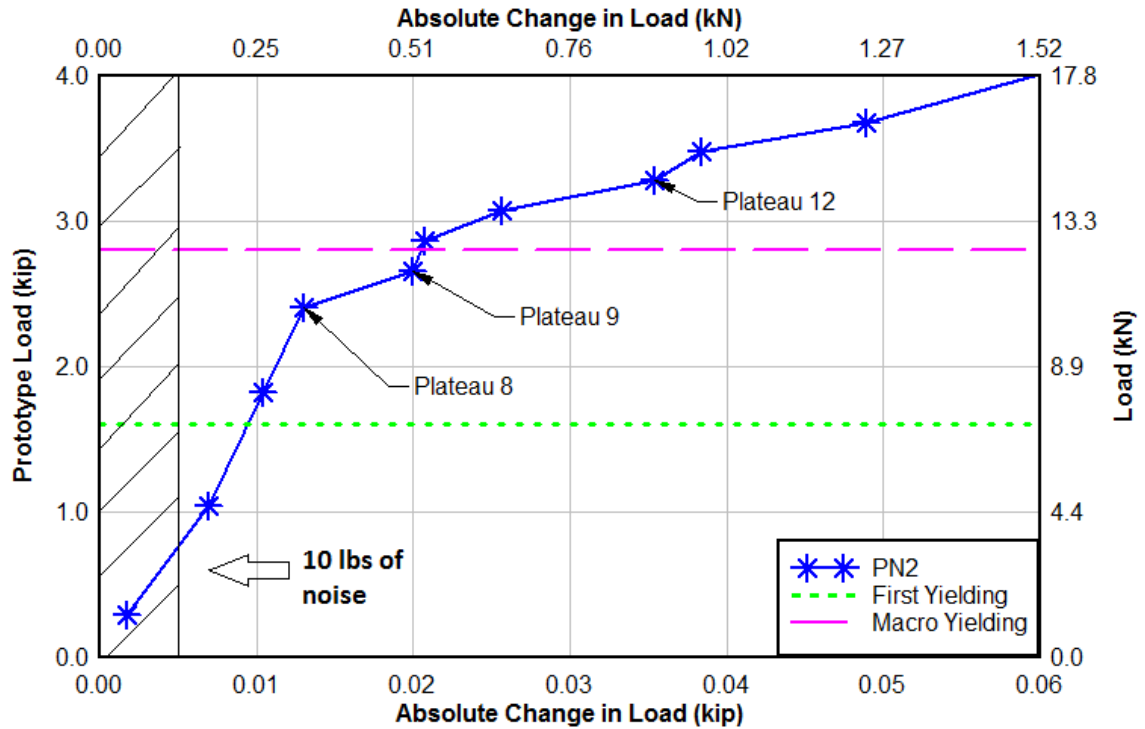


Figure 5-10: Absolute change in load at each 60 sec. hold interval.

5.5 Prototype Load vs. Plate Deflection

P_Y was also determined from the load and deflection data where the load-deformation response is linear when the plate is elastic and then becomes progressively nonlinear as the plate yields. It is necessary to establish a load which can be correlated with yield stress enabling correlation with the FE analyses once the plate becomes inelastic. The very first observation of nonlinearity (indicating first yielding) can be difficult to detect in different plate materials and thicknesses. Further, the change from linear to nonlinear response is gradual without an abrupt transition. Thus, a definition is required for the load magnitude that can be correlated with yielding of the plate. This is described subsequently and compared with the other methods used to identify the

prototype device load that corresponds to yielding.

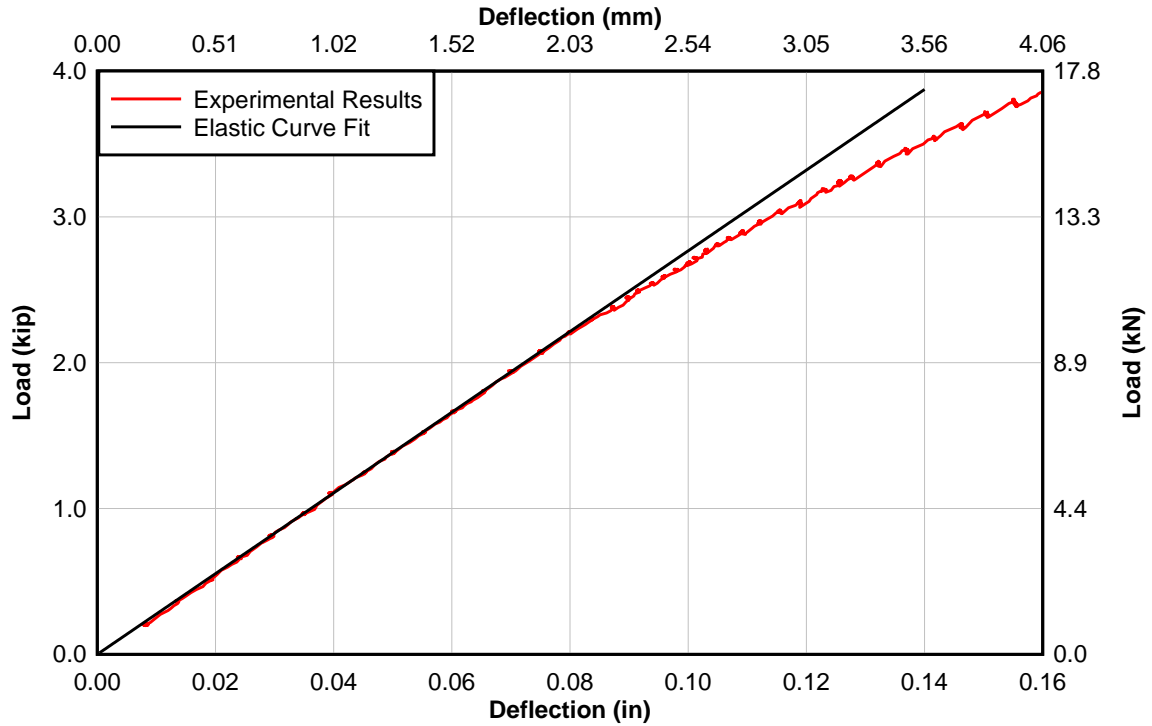


Figure 5-11: Typical experimental results load vs. deflection plot

5.6 Prototype Load Correlation with Finite Element Model

Once all of the various experimental measurements were developed, they were correlated with the FE results. The 3/8 in. thick, A36 plate results are used in the following discussion. First yielding of the plate was identified from the FE results (using the known yield stress of the plate material as an input in the FE model) where the load-deformation curves from the static and dynamic yield material inputs deviate (Figure 5-12) and when the plate element stress meets the von Mises yield criterion. This value corresponds to 1.6 kip (7.1 kN) and was similar to that calculated from the strain gauge data on the experimental plates.

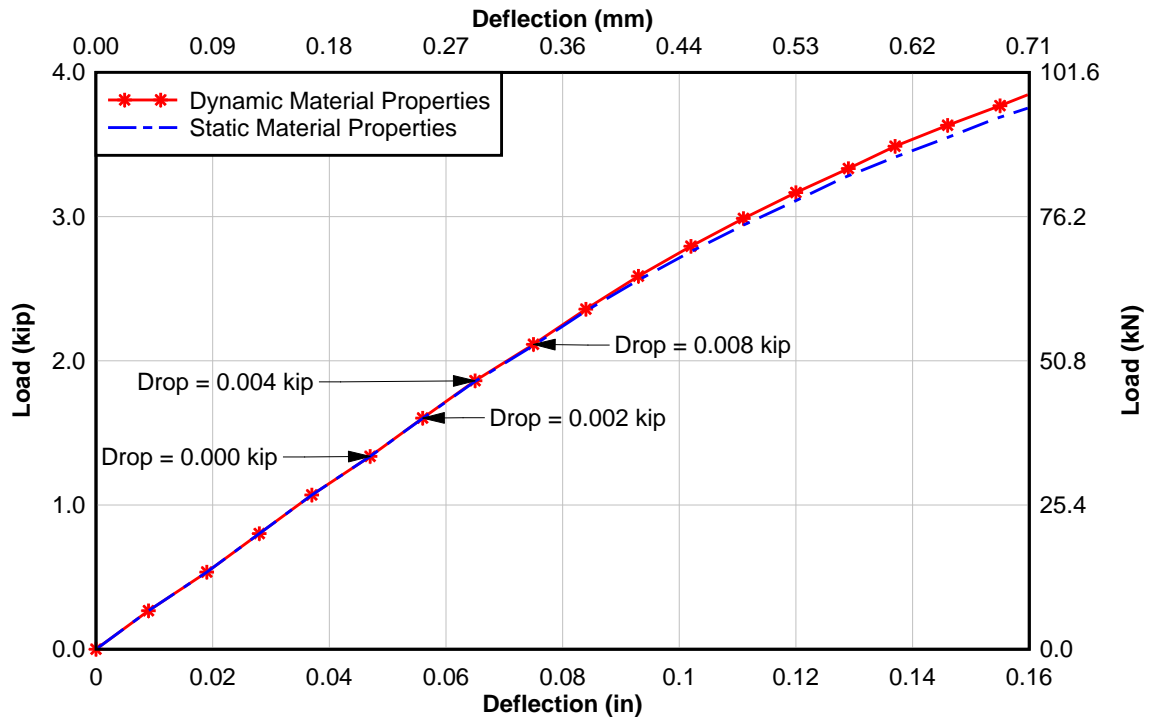


Figure 5-12: Load drop between dynamic and static yield properties giving first yielding

Macro yielding was defined as a spread of plasticity that corresponds with visual flaking of the mill scale and an abrupt drop in the load vs. time response. This P_Y was approximately 2.9 kips (12.5 kN) and coincided with a spread of plasticity along the free edge of the plate of roughly 2 in. (50.8 mm) at the load point, as shown in Figure 5-14.

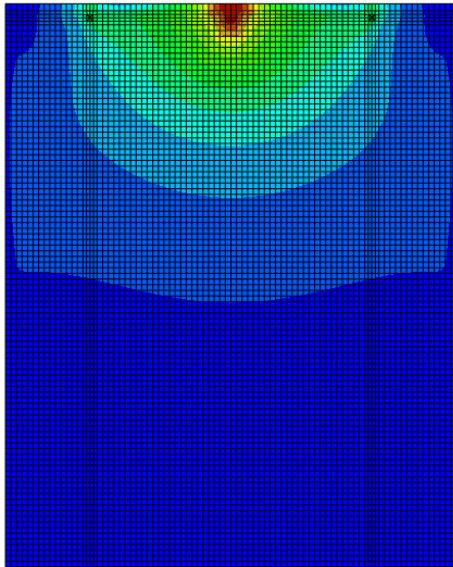


Figure 5-13: FE model - first yielding

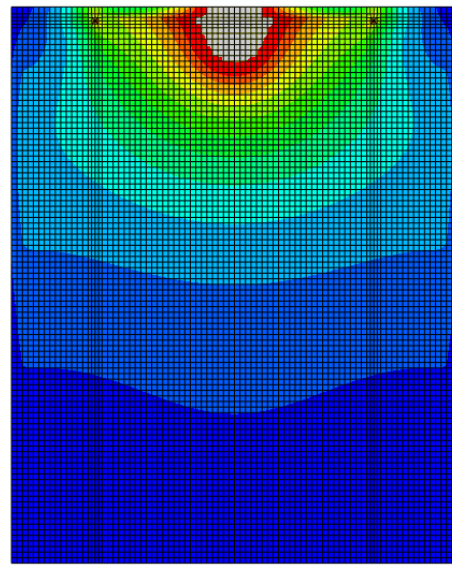


Figure 5-14: FE model - 2 in. spread of plasticity at the load point

5.7 Analysis Results

After comparison of the above procedures, it was decided that P_Y was best associated with macro yielding because it can be easily detected through both the load vs. deflection and load vs. time methods. The approach was to determine P_Y from the load vs. deflection curve using an offset similar to that of the ASTM E8 standard for materials without well-defined yield plateaus. An offset of 0.005 in. (0.127 mm) was found to provide a load magnitude that was sufficiently distinguished from the elastic response.

5.7.1 Development of Offset Method Concept

To demonstrate the selected offset was applicable to a wide range of plate thicknesses and materials, four additional FE analyses were performed for plates loaded with the prototype device. Plate thicknesses of 3/8 in. and 1 in. were used with A36 (36 ksi yield) and A514 (100

ksi yield) material properties. Three different material property inputs were used for the FE models which included 1) post-yield strain hardening based on the actual tensile test data 2) linear post-yield strain hardening and 3) elastic-plastic properties. The material input models are shown in Figure 5-15 and Figure 5-16.

The predicted load-displacement response of the plates is shown in Figure 5-17 for the different material inputs. As seen in this figure, the material models did not affect the load vs. deflection results. Therefore, the simplified elastic-plastic material model was used for the subsequent FE analysis to develop the relationship between P_Y and yield stress for varying materials.

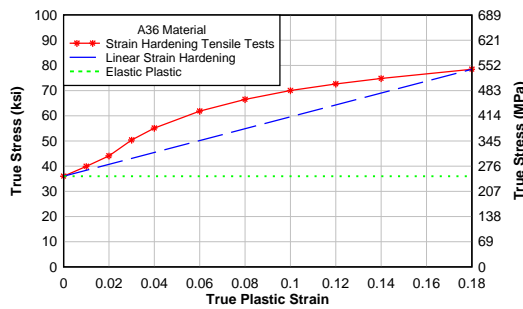


Figure 5-15: A36 various material inputs

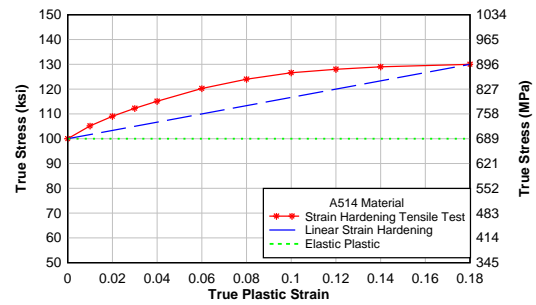


Figure 5-16: A514 various material inputs

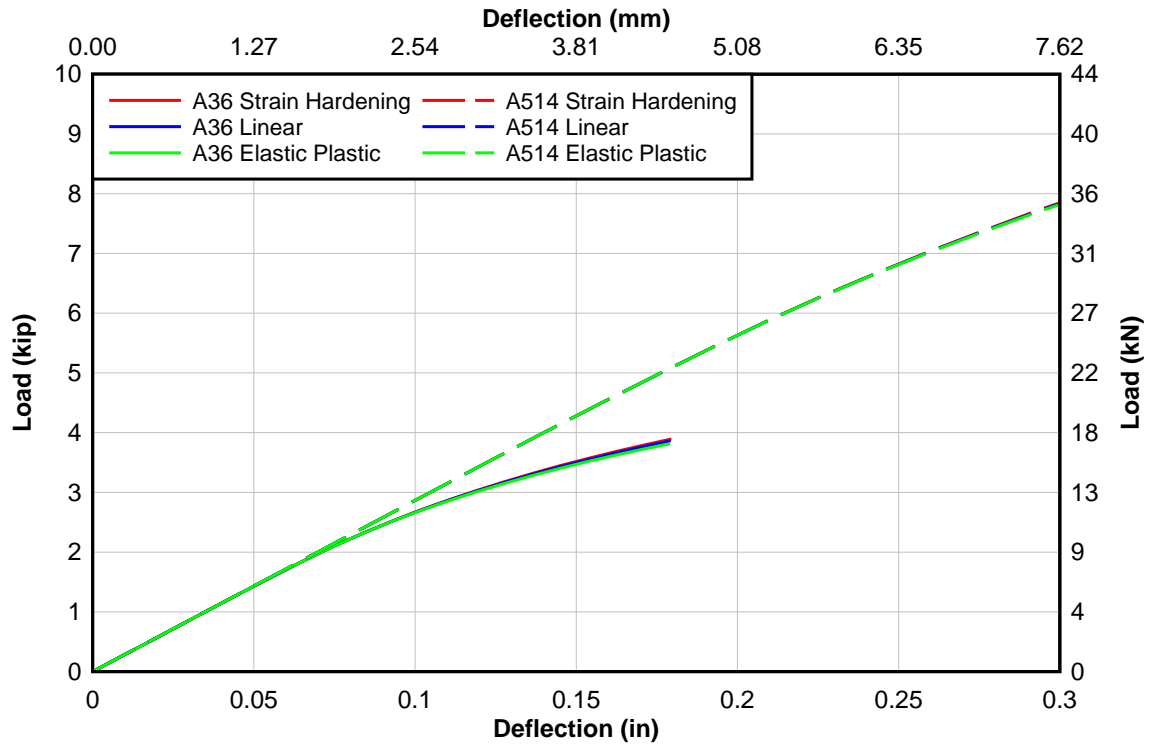


Figure 5-17: Load-deformation response for analyses of different material models.

Using the elastic-plastic material model, the different plate thickness and material models were analyzed and the 0.005 in. offset was used to identify the P_Y value and the corresponding spread of plasticity at the load point. Figure 5-18 and Figure 5-19 show the load deformation response and Figure 5-20 to Figure 5-23 show the spread of plasticity around the load point at the P_Y values. This comparison analysis demonstrates that the offset allows for P_Y to be correlated with yield stress for a wide range of plate thickness and yield stress ranges. The selected offset also provides approximately the same spread of plasticity at the edge of the plate as in Figure 5-14. The offset method to identify P_Y was applied to all the experimental data and the results were quantified as described subsequently.

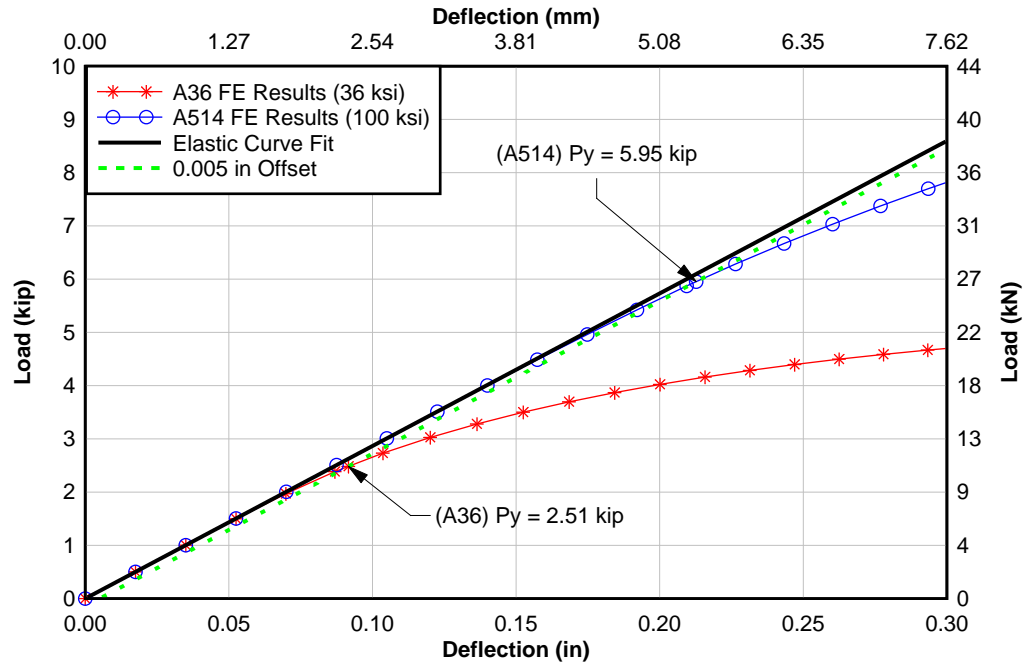


Figure 5-18: Load vs. deflection response and device load at 0.005 in. offset for 3/8 in. thick plate

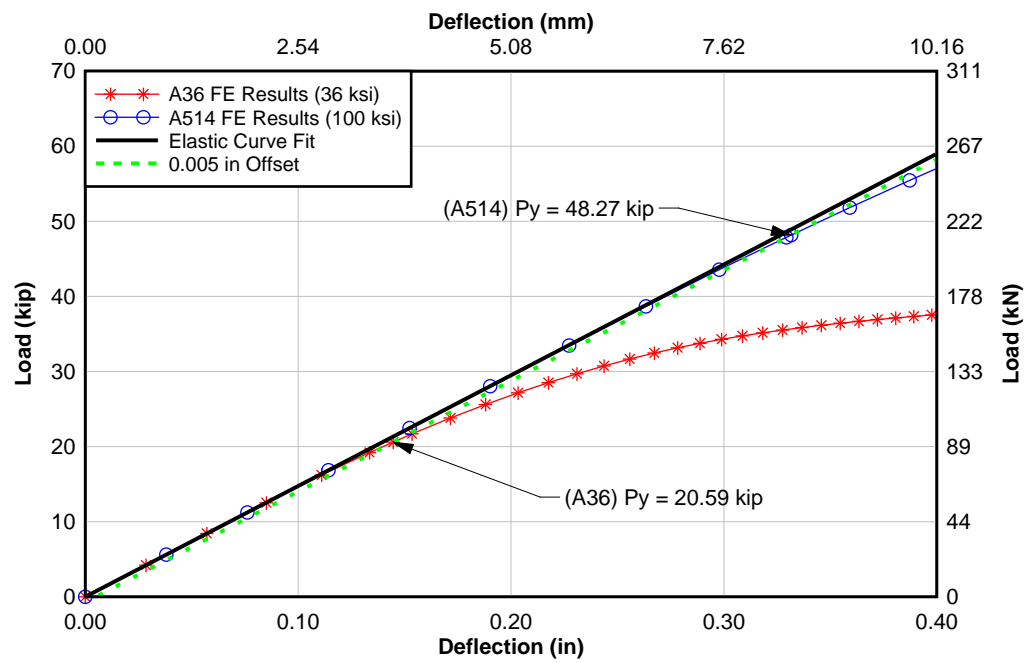


Figure 5-19: Load vs. deflection response and device load at 0.005 in. offset for 1 in. thick plate

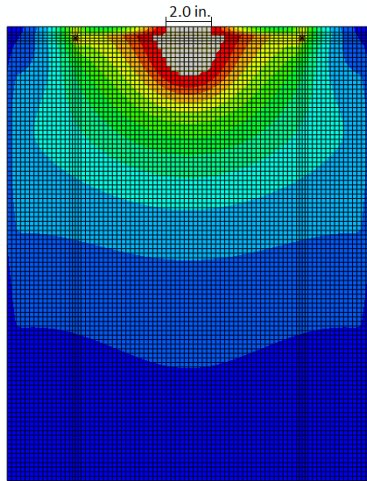


Figure 5-20: 3/8 in. thick A36 (2.51 kip) spread of plasticity

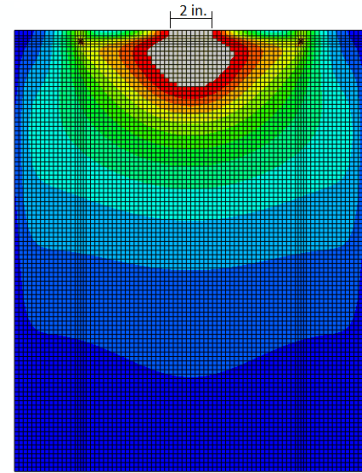


Figure 5-22: 1 in. thick A36 (19.21 kip) spread of plasticity

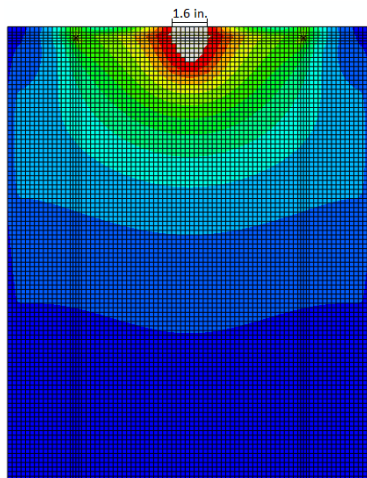


Figure 5-21: 3/8 in. thick A514 (5.87 kip) spread of plasticity

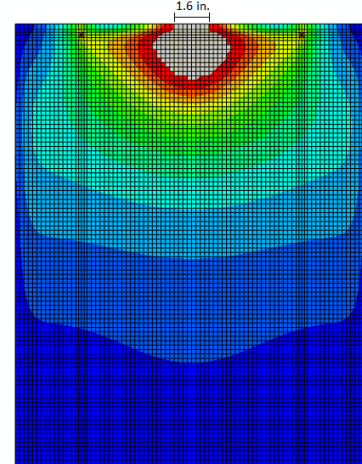


Figure 5-23: 1 in. thick A514 (47.86 kip) spread of plasticity

5.7.2 Demonstration of Offset Method

Typical load-deformation response for the 3/8 in. thick, A36 steel specimens is described here.

The prototype device load, P_Y , taken at the offset value of 0.005 in. correlates to the dynamic yield properties of the plate. The load-deformation response with the identified P_Y is shown in Figure 5-23.

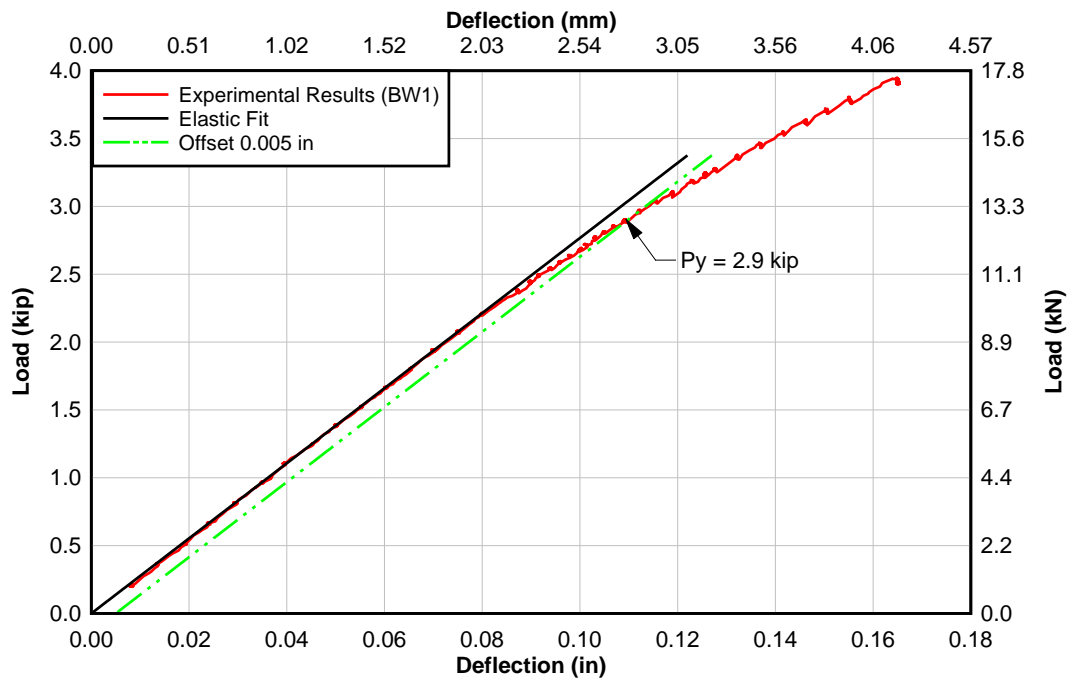


Figure 5-24: Prototype device yielding load using offset method for 3/8 in. thick A36 plate BW1

The axially-loaded plate response with identified P_Y , is shown in Figure 5-25. Pulling the plate specimen in the UTM created unintended bending stresses. These stress components were resolved by the strain gages mounted to the specimens shown in Figure 4-9 and Figure 5-26. The weak axis bending was larger than the strong axis bending as shown in

Figure 5-28. The axial stresses are the largest component and the weak-axis bending induces +/- 1.8 ksi (25 MPa) at the plate surface. This results in earlier yielding than would be expected without the bending contributions. The expected device load for the 12 ksi surface stress effect was interpolated between the 10 ksi and 20 ksi models.

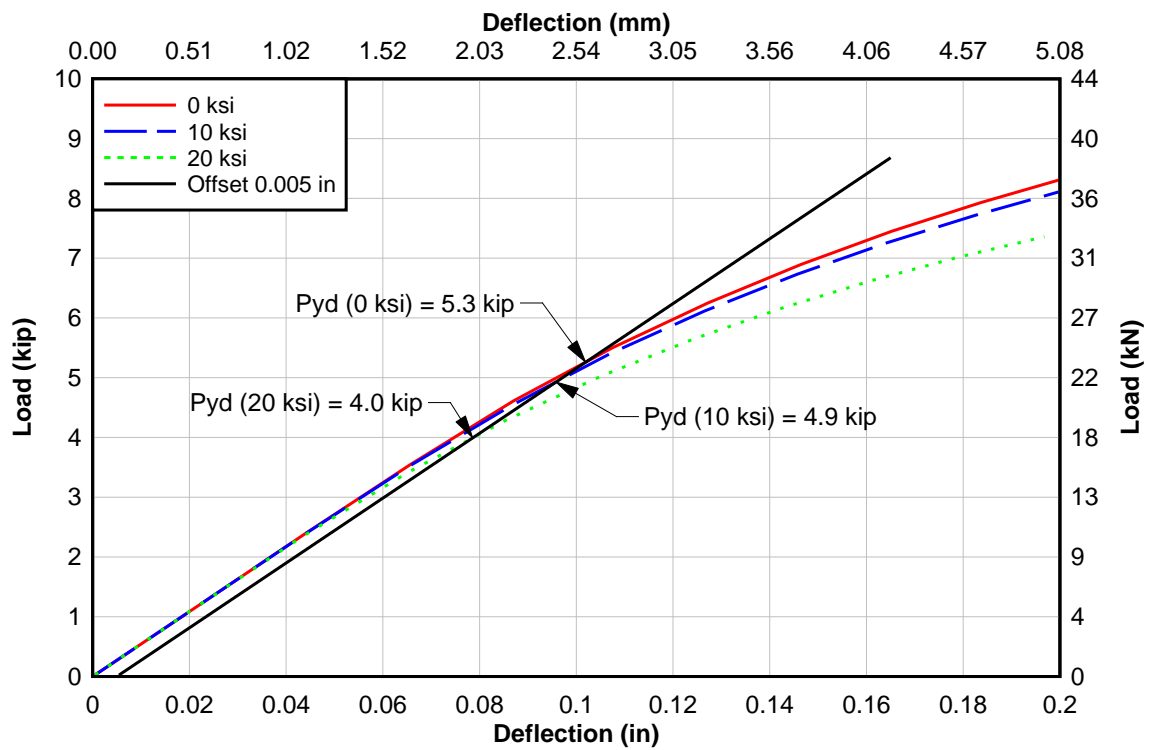


Figure 5-25: FE predicted effect of axial stresses on P_Y for 1/2 in. thick A36 plate

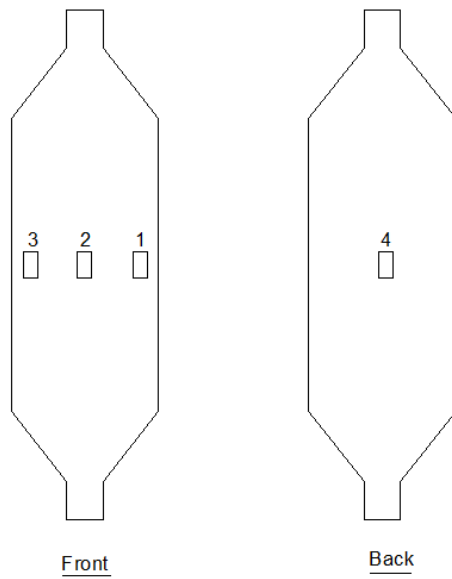


Figure 5-26: Strain gauge locations on specimen

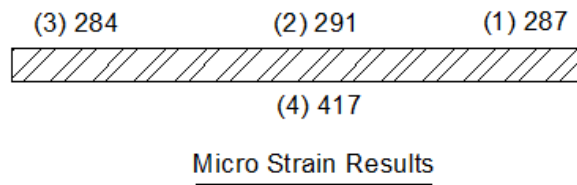


Figure 5-27: Measured strain gauge readings (microstrain) in 1/2 in. thick A36 plate with 10 ksi nominal axial stresses

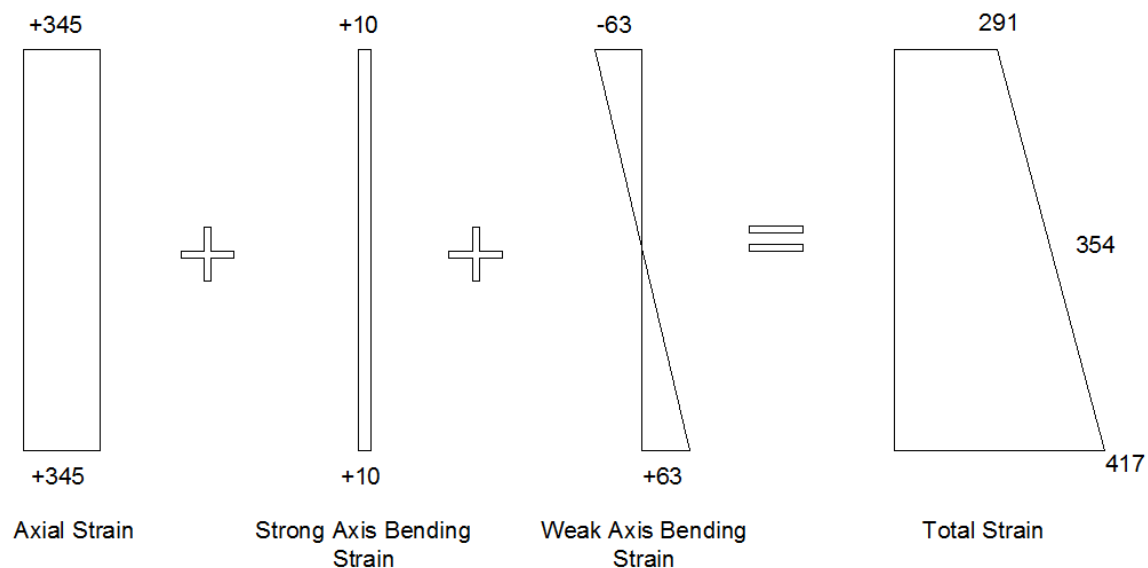


Figure 5-28: Stresses in plate when pulled in UTM (microstrain)

The experimentally measured P_Y values for the different specimens were determined at the prescribed 0.005 in. offset. The loads were correlated to the predicted load-deformation response from FE analysis of plate specimens with a range of dynamic yield stresses shown in Figure 5-29. The relationship between P_Y and yield stress was developed by performing FE analysis for a range of material properties considering the different plate thicknesses and types (free and axially loaded) at the 0.005 in. offset for each curve. An example is presented in Figure 5-30 and the relationship between the device load at 0.005 in. offset and yield stress is seen to vary linearly.

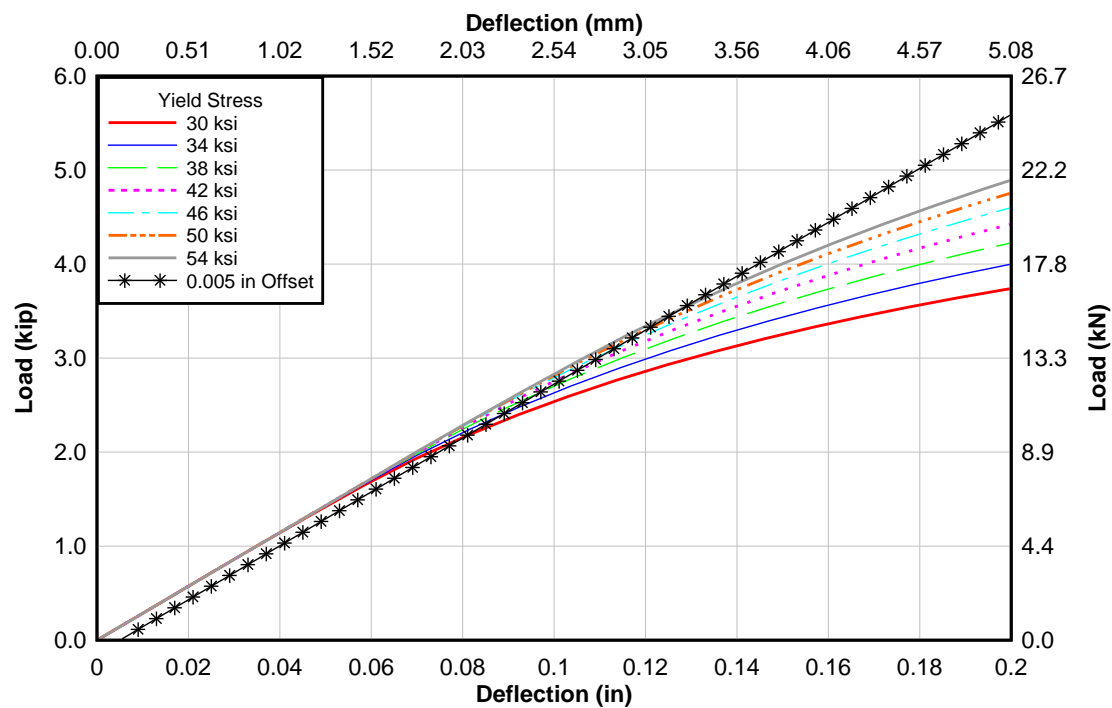


Figure 5-29: Load-deformation response for 3/8 in. thick plate with different yield stress materials

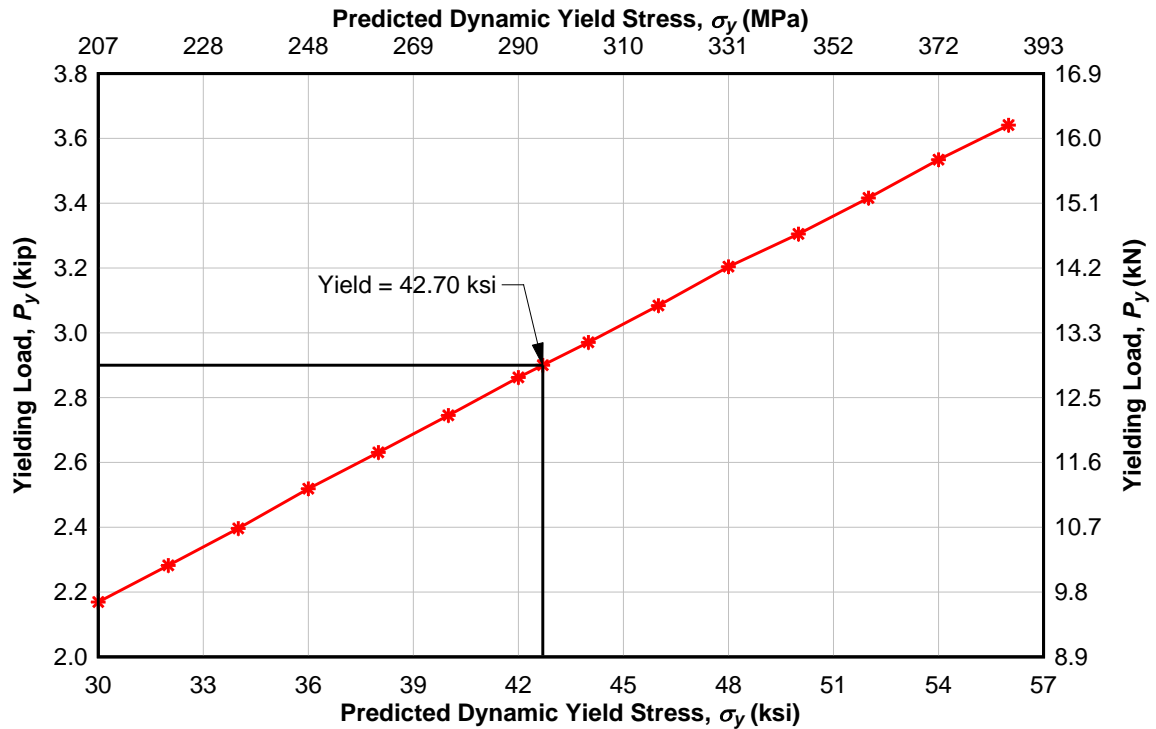


Figure 5-30: Prototype device load at 0.005 in. offset correlated to yield stress for 3/8 in. thick steel plate

The predicted yield stress value for each specimen is presented in Table 5-3. Statistical analysis was performed on the data to calculate the mean and standard deviation of the predicted yield stress. The data could be reasonably modeled as normally distributed. Because there is variability in the data, a yield stress prediction safety factor, α was introduced to account for the uncertainty in the test method and reduce the likelihood of overestimating the yield stress of the plate.

Table 5-3: Predicted yield stress results from plate specimens

A36 3/8 in			A36 1/2 in			Gr. 50 3/8 in		
Sample	P_y (kip)	Predicted σ_y (ksi)	Sample	P_y (kip)	Predicted σ_y (ksi)	Sample	P_y (kip)	Predicted σ_y (ksi)
PW1	3.03	45.05	PN1	4.85	39.57	PN3	3.18	49.49
PW1s	2.83	41.45	PN3	4.92	40.27	TN1	3.55	56.15
PW2	2.95	43.62	TN3	5.9	50.28	TN3	4.09	65.86
PW2s	2.90	42.70	σ	0.59	5.99	σ	0.46	8.23
PW3	2.84	41.62	μ (ksi)	5.22	43.38	μ (ksi)	3.61	57.16
PW3s	2.78	40.59	COV	0.11	0.14	COV	0.13	0.14
TW1s1	2.88	42.33	A36 1/2 in (10 ksi)			Gr. 50 3/8 in (10 ksi)		
TW2	3.08	45.93	Sample	P_y (kip)	Predicted σ_y (ksi)	Sample	P_y (kip)	Predicted σ_y (ksi)
TW2s	2.91	42.88	TN2a	5.15	47.77	PN1a	3.34	57.76
TW3s	2.86	41.96	TN2b	5.65	52.44	PN1b	3.82	65.45
BW1	2.90	42.70	σ	0.35	3.30	σ	0.34	5.44
BW1s	3.17	47.43	μ (ksi)	5.40	50.11	μ (ksi)	3.58	61.61
BW2	2.87	42.14	COV	0.07	0.07	COV	0.09	0.09
BW2s	3.05	45.40	A36 1/2 in (20 ksi)			Gr. 50 3/8 in (20 ksi)		
σ	0.11	1.96	Sample	P_y (kip)	Predicted σ_y (ksi)	Sample	P_y (kip)	Predicted σ_y (ksi)
μ (ksi)	2.93	43.27	PN2a	3.82	40.05	TN2a	2.95	53.80
COV	0.04	0.05	PN2b	3.82	40.05	TN2b	3.11	56.41
			σ	0.00	0.00	σ	0.11	1.85
			μ (ksi)	3.82	40.05	μ (ksi)	3.03	55.10
			COV	0.00	0.00	COV	0.04	0.03

The yield stress prediction safety factor was calculated by normalizing all predicted yield stress results from the prototype device in relation to the nominal stress from the coupon samples as:

$$Bias = \frac{\sigma_{prototype\ device}}{\sigma_{nominal\ coupon}} \quad [5.1]$$

A probability of underestimating the yield stress of 1/10,000 (~3.5 standard deviations from the mean) was selected and for the bias and standard deviation (normalized standard deviation = 0.076 and mean = 1.023) results in an α of 0.74. This significantly reduces the predicted yield stress from the likely yield stress as shown in Table 5-4.

Table 5-4: Predicted yield stress

	Sample	Predicted σ_y (ksi)	Actual σ_y (ksi)	Bias	Factored by α_1, σ_y (ksi)	Factored by α_3, σ_y (ksi)
A36 3/8 in	PW1	45.05	41.79	1.08	32.68	38.29
	PW1s	41.45	41.79	0.99	30.07	35.23
	PW2	43.62	41.79	1.04	31.65	37.08
	PW2s	42.70	41.79	1.02	30.98	36.29
	PW3	41.62	41.79	1.00	30.20	35.38
	PW3s	40.59	41.79	0.97	29.45	34.51
	TW1s1	42.33	41.79	1.01	30.71	35.98
	TW2	45.93	41.79	1.10	33.32	39.04
	TW2s	42.88	41.79	1.03	31.11	36.45
	TW3s	41.96	41.79	1.00	30.44	35.67
	BW1	42.70	41.79	1.02	30.98	36.29
	BW1s	47.43	41.79	1.14	34.41	40.32
	BW2	42.14	41.79	1.01	30.57	35.82
	BW2s	45.40	41.79	1.09	32.94	38.59
A36 1/2 in	PN1	39.57	42.13	0.94	28.71	33.64
	PN3	40.27	42.13	0.96	29.22	34.23
	TN3	50.28	44.89	1.12	36.48	42.74
Gr. 50 3/8 in	PN3	49.49	56.84	0.87	35.91	42.07
	TN1	56.15	58.72	0.96	40.74	47.72
	TN3	65.86	58.72	1.12	47.78	55.98
A36 1/2 in (10 ksi)	TN2a	45.93	44.89	1.02	33.32	39.04
	TN2b	50.53	44.89	1.13	36.66	42.95
Gr. 50 3/8 in (10 ksi)	PN1a	55.98	56.84	0.98	40.62	47.58
	PN1b	63.59	56.84	1.12	46.14	54.05
A36 1/2 in (20 ksi)	PN2a	38.51	42.13	0.91	27.94	32.73
	PN2b	38.51	42.13	0.91	27.94	32.73
Gr. 50 3/8 in (20 ksi)	TN2a	51.82	58.72	0.88	37.60	44.05
	TN2b	54.21	58.72	0.92	39.33	46.08

The conservativeness of using an α_1 of 0.74 may result in low bridge ratings when the intended use of this device is to determine the in-situ yield stress of a plate to obtain greater accuracy during bridge evaluation. Therefore to increase α , multiple replicate measurements can be taken, which will reduce the standard deviation. If three replicate tests are made on a plate, α_3 increases to 0.86. A value of 0.85 was chosen as the final factor for three (3) readings. Using this value would predict the yield stress of the plates very close to the nominal value in the previous table.

Table 5-5: Yield stress prediction safety factor for various test readings

Number of Tests	Factor, α
1	0.74
2	0.82
3	0.86
4	0.88
5	0.9

Similarly to Figure 5-30, Figure 5-31 correlates the calculated prototype device load to the dynamic yield stress of a steel plate for multiple plate thicknesses. Once a yield stress is calculated then the chosen safety factor can be applied. While this report states using a factor of 0.85 for three (3) readings, there is flexibility for bridge owners and rating engineers to decide what probability of over estimation they are willing to tolerate and may adjust the factors accordingly.

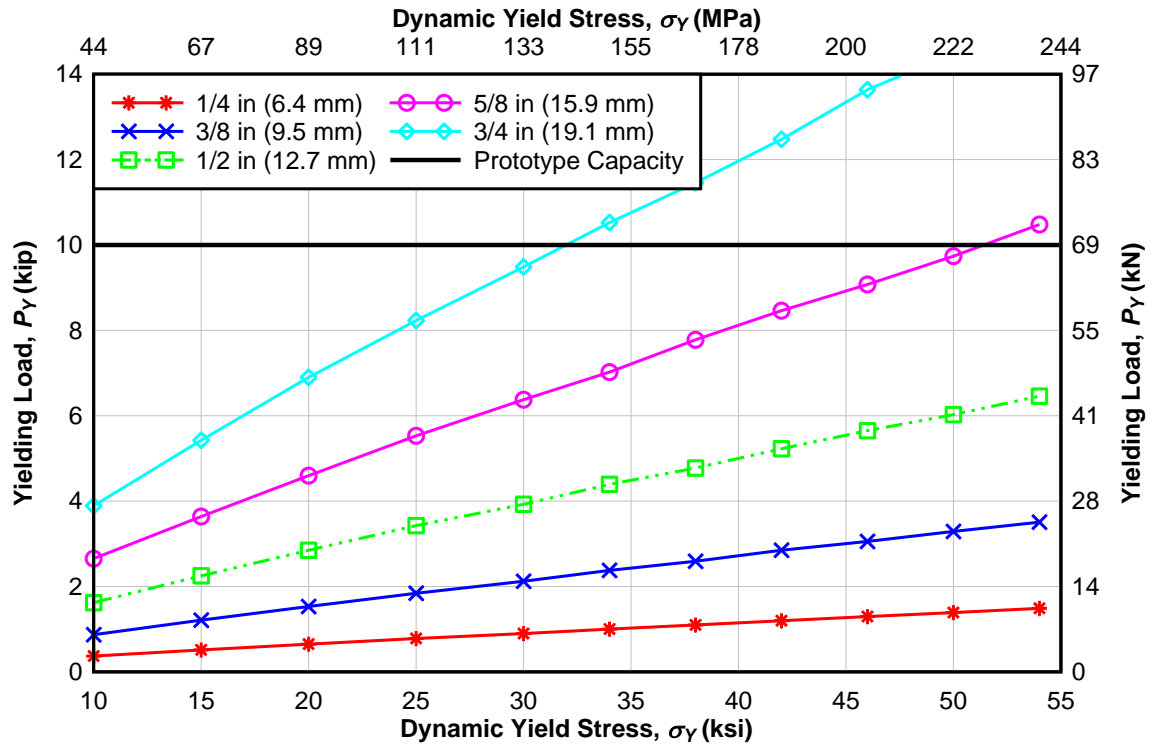


Figure 5-31: Relationship between dynamic yield stress and prototype device load for various plate thicknesses with no yield stress prediction safety factor

5.7.3 Prototype Device Testing on Spare Gusset Plate

To examine the finalized method, a spare 3/8 in. thick gusset plate left in the Oregon State Laboratory was tested. The prototype device was applied to the edge of the plate, and three measurements were taken (See Figure 5-32).



Figure 5-32: Gusset plate test with spare plate in OSU laboratory

Averaging the offset results from the three measurements resulted in a P_Y of 3.23 kips (14.37 kN). Using Figure 5-31, the yield stress associated with a 3/8 in. thick plate was determined to be 48.99 ksi (337.8 MPa). Multiplying the yield stress by the safety factor of 0.85, the final dynamic yield stress is calculated to be 41.64 ksi (287.1 MPa). Based on the material results for the gusset plate, the dynamic yield stress was specified as 50.3 ksi (346.8 MPa) which is within 2% of the non-factored yield stress calculated by the prototype device. This test verifies that the prototype can appropriately determine the yield stress of a gusset plate non-destructively. Additionally, when these plates were ordered they were ordered as A36 material. The prototype results allow for the engineer giving a load rating to use 41.64 ksi instead of the nominal 36 ksi which will help increase the rating of the bridge and diminish unnecessary retrofits.

6 CONCLUSIONS

In order to allow bridge owners to improve the evaluation and rating of gusset plate connections, a prototype device was developed to non-destructively obtain the material properties for steel gusset plates. The prototype device applies an out-of-plane load to the edge of a plate causing bending of the plate. As the applied load is increased, the plate eventually begins to yield. This produces nonlinear load-deformation response which was used to identify the transition from elastic to inelastic behavior. The dynamic yield stress of the plate was correlated to the prototype device load through calibrated finite element analysis. The device was applied to several plate thickness and material types and the yield stress was correlated to the dynamic yield stress over a wide range of material thicknesses. Based on the testing and analysis conducted in this research, the following conclusions are presented:

- A prototype device was developed to nondestructively estimate the dynamic yield stress of gusset plates.
- Yield stress was ascertained from the device by measuring the applied load-plate deformation response and taking an offset of 0.005 in. from the elastic portion of the curve. (Similar to the 0.2% offset specified in the ASTM E8 standard)
- The yield stress for a given plate thickness can be established by observing the applied device load at the prescribed offset. This yield stress correlates to an approximate spread of plasticity of 2 in. on the free edge where the load is applied.
- Secondary identification of yielding can be detected by observing if the load magnitude drops when device loading is halted.
- Internal stresses from possible dead loads in the plates influenced the device by producing a yielding load earlier than if there are no stresses in the plate.

- Based on the statistical analysis of the device predicted and actual yield stress, a test reliability factor of 0.85 is used to ensure the yield stress is not over-predicted with a 1/10,000 probability when three (3) replicate tests are performed.

Future Work

Future work to be considered with the prototype device include implementing an alternate way to measure deflection of the plate directly under the load point, using a larger bottle jack in order to test thicker and higher strength plates, testing plates with multiple paint layers and full size gusset plates with known material properties, and implementing the prototype device in the field on an actual bridge. Additional methods of determining the load and support conditions to be implemented in the FE model as well as calculating the stiffness of the system should be researched as well. Hardness correlations to yield stress may be considered if additional testing is performed on lower strength bridge steels.

7 BIBLIOGRAPHY

- Abaqus Theory Manual (6.11), Simulia, Web. 05 Sept. 2013.
- AISC (1986) Steel Construction Manual, LRFD 1st Edition, *American Institute of Steel Construction*, Chicago, Illinois
- ASTM A36/A36M – 08 (2008) “Standard Specification for Carbon Structural Steel,” *ASTM International*, West Conshohocken, PA.
- ASTM A370 – 12a (2012) “Standard Test Methods and Definitions for Mechanical Testing of Steel Products,” *ASTM International*, West Conshohocken, PA.
- ASTM A514/A514M - 05 (2009) “Standard Specification for High-Yield stress, Quenched and tempered Alloy Steel Plate, Suitable for Welding,” *ASTM International*, West Conshohocken, PA.
- ASTM A572/A572M - 12 (2012) “Standard Specification for High-Strength Low-Alloy Columbium-Vanadium Structural Steel,” *ASTM International*, West Conshohocken, PA.
- ASTM B265 - 12 (2012) “Standard Specification for High-Strength Low-Alloy Columbium-Vanadium Structural Steel,” *ASTM International*, West Conshohocken, PA.
- ASTM E6 – 09b^{e1} (2009) “Standard Terminology Relating to Methods of Mechanical Testing,” *ASTM International*, West Conshohocken, PA.
- ASTM E8/E8M - 11 (2011) “Standard Test Method for Tension Testing of Metallic Materials,” *ASTM International*, West Conshohocken, PA.
- Beedle, L.S., Tall, I. (1959) “Basic column strength. Original manuscript for “Basic Column Strength.” September 1959 and publications Proc. ASCE, 86 (ST7), pp. 139, (July 1960).” *Fritz Laboratory Reports*. Paper 1507
- Cahoon, J.R., Broughton, W.H., Kutzak, A.R. (1971) “The Determination of Yield stress from Hardness Measurements,” *Journal of Metallurgical Transactions*, V. 2, No. 7, July, pp. 1979-1983.
- Callister Jr., W.D (2000) *Materials Science and Engineering*, Oxford University Press, New York
- Datsko, J., Hartwig, L., McClory, B. (2001) “On the Tensile Strength and Hardness Relation for Metals,” *Journal of Materials Engineering and Performance*, V. 10, No. 6, December, pp. 718-722.
- Hibbitt, Karlsson & Sorensen, Inc. (2002) ABAQUS/Standard (Version 6.3-8) [Computer Software]
- Hitchings, I.M (2009) “The contributions of David Tabor to the science of indentation hardness,” *Journal of Materials Research*, V. 24, No. 3, March, pp. 581-589.

- Kowalkowski, K.J., Varma, A.H. (2007) "Structural Properties of Steels Subjected to Multiple Cycles of Damage Followed by Heating Repair," *Journal of Structural Engineering*, V. 133, pp. 283-296.
- Moore, M., Beshah, F., and Washer, G. (2001) "Investigation of Properties of Historic Steels," unpublished Federal Highway Report, Non Destructive Evaluation Validation Center, Contract no. DTFH61-96-C-00054, McLean, VA.
- Murty, K., Mathew, M.D., Miraglia, P.Q., Snah, V.N., Haggag, F.M. (1998) "Non-Destructive Evaluation of Deformation and Fracture Properties of Materials Using Stress-Strain Microprobe," *Journal of Nondestructive characterization of materials in aging system*, V. 503, pp. 327-337.
- NagarajaRao, N., Lohrmann, M., and Tall, L. (1966) "Effect of strain rate on the yield stress of structural steel." *ASTM Journal of Materials*, V. 1, No. 1, March.
<<http://preserve.lehigh.edu/engr-civil-environmental-fritz-lab-reports/1684>>
- Pavlina, E.J., Van Tyne, C.J. (2008) "Correlation of Yield stress and Tensile Strength with Hardness for Steels," *Journal of Materials Engineering and Performance*, V. 17, No. 6, December, pp. 888-893.
- Speich, G.R., Warlimont, H. (1968) "Yield stress and Transformation Substructure of Low-Carbon Martensite," *Journal of Iron and Steel Institute*, V. 206, April, pp. 385-392.
- Szilar, R. (1974) *Theory and Analysis of Plates: Classical and Numerical Methods*, Prentice-Hall, New Jersey.
- Tabor, D., (1951) *The Hardness of Metals*, Oxford University Press, New York

APPENDECIES

A. MATERIALS TESTING RESULTS

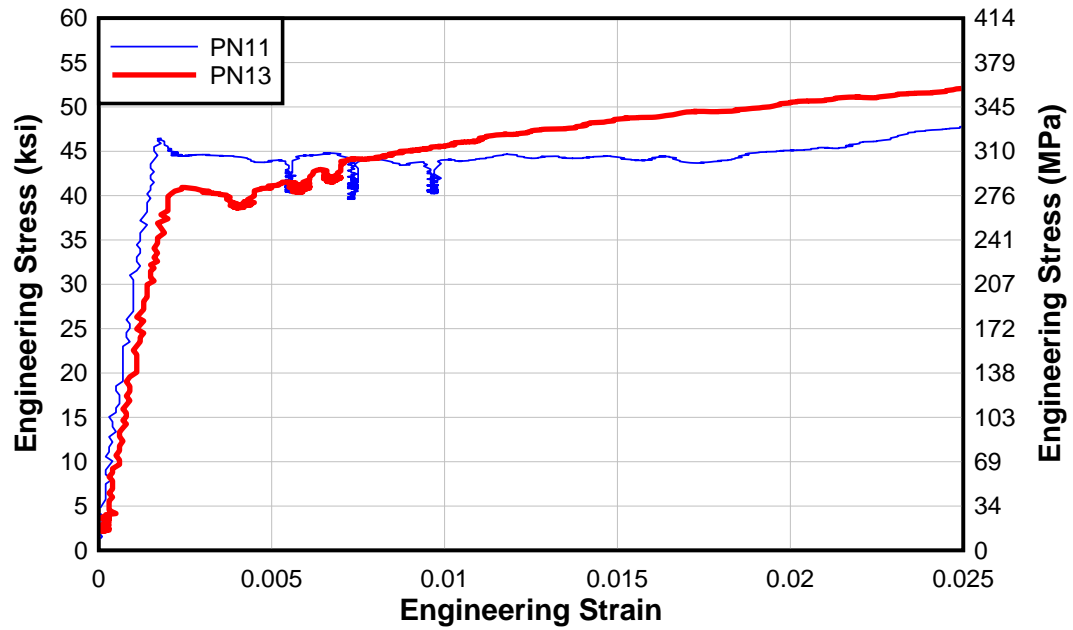


Figure A-1: Engineering stress vs. engineering strain for the parallel rolling direction 3/8 in. thick A36 sample PN1

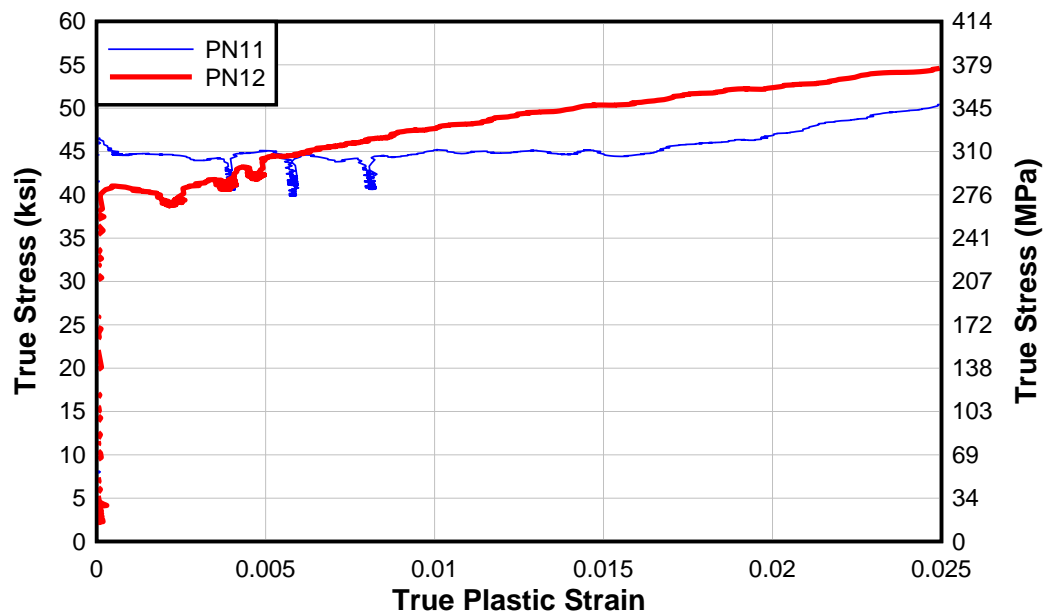


Figure A-2: True stress vs. true plastic strain for the parallel rolling direction 3/8 in. thick A36 sample PN1

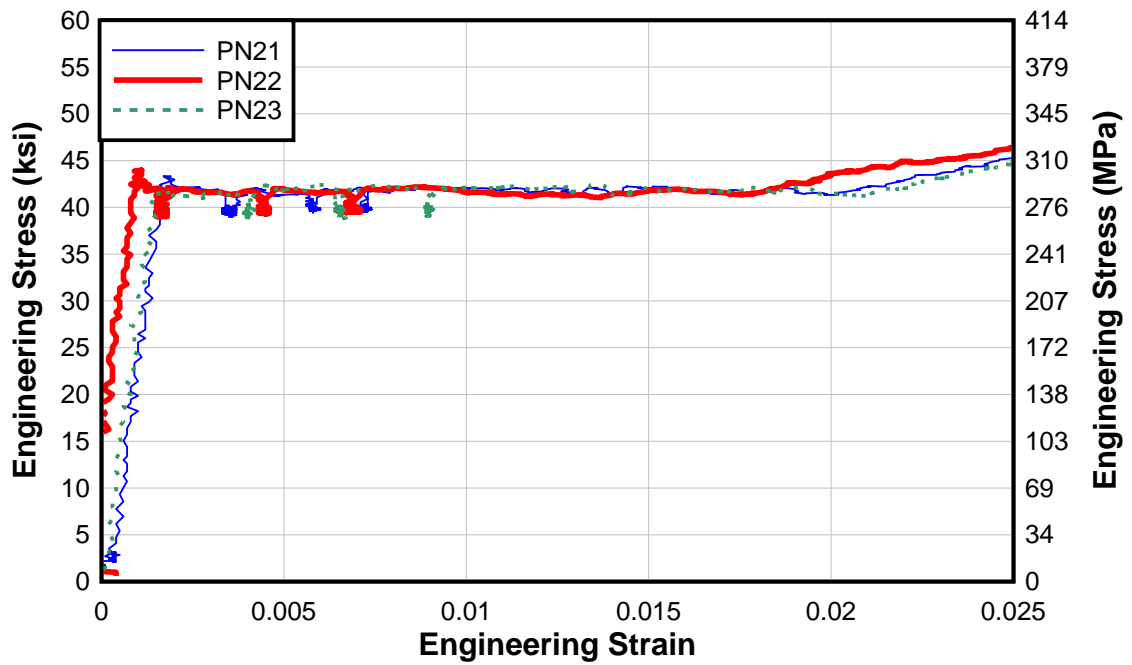


Figure A-3: Engineering stress vs. engineering strain for the parallel rolling direction 3/8 in. thick A36 sample PN2

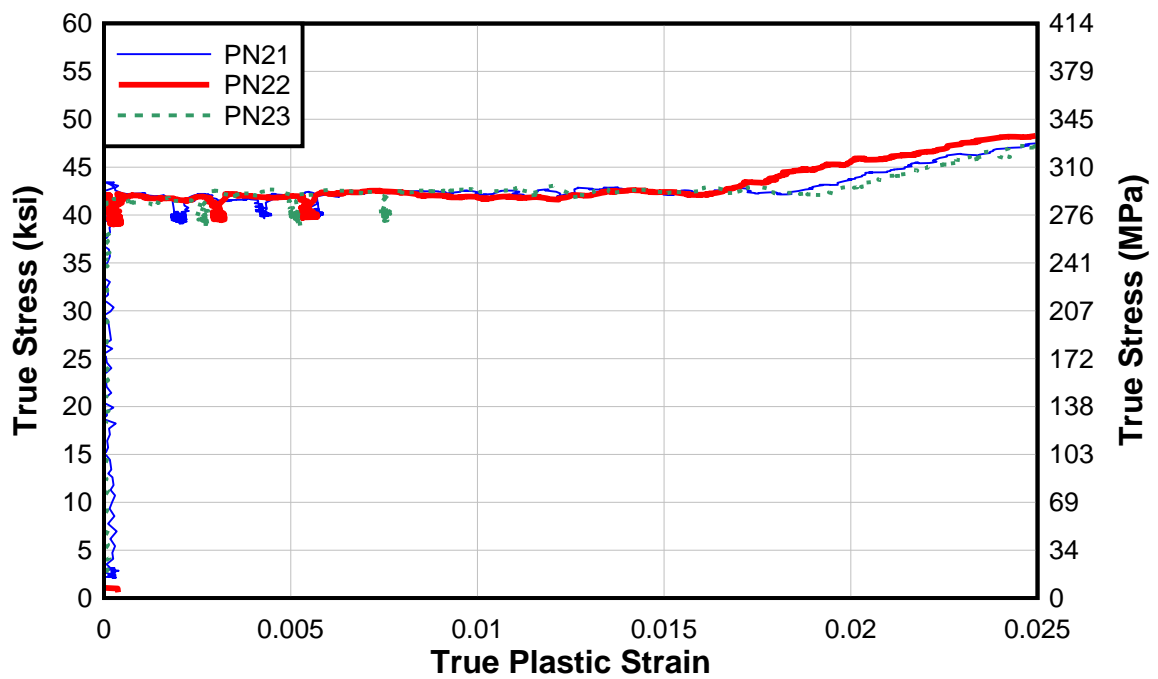


Figure A-4: True stress vs. true plastic strain for the parallel rolling direction 3/8 in. thick A36 sample PN2

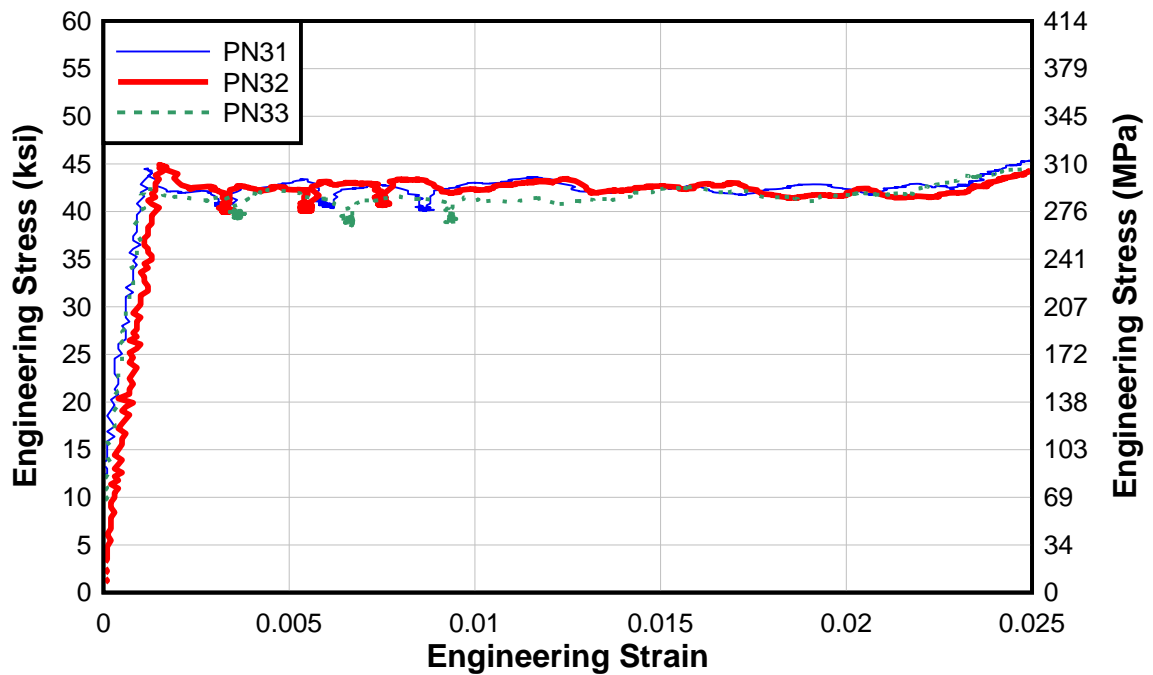


Figure A-5: Engineering stress vs. engineering strain for the parallel rolling direction 3/8 in. thick A36 sample PN3

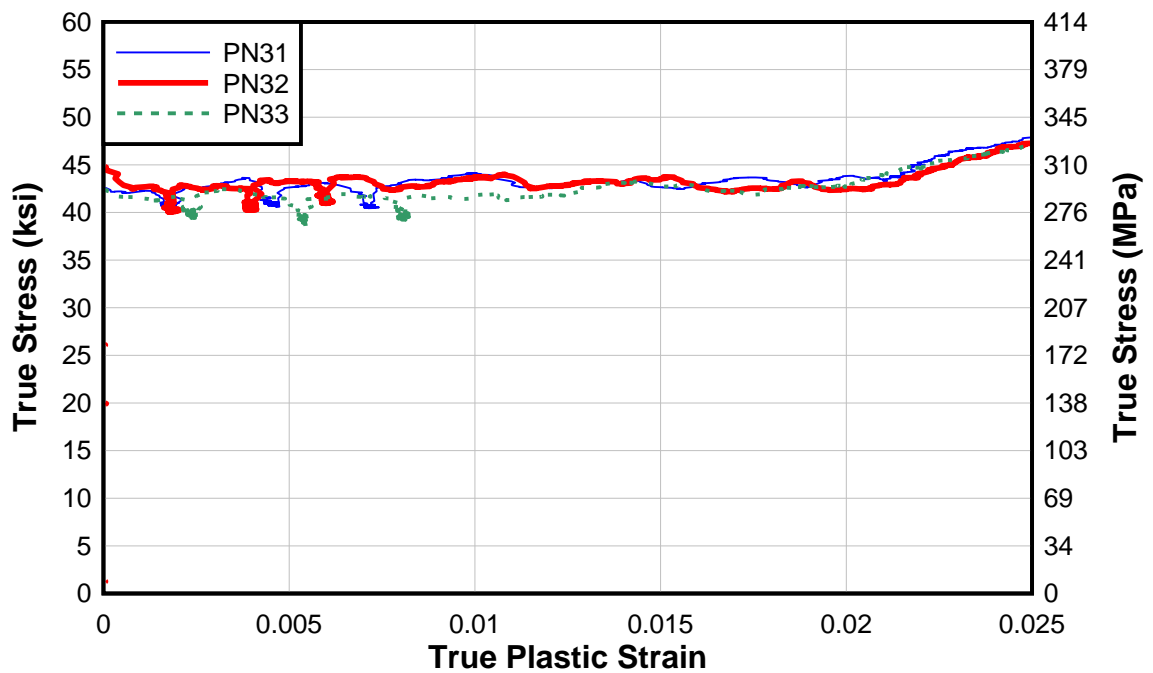


Figure A-6: True stress vs. true plastic strain for the parallel rolling direction 3/8 in. thick A36 sample PN3

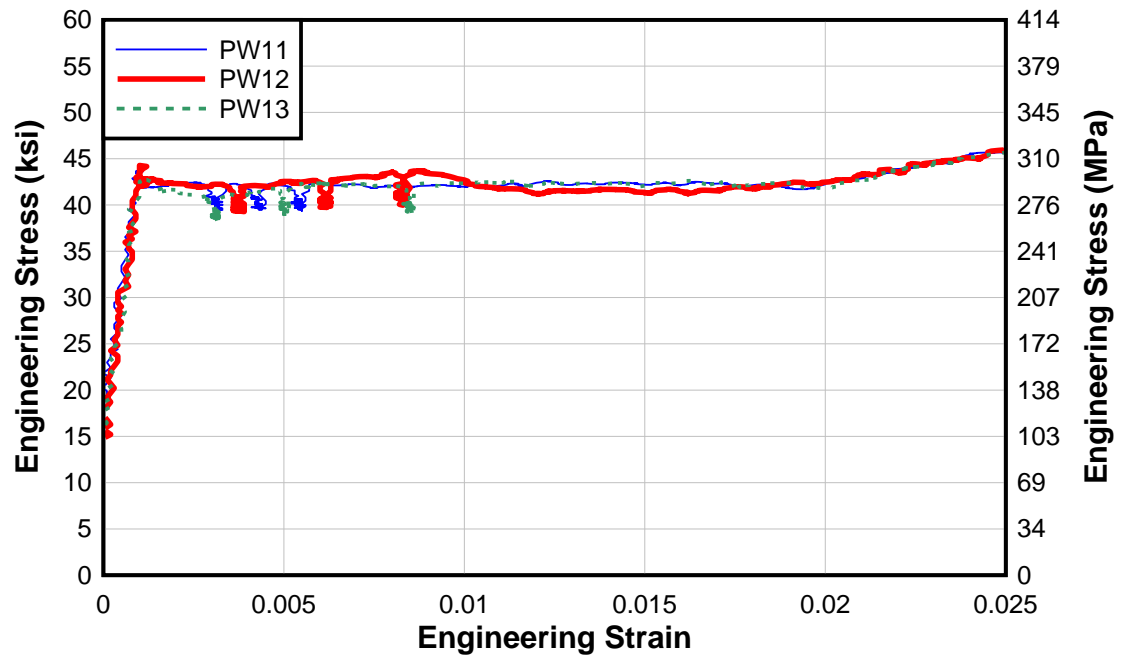


Figure A-7: Engineering stress vs. engineering strain for the parallel rolling direction 3/8 in. thick A36 sample PW1

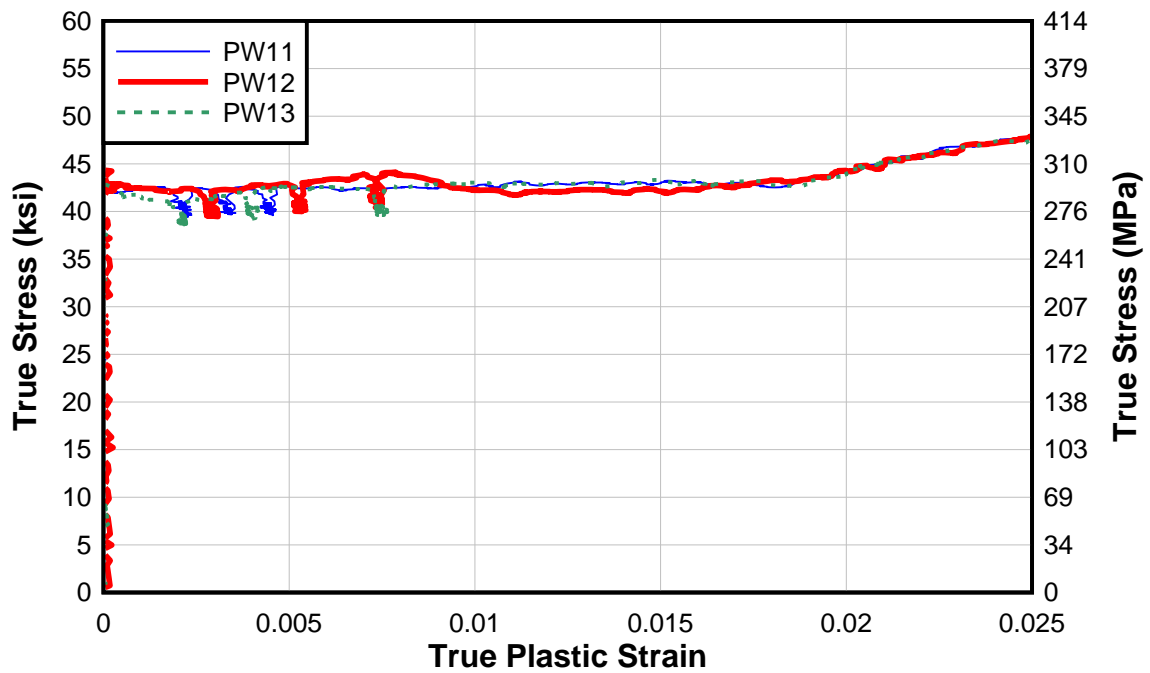


Figure A-8: True stress vs. true plastic strain for the parallel rolling direction 3/8 in. thick A36 sample PW1

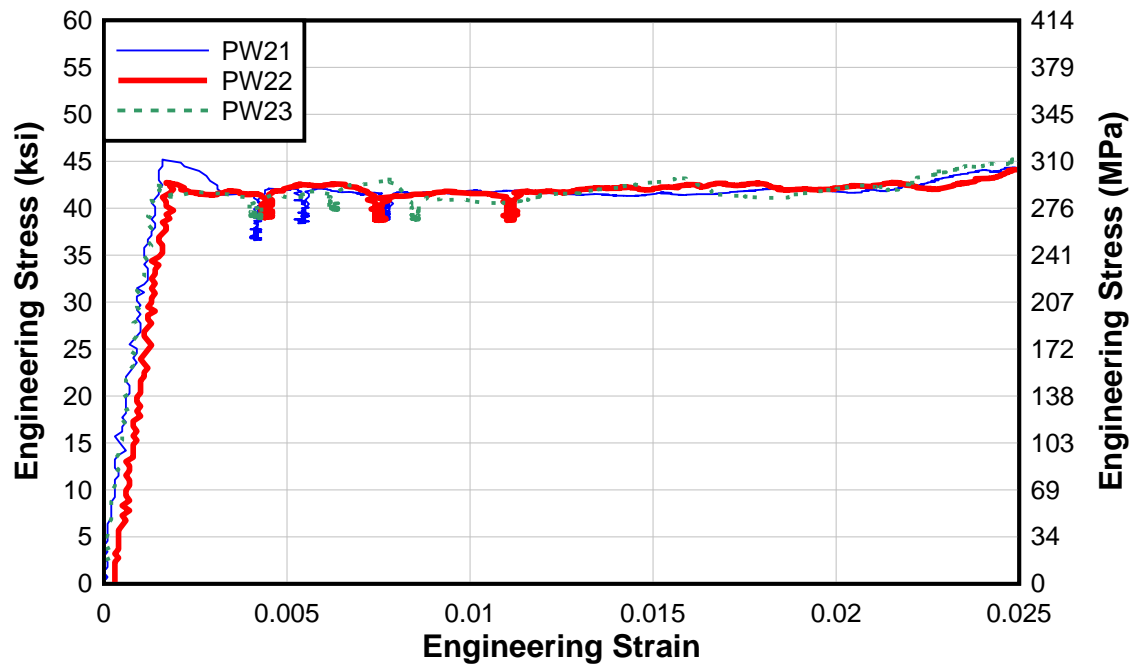


Figure A-9: Engineering stress vs. engineering strain for the parallel rolling direction 3/8 in. thick A36 sample PW2

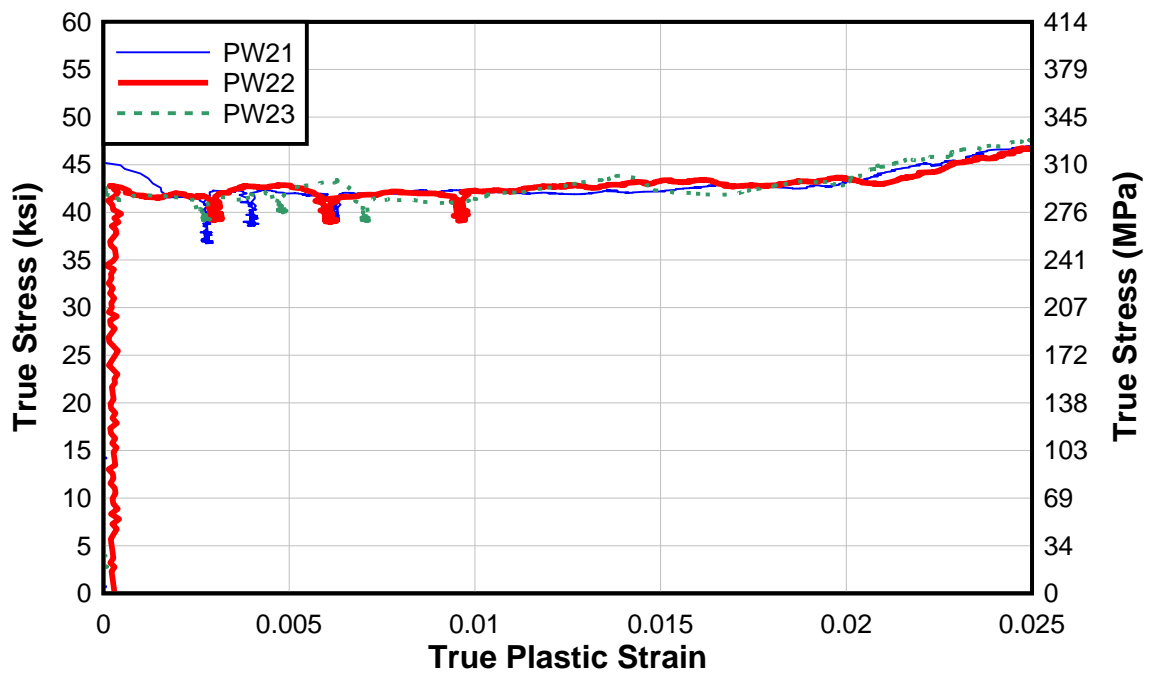


Figure A-10: True stress vs. true plastic strain for the parallel rolling direction 3/8 in. thick A36 sample PW2

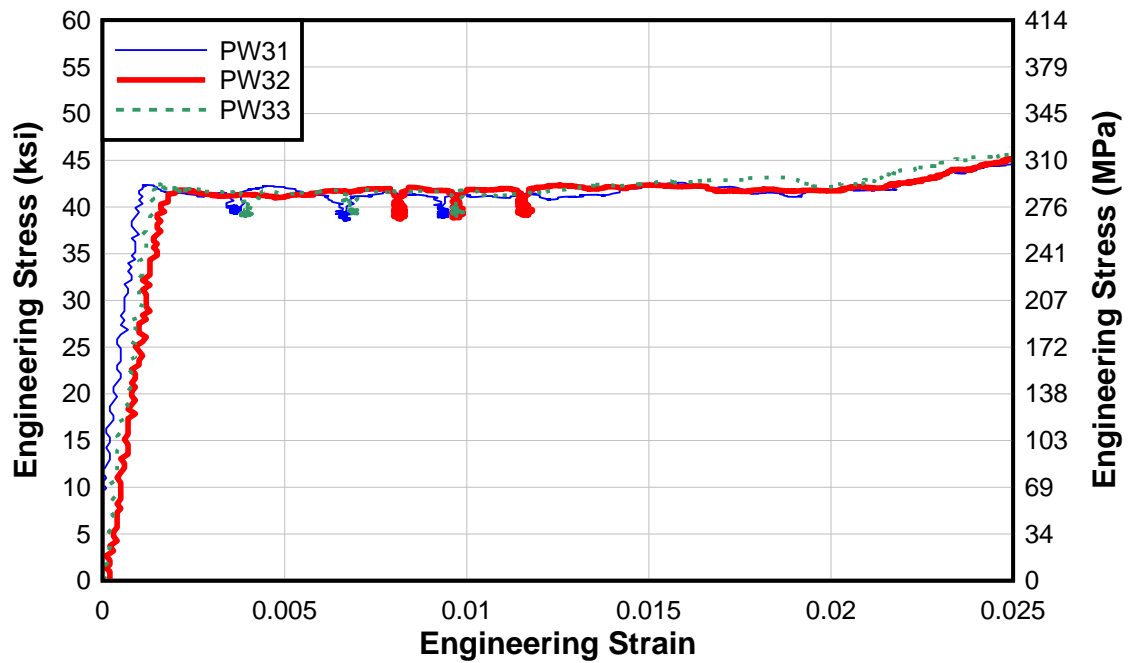


Figure A-11: Engineering stress vs. engineering strain for the parallel rolling direction 3/8 in. thick A36 sample PW3

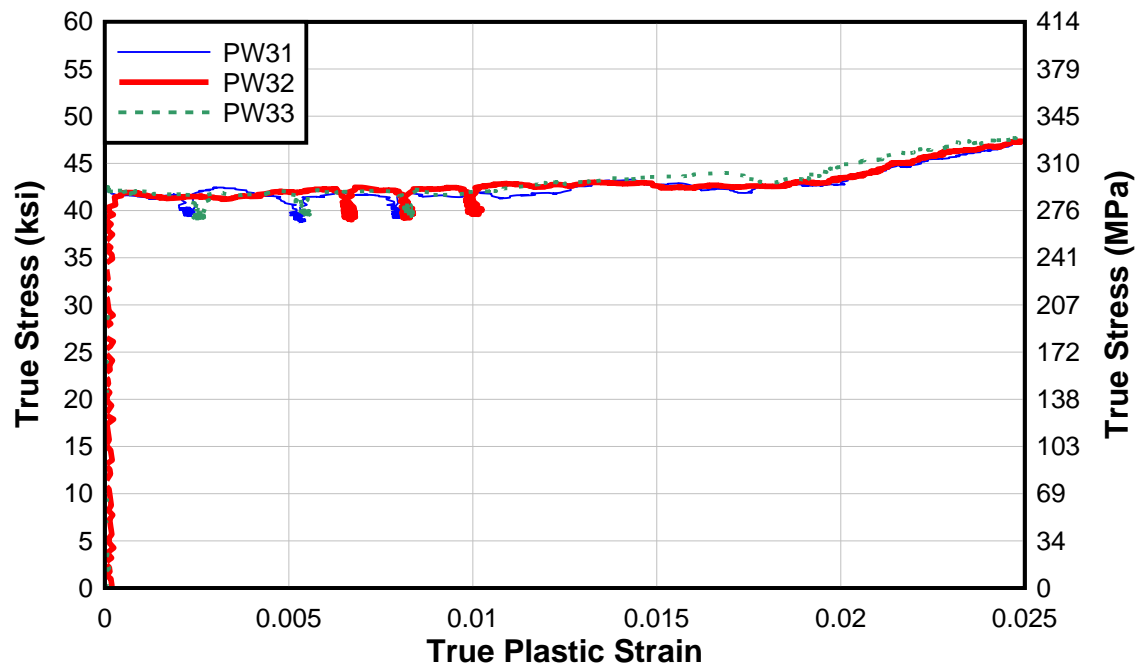


Figure A-12: True stress vs. true plastic strain for the parallel rolling direction 3/8 in. thick A36 sample PW3

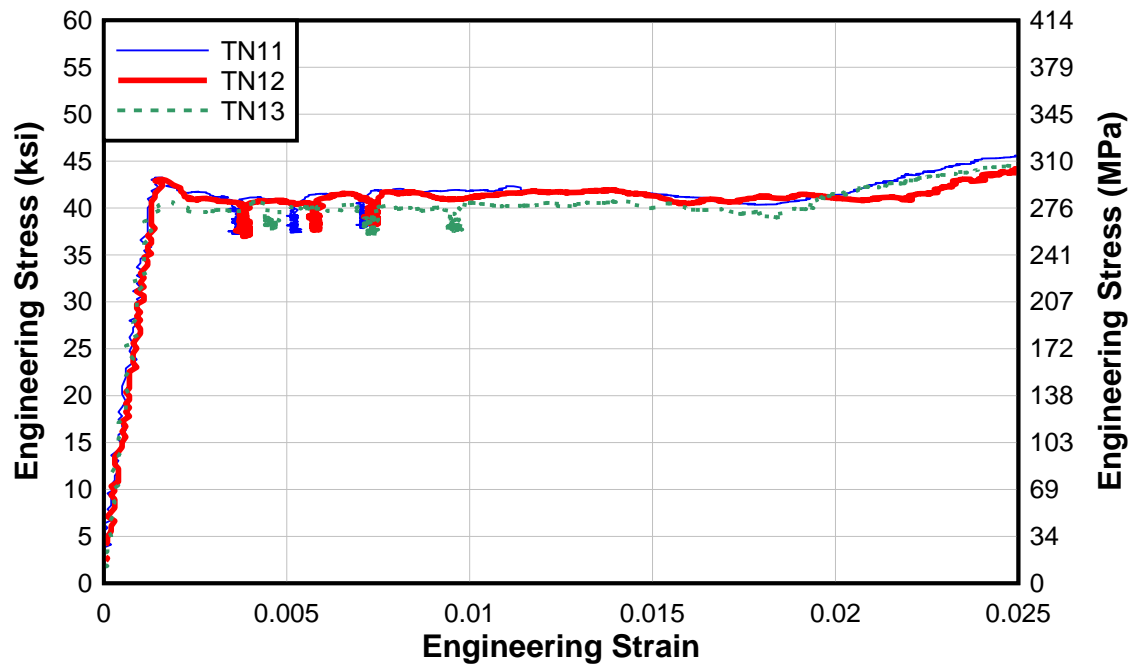


Figure A-13: Engineering stress vs. engineering strain for the transverse rolling direction 3/8 in. thick A36 sample TN1

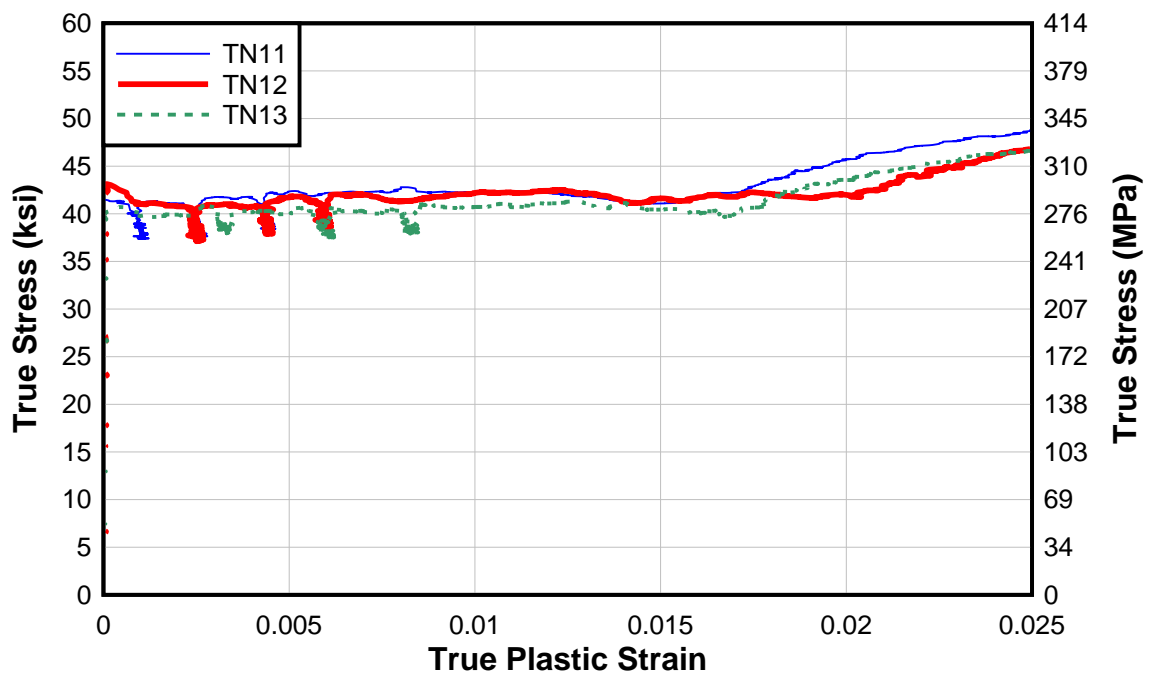


Figure A-14: True stress vs. true plastic strain for the transverse rolling direction 3/8 in. thick A36 sample TN1

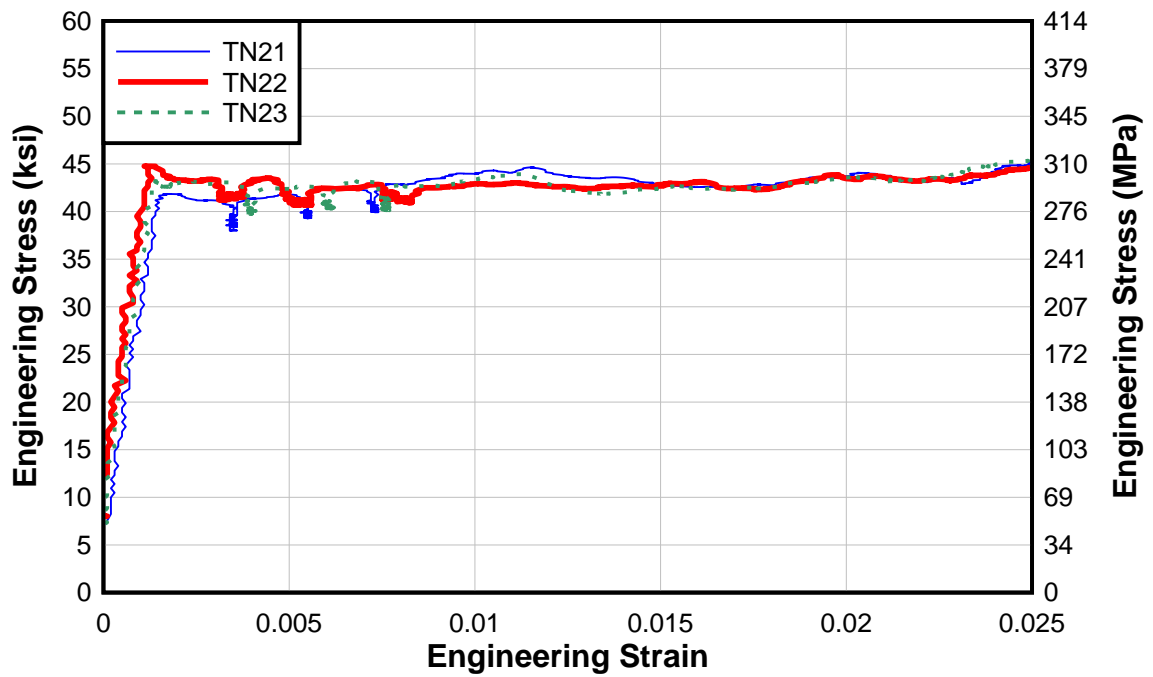


Figure A-15: Engineering stress vs. engineering strain for the transverse rolling direction 3/8 in. thick A36 sample TN2

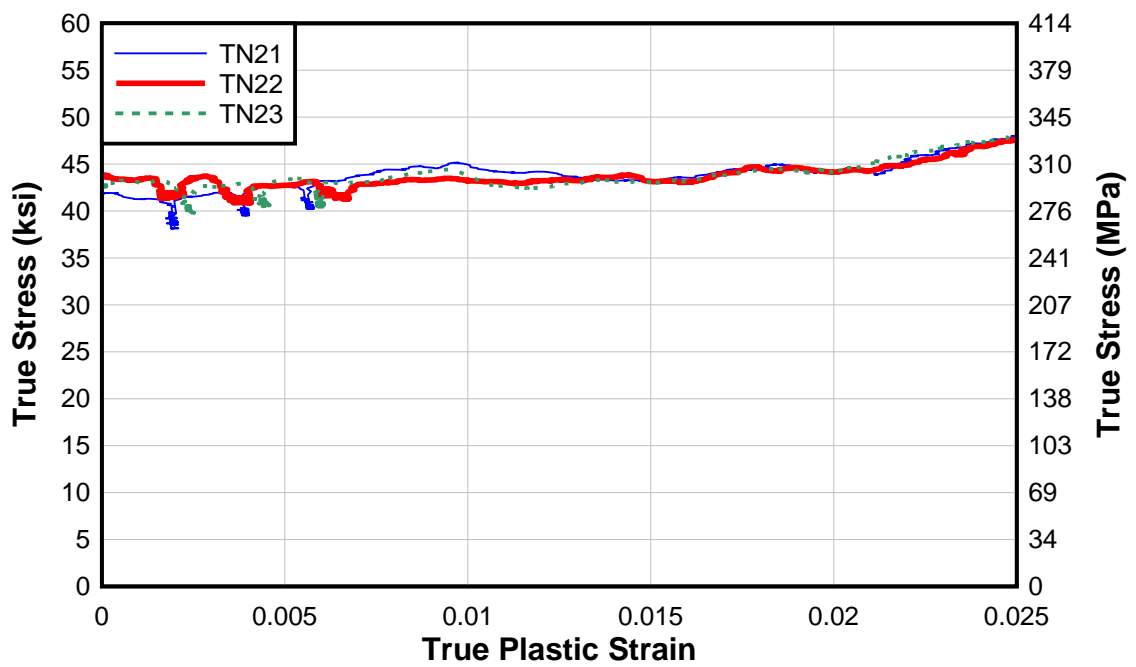


Figure A-16: True stress vs. true plastic strain for the transverse rolling direction 3/8 in. thick A36 sample TN2

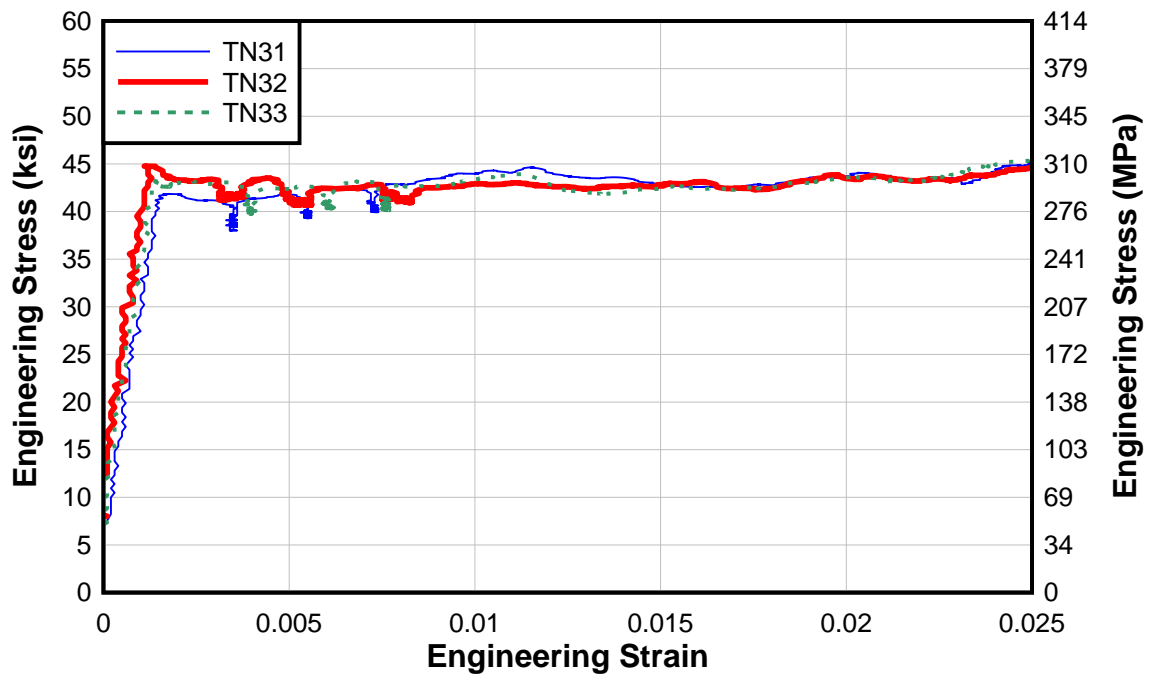


Figure A-17: Engineering stress vs. engineering strain for the transverse rolling direction 3/8 in. thick A36 sample TN3

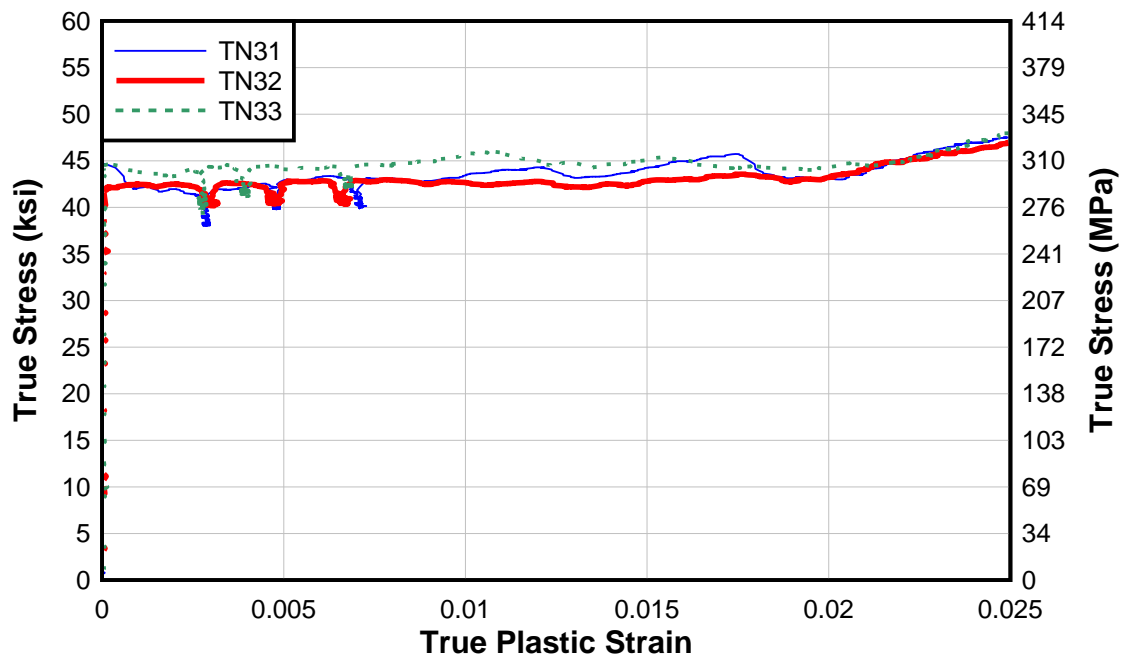


Figure A-18: True stress vs. true plastic strain for the transverse rolling direction 3/8 in. thick A36 sample TN3

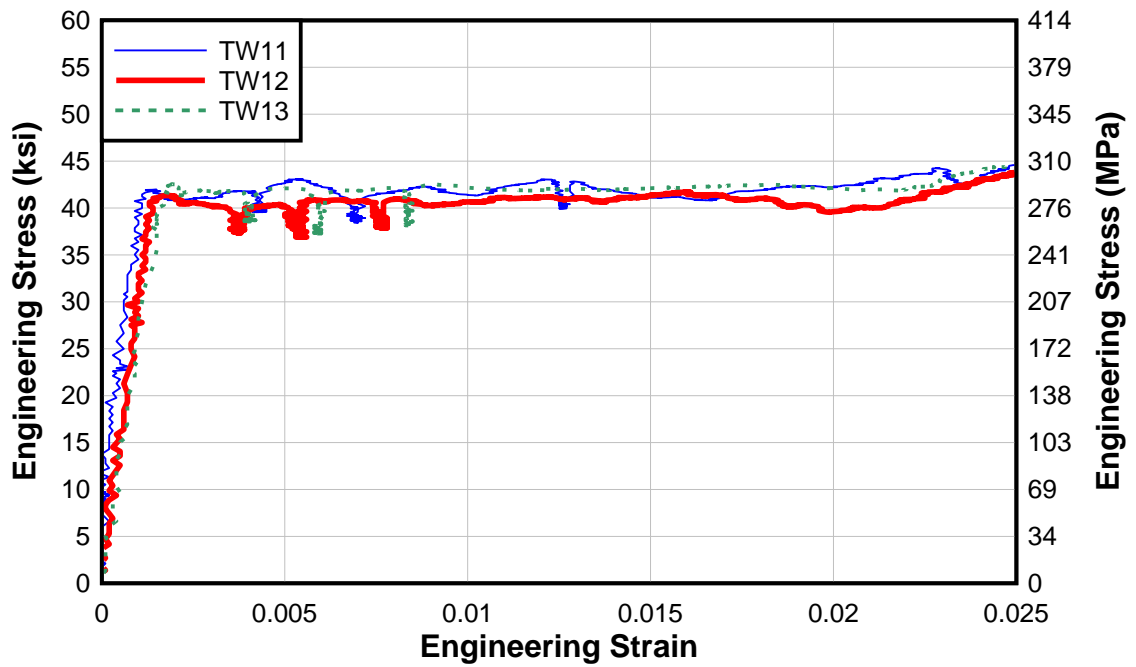


Figure A-19: Engineering stress vs. engineering strain for the transverse rolling direction 3/8 in. thick A36 sample TW1

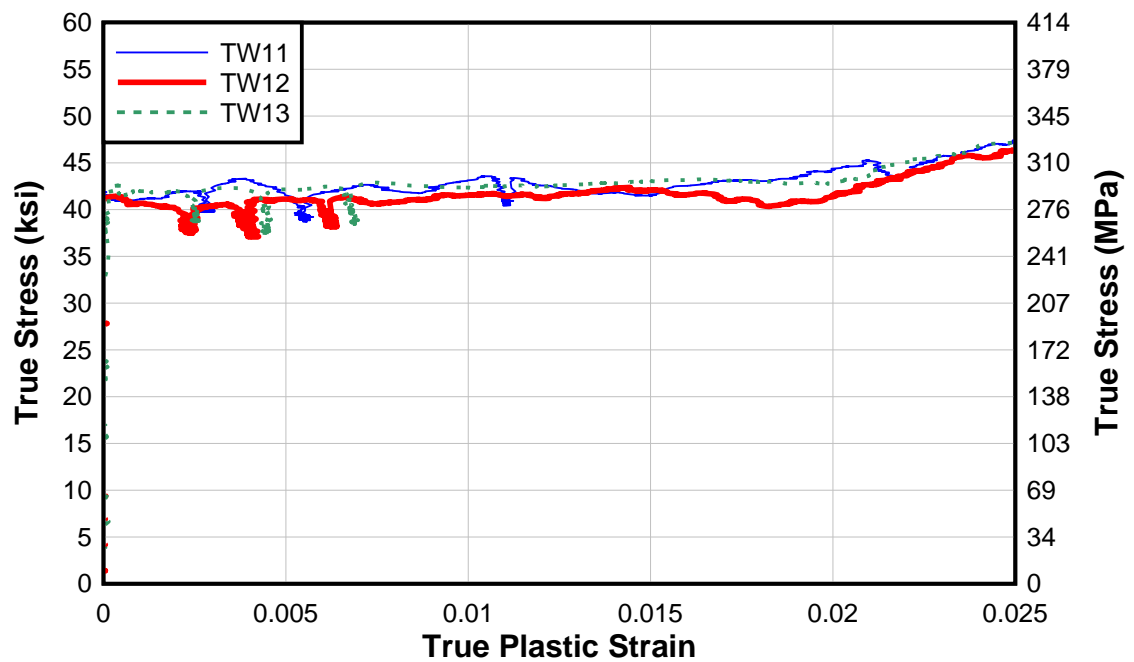


Figure A-20: True stress vs. true plastic strain for the transverse rolling direction 3/8 in. thick A36 sample TW1

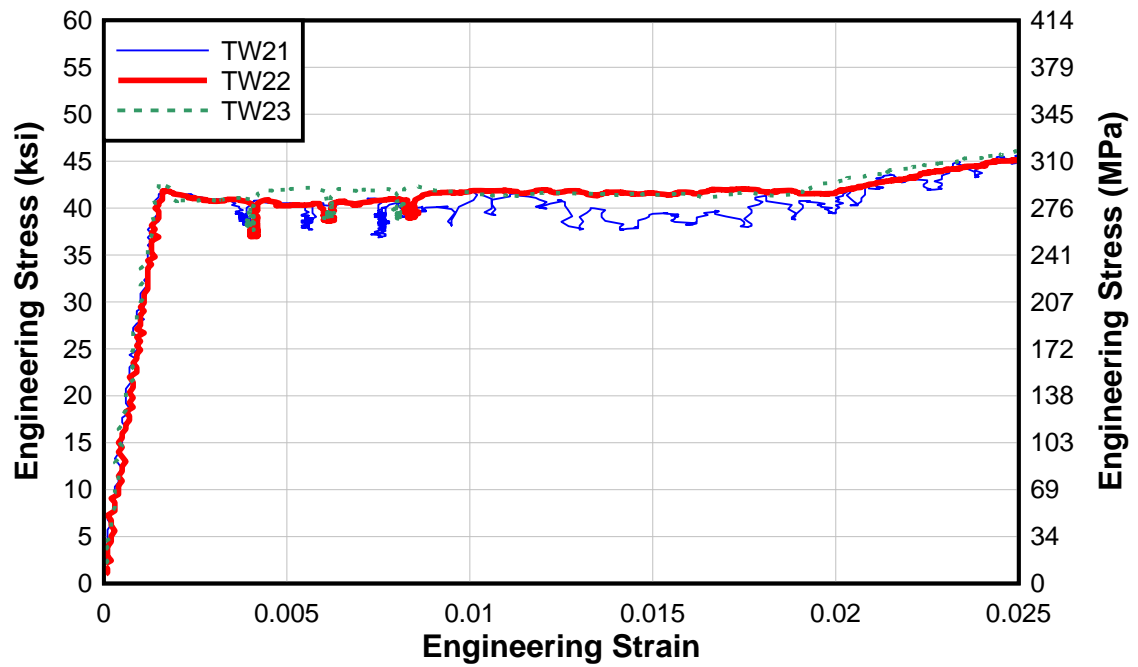


Figure A-21: Engineering stress vs. engineering strain for the transverse rolling direction 3/8 in. thick A36 sample TW2

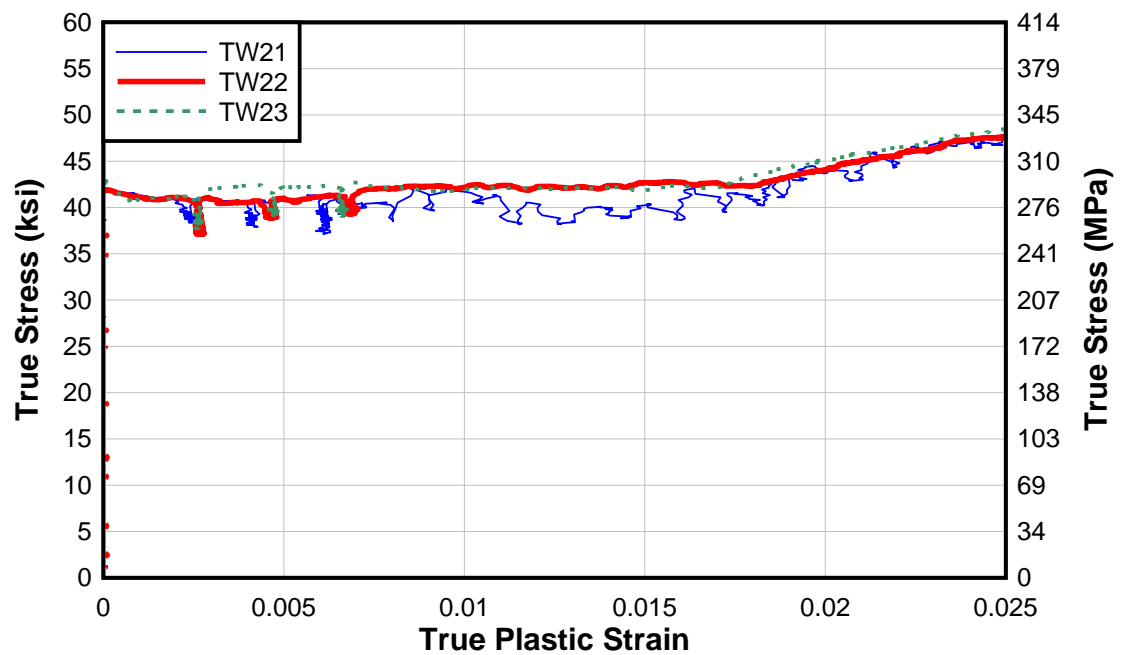


Figure A-22: True stress vs. true plastic strain for the transverse rolling direction 3/8 in. thick A36 sample TW2

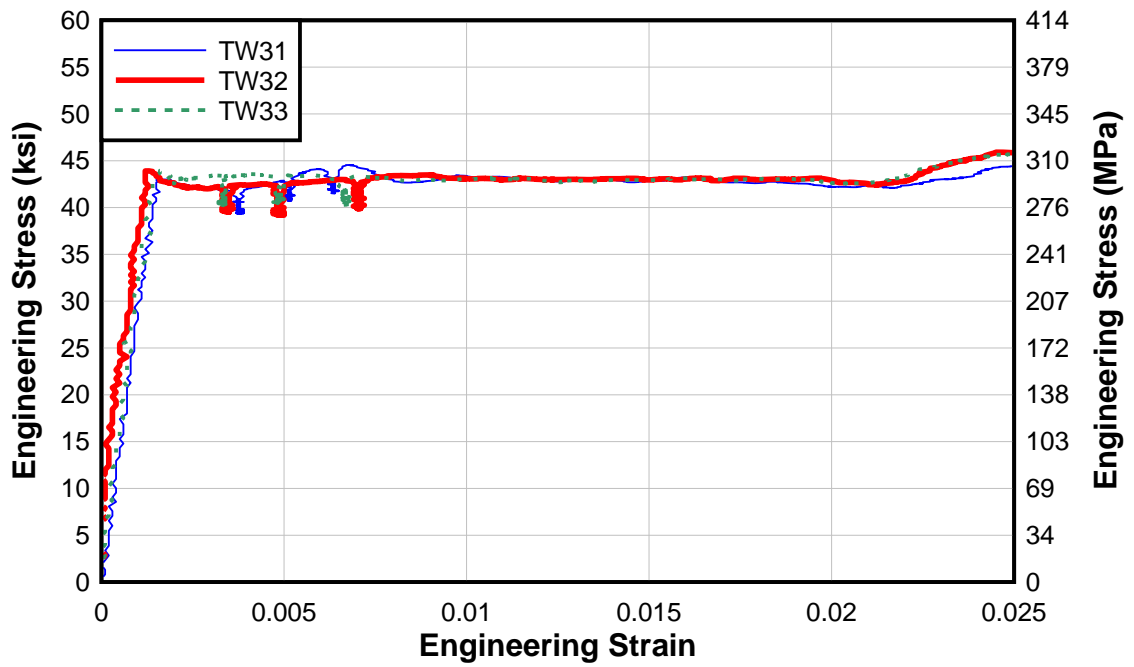


Figure A-23: Engineering stress vs. engineering strain for the transverse rolling direction 3/8 in. thick A36 sample TW3

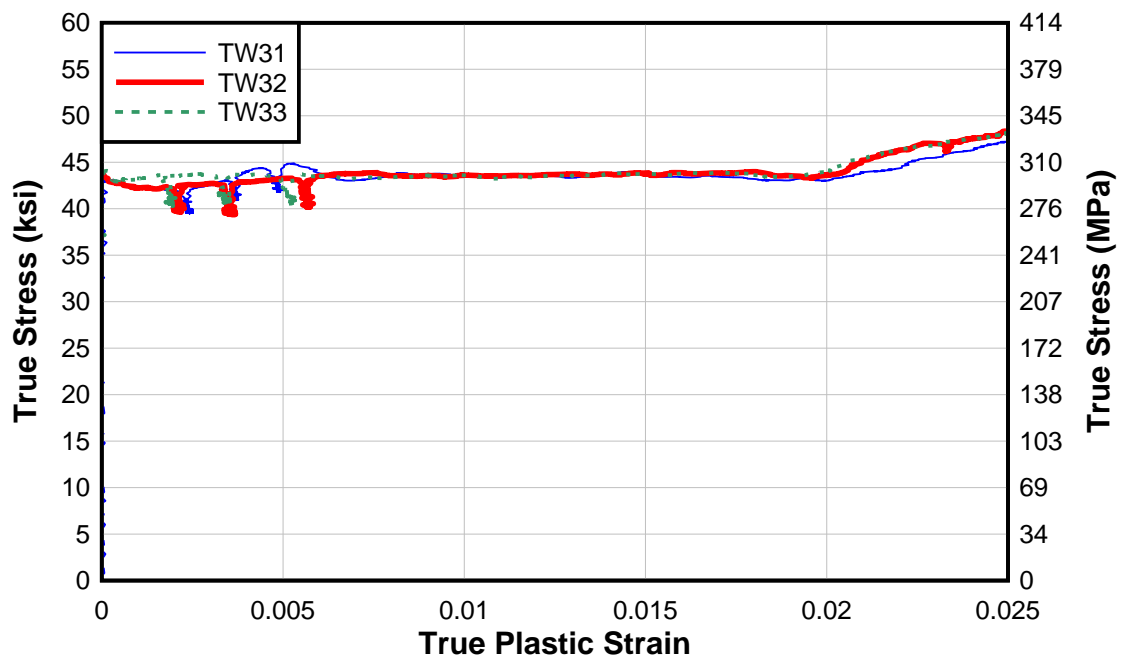


Figure A-24: True stress vs. true plastic strain for the transverse rolling direction 3/8 in. thick A36 sample TW3

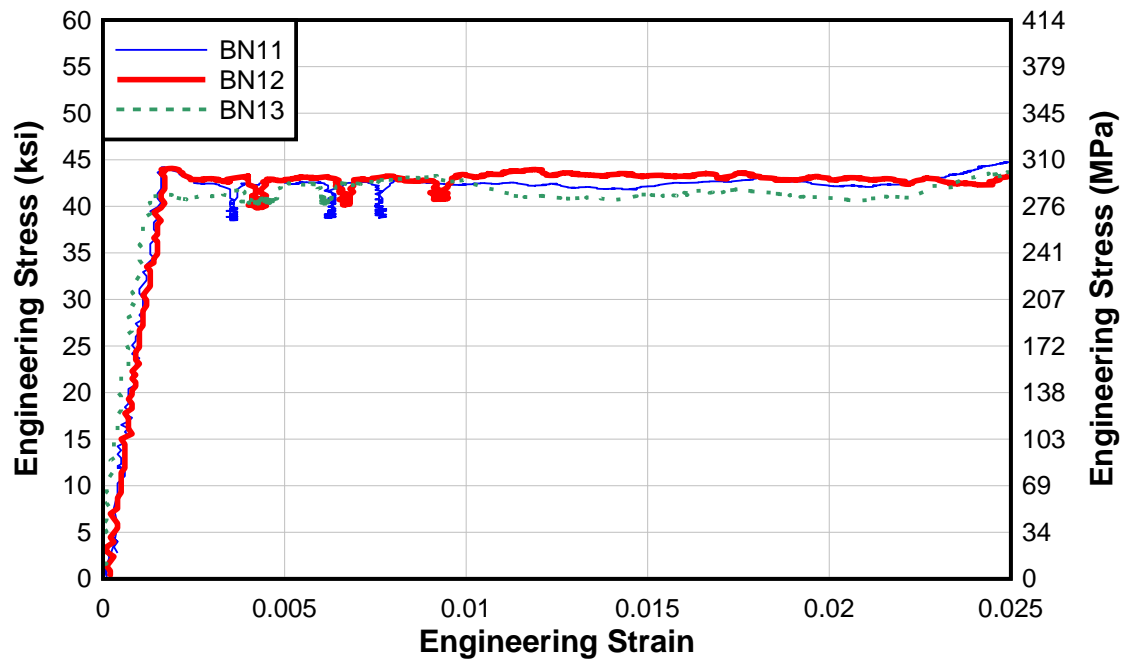


Figure A-25: Engineering stress vs. engineering strain for the 45° bias rolling direction 3/8 in. thick A36 sample BN1

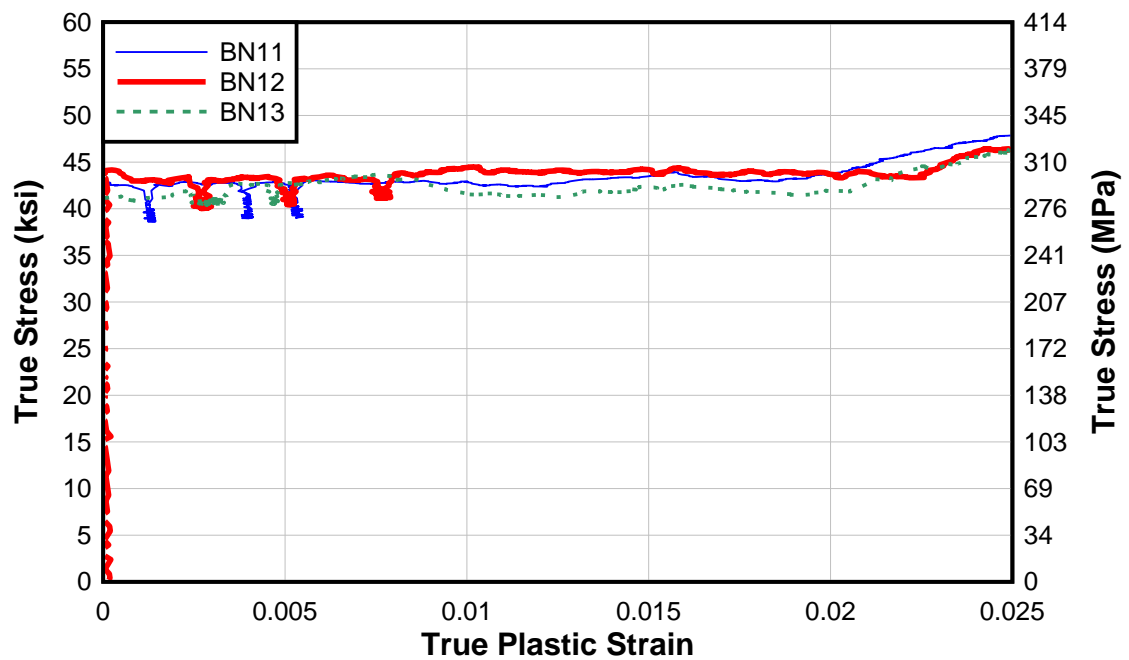


Figure A-26: True stress vs. true plastic strain for the 45° bias rolling direction 3/8 in. thick A36 sample BN1

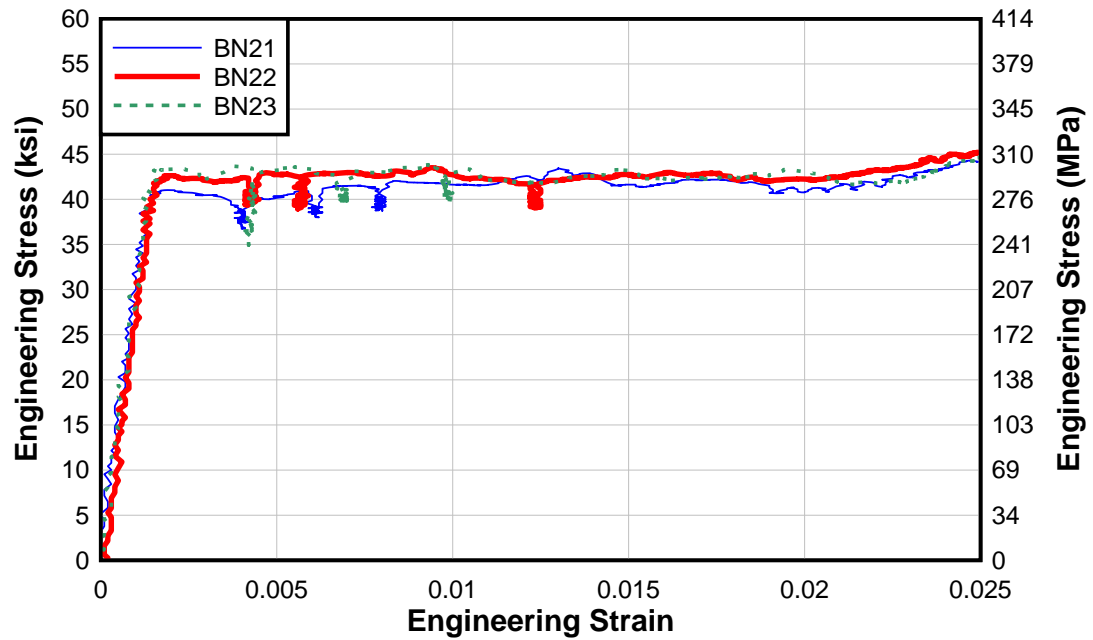


Figure A-27: Engineering stress vs. engineering strain for the 45° bias rolling direction 3/8 in. thick A36 sample BN2

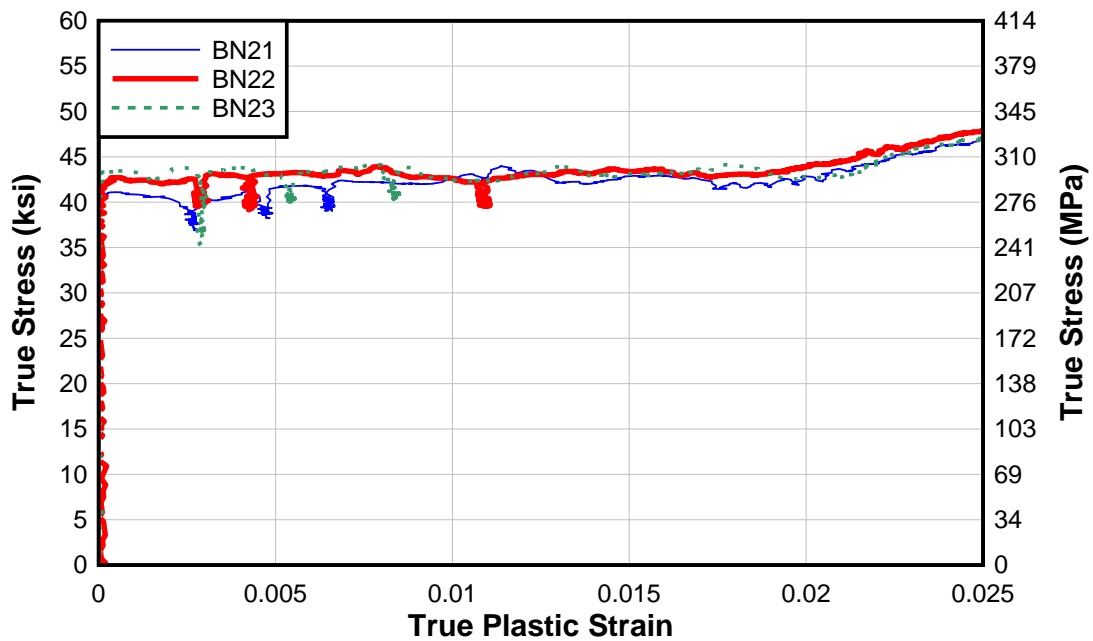


Figure A-28: True stress vs. true plastic strain for the 45° bias rolling direction 3/8 in. thick A36 sample BN2

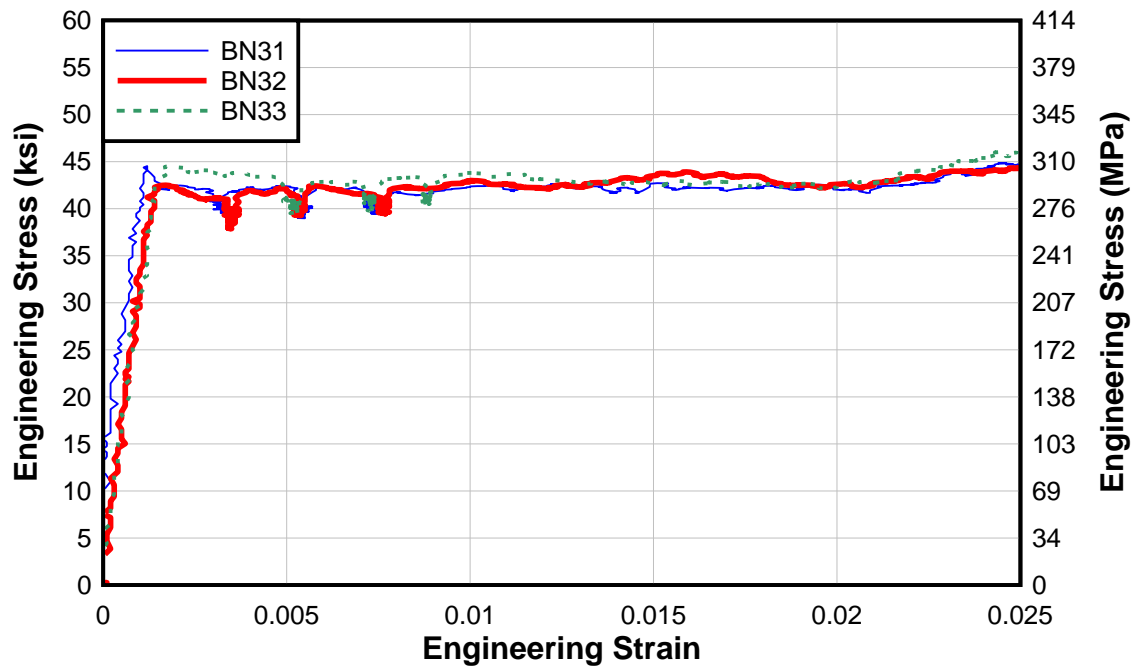


Figure A-29: Engineering stress vs. engineering strain for the 45° bias rolling direction 3/8 in. thick A36 sample BN3

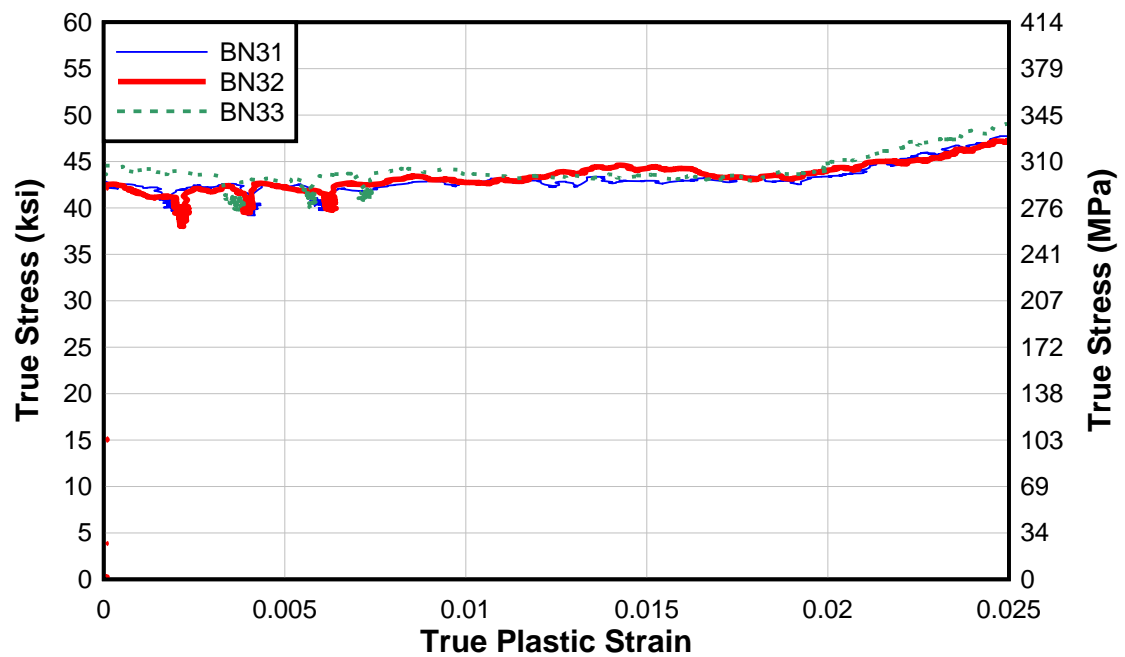


Figure A-30: True stress vs. true plastic strain for the 45° bias rolling direction 3/8 in. thick A36 sample BN3

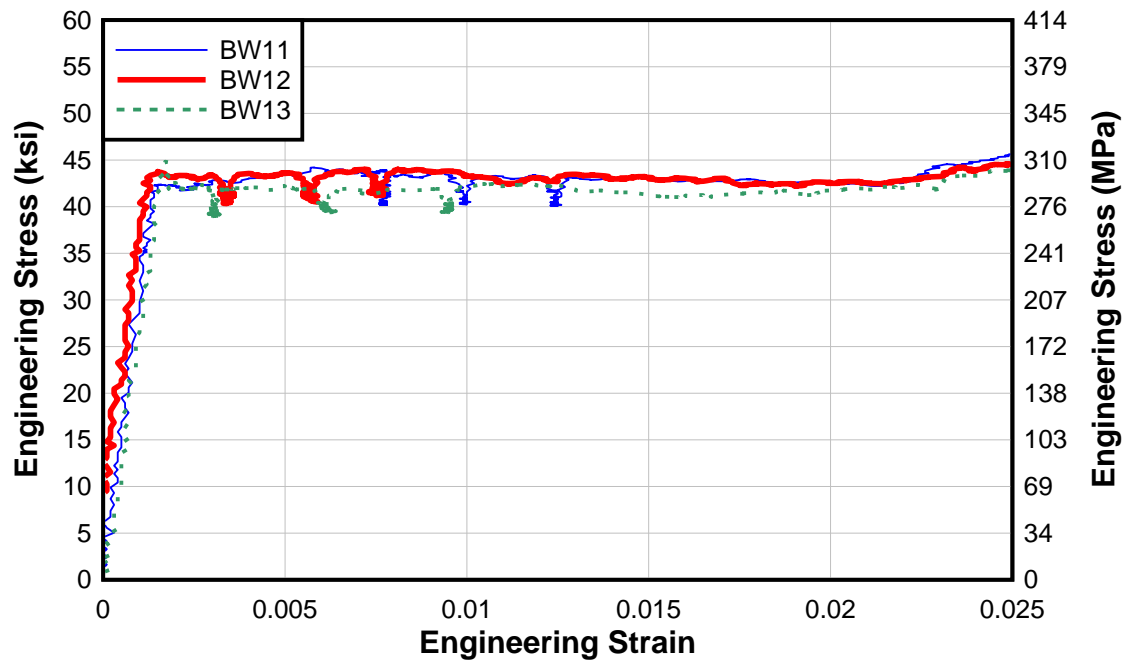


Figure A-31: Engineering stress vs. engineering strain for the 45° bias rolling direction 3/8 in. thick A36 sample BW1

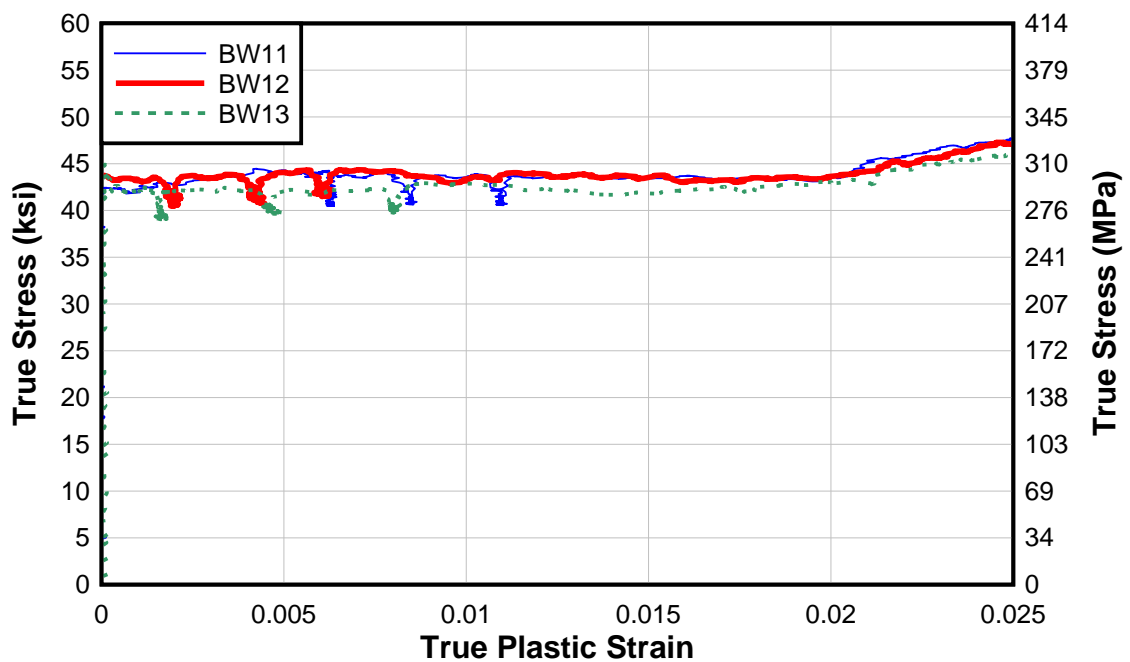


Figure A-32: True stress vs. true plastic strain for the 45° bias rolling direction 3/8 in. thick A36 sample BW1

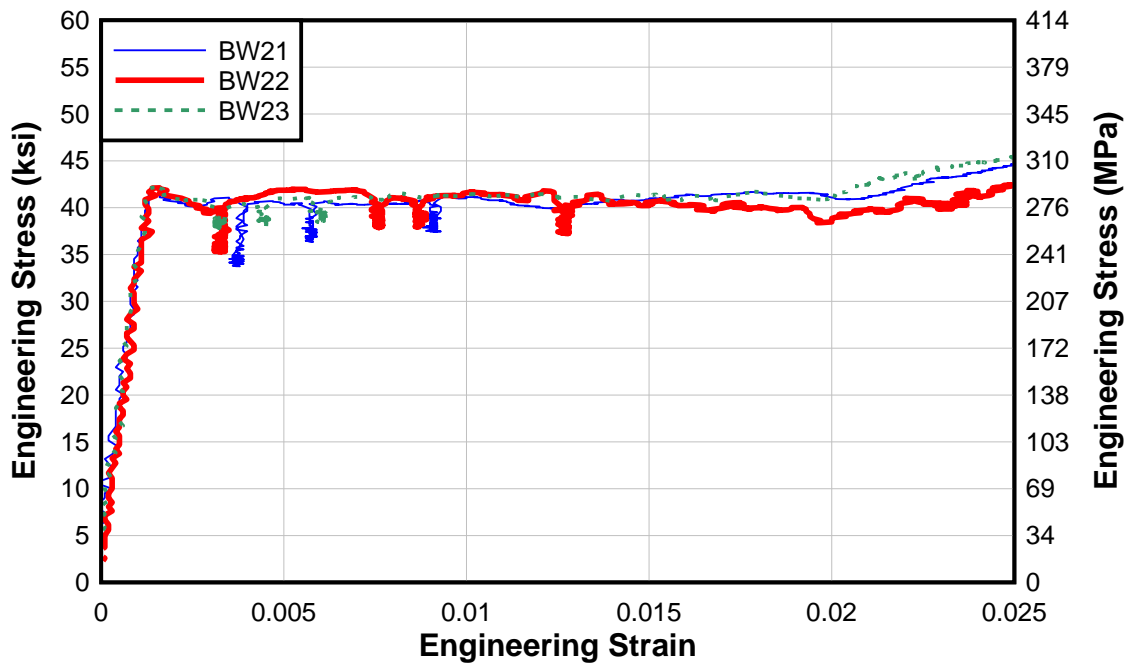


Figure A-33: Engineering stress vs. engineering strain for the 45° bias rolling direction 3/8 in. thick A36 sample BW2

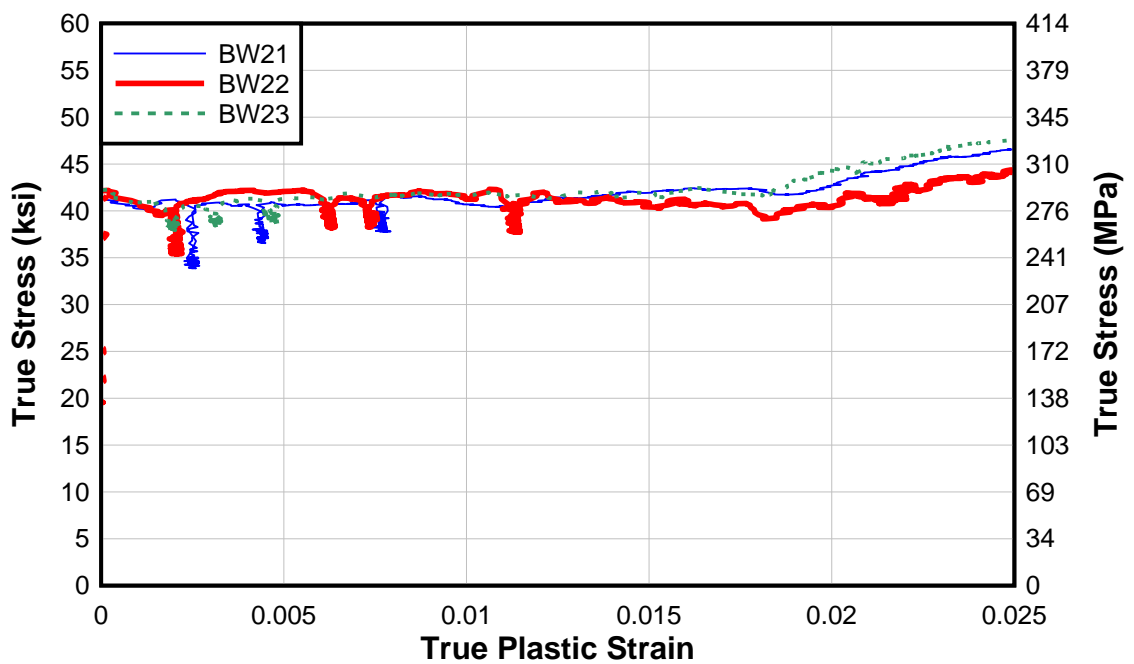


Figure A-34: True stress vs. true plastic strain for the 45° bias rolling direction 3/8 in. thick A36 sample BW2

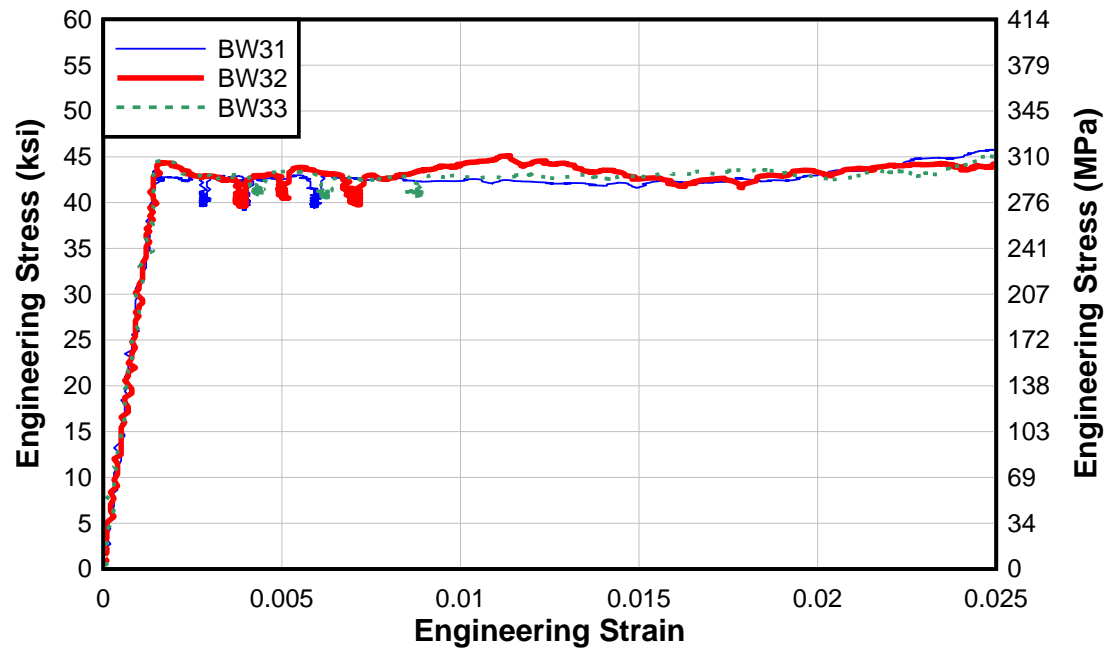


Figure A-35: Engineering stress vs. engineering strain for the 45° bias rolling direction 3/8 in. thick A36 sample BW3

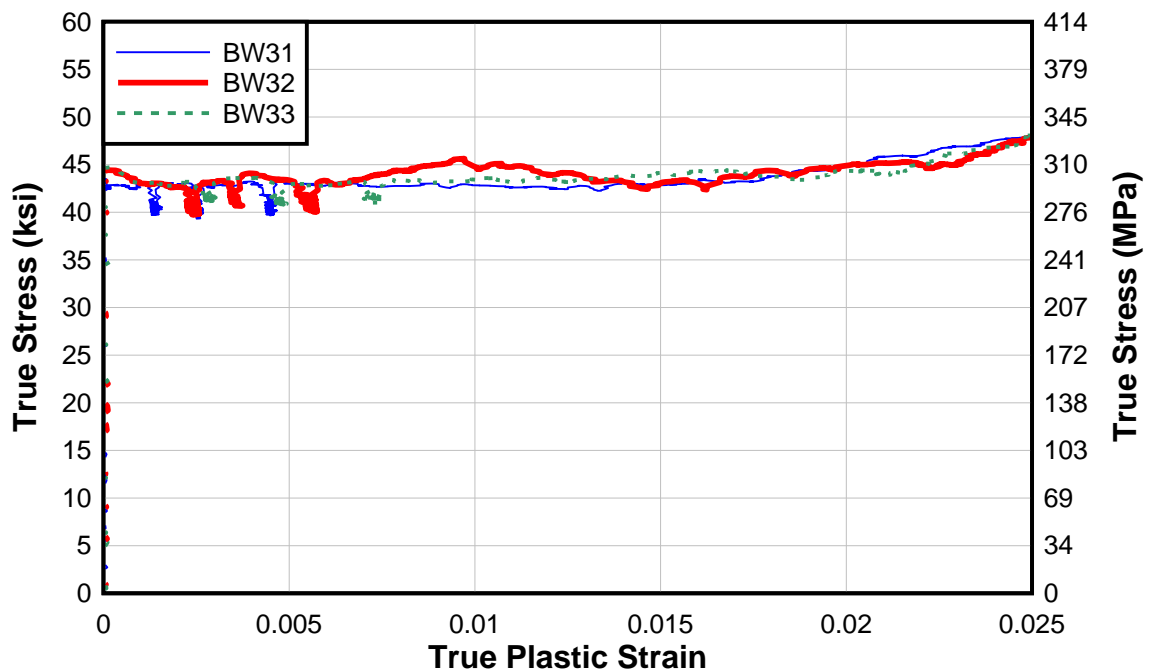


Figure A-36: True stress vs. true plastic strain for the 45° bias rolling direction 3/8 in. thick A36 sample BW3

Table A-1: Static yield stress for the parallel rolling direction 3/8 in. thick A36 plate

	Plateau 1					Plateau 2				
Sample ID	Min Value (ksi)	Min Value (MPa)	Mean Value (ksi)	Mean Value (MPa)	Standard Deviation	Min Value (ksi)	Min Value (MPa)	Mean Value (ksi)	Mean Value (MPa)	Standard Deviation
PN11	40.36	278	40.50	279	0.09	39.61	273	39.90	275	0.30
PN12	Incorrect Loading Rate									
PN13	39.28	271	39.16	270	0.10	40.85	282	41.10	283	0.18
PN21	38.96	269	39.46	272	0.32	39.42	272	39.72	274	0.16
PN22	38.94	268	39.18	270	0.18	39.27	271	39.50	272	0.17
PN23	38.85	268	39.31	271	0.25	38.74	267	39.25	271	0.32
PN31	40.18	277	40.62	280	0.23	40.35	278	40.62	280	0.16
PN32	39.94	275	40.07	276	0.11	40.06	276	40.20	277	0.12
PN33	39.27	271	39.57	273	0.16	38.51	266	38.92	268	0.30
PW11	39.31	271	39.64	273	0.26	39.50	272	39.59	273	0.07
PW12	39.29	271	39.75	274	0.25	39.74	274	40.11	277	0.24
PW13	38.35	264	38.72	267	0.18	39.00	269	39.33	271	0.20
PW21	36.59	252	39.79	274	0.11	38.40	265	38.54	266	0.08
PW22	39.00	269	39.32	271	0.23	38.71	267	38.79	267	0.05
PW23	38.92	268	39.10	270	0.10	39.74	274	39.88	275	0.08
PW31	37.15	256	37.40	258	0.15	38.83	268	38.89	268	0.05
PW32	38.72	267	38.98	269	0.16	38.86	268	39.20	270	0.22
PW33	38.98	269	39.14	270	0.08	39.27	271	39.48	272	0.16

Sample ID	Plateau 3				
	Min Value (ksi)	Min Value (MPa)	Mean Value (ksi)	Mean Value (MPa)	Standard Deviation
PN11	40.24	277	40.43	279	0.09
PN12	Incorrect Loading Rate				
PN13	41.78	288	42.09	290	0.10
PN21	39.61	273	39.76	274	0.09
PN22	39.50	272	39.76	274	0.18
PN23	39.05	269	39.47	272	0.26
PN31	40.11	277	40.23	277	0.09
PN32	40.66	280	40.88	282	0.17
PN33	39.02	269	39.26	271	0.18
PW11	39.36	271	39.79	274	0.28
PW12	39.98	276	40.72	281	0.42
PW13	39.28	271	39.62	273	0.27
PW21	38.80	268	38.94	268	0.12
PW22	38.72	267	39.10	270	0.24
PW23	38.80	267	38.80	267	0.05
PW31	39.00	269	39.11	270	0.07
PW32	39.15	270	39.44	272	0.17
PW33	39.31	271	39.48	272	0.10

Table A-2: Static yield stress for the transverse rolling direction 3/8 in. thick A36 plate

Sample ID	Plateau 1					Plateau 2				
	Min Value (ksi)	Min Value (MPa)	Mean Value (ksi)	Mean Value (MPa)	Standard Deviation	Min Value (ksi)	Min Value (MPa)	Mean Value (ksi)	Mean Value (MPa)	Standard Deviation
TN11	37.23	257	37.58	259	0.33	37.40	258	37.61	259	0.13
TN12	36.99	255	37.23	257	0.15	37.67	260	38.00	262	0.17
TN13	37.77	260	38.14	263	0.24	37.33	257	37.55	259	0.18
TN21	37.99	262	38.38	265	0.24	39.28	271	39.41	272	0.07
TN22	41.36	285	41.54	286	0.13	40.68	280	40.93	282	0.21
TN23	39.65	273	39.74	274	0.06	40.27	278	40.35	278	0.04
TN31	37.84	261	37.97	262	0.06	39.54	273	39.69	274	0.10
TN32	40.00	276	40.19	277	0.12	40.17	277	40.38	278	0.10
TN33	39.90	275	40.41	279	0.34	41.31	285	41.56	287	0.10
TW11	39.56	273	39.90	275	0.23	38.41	265	38.65	266	0.15
TW12	37.55	259	37.69	260	0.09	36.91	254	37.02	255	0.08
TW13	38.55	266	38.64	266	0.05	37.28	257	37.47	258	0.11
TW21	38.23	264	38.49	265	0.17	37.68	260	38.27	264	0.35
TW22	37.03	255	37.25	257	0.17	38.70	267	38.84	268	0.13
TW23	37.61	259	38.10	263	0.24	38.82	268	39.17	270	0.15
TW31	39.31	271	39.46	272	0.08	40.72	281	40.85	282	0.07
TW32	39.51	272	39.70	274	0.09	39.18	270	39.31	271	0.07
TW33	40.14	277	40.42	279	0.10	40.45	279	40.63	280	0.14

Sample ID	Plateau 3				
	Min Value (ksi)	Min Value (MPa)	Mean Value (ksi)	Mean Value (MPa)	Standard Deviation
TN11	37.84	261	38.19	263	0.18
TN12	38.30	264	38.55	266	0.25
TN13	37.67	260	38.02	262	0.21
TN21	39.92	275	40.13	277	0.14
TN22	40.93	282	41.16	284	0.14
TN23	40.13	277	40.41	279	0.12
TN31	39.55	273	39.77	274	0.15
TN32	40.04	276	40.41	279	0.18
TN33	41.87	289	42.00	290	0.06
TW11	39.93	275	40.26	278	0.18
TW12	37.88	261	38.07	262	0.12
TW13	38.14	263	38.23	264	0.06
TW21	36.87	254	37.94	262	0.74
TW22	38.96	269	39.30	271	0.14
TW23	38.77	267	38.96	269	0.10
TW31	41.52	286	41.81	288	0.13
TW32	39.89	275	40.09	276	0.09
TW33	40.27	278	40.42	279	0.09

Table A-3: Static yield stress for the 45° bias rolling direction 3/8 in. thick A36 plate

Sample ID	Plateau 1					Plateau 2				
	Min Value (ksi)	Min Value (MPa)	Mean Value (ksi)	Mean Value (MPa)	Standard Deviation	Min Value (ksi)	Min Value (MPa)	Mean Value (ksi)	Mean Value (MPa)	Standard Deviation
BN11	38.49	265	38.61	266	0.07	38.77	267	38.87	268	0.06
BN12	39.87	275	40.02	276	0.14	40.18	277	40.53	279	0.28
BN13	40.30	278	40.58	280	0.15	40.26	278	40.54	280	0.16
BN21	37.40	258	37.85	261	0.39	38.42	265	38.53	266	0.06
BN22	39.38	271	39.95	275	0.36	38.94	268	39.29	271	0.21
BN23	34.93	241	37.76	260	1.83	39.69	274	39.96	276	0.16
BN31	35.54	245	40.23	277	0.30	38.98	269	39.82	275	0.37
BN32	38.75	267	39.57	273	0.38	39.52	272	39.78	274	0.17
BN33	39.49	272	40.21	277	0.47	39.71	274	40.66	280	0.52
BW11	40.24	277	40.37	278	0.11	40.25	277	40.48	279	0.16
BW12	40.33	278	41.06	283	0.32	40.53	279	41.16	284	0.44
BW13	38.90	268	39.10	270	0.17	39.39	272	39.57	273	0.12
BW21	34.02	235	34.40	237	0.29	36.34	251	36.75	253	0.21
BW22	35.33	244	35.54	245	0.22	37.95	262	38.79	267	0.52
BW23	38.22	264	38.69	267	0.25	38.22	264	38.63	266	0.25
BW31	39.82	275	40.24	277	0.26	39.71	274	40.04	276	0.20
BW32	39.59	273	39.87	275	0.22	40.48	279	40.61	280	0.07
BW33	40.83	282	41.17	284	0.21	40.53	279	40.62	280	0.07

Sample ID	Plateau3				
	Max Value (ksi)	Max Value (MPa)	Mean Value (ksi)	Mean Value (MPa)	Standard Deviation
BN11	38.76	267	39.03	269	0.17
BN12	40.76	281	40.87	282	0.08
BN13	40.61	280	40.87	282	0.17
BN21	38.71	267	39.18	270	0.28
BN22	39.07	269	39.36	271	0.21
BN23	39.93	275	40.34	278	0.25
BN31	39.68	274	39.92	275	0.14
BN32	39.47	272	39.59	273	0.07
BN33	40.79	281	41.03	283	0.22
BW11	40.06	276	40.30	278	0.13
BW12	41.23	284	41.31	285	0.06
BW13	39.39	272	39.68	274	0.16
BW21	37.42	258	37.66	260	0.14
BW22	37.25	257	37.35	258	0.09
BW23	38.78	267	39.11	270	0.23
BW31	39.51	272	40.09	276	0.45
BW32	39.76	274	40.51	279	0.48
BW33	40.65	280	40.97	282	0.20

Table A-4: Dynamic yield stress for the parallel rolling direction 3/8 in. thick A36 plate

Sample ID	Plateau 1					Plateau 2				
	Max Value (ksi)	Max Value (MPa)	Mean Value (ksi)	Mean Value (MPa)	Standard Deviation	Max Value (ksi)	Max Value (MPa)	Mean Value (ksi)	Mean Value (MPa)	Standard Deviation
PN11	46.46	320	45.26	312	1.02	44.81	309	43.95	303	0.84
PN12	Set at Incorrect Loading Rate									
PN13	40.92	282	40.33	278	0.65	41.54	286	41.21	284	0.24
PN21	43.36	299	42.66	294	0.49	39.91	275	39.46	272	0.30
PN22	43.98	303	43.28	298	0.57	42.11	290	41.71	288	0.19
PN23	41.65	287	41.33	285	0.21	42.41	292	42.01	290	0.20
PN31	44.53	307	43.78	302	0.63	43.41	299	45.90	316	0.37
PN32	44.92	310	43.90	303	0.81	42.69	294	42.36	292	0.26
PN33	42.36	292	42.19	291	0.16	42.25	291	42.05	290	0.16
PW11	43.64	301	42.73	295	0.75	42.29	292	41.42	286	0.68
PW12	44.27	305	43.22	298	0.83	42.65	294	45.17	311	0.42
PW13	43.80	302	42.08	290	0.54	41.76	288	41.40	285	0.22
PW21	45.19	312	43.44	299	1.47	42.09	290	41.74	288	0.52
PW22	42.72	295	41.80	288	0.84	42.58	294	42.35	292	0.21
PW23	42.63	294	42.03	290	0.51	41.85	289	41.43	286	0.25
PW31	43.00	296	42.57	293	0.41	41.56	287	41.31	285	0.19
PW32	41.95	289	41.46	286	0.27	42.11	290	41.49	286	0.61
PW33	41.68	287	41.95	289	0.22	41.82	288	41.55	286	0.19

Plateau 3						Plateau 4				
Sample ID	Max Value (ksi)	Max Value (MPa)	Mean Value (ksi)	Mean Value (MPa)	Standard Deviation	Max Value (ksi)	Max Value (MPa)	Mean Value (ksi)	Mean Value (MPa)	Standard Deviation
PN11	44.26	305	43.44	300	0.88	44.69	308	44.18	305	0.27
PN12	Set at Incorrect Loading Rate									
PN13	42.95	296	42.37	292	0.48	44.14	304	43.64	301	0.61
PN21	42.13	290	41.65	287	0.42	42.25	291	41.82	288	0.25
PN22	42.00	290	41.61	287	0.30	42.18	291	41.59	287	0.29
PN23	42.32	292	41.96	289	0.28	42.48	293	41.80	288	0.27
PN31	42.79	295	42.42	292	0.29	43.59	301	42.49	293	0.42
PN32	43.16	298	42.92	296	0.15	43.44	300	42.68	294	0.42
PN33	41.60	287	41.31	285	0.15	42.61	294	41.71	288	0.47
PW11	42.36	292	41.50	286	0.82	42.59	294	42.19	291	0.17
PW12	43.57	300	42.93	296	0.39	43.68	301	42.70	294	0.71
PW13	42.36	292	42.18	291	0.11	42.61	294	42.27	291	0.18
PW21	42.08	290	41.75	288	0.20	42.08	290	41.68	287	0.21
PW22	41.80	288	41.50	286	0.20	42.73	295	42.27	291	0.23
PW23	43.06	297	42.58	294	0.34	43.20	298	41.80	288	0.70
PW31	42.46	293	42.21	291	0.20	42.35	292	41.92	289	0.26
PW32	41.97	289	41.73	288	0.03	42.36	292	42.03	290	0.23
PW33	41.85	289	41.66	287	0.11	43.20	298	42.70	294	0.30

Table A-5: Dynamic yield stress for transverse rolling direction for 3/8 in. thick A36 plate

Sample ID	Plateau 1					Plateau 2				
	Min Value (ksi)	Min Value (MPa)	Mean Value (ksi)	Mean Value (MPa)	Standard Deviation	Min Value (ksi)	Min Value (MPa)	Mean Value (ksi)	Mean Value (MPa)	Standard Deviation
TN11	43.25	298	42.93	296	0.34	41.14	284	40.92	282	0.17
TN12	43.05	297	42.55	293	0.44	40.82	281	40.64	280	0.14
TN13	40.66	280	40.04	276	0.40	40.40	279	40.02	276	0.19
TN21	41.85	289	41.61	287	0.22	41.79	288	41.54	286	0.19
TN22	44.76	309	44.03	304	0.63	43.53	300	42.92	296	0.61
TN23	43.24	298	42.84	295	0.28	42.67	294	42.49	293	0.11
TN31	44.61	308	43.95	303	0.58	42.30	292	41.92	289	0.21
TN32	42.37	292	42.22	291	0.11	42.43	293	42.16	291	0.26
TN33	44.58	307	43.69	301	0.50	44.32	306	43.88	303	0.50
TW11	41.96	289	41.33	285	0.39	43.06	297	42.68	294	0.27
TW12	41.35	285	40.78	281	0.36	40.37	278	39.08	269	0.69
TW13	42.54	293	41.81	288	0.30	42.10	290	41.86	289	0.28
TW21	42.01	290	41.39	285	0.37	40.80	281	40.34	278	0.46
TW22	41.82	288	41.69	287	0.11	40.89	282	40.45	279	0.20
TW23	42.87	296	42.30	292	0.60	42.17	291	41.95	289	0.22
TW31	42.99	296	42.87	296	0.12	42.87	296	42.39	292	0.29
TW32	43.92	303	43.46	300	0.40	42.53	293	42.39	292	0.13
TW33	44.01	303	43.89	303	0.14	43.58	300	43.45	300	0.07

Sample ID	Plateau 3					Plateau 4				
	Min Value (ksi)	Min Value (MPa)	Mean Value (ksi)	Mean Value (MPa)	Standard Deviation	Min Value (ksi)	Min Value (MPa)	Mean Value (ksi)	Mean Value (MPa)	Standard Deviation
TN11	41.52	286	41.33	285	0.20	42.33	292	41.84	289	0.16
TN12	41.54	286	41.23	284	0.27	41.93	289	41.28	285	0.39
TN13	40.28	278	39.92	275	0.20	40.73	281	40.37	278	0.20
TN21	42.35	292	42.22	291	0.19	44.06	304	43.43	299	0.32
TN22	42.83	295	42.48	293	0.19	43.84	302	42.80	295	0.35
TN23	43.19	298	43.00	297	0.13	43.92	303	42.85	295	0.60
TN31	43.03	297	42.81	295	0.16	44.87	309	43.43	299	0.69
TN32	42.54	293	42.32	292	0.31	42.75	295	42.13	291	0.31
TN33	44.20	305	43.96	303	0.14	45.42	313	44.25	305	0.61
TW11	43.05	297	42.15	291	0.54	44.26	305	42.78	295	0.73
TW12	40.88	282	40.71	281	0.16	41.68	287	41.15	284	0.25
TW13	42.14	291	41.98	289	0.12	42.49	293	42.15	291	0.18
TW21	41.03	283	40.28	278	0.59	41.73	288	39.98	276	1.03
TW22	40.97	283	40.68	281	0.21	42.05	290	41.71	288	0.18
TW23	42.04	290	41.93	289	0.07	41.75	288	41.47	286	0.13
TW31	44.11	304	43.74	302	0.33	43.24	298	42.73	295	0.30
TW32	43.00	296	42.76	295	0.17	43.16	298	43.03	297	0.07
TW33	43.46	300	43.33	299	0.16	43.13	297	42.97	296	0.10

Table A-6: Dynamic yield stress for 45° bias rolling direction for 3/8 in. thick A36 plate

Sample ID	Plateau 1					Plateau 2				
	Min Value (ksi)	Min Value (MPa)	Mean Value (ksi)	Mean Value (MPa)	Standard Deviation	Min Value (ksi)	Min Value (MPa)	Mean Value (ksi)	Mean Value (MPa)	Standard Deviation
BN11	44.22	305	43.74	302	0.43	42.73	295	42.53	293	0.12
BN12	44.07	304	43.19	298	0.71	43.18	298	42.94	296	0.22
BN13	41.70	288	41.17	284	0.27	42.47	293	42.38	292	0.07
BN21	41.03	283	40.41	279	0.51	40.95	282	40.47	279	0.32
BN22	42.62	294	42.22	291	0.21	42.95	296	42.39	292	0.74
BN23	43.66	301	43.06	297	0.41	43.57	300	43.22	298	0.33
BN31	44.52	307	49.94	344	1.27	42.39	292	41.98	289	0.30
BN32	42.50	293	41.80	288	0.67	42.19	291	41.53	286	0.49
BN33	44.48	307	43.96	303	0.31	42.91	296	42.45	293	0.52
BW11	44.21	305	43.41	299	0.49	43.66	301	43.35	299	0.15
BW12	43.76	302	43.23	298	0.27	43.62	301	43.36	299	0.18
BW13	44.83	309	44.04	304	0.66	42.22	291	41.92	289	0.58
BW21	41.40	285	40.31	278	0.50	40.70	281	40.38	278	0.28
BW22	42.12	290	40.99	283	0.85	41.96	289	41.62	287	0.35
BW23	42.20	291	41.51	286	0.49	40.40	279	39.93	275	0.49
BW31	43.41	299	42.85	295	0.34	42.93	296	42.49	293	0.41
BW32	44.36	306	43.78	302	0.56	43.11	297	42.80	295	0.28
BW33	44.63	308	43.61	301	0.87	43.39	299	43.10	297	0.47

Sample ID	Plateau 3					Plateau 4				
	Min Value (ksi)	Min Value (MPa)	Mean Value (ksi)	Mean Value (MPa)	Standard Deviation	Min Value (ksi)	Min Value (MPa)	Mean Value (ksi)	Mean Value (MPa)	Standard Deviation
BN11	42.61	294	42.40	292	0.22	43.17	298	42.41	292	0.32
BN12	43.25	298	42.89	296	0.02	43.96	303	43.24	298	0.33
BN13	43.28	298	42.97	296	0.17	No Final Plateau				
BN21	41.52	286	41.21	284	0.40	43.45	300	42.15	291	0.51
BN22	43.51	300	42.88	296	0.27	42.98	296	42.60	294	0.21
BN23	43.83	302	43.37	299	0.31	43.29	299	42.59	294	0.36
BN31	42.25	291	41.98	289	0.33	42.71	295	42.19	291	0.23
BN32	42.42	292	41.89	289	0.32	43.91	303	43.11	297	0.52
BN33	43.35	299	42.92	296	0.52	43.14	297	42.66	294	0.24
BW11	43.36	299	43.13	297	0.19	43.23	298	42.76	295	0.21
BW12	44.01	303	43.62	301	0.31	43.84	302	43.02	297	0.39
BW13	41.93	289	41.65	287	0.28	42.47	293	41.64	287	0.43
BW21	40.78	281	40.42	279	0.19	41.67	287	41.24	284	0.34
BW22	41.80	288	41.29	285	0.35	41.43	286	40.37	278	0.40
BW23	41.08	283	40.65	280	0.43	41.53	286	41.18	284	0.20
BW31	42.99	296	42.47	293	0.49	42.57	294	42.20	291	0.20
BW32	43.85	302	43.31	299	0.39	44.25	305	43.69	301	0.42
BW33	42.94	296	42.66	294	0.13	43.58	300	43.01	297	0.29

Table A-7: Final strain and tensile strength for the parallel rolling direction 3/8 in. thick A36 plate –US Customary Units

Sample ID	Area (in ²)	Ultimate Load (kip)	Original Length (in)	Final Length (in)	Δ Length (in)	Final Strain (in/in)	Final Strain %	F _u (ksi)
PN11*	0.194	12.860	3.000	3.767	0.767	0.361	36.15	66.43
PN12*	Set at Incorrect Loading Rate							
PN13*	0.195	12.827	3.000	3.807	0.807	0.380	38.04	65.68
PN21*	0.191	12.545	3.000	3.839	0.839	0.395	39.52	65.72
PN22*	0.193	12.656	3.000	3.823	0.823	0.388	38.79	65.73
PN23*	0.192	12.595	3.000	3.843	0.843	0.397	39.72	65.50
PN31	0.198	13.075	2.003	2.757	0.754	0.376	37.64	65.97
PN32	0.199	13.069	2.004	2.749	0.745	0.372	37.18	65.76
PN33	0.197	12.921	2.003	2.731	0.728	0.363	36.35	65.68
PW11*	0.190	12.525	3.000	3.815	0.815	0.384	38.40	65.78
PW12*	0.190	12.538	3.000	3.809	0.809	0.381	38.14	65.93
PW13*	0.190	12.572	3.000	3.845	0.845	0.398	39.82	66.19
PW21	0.194	12.693	2.000	2.739	0.739	0.370	36.95	65.55
PW22	0.193	12.716	2.000	2.713	0.713	0.357	35.65	65.97
PW23	0.194	12.719	2.001	2.743	0.742	0.371	37.08	65.67
PW31	0.191	12.625	1.996	2.790	0.794	0.398	39.78	65.98
PW32	0.189	12.548	2.005	2.730	0.725	0.362	36.16	66.36
PW33	0.190	12.615	2.004	2.785	0.781	0.390	38.97	66.37
							Average	65.90

*Elongations were calculated using an adjustment factor

Table A-13: Results summary for the parallel rolling direction 3/8 in. thick plate

Sample ID	Measured Modulus of Elasticity (ksi)	Measured Modulus of Elasticity (MPa)	0.2% Offset Yield Stress (ksi)	0.2% Offset Yield Stress (Mpa)	Static Yield Stress (ksi)	Static Yield Stress (MPa)
PN11	27242	187828	44.49	307	40.28	278
PN12	Set at Incorrect Loading Rate					
PN13	21026	144970	40.05	276	40.78	281
PN21	26613	183491	41.74	288	39.65	273
PN22	29115	200742	41.39	285	39.48	272
PN23	28849	198908	41.29	285	39.34	271
PN31	28073	193558	42.28	292	40.49	279
PN32	27518	189731	42.60	294	40.38	278
PN33	32110	221392	41.55	286	39.25	271
PW11	26009	179327	42.20	291	39.67	274
PW12	28079	193599	41.95	289	40.19	277
PW13	26403	182043	40.25	278	39.22	270
PW21	27459	189324	41.47	286	39.09	270
PW22	27992	192999	41.99	290	39.07	269
PW23	27694	190945	41.48	286	39.26	271
PW31	29348	202349	41.58	287	38.47	265
PW32	26988	186077	41.58	287	39.21	270
PW33	28242	194723	41.60	287	39.37	271
Average	27574	190118	41.73	288	39.60	273
COV	0.08	0.08	0.02	0.02	0.02	0.02

Sample ID	Dynamic Yield Stress (ksi)	Dynamic Yield Stress (MPa)	Tensile Strength (ksi)	Tensile Strength (Mpa)	Elongation (%)	Area Reduction (%)
PN11	44.21	305	66.43	458	36.15	70.72
PN12	Set at Incorrect Loading Rate					
PN13	41.89	289	65.68	453	38.04	71.53
PN21	41.40	285	65.72	453	39.52	68.45
PN22	42.05	290	65.73	453	38.79	69.02
PN23	41.78	288	65.50	452	39.72	68.61
PN31	43.65	301	65.97	455	37.64	66.23
PN32	42.96	296	65.76	453	37.18	70.04
PN33	41.82	288	65.68	453	36.35	70.18
PW11	41.96	289	65.78	454	38.40	70.92
PW12	43.51	300	65.93	455	72.05	72.05
PW13	41.98	289	66.19	456	39.82	67.44
PW21	42.15	291	65.55	452	36.95	70.21
PW22	41.98	289	65.97	455	35.65	72.00
PW23	41.96	289	65.67	453	37.08	70.31
PW31	42.00	290	65.98	455	39.78	69.09
PW32	41.68	287	66.36	458	36.16	69.49
PW33	41.97	289	66.37	458	38.97	65.81
Average	42.29	292	65.90	454	0.38	69.53
COV	0.02	0.02	0.00	0.00	0.04	0.03

Table A-14: Results summary for the transverse rolling direction 3/8 in. thick plate

Sample ID	Measured Modulus of Elasticity (ksi)	Measured Modulus of Elasticity (MPa)	0.2% Offset Yield Stress (ksi)	0.2% Offset Yield Stress (Mpa)	Static Yield Stress (ksi)	Static Yield Stress (MPa)
TN11	29108	200697	41.14	284	37.79	261
TN12	28679	197739	40.69	281	-	-
TN13	29802	205482	39.80	274	37.90	261
TN21	25412	175213	40.96	282	39.31	271
TN22	27254	187914	42.80	295	41.21	284
TN23	25451	175482	42.57	294	40.17	277
TN31	28874	199083	41.82	288	39.14	270
TN32	28680	197746	42.36	292	40.33	278
TN33	28495	196470	43.19	298	41.32	285
TW11	27572	190106	41.65	287	39.60	273
TW12	27840	191954	40.04	276	37.59	259
TW13	26251	180998	41.80	288	38.11	263
TW21	26958	185873	40.78	281	38.23	264
TW22	26306	181377	41.08	283	38.46	265
TW23	28247	194760	41.03	283	38.75	267
TW31	28785	198470	41.79	288	40.71	281
TW32	30307	208964	42.12	290	39.70	274
TW33	28305	195160	43.40	299	40.49	279
Average	27907	192416	41.61	287	39.34	271
COV	0.05	0.05	0.02	0.02	0.03	0.03

Sample ID	Dynamic Yield Stress (ksi)	Dynamic Yield Stress (MPa)	Tensile Strength (ksi)	Tensile Strength (Mpa)	Elongation (%)	Area Reduction (%)
TN11	41.76	288	65.89	454	37.40	67.61
TN12	41.43	286	65.51	452	37.50	69.06
TN13	40.09	276	66.46	458	39.34	68.30
TN21	42.20	291	66.30	457	36.02	66.95
TN22	43.06	297	66.47	458	39.11	66.62
TN23	42.80	295	66.64	459	39.79	62.66
TN31	43.03	297	66.23	457	39.71	65.44
TN32	42.21	291	65.90	454	38.02	65.75
TN33	43.94	303	67.11	463	36.48	62.21
TW11	42.24	291	66.29	457	-	-
TW12	40.43	279	65.88	454	37.86	66.62
TW13	41.95	289	65.64	453	38.10	62.66
TW21	40.50	279	65.02	448	37.17	69.96
TW22	41.13	284	65.34	450	37.41	66.57
TW23	41.91	289	66.17	456	38.68	70.08
TW31	42.93	296	66.51	459	36.92	64.93
TW32	42.91	296	66.82	461	37.26	62.45
TW33	43.41	299	66.87	461	37.38	64.70
Average	42.11	290	66.17	456	37.89	65.76
COV	0.03	0.03	0.01	0.01	0.03	.05

Table A-15: Results summary for the 45° bias rolling direction 3/8 in. thick plate

Sample ID	Measured Modulus of Elasticity (ksi)	Measured Modulus of Elasticity (MPa)	0.2% Offset Yield Stress (ksi)	0.2% Offset Yield Stress (Mpa)	Static Yield Stress (ksi)	Static Yield Stress (MPa)
BN11	28476	196339	41.84	288	38.84	268
BN12	26593	183356	43.02	297	40.48	279
BN13	29675	204606	41.48	286	40.66	280
BN21	28380	195677	40.29	278	38.52	266
BN22	29142	200931	42.05	290	39.53	273
BN23	28304	195153	42.99	296	39.35	271
BN31	28189	194360	41.81	288	39.99	276
BN32	29577	203930	41.41	286	39.65	273
BN33	26805	184818	43.81	302	40.63	280
BW11*	29090	200573	42.73	295	40.38	278
BW12	28916	199373	42.91	296	41.18	284
BW13	27788	191595	41.96	289	39.45	272
BW21	28362	195553	41.07	283	36.27	250
BW22	30107	207585	40.34	278	37.23	257
BW23	29904	206185	40.06	276	38.81	268
BW31	28369	195601	42.99	296	40.12	277
BW32	28257	194829	42.58	294	40.33	278
BW33	28348	195457	42.78	295	40.92	282
Average	28571	196996	42.01	290	39.57	273
COV	0.03	0.03	0.03	0.03	0.03	0.03

Sample ID	Dynamic Yield Stress (ksi)	Dynamic Yield Stress (MPa)	Tensile Strength (ksi)	Tensile Strength (Mpa)	Elongation (%)	Area Reduction (%)
BN11	42.77	295	66.14	456	37.24	69.36
BN12	43.06	297	66.69	460	36.36	68.69
BN13	42.17	291	65.95	455	37.21	67.19
BN21	41.06	283	66.51	459	38.07	71.26
BN22	42.52	293	66.68	460	39.17	66.99
BN23	43.06	297	66.58	459	39.22	71.08
BN31	44.02	304	66.28	457	38.96	70.47
BN32	42.08	290	66.14	456	37.32	69.51
BN33	43.00	296	67.19	463	34.98	66.36
BW11*	43.17	298	66.72	460	-	
BW12	43.31	299	66.24	457	38.69	69.94
BW13	42.31	292	65.24	450	69.03	69.03
BW21	40.59	280	66.49	458	68.47	69.65
BW22	41.07	283	66.12	456	40.88	68.47
BW23	40.81	281	65.43	451	37.04	69.54
BW31	42.50	293	66.38	458	37.83	70.78
BW32	43.40	299	66.38	458	37.72	69.18
BW33	43.09	297	66.29	457	36.93	70.87
Average	42.44	293	66.30	457	37.91	69.32
COV	0.02	0.02	0.01	0.01	0.04	0.02

* Sample was damaged before a final measurement could be taken

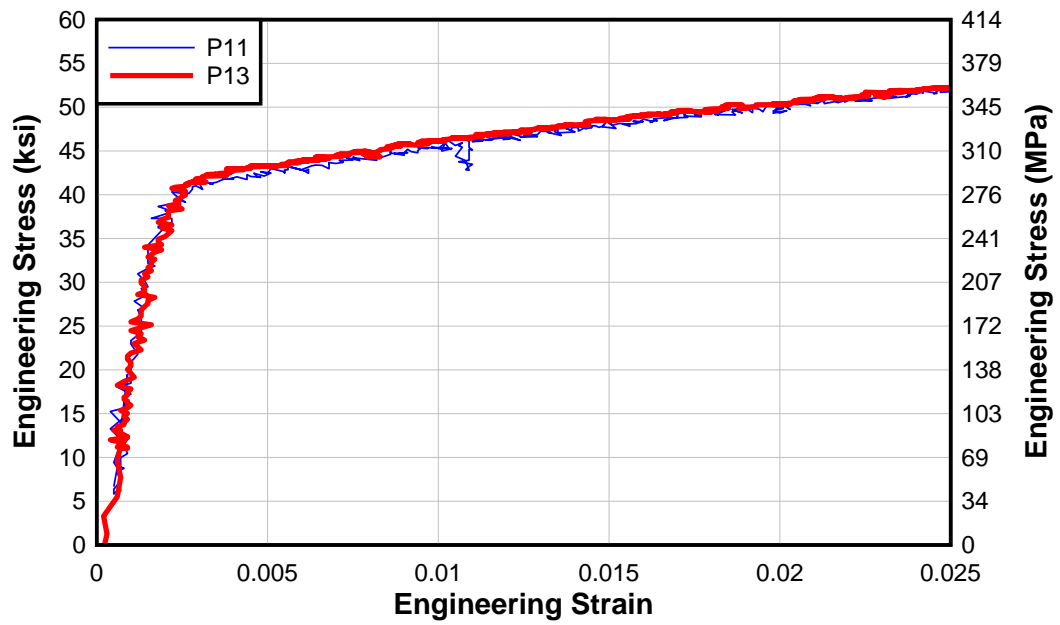


Figure A-37: Engineering stress vs. engineering strain for the parallel rolling direction 1/2 in. thick A36 sample P1

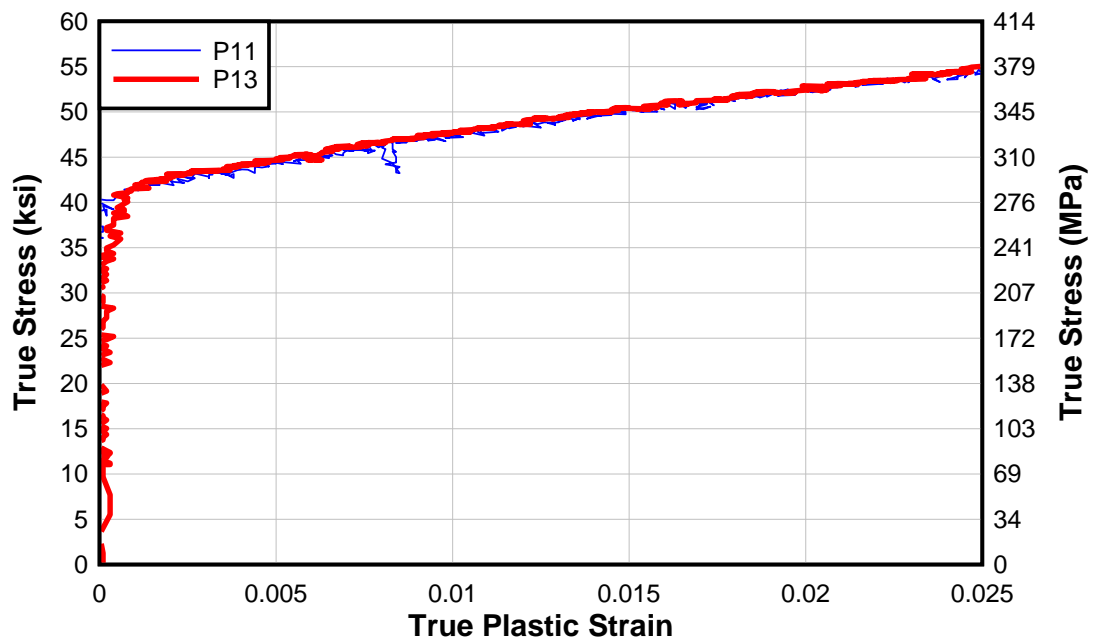


Figure A-38: True stress vs. true plastic strain for the parallel rolling direction 1/2 in. thick A36 sample P1

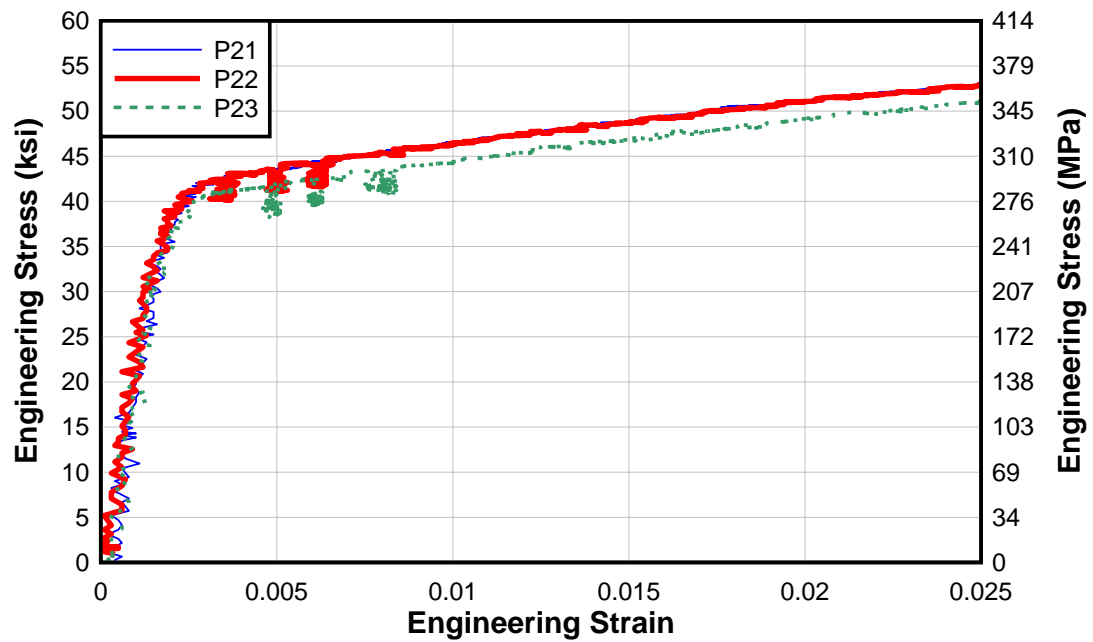


Figure A-39: Engineering stress vs. engineering strain for the parallel rolling direction 1/2 in. thick A36 sample P2

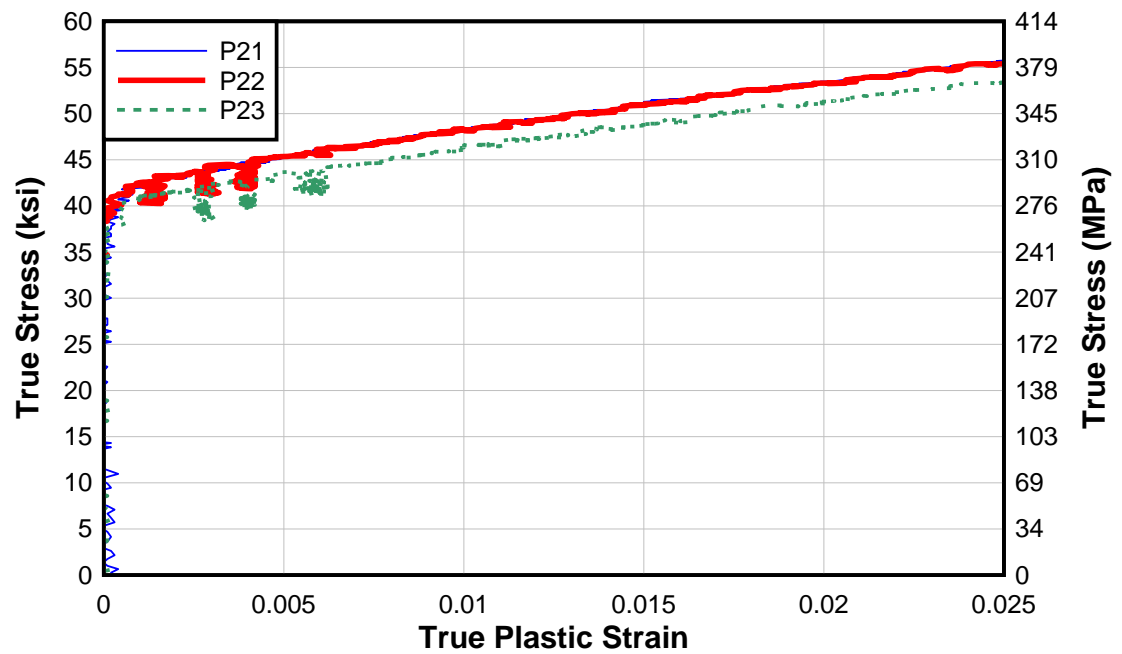


Figure A-40: True stress vs. true plastic strain for the parallel rolling direction 1/2 in. thick A36 sample P2

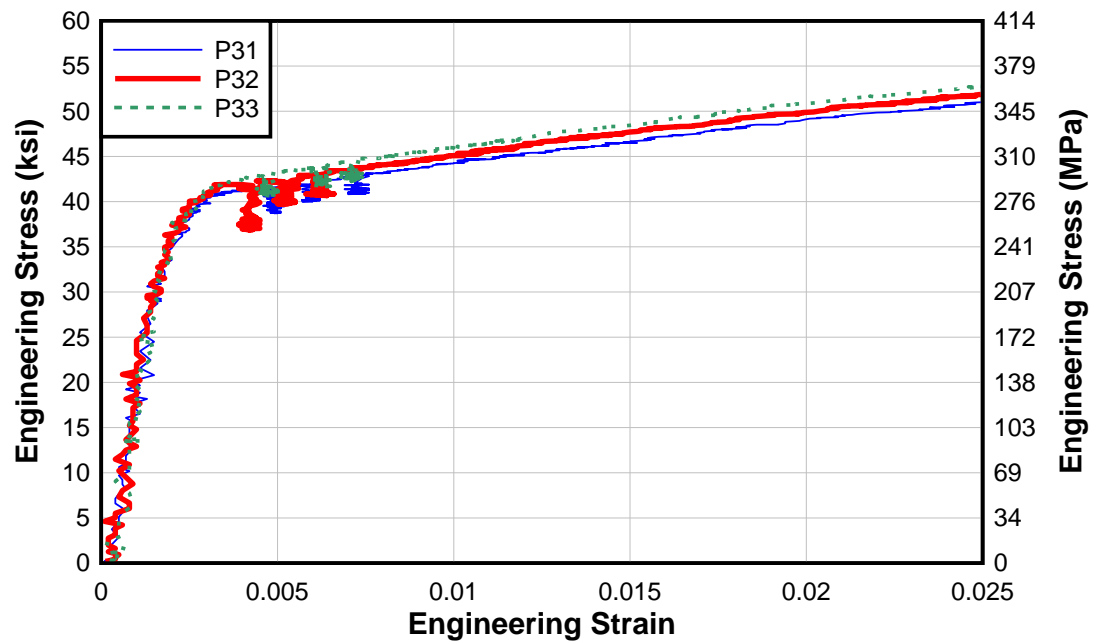


Figure A-41: Engineering stress vs. engineering strain for the parallel rolling direction 1/2 in. thick A36 sample P3

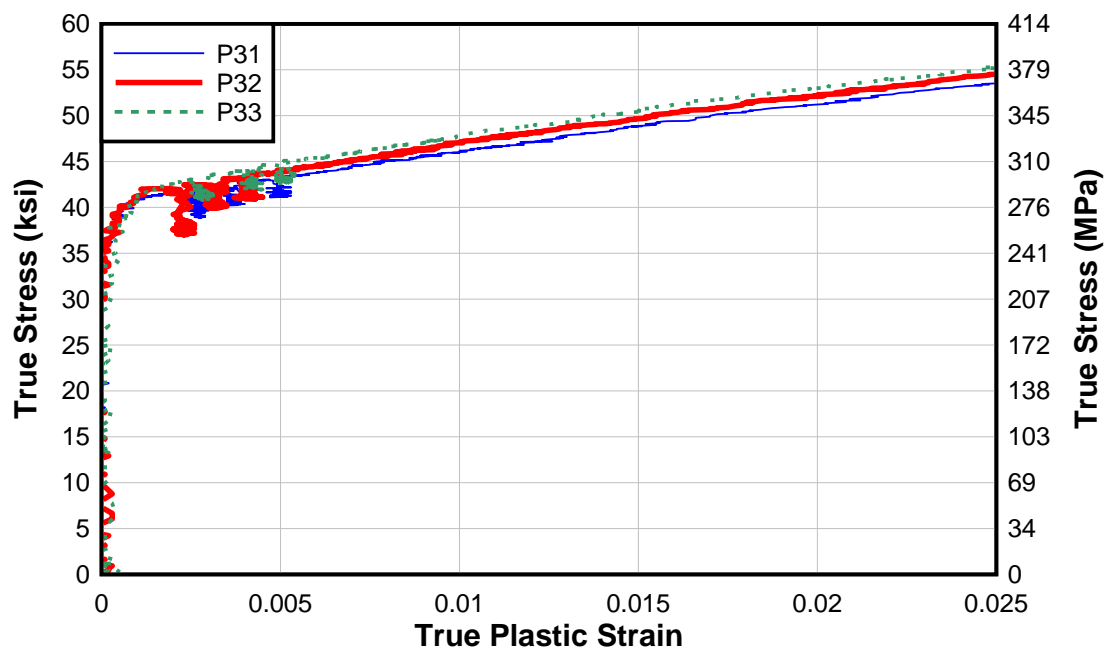


Figure A-42: True stress vs. true plastic strain for the parallel rolling direction 1/2 in. thick A36 sample P3

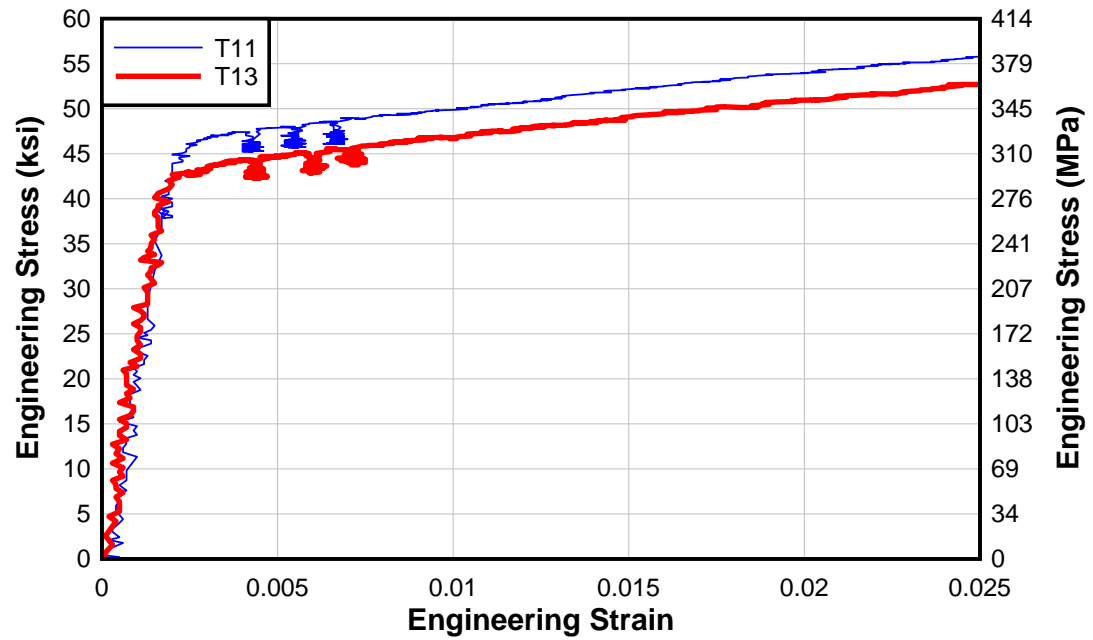


Figure A-43: Engineering stress vs. engineering strain for the transverse rolling direction 1/2 in. thick A36 sample T1

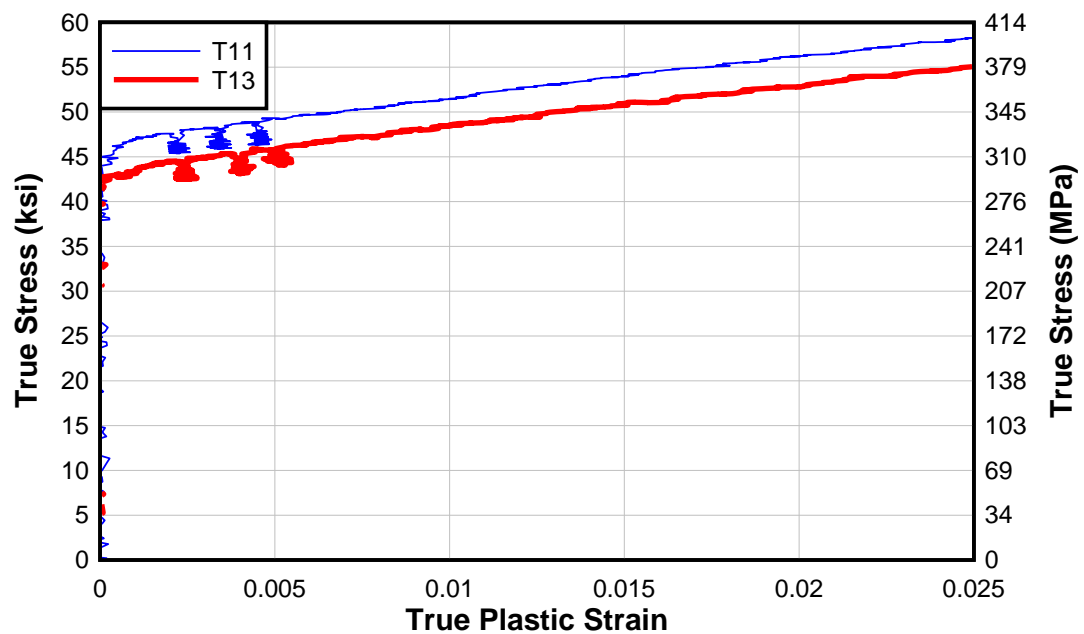


Figure A-44: True stress vs. true plastic strain for the transverse rolling direction 1/2 in. thick A36 sample T1

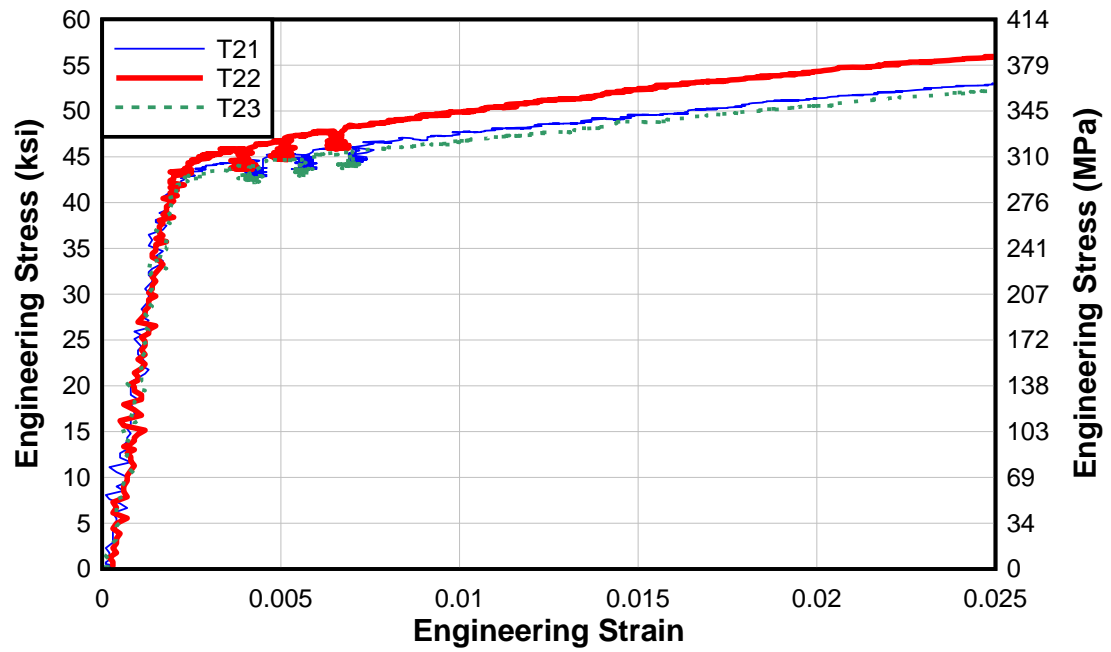


Figure A-45: Engineering stress vs. engineering strain for the transverse rolling direction 1/2 in. thick A36 sample T2

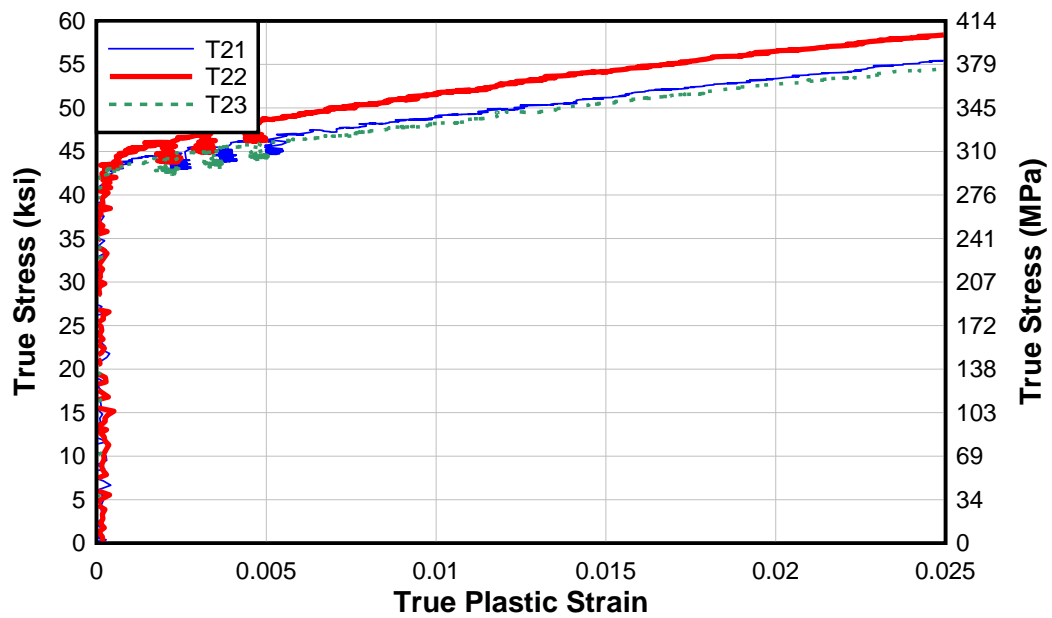


Figure A-46: True stress vs. true plastic strain for the transverse rolling direction 1/2 in. thick A36 sample T2

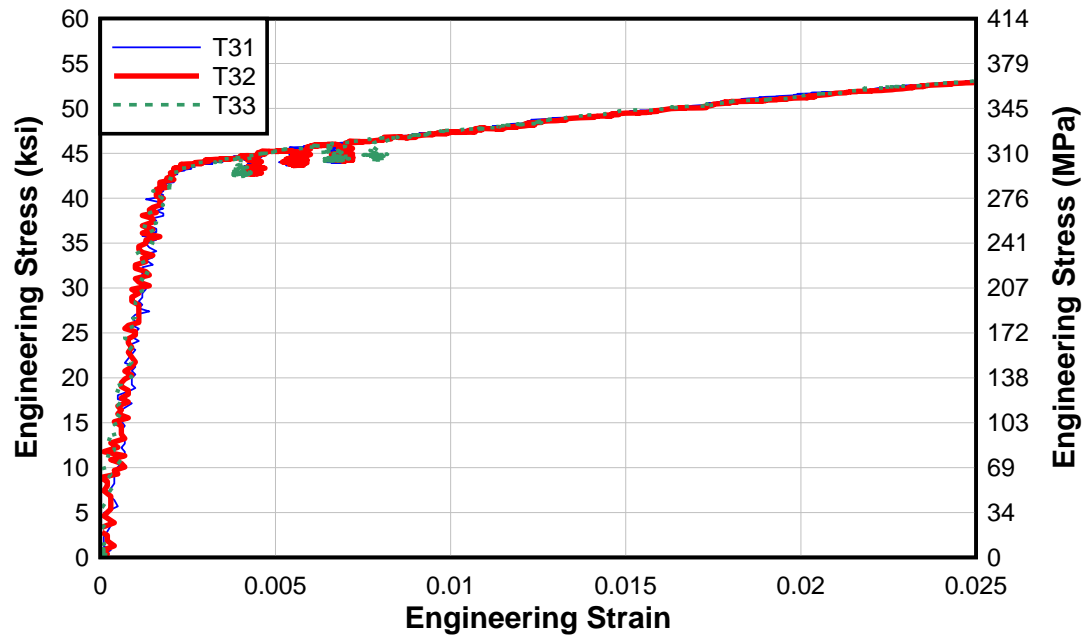


Figure A-47: Engineering stress vs. engineering strain for the transverse rolling direction 1/2 in. thick A36 sample T3

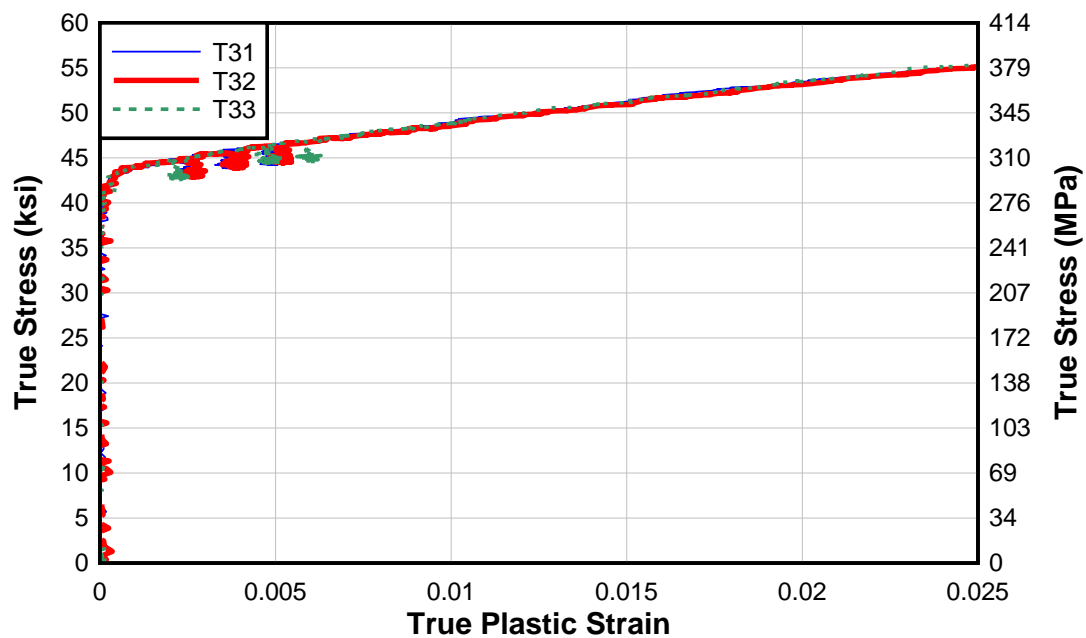


Figure A-48: True stress vs. true plastic strain for the transverse rolling direction 1/2 in. thick A36 sample T3

Table A-16: Results summary for the parallel rolling direction 1/2 in. thick A36 plate

Sample ID	Measured Modulus of Elasticity (ksi)	Measured Modulus of Elasticity (MPa)	0.2% Offset Dynamic Yield Stress (ksi)	0.2% Offset Dynamic Yield Stress (Mpa)	Yield Stress Drop (ksi)	Yield Stress Drop (MPa)
P11	22843	157500	41.76	288	-	-
P12	-	-	-	-	-	-
P13	23858	164499	42.49	293	-	-
P21	22511	155211	42.84	295	-	-
P22	23942	165078	43.15	298	2.46	17
P23	22615	155928	41.24	284	2.95	20
P31	22054	152060	41.29	285	2.18	15
P32	22092	152322	41.97	289	3.28	23
P33	24240	167132	42.31	292	2.14	15
Average	23019	158716	42.18	290	2.60	18
COV	0.038	0.038	0.017	0.016	0.191	0.191
Sample ID	Static Yield Stress (ksi)	Static Yield Stress (MPa)	Tensile Strength (ksi)	Tensile Strength (Mpa)	Elongation (%)	Area Reduction (%)
P11	-	-	64.93	448	41.65%	73.17
P12	-	-	-	-	-	-
P13	-	-	66.12	456	40.15%	70.51
P21	-	-	67.03	462	40.28%	70.68
P22	40.69	281	66.67	460	37.35%	73.90
P23	38.29	264	65.59	452	41.53%	70.25
P31	39.11	270	65.32	450	38.68%	73.00
P32	38.69	267	65.91	454	38.93%	71.03
P33	40.17	277	66.83	461	39.90%	69.73
Average	39.39	272	66.05	455	0.40	71.54
COV	0.03	0.03	0.01	0.01	0.04	0.02

Table A-17: Results summary for the transverse rolling direction 1/2 in. thick A36 plate

Sample ID	Measured Modulus of Elasticity (ksi)	Measured Modulus of Elasticity (MPa)	0.2% Offset Dynamic Yield Stress (ksi)	0.2% Offset Dynamic Yield Stress (Mpa)	Yield Stress Drop (ksi)	Yield Stress Drop (MPa)
T11	26570	183197	47.35	326	2.34	16
T12	-	-	-	-	-	-
T13	24776	170828	44.23	305	2.01	14
T21	23830	164305	44.61	308	1.86	13
T22	25883	178461	45.91	317	2.06	14
T23	24362	167974	43.96	303	1.78	12
T31	25790	177819	44.34	306	1.87	13
T32	25896	178550	44.35	306	1.84	13
T33	24190	166788	44.4	306	2.05	14
Average	25162	173490	44.89	310	1.98	14
COV	0.040	0.040	0.026	0.026	0.092	0.092
Sample ID	Static Yield Stress (ksi)	Static Yield Stress (MPa)	Tensile Strength (ksi)	Tensile Strength (Mpa)	Elongation (%)	Area Reduction (%)
T11	45.01	310	68.98	476	34.53	68.45
T12	-	-	-	-	-	-
T13	42.22	291	65.57	452	33.93	66.79
T21	42.75	295	66.06	455	35.73	66.37
T22	43.85	302	66.73	460	31.85	69.62
T23	42.18	291	64.78	447	33.98	68.59
T31	42.47	293	64.66	446	33.95	69.53
T32	42.51	293	65.39	451	33.90	67.15
T33	42.35	292	65.22	450	35.45	67.73
Average	42.92	296	65.92	455	0.34	68.03
COV	0.02	0.02	0.02	0.02	0.03	0.02

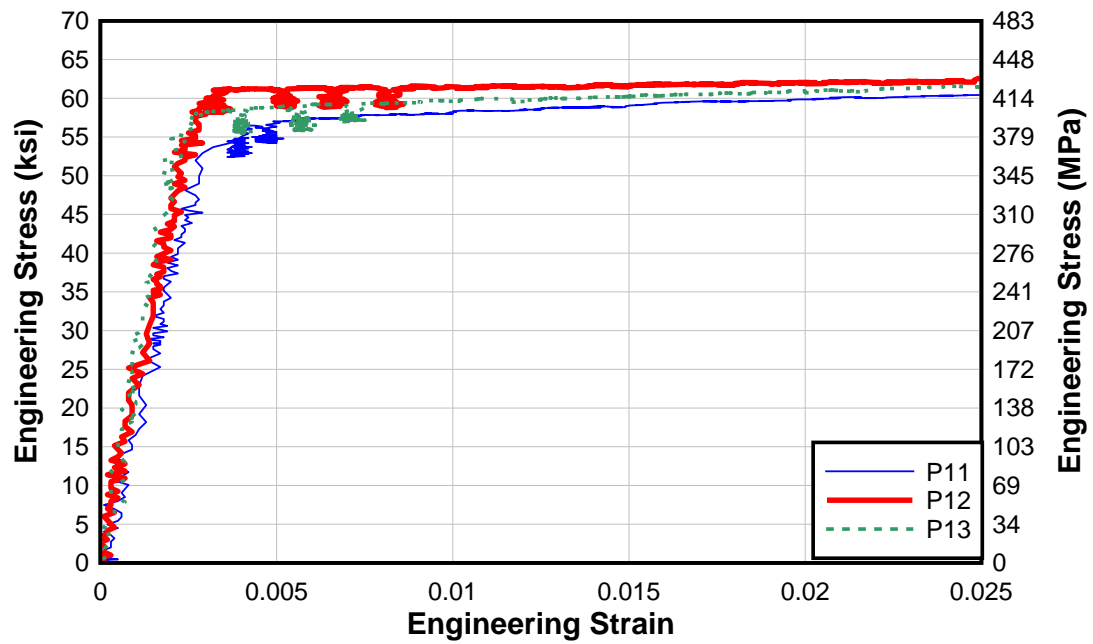


Figure A-49: Engineering stress vs. engineering strain for the parallel rolling direction 3/8 in. thick Gr. 50 sample P1

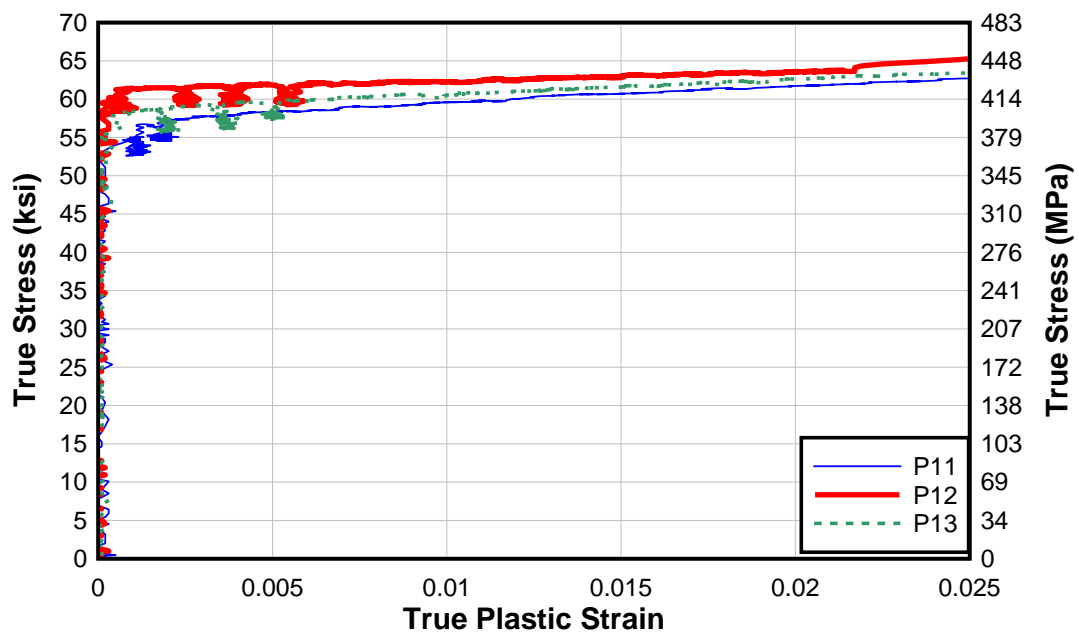


Figure A-50: Engineering stress vs. engineering strain for the parallel rolling direction 3/8 in. thick Gr. 50 sample P1

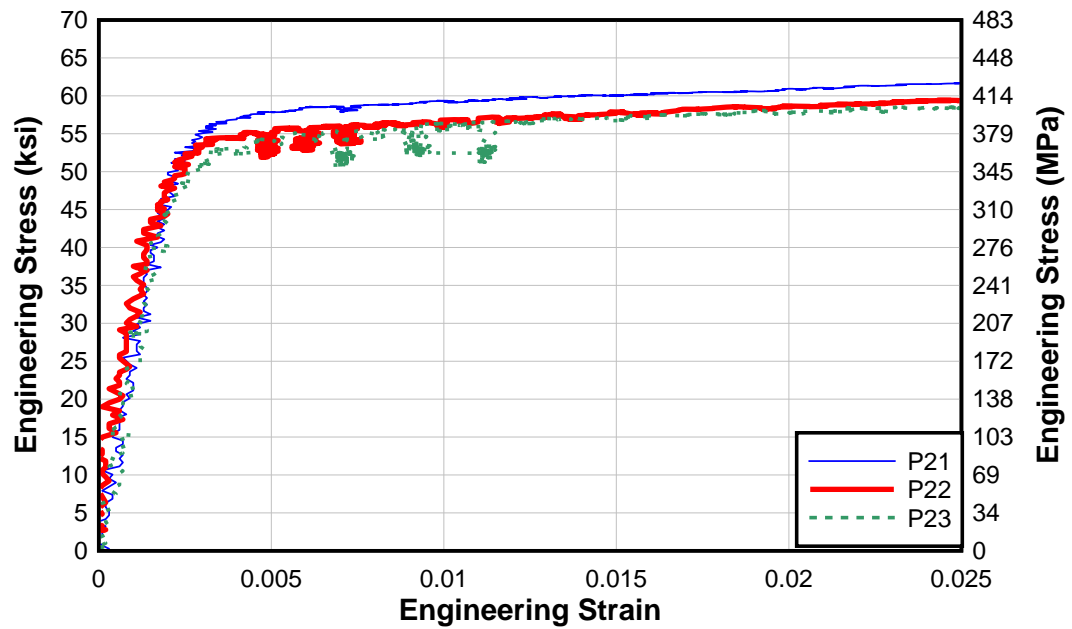


Figure A-51: Engineering stress vs. engineering strain for the parallel rolling direction 3/8 in. thick Gr. 50 sample P2

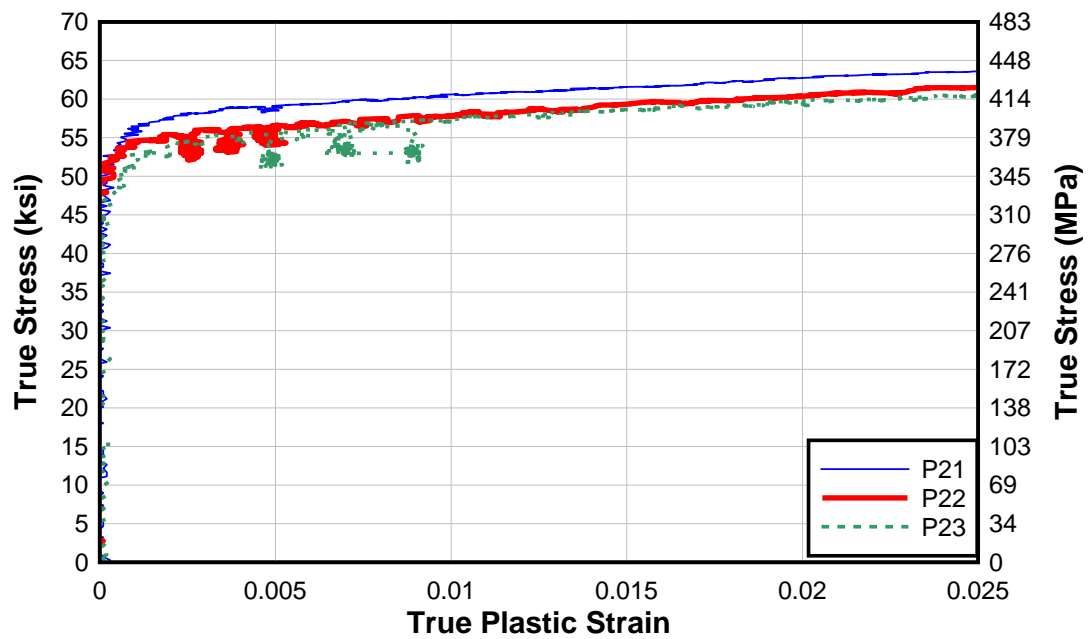


Figure A-52: Engineering stress vs. engineering strain for the parallel rolling direction 3/8 in. thick Gr. 50 sample P2

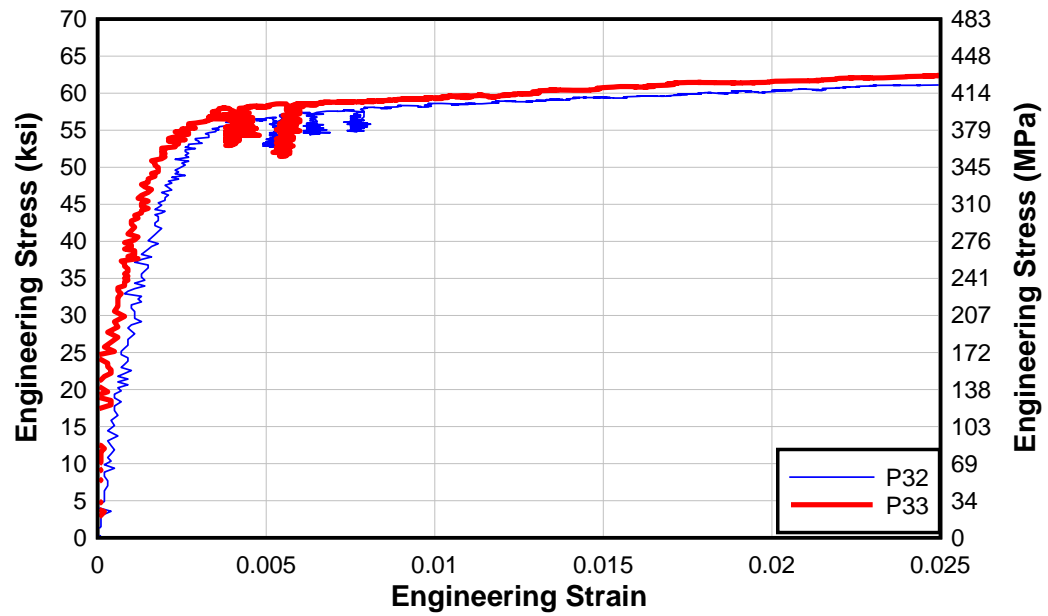


Figure A-53: Engineering stress vs. engineering strain for the parallel rolling direction 3/8 in. thick Gr. 50 sample P3

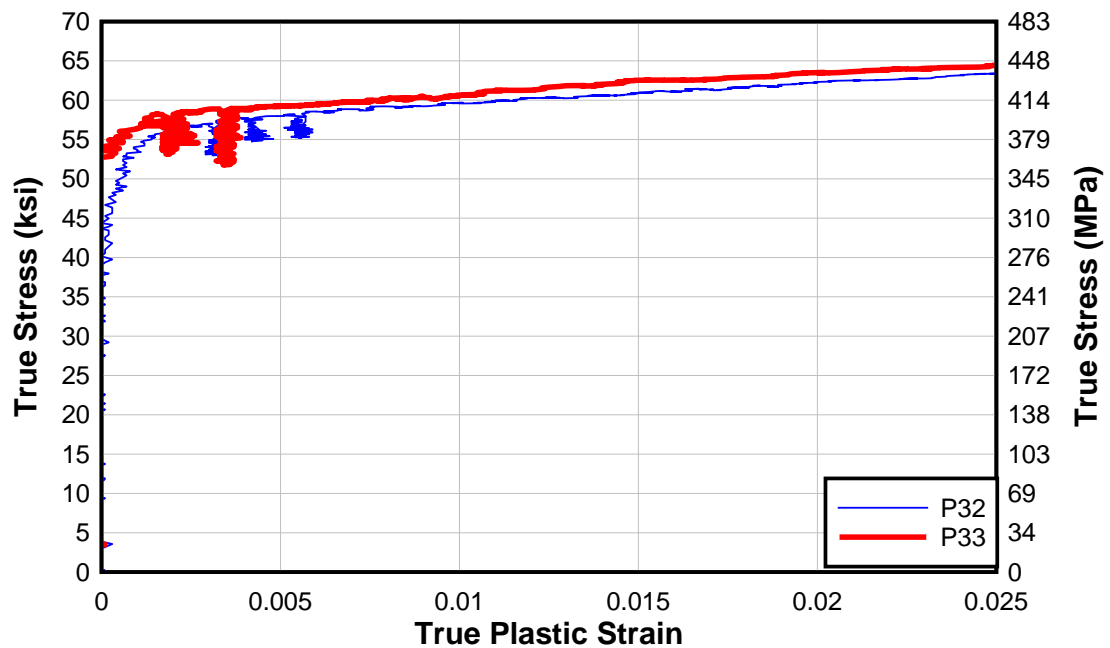


Figure A-54: Engineering stress vs. engineering strain for the parallel rolling direction 3/8 in. thick Gr. 50 sample P3

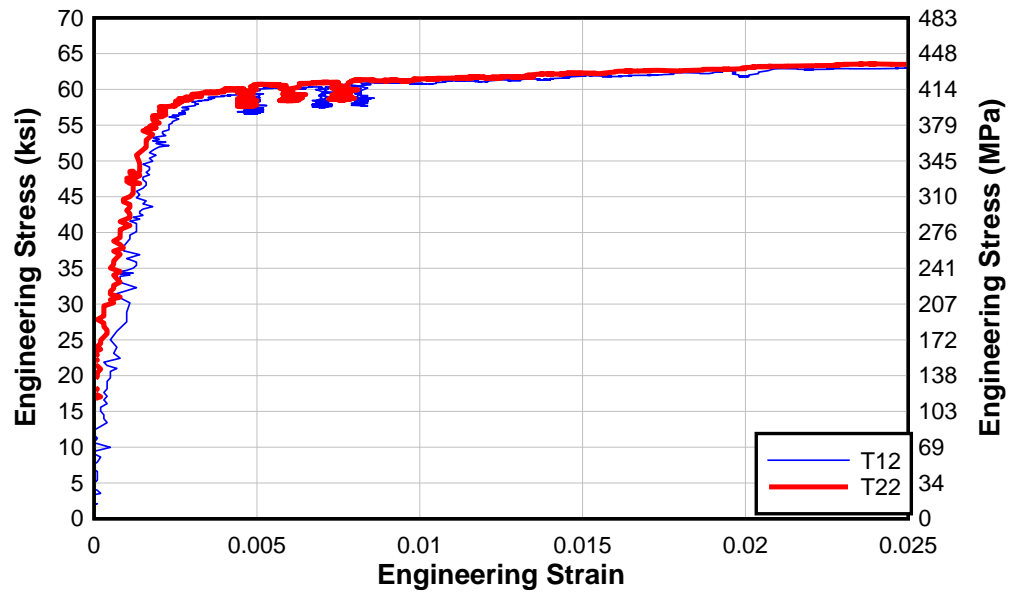


Figure A-55: Engineering stress vs. engineering strain for the transverse rolling direction 3/8 in. thick Gr. 50 sample T1

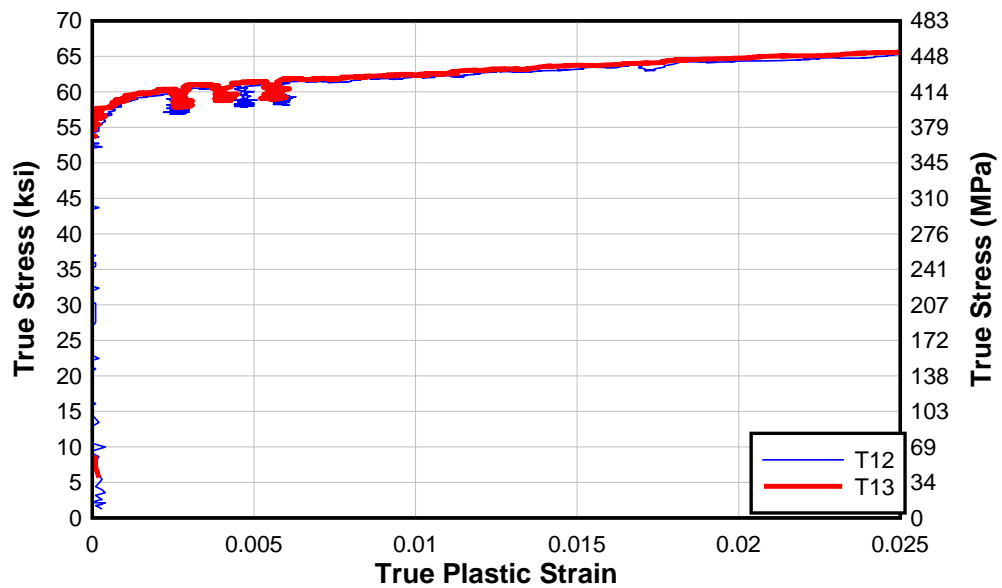


Figure A-56: True stress vs. true plastic strain for the transverse rolling direction 3/8 in. thick Gr. 50 sample T1

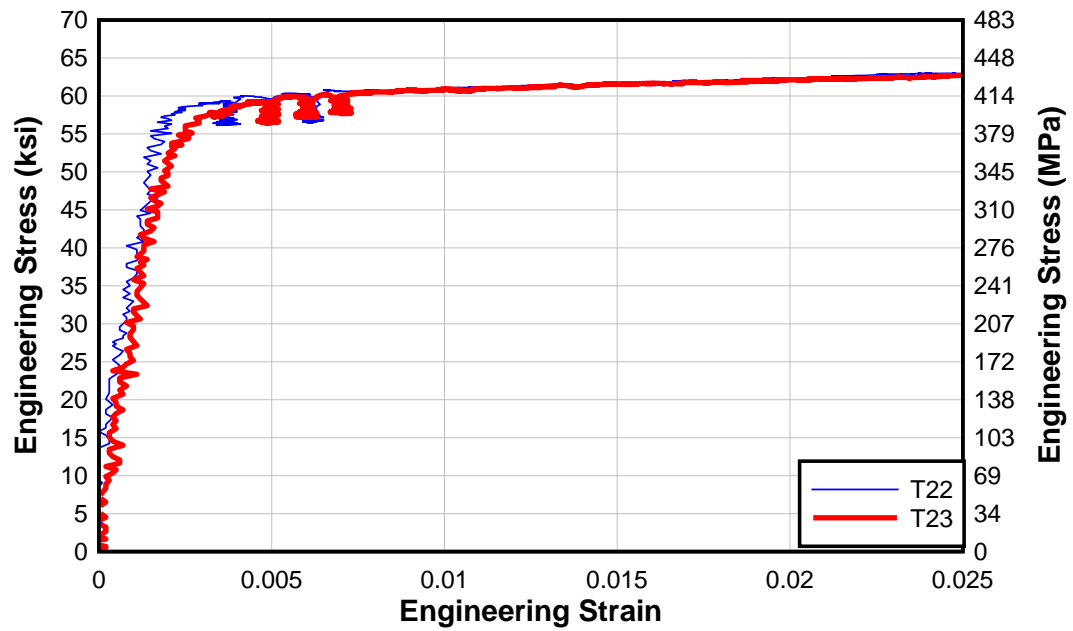


Figure A-57: Engineering stress vs. engineering strain for the transverse rolling direction 3/8 in. thick Gr. 50 sample T2

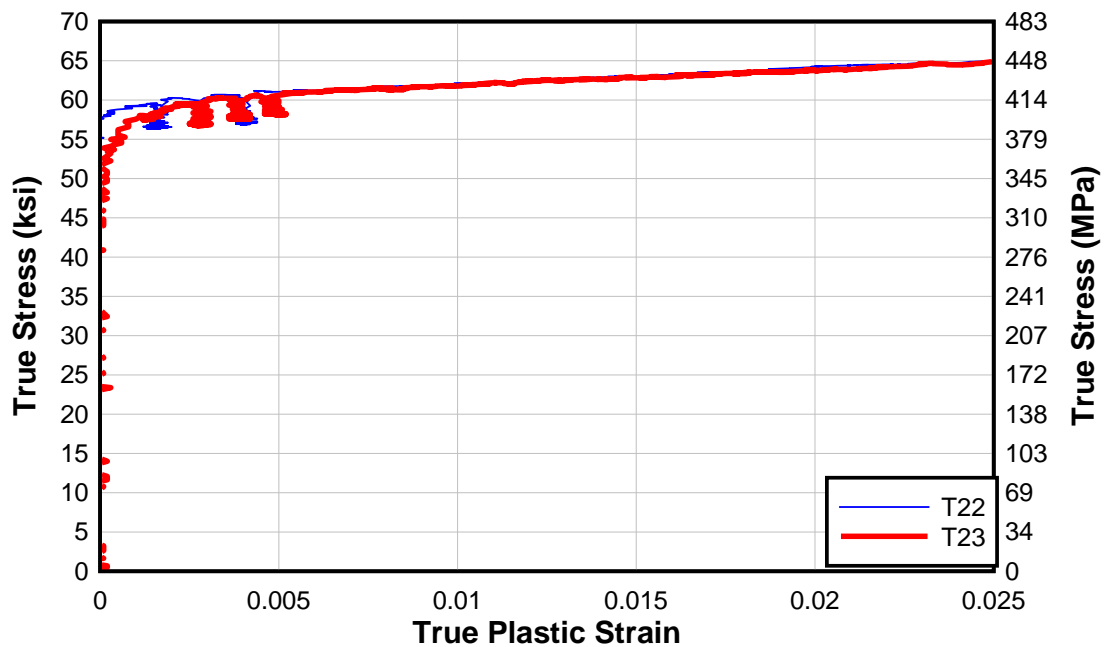


Figure A-58: True stress vs. true plastic strain for the transverse rolling direction 3/8 in. thick Gr. 50 sample T2

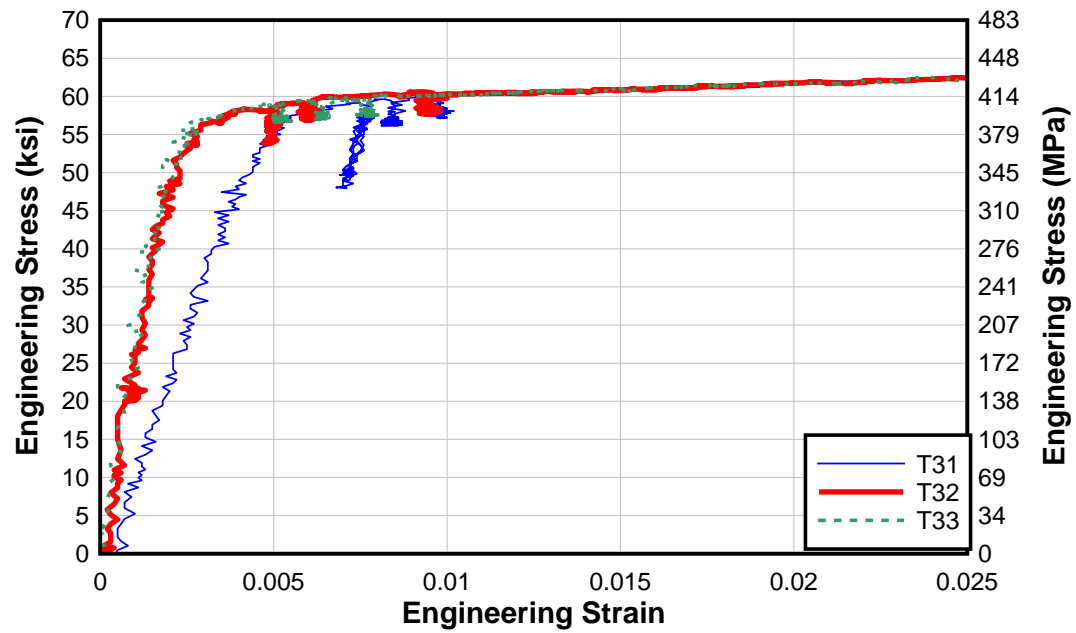


Figure A-59: Engineering stress vs. engineering strain for the transverse rolling direction 3/8 in. thick Gr. 50 sample T3

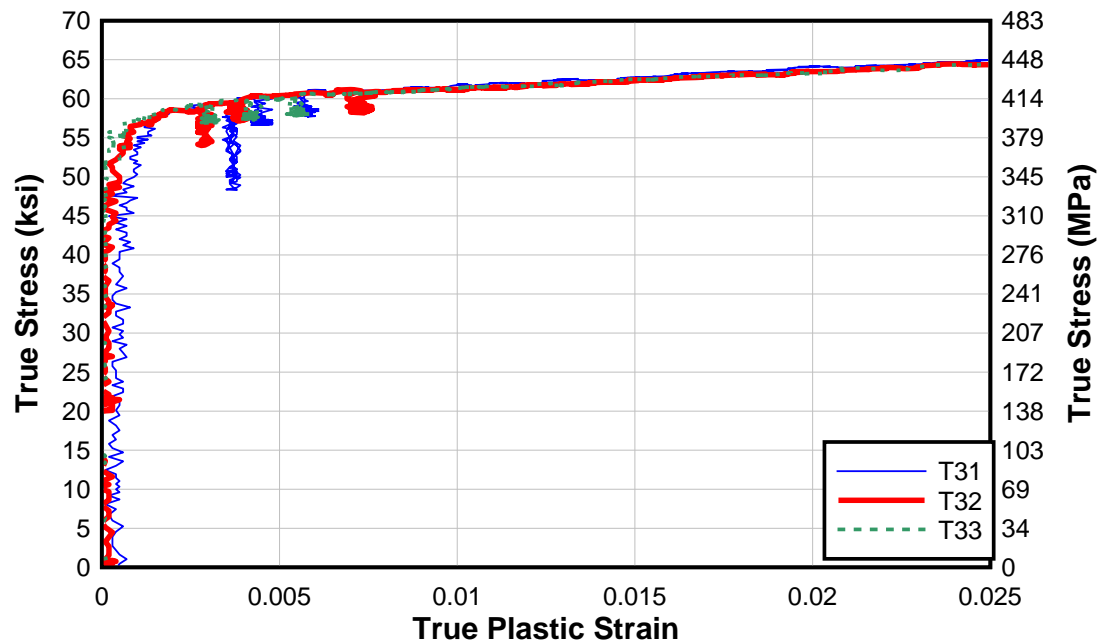


Figure A-60: True stress vs. true plastic strain for the transverse rolling direction 3/8 in. thick Gr. 50 sample T3

Table A-18: Results for parallel rolling direction 3/8 in. thick Gr. 50 plate

Sample ID	Measured Modulus of Elasticity (ksi)	Measured Modulus of Elasticity (MPa)	0.2% Offset Dynamic Yield Stress (ksi)	0.2% Offset Dynamic Yield Stress (MPa)	Yield Stress Drop (ksi)	Yield Stress Drop (MPa)
P11	19109	131755	56.59	390	2.15	15
P12	22471	154935	61.19	422	2.48	17
P13	27949	192706	58.34	402	2.79	19
P21	24979	172228	57.22	395	-	-
P22	23484	161920	54.46	375	2.83	20
P23	29346	202338	52.78	364	4.21	29
P31	-	-	-	-	-	-
P32	26447	182349	56.21	388	3.31	23
P33	26056	179654	57.96	400	5.10	35
Average	24980	172235	56.88	392	3.27	23
COV	0.13	0.13	0.05	0.04	0.32	0.32
Sample ID	Static Yield Stress (ksi)	Static Yield Stress (MPa)	Tensile Strength (ksi)	Tensile Strength (Mpa)	Elongation (%)	Area Reduction (%)
P11	54.44	375	66.15	456	38.08	72.59
P12	58.71	405	65.61	452	37.53	72.88
P13	55.55	383	67.05	462	36.20	74.50
P21	-	-	67.08	462	35.48	75.88
P22	51.63	356	65.64	453	35.13	75.32
P23	48.57	335	65.12	449	37.28	74.50
P31	-	-	-	-	-	75.90
P32	52.90	365	67.69	467	38.65	71.83
P33	52.86	364	68.68	474	39.33	74.64
Average	53.52	369	66.63	459	0.37	74.23
COV	0.06	0.06	0.02	0.02	0.04	0.02

Table A-19: Results for transverse rolling direction 3/8 in. thick Gr. 50 plate

Sample ID	Measured Modulus of Elasticity (ksi)	Measured Modulus of Elasticity (MPa)	0.2% Offset Dynamic Yield Stress (ksi)	0.2% Offset Dynamic Yield Stress (MPa)	Yield Stress Drop (ksi)	Yield Stress Drop (MPa)
T11	-	-	-	-	-	-
T12	21930	151205	59.31	409	2.92	20
T13	25226	173931	59.86	413	2.44	17
T21	-	-	-	-	-	-
T22	27529	189810	59.35	409	3.56	25
T23	27522	189761	58.18	401	2.68	18
T31	14653	101031	58.05	400	3.22	22
T32	27527	189796	58.18	401	3.26	22
T33	26857	185176	58.12	401	2.44	17
Average	24463	168673	58.72	405	2.93	20
COV	0.20	0.20	0.01	0.01	0.15	0.15
Sample ID	Static Yield Stress (ksi)	Static Yield Stress (MPa)	Tensile Strength (ksi)	Tensile Strength (Mpa)	Elongation (%)	Area Reduction (%)
T11	-	-	-	-	-	63.24
T12	56.39	389	68.44	472	35.65%	61.57
T13	57.42	396	68.65	473	38.73%	62.02
T21	-	-	-	-	-	61.04
T22	55.79	385	68.08	469	35.60%	65.64
T23	55.50	383	68.04	469	36.30%	60.97
T31	54.84	378	68.41	472	38.13%	63.50
T32	54.92	379	67.91	468	36.08%	61.26
T33	55.68	384	67.84	468	37.75%	58.83
Average	55.79	385	68.20	470	0.37	62.01
COV	0.02	0.02	0.00	0.00	0.03	0.03

B. MATERIAL FABRICATION DOCUMENTS

TICO TITANIUM, INC *Certification of Tests*

30150 S Wixom Rd • Wixom • MI • 48393-3340 • 248-446-0400 • 800-521-4392 • Fax 248-446-1991
 519 Todd Dr • Oak Ridge North • TX • 77385-7332 • 281-355-6555 • 888-676-7575 • Fax 281-355-6676

TO: ORSTA
 OREGON STATE UNIVERSITY
 ELECTRICAL & COMPUTER ENGINEER
 CORVALLIS, OR 97331-3211

DATE: 12/10/2012
CUSTOMER PO: VERBAL THERESE
TICO SO: 6630

HEAT NUMBER: 61003-1

SPECIFICATION: ASTM B-265-10/ASME SB-265/AMS 4911L **** GR. 5 ****
 TI 6AL-4V/EN 10204:2004 TYPE 3.1

DESCRIPTION: PLATE 1.00" TK X 4.25" X 8.5" 1 PC.

COMMENTS:

CHEMISTRY %:

Al	ALUMINUM	6.11
V	VANADIUM	4.275
Fe	IRON	0.22
O	OXYGEN	0.16
N ₂	NITROGEN	0.007
C	CARBON	0.05

RESIDUAL ELEMENTS (EACH) LESS THAN 0.10
 RESIDUAL ELEMENTS (TOTAL) LESS THAN 0.40

FINAL PRODUCT HYDROGEN: <.003
 TITANIUM REMAINDER

TENSILE DATA:	TEST 1	TEST 2	TEST 3	TEST 4
TENSILE PSI:	142000		149000	
YIELD 0.2% OFFSET:	133000		142000	
ELONGATION % IN 4D:	13		13	
RA %:				

PRODUCT ANNEALED: YES

PHYSICAL/MECHANICAL TEST DATA:

HYDROSTATIC:	ULTRASONIC:	GUIDED BEND:
FLATTENING:	PNEUMATIC:	
FLARE:	EDDY CURRENT:	

MATERIAL FREE FROM MERCURY CONTAMINATION
MATERIAL CONFORMS TO ALL TECHNICAL AND WORKMANSHIP REQUIREMENTS OF SPECIFICATIONS

PRINTED: 12/10/2012 2:12:50PM

Carie Westfal
 Carie Westfal, Certification Clerk

Figure B-1: Mill certification for titanium plate 1

TICO TITANIUM, INC *Certification of Tests*

30150 S Wixom Rd • Wixom • MI • 48393-3340 • 248-446-0400 • 800-521-4392 • Fax 248-446-1911
 519 Todd Dr • Oak Ridge North • TX • 77385-7332 • 281-355-6555 • 888-676-7575 • Fax 281-355-6611

TO: ORSTA
 OREGON STATE UNIVERSITY
 ELECTRICAL & COMPUTER ENGINEER
 CORVALLIS, OR 97331-3211

DATE: 10/4/2012
CUSTOMER PO: J1672A
TICO SO: 3888

HEAT NUMBER: 61002-1

SPECIFICATION: ASTM B-265-10/ASME SB-265/AMS 4911L **** GR. 5 ****
 TI 6AL-4V/EN 10204:2004 TYPE 3.1

DESCRIPTION: PLATE .500" TK X 3" X 3" 1 PC.

COMMENTS:

CHEMISTRY %:

Al	ALUMINUM	6.075
V	VANADIUM	4.225
Fe	IRON	0.09
O	OXYGEN	0.165
N	NITROGEN	0.018
C	CARBON	0.05
H	HYDROGEN	0.01

RESIDUAL ELEMENTS (EACH) LESS THAN 0.10
 RESIDUAL ELEMENTS (TOTAL) LESS THAN 0.40

FINAL PRODUCT HYDROGEN: <.003
 TITANIUM REMAINDER

TENSILE DATA:	TEST 1	TEST 2	TEST 3	TEST 4
TENSILE PSI:	143000		147000	
YIELD 0.2% OFFSET:	131000		140000	
ELONGATION % IN 4D:	13		13	
RA %:				

PRODUCT ANNEALED: YES

PHYSICAL/MECHANICAL TEST DATA:

HYDROSTATIC:	ULTRASONIC:	GUIDED BEND:
FLATTENING:	PNEUMATIC:	
FLARE:	EDDY CURRENT:	

MATERIAL FREE FROM MERCURY CONTAMINATION
 MATERIAL CONFORMS TO ALL TECHNICAL AND WORKMANSHIP REQUIREMENTS OF SPECIFICATIONS

PRINTED: 10/4/2012 4:50:51PM

Carie Westfal
 Carie Westfal, Certification Clerk

Figure B-2: Mill certification for titanium plate 2

TICO TITANIUM, INC *Certification of Tests*

30150 S Wixom Rd • Wixom • MI • 48393-3340 • 248-446-0400 • 800-521-4392 • Fax 248-446-199
519 Todd Dr • Oak Ridge North • TX • 77385-7332 • 281-355-6555 • 888-676-7575 • Fax 281-355-667

TO: ORSTA
OREGON STATE UNIVERSITY
ELECTRICAL & COMPUTER ENGINEER
CORVALLIS, OR 97331-3211

DATE: 10/4/2012
CUSTOMER PO: J1672A
TICO SO: 3888

HEAT NUMBER: 61003-1

SPECIFICATION: ASTM B-265-10/ASME SB-265/AMS 4911L **** GR. 5 ****
TI 6AL-4V/EN 10204:2004 TYPE 3.1

DESCRIPTION: PLATE 1.00" TK X 1.5" X 11" 1 PC.

COMMENTS:

CHEMISTRY %:

Al	ALUMINUM	6.11
V	VANADIUM	4.275
Fe	IRON	0.22
O	OXYGEN	0.16
N	NITROGEN	0.007
C	CARBON	0.05

RESIDUAL ELEMENTS (EACH) LESS THAN 0.10
RESIDUAL ELEMENTS (TOTAL) LESS THAN 0.40

FINAL PRODUCT HYDROGEN: <.003
TITANIUM REMAINDER

TENSILE DATA:	TEST 1	TEST 2	TEST 3	TEST 4
TENSILE PSI:	142000		149000	
YIELD 0.2% OFFSET:	133000		142000	
ELONGATION % IN 4D:	13		13	
RA %:				

PRODUCT ANNEALED: YES

PHYSICAL/MECHANICAL TEST DATA:

HYDROSTATIC:	ULTRASONIC:	GUIDED BEND:
FLATTENING:	PNEUMATIC:	
FLARE:	EDDY CURRENT:	

MATERIAL FREE FROM MERCURY CONTAMINATION
MATERIAL CONFORMS TO ALL TECHNICAL AND WORKMANSHIP REQUIREMENTS OF SPECIFICATIONS

PRINTED: 10/4/2012 4:50:24PM

Carie Westfal
Carie Westfal, Certification Clerk

Figure B-3: Mill certification for titanium plate 3

Exova
4949 SE Johnson Creek Blvd
Portland
Oregon
USA
97222

T: +1 (503) 777-7458
F: +1 (503) 777-7453
E: sales@exova.com
W: www.exova.com

EXOVA

Test Certificate

FARWEST STEEL CORP.
2000 HENDERSON AVE.
EUGENE, OR
97043

Attn: TERRY TETER

REF No P 164587 : Issue 1
Page 1 of 1
Ord No PO #301-10846
Date Reported 09/10/12
Date Received 09/06/12

Item - TAG #9466, HEAT #M93567, MILL COIL #G94327
TRANSVERSE TENSILE TESTING - COIL SIZE: 5000 X 72.000

Specification - **ASTM A36-08**

TENSILE TEST - ASTM E8/E8M 4D								
	Dimensions [in]	Area [in ²]	GL [in]	0.20%YS [ksi]	UTS [ksi]	%EL	%RA	Comments
001: Flat RT Tensile	0.4910 x 0.5020	0.2465	2.000	49.1	64.4	38	N/A	IL
Specification Minimum				36	58	21	-	
Specification Maximum				-	80	-	-	

Certificate Comments

Material conforms to specification requirements.

Approved By Exova Portland Laboratory

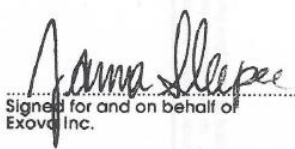

 Signed for and on behalf of
 Exova Inc.

Figure B-4: Mill certification for steel ½ in. thick A36 plate

POSCO Mill Test Certificate/검사증명서

Certificate No./증명서번호: 120720-PPSE-002-001
Date of Issue/발행일자: Jul., 30, 2012

Order No./계약번호: 0005237450

PO No./주문번호: 109-2830S

Supplier/주문자: GS GLOBAL CORP.

Commodity/품명: PLATE

Customer/고객사: FARWEST STEEL

Spec & Type/규격: A36/ASMESA36/A709-36

Size/치수	Product No. 제품번호	Quantity 수량	Weight 중량 (kg)	Heat No. 재질번호	POSITION	Tensile/인장시험 (%)			DIVISION	Chemical Composition/화학성분(%)												
						YP	TS	EL		C	Si	Mn	P	S	Cr	Ni	Cu	Mo	Nb	V		
0.3750"x96"x240"	PA88126103-5104	2	2,222	SF16664	T	337	476	26		L	1431	249	818	89	38	2	1	20	0	0	1	
0.3750"x96"x240"	PA88030101	1	1,111	SF16665	T	361	483	27		P	1472	240		90	40	3	1	19	0	0	2	
0.3750"x96"x240"	PA88148903-8904	2	2,222	SF16769	T	317	472	27		L	1451	267	792	126	44	3	1	21	0	0	1	
										P	1467	259		133	45	3	1	20	0	0	2	
0.3750"x96"x240"	PA88149002-9004	3	3,333	SF18789	T	317	472	27		L	1395	250	831	103	14	2	1	9	0	1	0	
										P	1432	244		112	25	2	1	9	0	1	1	
*** Sub Total (010) ***		8	8,868 (kg)							L	1395	250	831	103	14	2	1	9	0	1	0	
										P	1432	244		112	25	2	1	9	0	1	1	
0.7500"x96"x240"	PA88023901	1	2,222	SF16664	T	308	469	30		L	1431	249	818	89	38	2	1	20	0	0	1	
0.7500"x96"x240"	PA88024201	1	2,222	SF16664	T	308	469	30		P	1472	240		90	40	3	1	19	0	0	2	
0.7500"x96"x240"	PA88023402-3403	2	4,444	SF16664	T	294	449	31		L	1431	249	818	89	38	2	1	20	0	0	1	
										P	1472	240		90	40	3	1	19	0	0	1	
0.7500"x96"x240"	PA88024101	1	2,222	SF16666	T	281	453	29		L	1451	267	792	126	44	3	1	21	0	0	1	
										P	1467	259		133	45	3	1	20	0	0	2	
0.7500"x96"x240"	PA88025601	1	2,222	SF16666	T	294	457	32		L	1451	267	792	126	44	3	1	21	0	0	1	
										P	1467	259		133	45	3	1	20	0	0	2	

* Position : T : Top, M : Middle, B : Bottom

* Tensile Test Direction : Transversal, Gauge Length : 200mm (Rectangular).

* YP Method : 0.2% offset

* Division : L: Ladle Analysis, P: Products Analysis

* Chemical Composition Unit : 2x1/100, 3x1/1000, 4x1/10000, 5x1/100000

* Supply Condition : As-Rolled unless otherwise Heat Treated

We hereby certify that the material herein has been made in accordance with the order and above specification.
This material has been fully killed and made by basic oxygen process.

Test Certificate is issued according to EN10204 3.1.

* This Mill Test Certificate cannot be copied for any purpose

Surveyor To:

M.S. JANG

POSCO Pohang Works, 5 Dongchon-dong, Nam-gu, Pohang-si, Gyeongsangbuk-do, 790-785, Korea

Chief of material testing section Man Soo, Jang

Figure B-5: Mill certification for steel 3/8 in. thick A36 plate



MILL TEST CERTIFICATE

1700 HOLY RD N.E.
Tuscaloosa, AL 35404-1000
800-827-8872

Page #...

Load Number		Tally	Mill Order Number		PO NO Line NO		Part Number		Certificate Number		Prepared									
R010394		00000000469570	N-114499-002		101-11202 2				L387767-1		09/21/2012 21:47									
Grade							Customer:													
Order Description:							Sold TO:													
A572 50, 0.3750 IN x 96.000 IN x 240.000 IN							FARMEST STEEL EUGENE OR													
Quality Plan Description:							Ship TO:													
A57250 FARMEST: ASTM A572-07 GR 50/A709-08 GR 50 FARMEST							FARMEST STEEL Eugene OR													
Shipped Item	Heat/Slab Number	Certified By	C	Mn	P	S	Si	Cu	Ni	Cr	Mo	Cb	V	Al	Ti	N2	B	Ca	Sn	CEV
2T0212B	B2V8414-04 ***	B2V8414	0.07	1.17	0.007	0.001	0.20	0.23	0.08	0.07	0.013	0.032	0.006	0.031	0.011	0.004	0.0000	0.0015	0.008	0.30
Shipped Item	Certified By	Heat Number	Yield ksi	Tensile ksi	Y/T %	ELONGATION %		Bend OK?	Hard HB	Charpy Impacts (ft-lbf)				Shear %				Test Temp		
						2"	8"			Size mm	1	2	3	Avg	1	2	3	Avg		
210212B	S210212FTT	B2V8414 ***	69.5	76.3	91.1	35.6														
210212B	S210212MTT	B2V8414 ***	65.3	74.3	87.9	28.8														

Items: 1 PCS: 8 Weight: 19602 LBS

Mercury has not come in contact with this product during the manufacturing process not has any mercury been used by the manufacturing process. Certified in accordance with EN 10204 3.1. No weld repair has been performed on this material. Manufactured to a fully killed fine grain practice. NUTEMPER TEMPER PASSED plate from coil ISO 9001:2008 Registered, PED Certified

We hereby certify that the product described above passed all of the tests required by the specifications.

April Pitts
April Pitts - QA Engineer

**** indicates Heats melted and Manufactured in the U.S.A.

Figure B-6: Mill certification for steel 3/8 in. thick Gr. 50 plate

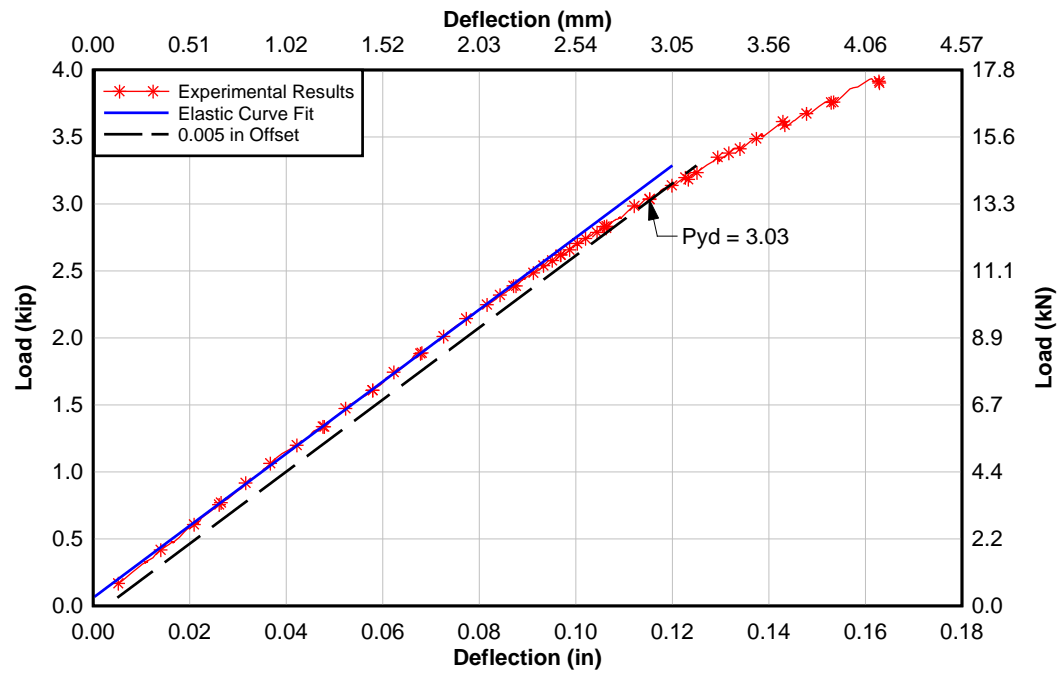
C. EXPERIMENTAL RESULTS 0.005 IN. OFFSET

Figure C-1: 3/8 in. thick A36 plate PW1

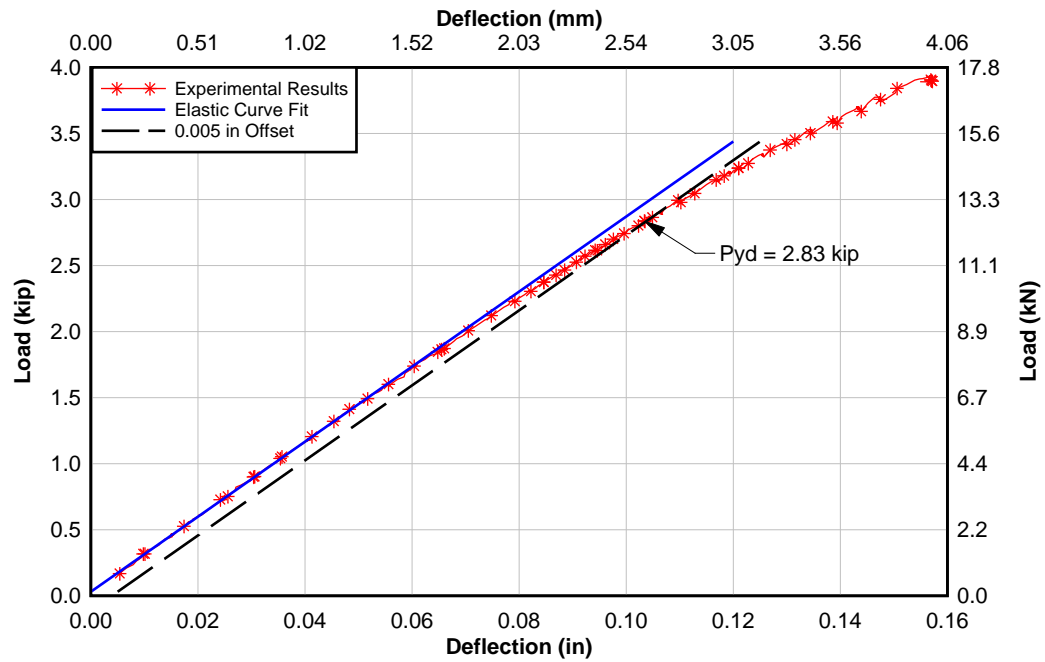


Figure C-2: 3/8 in. thick A36 plate PW1s

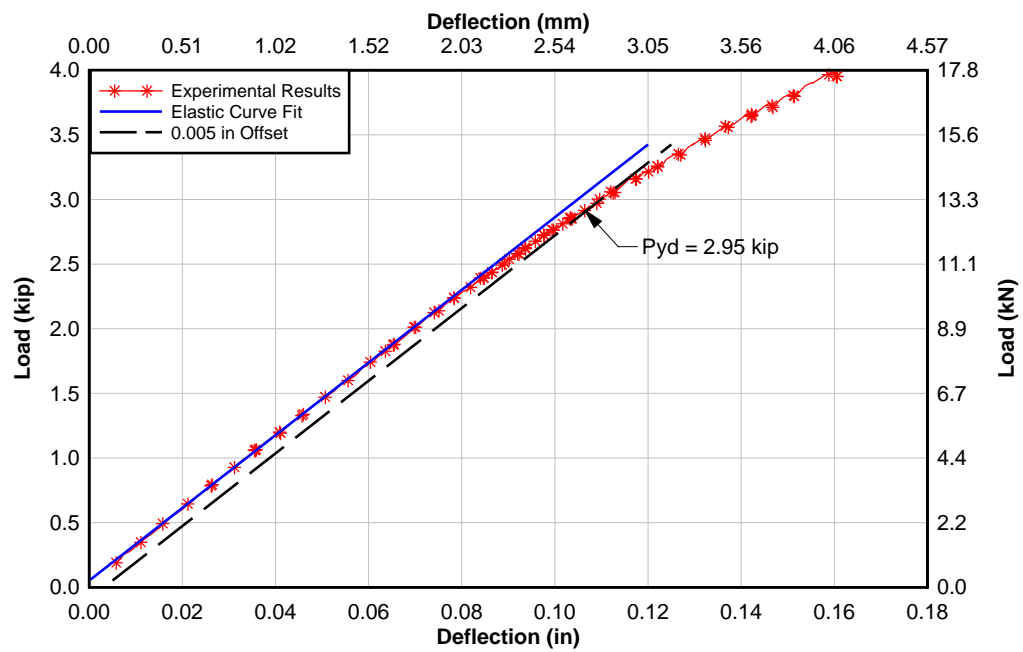


Figure C-3: 3/8 in. thick A36 plate PW2

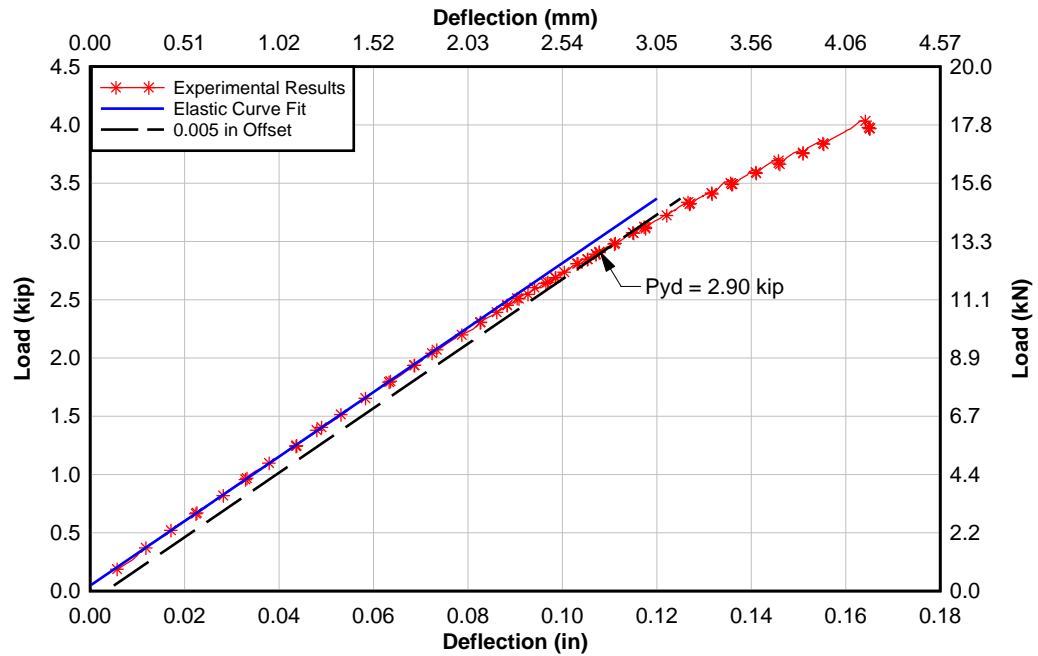


Figure C-4: 3/8 in. thick A36 plate PW2s

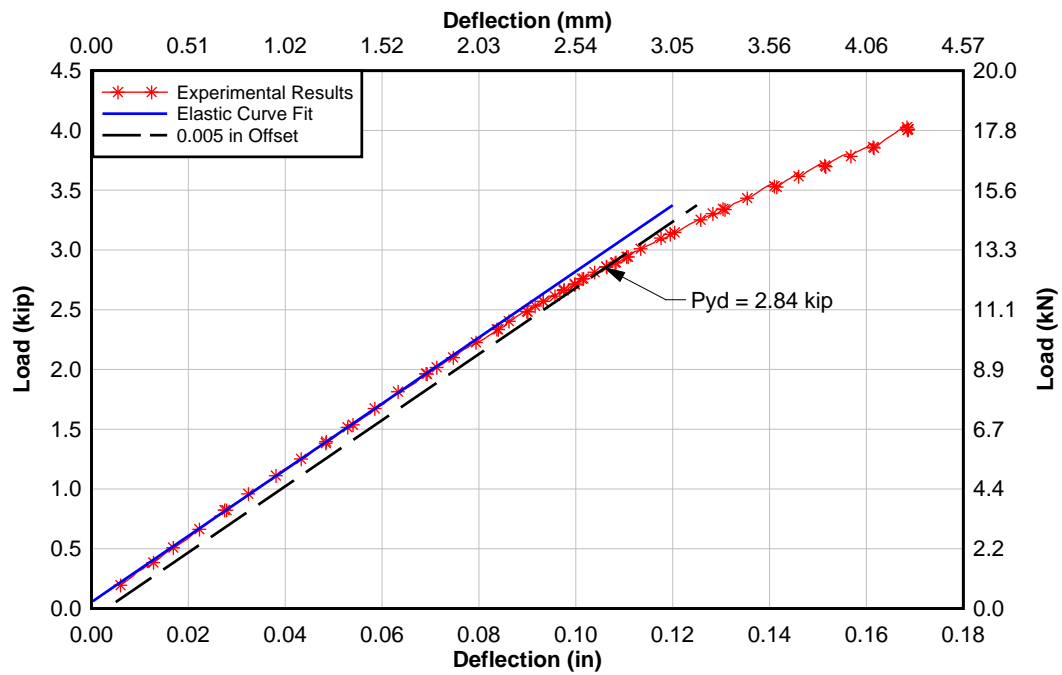


Figure C-5: 3/8 in. thick A36 plate PW3

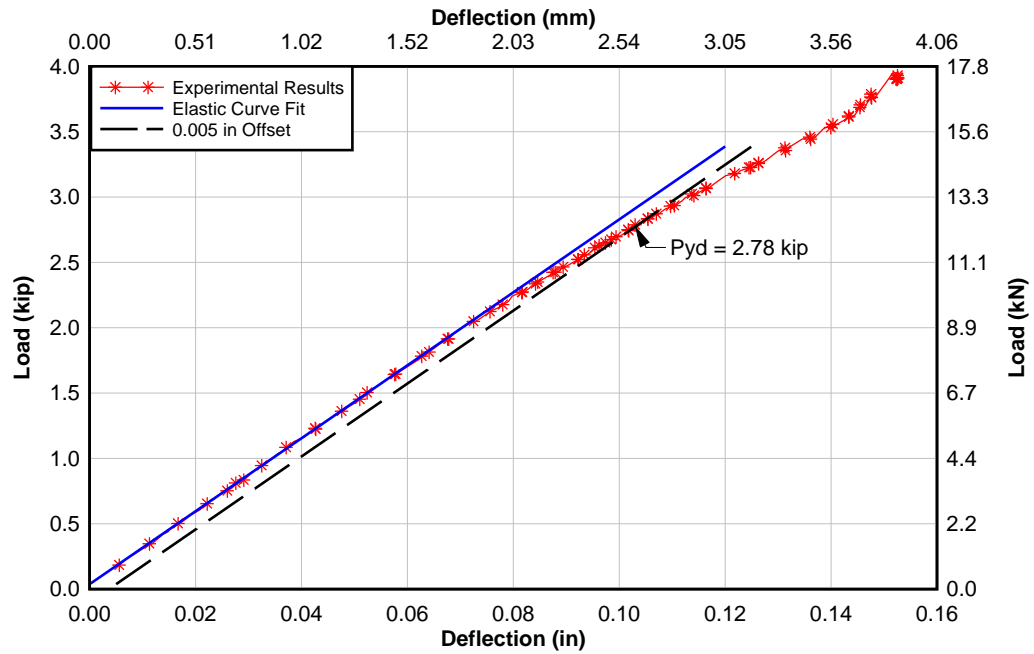


Figure C-6: 3/8 in. thick A36 plate PW3s

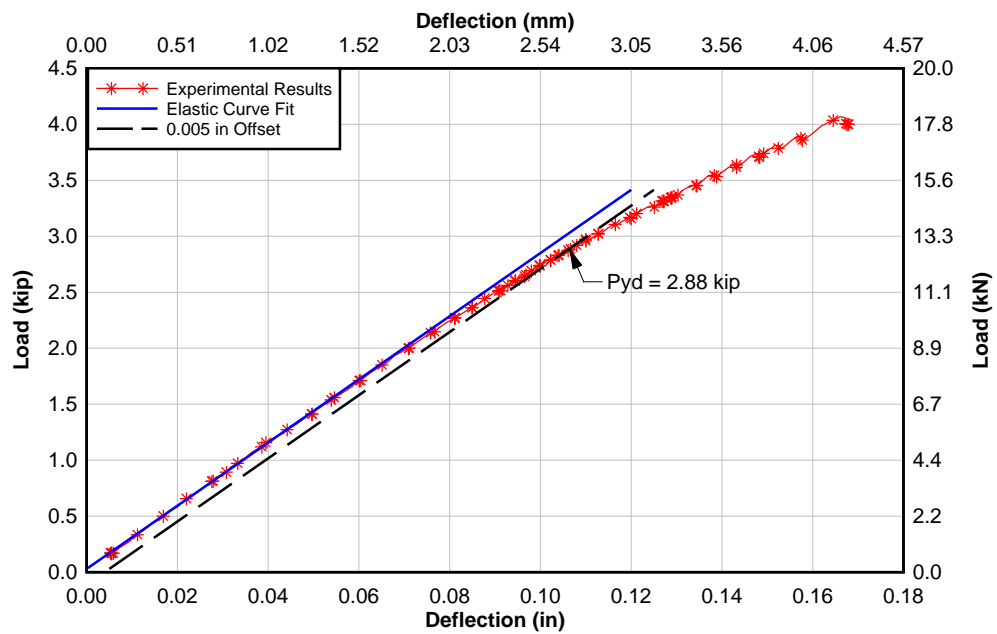


Figure C-7: 3/8 in. thick A36 plate TW1s1

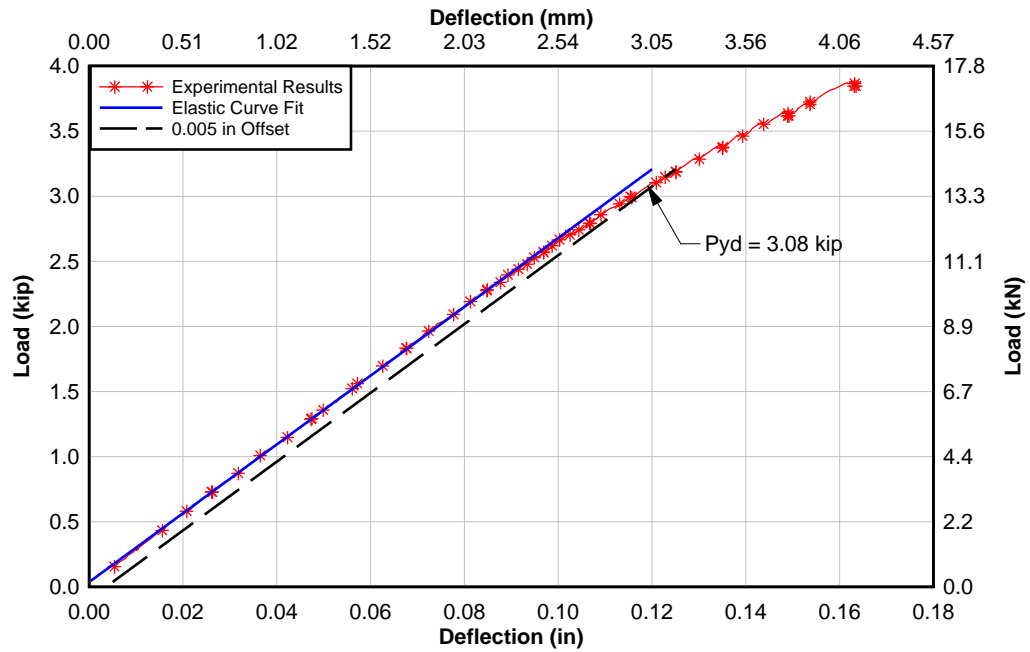


Figure C-8: 3/8 in. thick A36 plate TW2

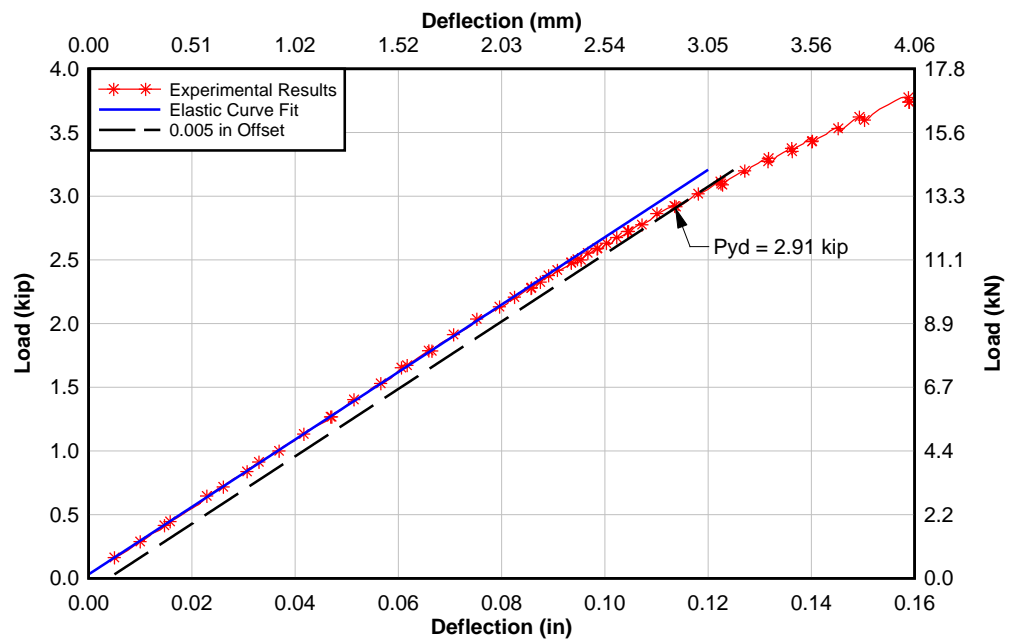


Figure C-9: 3/8 in. thick A36 plate TW2s

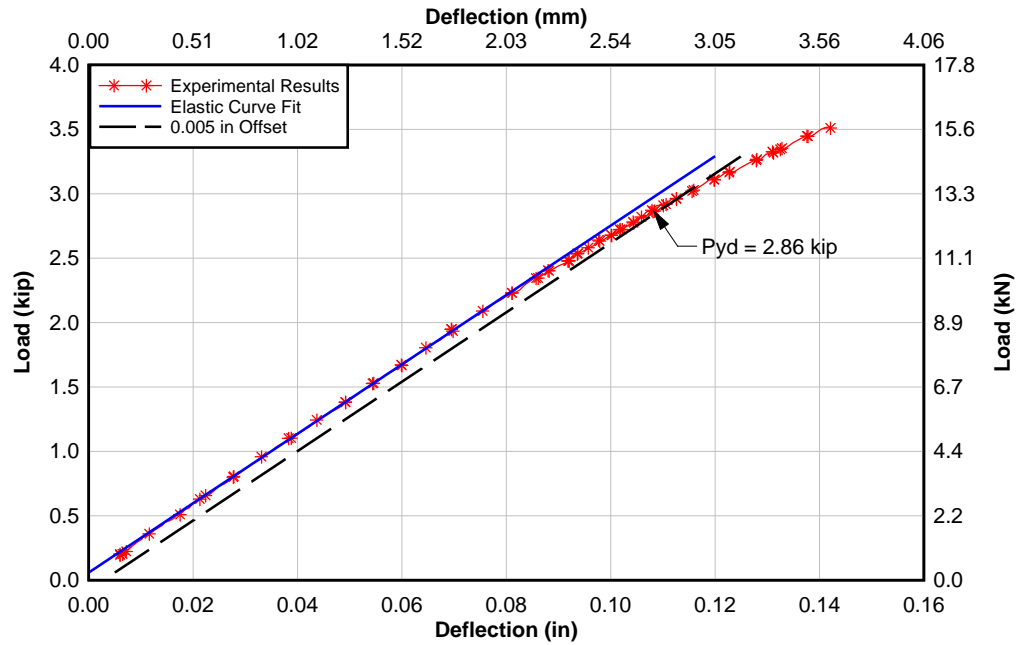


Figure C-10: 3/8 in. thick A36 plate TW3s

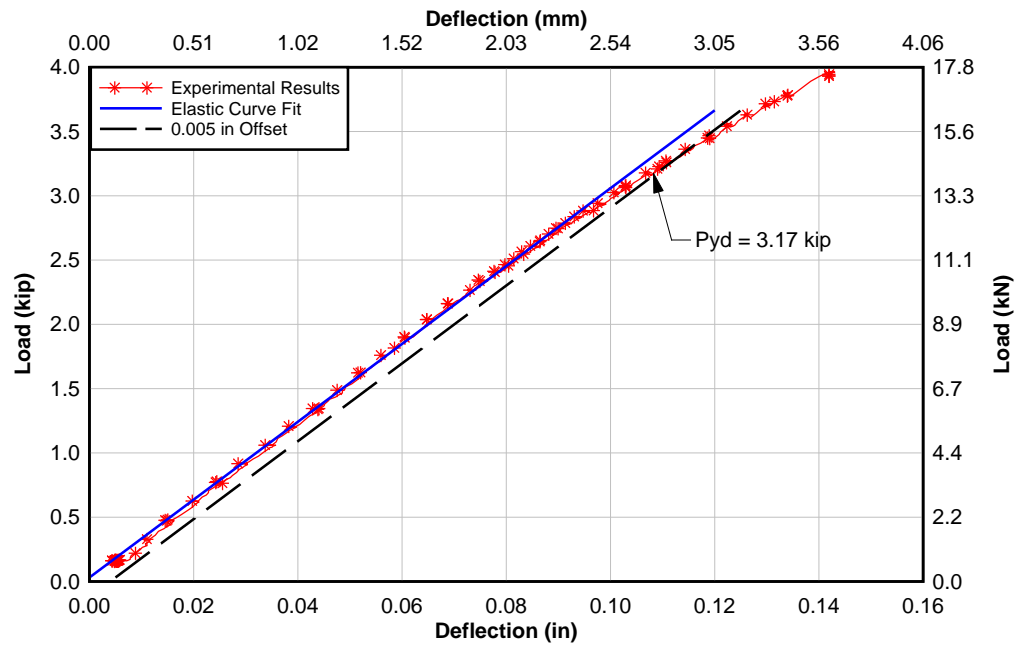


Figure C-11: 3/8 in. thick A36 plate BW1s

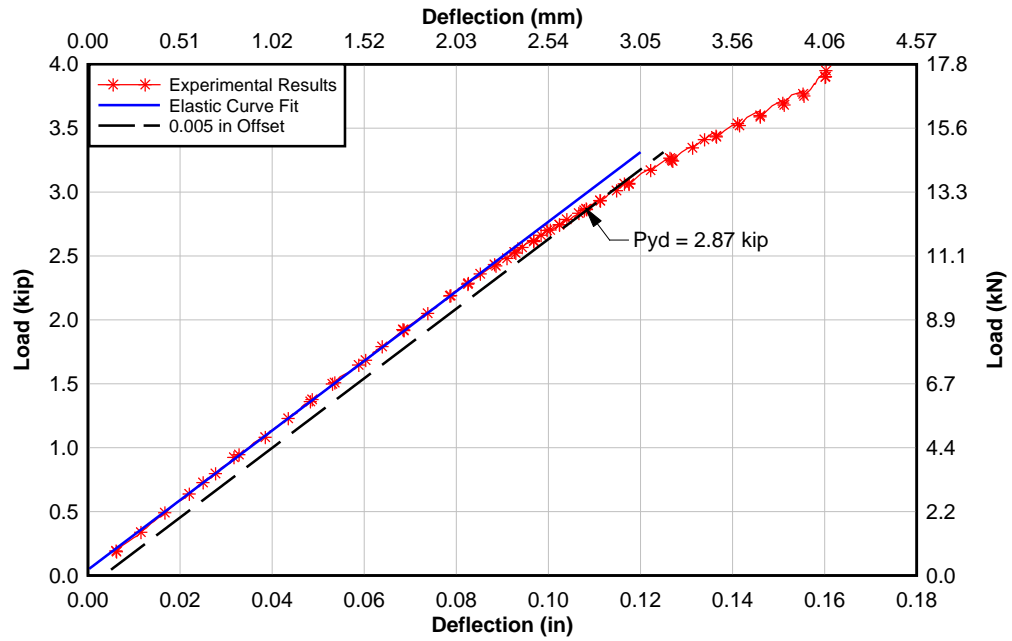


Figure C-12: 3/8 in. thick A36 plate BW2

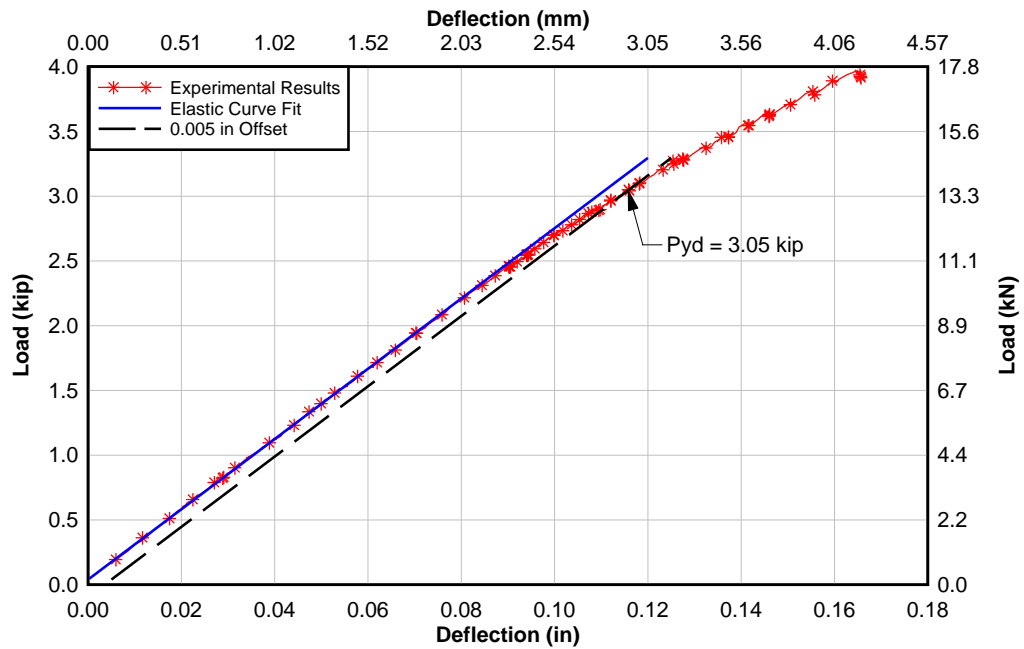


Figure C-13: 3/8 in. thick A36 plate BW2s

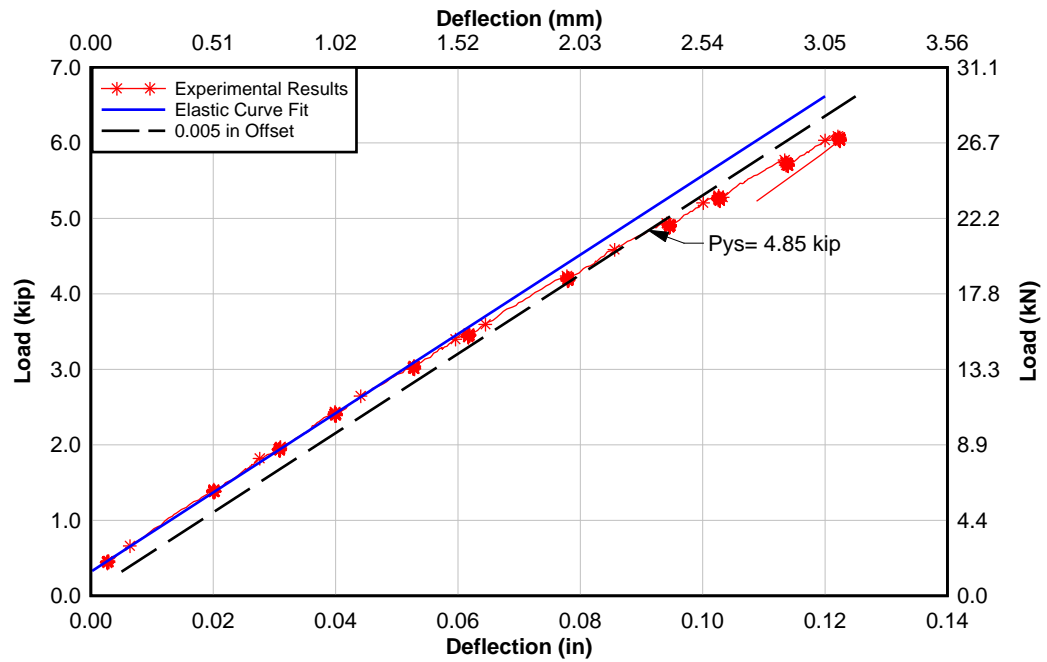


Figure C-14: 1/2 in. thick A36 plate PN1

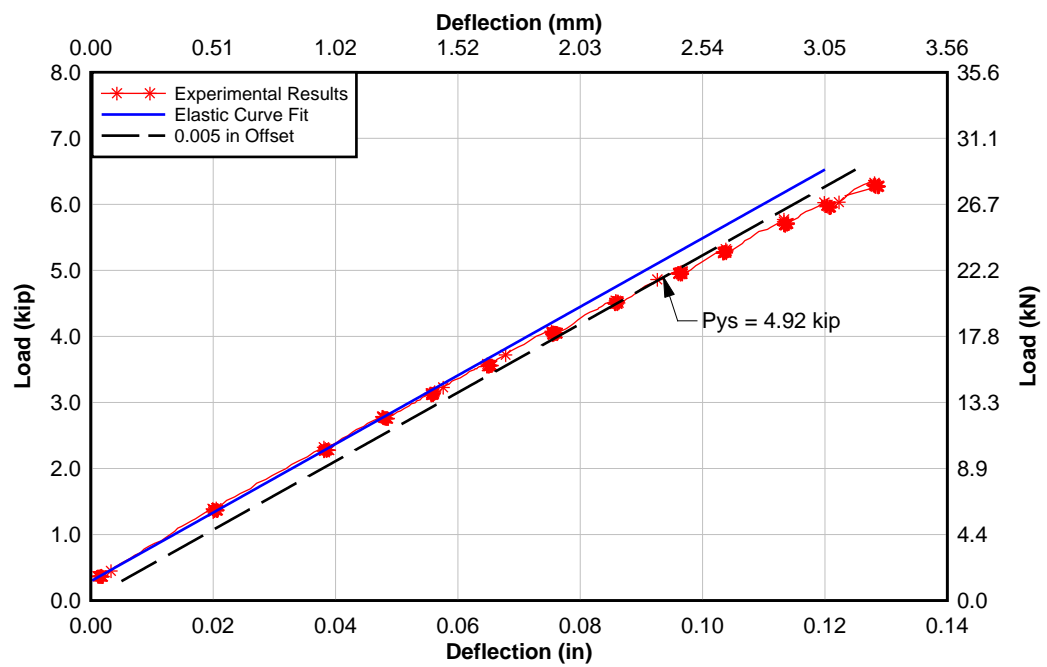


Figure C-15: 1/2 in. thick A36 plate PN3

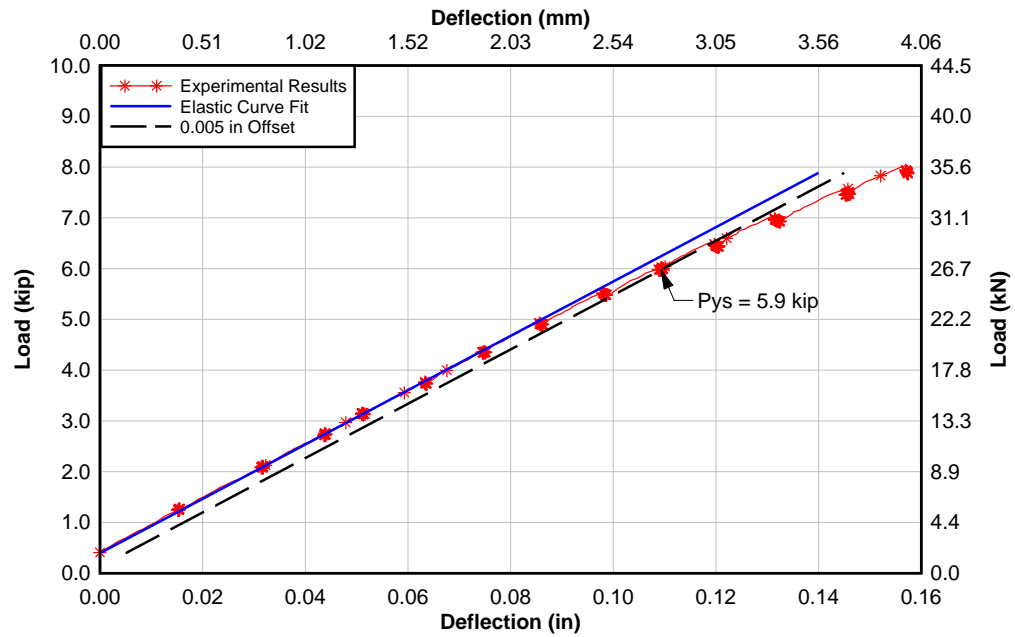


Figure C-16: 1/2 in. thick A36 plate TN3

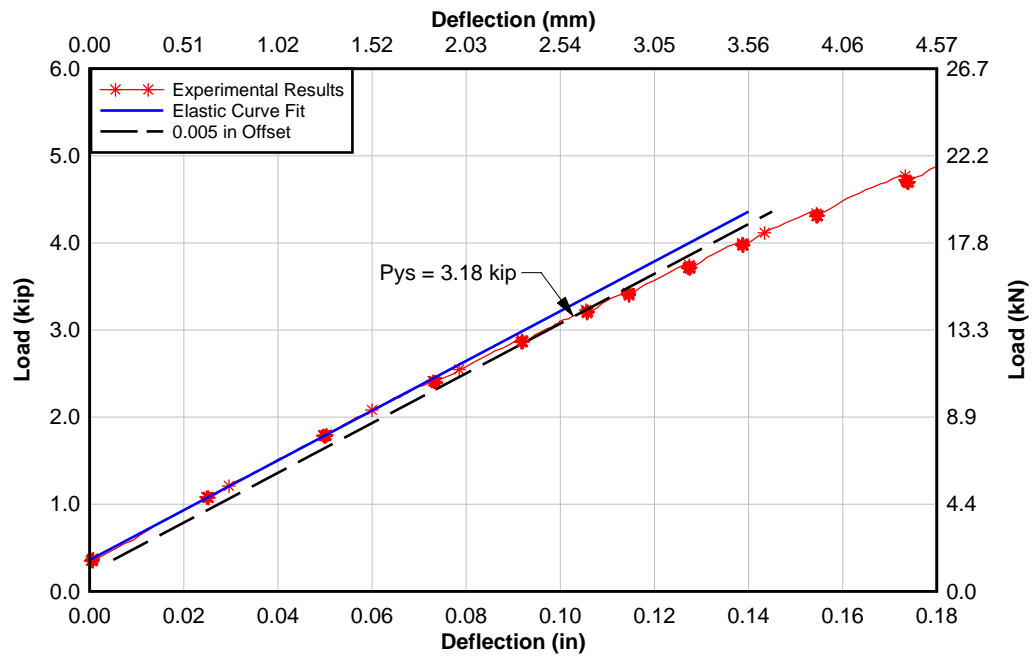


Figure C-17: 3/8 in. thick Gr 50 plate PN3

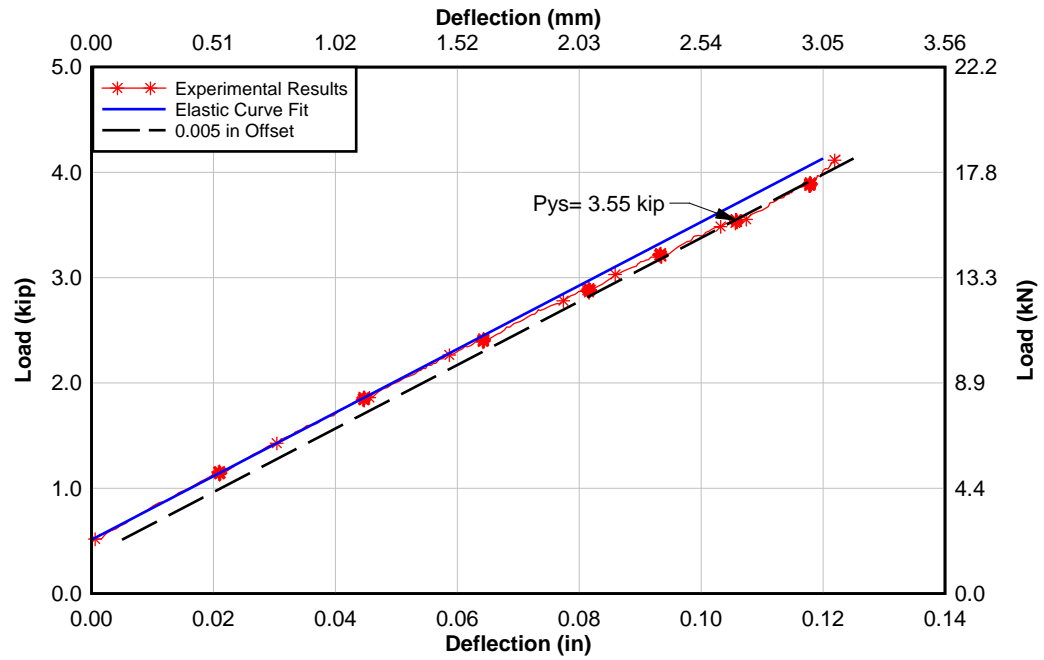


Figure C-18: 3/8 in. thick Gr 50 plate TN1

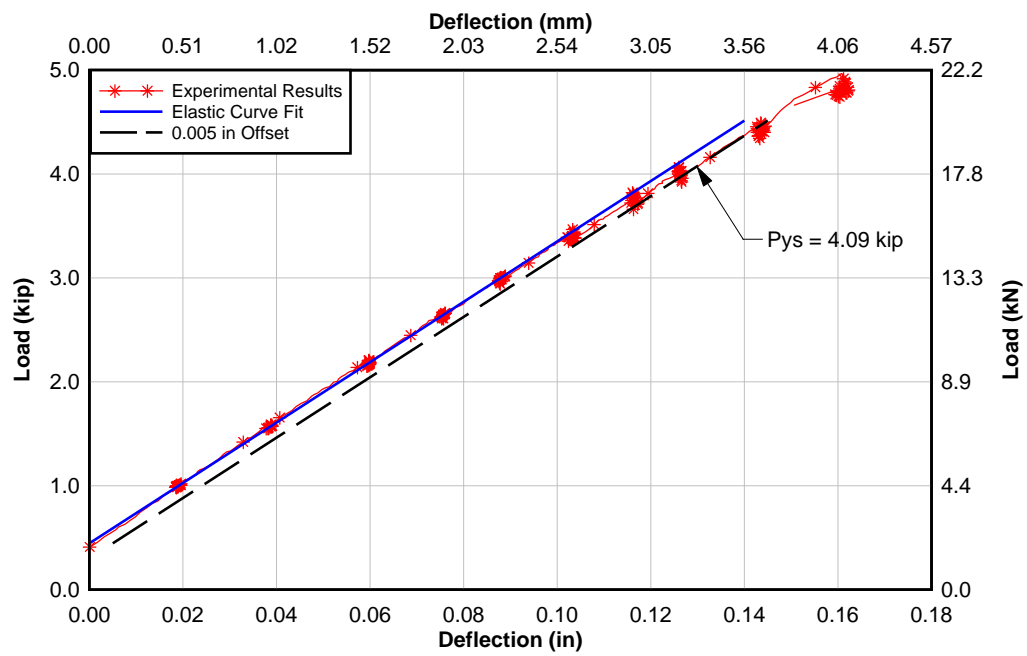


Figure C-19: 3/8 in. thick Gr 50 plate TN3